AN ABSTRACT OF THE DISSERTATION OF

Joshua R. Wyrick for the degree of Doctor of Philosophy in Civil Engineering presented on March 31, 2005.

Title: On the Formation of Fluvial Islands

Abstract approved:

Signature redacted for privacy.

Peter C. Klingeman

This research analyzes the effects of islands on river process and the effects river processes have on island formation. A fluvial island is defined herein as a land mass within a river channel that is separated from the floodplain by water on all sides, exhibits some stability, and remains exposed during bankfull flow. Fluvial islands are present in nearly all major rivers. They must therefore have some impact on the fluid mechanics of the system, and yet there has never been a detailed study on fluvial islands. Islands represent a more natural state of a river system and have been shown to provide hydrologic variability and biotic diversity for the river.

This research describes the formation of fluvial islands, investigates the formation of fluvial islands experimentally, determines the main relations between fluvial islands and river processes, compares and describes relationships between fluvial islands and residual islands found in megaflood outwash plains, and reaches conclusions regarding island shape evolution and flow energy loss optimization.

Fluvial islands are known to form by at least nine separate processes: avulsion, gradual degradation of channel branches, lateral shifts in channel position, stabilization of a bar or riffle, isolation of structural features, rapid incision of flood deposits, sediment deposition in the lee of an obstacle, isolation of material deposited by mass movement, and isolation of riparian topography after the installation of a dam. A classification scheme is proposed in order to describe the islands and relate them to the river processes.

Several physical experiments were performed to analyze both the processes involved with island formation and the effects islands have on river processes. The experiments performed herein ranged in scale from a 0.45-meter wide flume to the 100-meter wide Willamette River. The analyses describe the effects of islands on flow processes, such as drag force, energy loss, and flow patterns. Previous research has shown that the drag force on a streamlined object in a water flow can be minimized by setting the object's aspect ratio to about three. This research analyzed the flow patterns behind a blunt object in a streamflow and showed that conditions can be conducive to creating a streamlined, depositional shape with an aspect ratio (length/width) of about three. By introducing islands of various aspect ratios into a streamflow and measuring the flow characteristics, it is shown that the energy loss is minimized with the island's aspect ratio around three.

Aerial photographs of fluvial islands were analyzed for thirteen American rivers and a watershed-independent correlation was found for the shape parameters. The average length/width ratio of all analyzed fluvial islands was 4.14. By describing the island shapes with a lemniscate form, the islands were compared with dimensionless properties. The use of dimensionless properties allowed for the analyses of terrestrial fluvial islands to be compared to analyses of fluvially-formed residual islands in unique megaflood areas, such as the Channeled Scablands and Mars Channels. The shape characteristics of the islands were found to be similar, therefore similar relationships between the islands and flow processes are assumed.

© Copyright by Joshua R. Wyrick
March 31, 2005
All Rights Reserved

On the Formation of Fluvial Islands

by
Joshua R. Wyrick

A DISSERTATION

submitted to

Oregon State University

in partial fulfillment of
the requirements for the
degree of

Doctor of Philosophy

Presented March 31, 2005
Commencement June 2005

ACKNOWLEDGEMENTS

Thou in thy narrow banks art pent:
The stream I love unbounded goes
Through flood and sea and firmament;
Through light, through life, it forward flows
from "Two Rivers" by Ralph Waldo Emerson

Thou hast taught me, Silent River!
Many a lesson, deep and long;
Thou hast been a generous giver;
I can give thee but a song.
from "To the River Charles" by Henry Wadsworth Longfellow

I could not have done this alone and am indebted to everyone who volunteered their time and expertise to assist with this project. In the field, Bob Bostedt, Derron Coles, Denise Hoffert-Hay, Anne Jefferson, Laura Kegley, Pete Klingeman, Stephanie Painter, and Josh Wells helped in collecting data on the Willamette River, Calapooia River, Oak Creek, and the coastal streams. I am especially thankful to Greg Stewart who volunteered his kayak expertise and the use of the ADP system for work on the Willamette River.

My analysis of the Martian and Scabland islands was done at Washington University's Department of Earth and Planetary Science with the help of Dr. Roger Phillips and several graduate students, including Brian Hynek, Kim Deal, and Frank Seelos. I was assisted in finding historical aerial photographs of Columbia River islands by Randy Montalbano, a records management technician for the Portland office of the U.S. Army Corps of Engineers. Manfred Dittrich, the mechanical technician for Department of Civil, Construction and Environmental Engineering at Oregon State University, volunteered his time and tools to help create or alter some of my field equipment. Unpublished flow data for Oak Creek was provided by Amy Simmons of OSU's Forest Engineering Department. Dr. Wayne Huber was always available to answer questions.

I wish to thank the Rohner Family, who allowed us access through their property to an island on the Willamette River. I am especially thankful to Bob and Pallie Bostedt for allowing us access through their property to an island on the Calapooia River. I also thank Curt Sorte and Alice Smith, other landowners on the Calapooia River, who allowed access to their properties to assess their islands.

I am very grateful to my committee members Drs. Richard Cuenca, Roy Haggerty, Pete Klingeman, and Paul Komar, as well as my graduate school representative, Roland Deszoecke for their assistance and advice through the course of this research.

Finally, I wish to express my sincere appreciation to my advisor, Dr. Pete Klingeman for his continuous guidance, assistance, encouragement, and inspiration, not only for this research, but also for my coursework and career decisions.

TABLE OF CONTENTS

TABLE OF CONTENTS (CONTINUED)

TABLE OF CONTENTS (CONTINUED)

LIST OF FIGURES

LIST OF FIGURES (CONTINUED)

LIST OF FIGURES (CONTINUED)

LIST OF FIGURES (CONTINUED)

LIST OF FIGURES (CONTINUED)

LIST OF TABLES

LIST OF APPENDIX FIGURES

LIST OF SYMBOLS AND VARIABLES

A	=	cross-sectional area
B, b	=	width
c	=	particle cohesive force
C	=	Chezy friction coefficient
C_d	=	drag force coefficient
C_V	=	sediment concentration by volume
d	=	flow depth
d_s	=	sediment particle diameter
D_h	=	hydraulic diameter
D_s	=	scour depth
E	=	specific energy
f	=	Darcy-Weisbach friction coefficient
F_b	=	buoyancy force
F_D	=	drag force
F_g	=	gravitational force
F_L	=	lift force
F_R	=	resisting force
Fr	=	Froude Number
g	=	acceleration due to gravity
H	=	total head
He	=	Hedstrom Number
i	=	sediment transport rate per unit width
k	=	degree of elongation
K	=	decay constant
L	=	length
L_m	=	mixing length
M, m	=	mass
n	=	Manning's roughness coefficient
P	=	wetted perimeter
P	=	hydrostatic pressure
Q	=	volumetric flowrate
Q_b	=	geothermal heat flux
R	=	hydraulic radius
R_A	=	aspect ratio
Re	=	Reynold's Number
s	=	storage coefficient
S_o	=	channel bed slope
SG	=	specific gravity
t	=	time
T	=	transmissivity
T_m	=	melting temperature
V, v	=	stream velocity
W	=	width
w_s	=	particle settling velocity

x	=	distance from a given location
y	=	flow depth
z	=	elevation
z_o	=	streambed elevation
α	=	angle of internal friction
γ	=	specific weight
η	=	plastic viscosity
θ	=	angle
κ	=	hydraulic diffusivity
μ	=	dynamic viscosity
ρ	=	density
σ	=	normal stress
τ	=	shear stress
τ_b	=	Bingham yield stress
τ_y	=	yield stress
Ω	=	stream power

CHAPTER 1 – INTRODUCTION

PURPOSE AND APPROACH OF RESEARCH

Fluvial islands are present in nearly all major rivers. They must therefore have some impact on the fluid mechanics of the system, and yet any discussion of islands is conspicuously absent in reviewed geomorphology texts [e.g., Chorley, 1971; Schumm, 1972; Richards, 1987; Hickin, 1995; Rodriguez-Iturbe & Rinaldo, 1997; Knighton, 1998; Bridge, 2003]. The purpose of this research is to make analyses and conduct experiments that will provide a better understanding of the formation of fluvial islands. More specifically, the research objectives are to (1) describe the formation of fluvial islands based on general evidence, (2) investigate the formation of fluvial islands experimentally, (3) determine the main relations between fluvial islands and river processes, including any relationships between island shape and river processes, (4) compare and describe relationships between fluvial islands and residual islands found in megaflood outwash plains, and (5) reach conclusions regarding island shape evolution and optimization. Some supporting purposes are to (a) create an island classification scheme, (b) analyze and compare the shapes of islands in several American rivers, and (c) determine the influence of island shape on the drag force exerted by river flow.

To accomplish the purposes set forth for this research, I will: (1) summarize previous research on the formation of fluvial islands, (2) examine aerial photographs and topographic maps, (3) perform quantitative analyses of island features measurable from aerial photographs and maps, (4) conduct field experiments of flow features at existing and experimentally fabricated islands of various shapes, (5) conduct laboratory flume experiments of fabricated islands, and (6) synthesize the analyses, measurements, and experiments to seek generalized relationships for describing the formation of fluvial islands and their shape characteristics.

DEFINITION OF A FLUVIAL ISLAND

For the purpose of this research, a fluvial island is defined as a land mass within a river channel that is separated from the floodplain by water on all sides, exhibits some stability [Osterkamp, 1998], and remains exposed during bankfull flow (whereas a *bar* would be submerged). Islands may not be permanent on the geologic time scale due to river meanders, climate changes, etc., but can remain in place over decadal or century time scales and hence exhibit stability. Stability, however, is a term that is not usually defined precisely in the literature. For the purpose of this research, a stable island is one that exists not only in an inter-flood time period, but also remains after the next high flow occurs. Vegetation is generally a good indicator of stability. Vegetation may also provide a distinction between an island and a bar, but is not necessarily a requirement for a fluvial island. Islands may be composed of material too coarse to allow establishment of vegetation (e.g., bedrock outcrops, see Chapter 3), or they may be located in regions of naturally sparse vegetation.

Chapter 2 – Background on Fluvial Islands

Hydrologic and Biotic Importance of Fluvial Islands

Fluvial islands are important in both hydrologic and biotic capacities, and can therefore be indicators of the general health and energy of the system. Although islands may be generally unstable in the long term, recent histories of magnitudes, frequencies, and durations of water and sediment fluxes can be recorded in the sediment and biota. In some instances, histories of older, extreme events could be preserved as well. Landforms, including islands, associated with a particular river can provide a detailed account of that river's past and present activity. Because islands separate the total river flow into at least two individual channels, they create varying hydraulic conditions due to different widths, depths, slopes, etc. The type of islands present in a riverine system can help describe the river processes as well (see Chapter 3). Islands represent a more natural state of a river system. Gurnell and Petts [2002] determined that most European rivers were once island-dominated (pre-1900), but have become devoid of islands following human interference. Away from areas of agricultural or urban development in Europe, islands remain a common feature of riverine landscapes, such as the Fiume Tagliamento in northeast Italy [Ward et al., 1999].

Since islands are separated from the floodplain, they may offer a safe haven for wildlife from many predators. Flow conditions near the island, such as river width, depth, and velocity, will minimize predation and increase species productivity. For this reason, many large rivers have wildlife refuges that include islands. River management that reduces total island area could have negative implications for migratory fowl. Plants have been shown to thrive on islands near heavy grazing lands [Hilbig, 1995]. The presence of a certain species of plant on the island can help determine the flow conditions in the area. Some plant species require specific growth conditions, such as inundation duration, gradient, and particle size. Ward et al. [1999] suggest that the key elements of optimum ecosystem functioning are islands and secondary channels. In fact, Arscott et al. [2000] found that on the Fiume Tagliamento, aquatic habitat complexity was greater in the island-braided section as compared to the island-devoid section. In the same river, van der Nat et al. [2003] showed that aquatic habitats were more stable in regions of vegetated islands even as compared to bar-braided regions. Stanford et al. [1996] state that islands are most likely to occur in areas of dynamic fluvial processes that would provide for high species diversity within a wide range of riparian habitat.

INFLUENCE OF ISLANDS ON POLITICAL BOUNDARIES

Rivers that were impassable or difficult to cross for early settlers were commonly used to establish political boundaries since they formed easily recognizable borders [Beckinsale, 1971]. When boundary rivers shift course, either naturally or artificially, the original physical border is usually retained and can create a geomorphic interest.

Several problems can arise from the use of rivers as boundaries. The first is that rivers naturally change course, which would then alter the political boundaries and could lead to conflicts if the abutting administrations are not on friendly terms. Most policies for border definition are that the boundaries will change with the small, lateral shifts of the river, but the original boundaries will be kept if the river avulses, or in some other way abruptly alters its course. A second complication is that most river management practices, such as withdrawals, dredging, and dams, affect both banks. Third, a flood plain that is attractive for farming, ranching, or settling, may be equally attractive on both banks. If a waterline is unstable, difficulties in boundary definition can arise. A constantly meandering, shifting river can cause problems for the administrations involved. Such problems can be resolved by building construction projects, such as dams and revetments, along the channel. The Rio Grande River marks part of the border between the United States and Mexico. Historically, this river was very active due to excessive silting and frequent meander cutoffs. When the border was defined, few settlers lived near the river. As populations on both sides of the river increased, however, the shifting river began to cause problems. In the 1930's, an International Boundary Commission installed a dam near Caballo, New Mexico, and straightened and revetted the channel such that silting virtually ceased [Beckinsale, 1971]. Islands along this section of the river have subsequently disappeared.

Several partitioning methods have been used to create a boundary at a river: (1) setting the boundary equidistant from both shorelines, (2) having the boundary follow the river's thalweg, (3) selecting one edge of water as the boundary, or (4) defining some arbitrary line. The latter is generally used for boundary lakes, such as through the Great Lakes that separate Canada from the United States. The third, selecting a shoreline as the boundary, is rare, but one such example exists along the Red River between Oklahoma and Texas. The border is set as the right bank of the river (i.e., Oklahoma controls the whole of the mainstem). The use of the thalweg as the demarcation is common for international boundaries where navigation interests are dominant. An example of the median line used as a boundary is the Rhine River in southwestern Germany. One problem of the median line method is that the border can change position with changing stage levels and cross-sectional shapes. Another is where to draw the median line when an island is present.

Fluvial islands are usually not specifically discussed, and can therefore create difficulties in boundary demarcation [Beckinsale, 1971]. If an island is split or wholly given to one administration, what then happens if the river shifts and connects the island to the mainland? If an island forms within the channel, who has ownership? In active meander zones or sediment transport areas, adjustment of island ownership may therefore be necessary.

Influence of Dams on Fluvial Islands

Nearly all large rivers are flow-regulated to some degree. This can have implications for fluvial island development and stability. Dams reduce flood peaks, increase baseflow, and store sediments (especially coarser material). The sediment transported past a dam can be only a fraction of the normal sediment load.

The amount of sediment transported past a dam can be estimated by determining the amount of sediment that will be trapped behind it. Trap efficiencies of dams can be estimated by simplifying the sediment continuity equation. Sediment fluxes through a control volume are dictated by a combination of advective, diffusive, and turbulent mixing motions. For reservoir sedimentation, advection is usually assumed to dominate over diffusion and mixing [Yang, 1996]. Several formulae have been set forth by researchers to determine the trapping efficiencies (E, in percent) of reservoirs [USACE, 1989]. Brown's Method is the simplest, using reservoir capacity (C, in acre-feet) and upstream watershed area (W, in square miles):

$$E = 100\,(1 - 1\,(1 + KC/W)) \tag{2-1}$$

where K is a constant ranging between 0.046 and 1.0, with a median value of 0.1. Brune's Method can be more accurate if the mean annual inflow (I, in units of volume) is known for the reservoir:

$$E = 100\,(0.97 \wedge (0.19 \wedge \log(C/I))) \tag{2-2}$$

Another common method is Churchill's Method, which uses a sedimentation index (SI). The sedimentation index is the ratio of the period of retention in a reservoir to the mean velocity through the reservoir:

$$SI = (C/I)^2/L \tag{2-3}$$

where L is the length of the reservoir (feet) during normal operating stage. Neither of these methods incorporates sediment characteristics into their analyses. All of the above formulae have a power function to their shape that quickly levels off between 90-100% efficiency. This means that almost all of the incoming sediment is trapped behind most large dams.

Because most sediment becomes trapped, the water released from the reservoir may be "hungry" and can scour the riverbed downstream of the reservoir and cause degradation of the bed elevation. Lane [1955] quantitatively expressed this as a proportional relationship:

$$Q_s d \sim QS \tag{2-4}$$

Here, Q_s is the sediment load discharge, d is the mean sediment particle diameter, Q is the water discharge, and S is the channel slope. QS is an estimate of the stream power, and $Q_s d$ is an estimate of the sediment transport capacity of the flow [Lane, 1955]. The balance of these two parameters is useful to the analysis of how flow characteristics change to compensate for a change in one of the variables.

This may be only a local effect, though, near the dam. Once the river has accumulated its capacity of sediment further downstream, streamflow processes may proceed as usual, but with increased base flows and decreased peak flows. The reduced flow peaks downstream of a dam eliminate most processes of channel erosion, overbank deposition, and sediment replenishment. This also generally reduces the biologic habitat, diversity, and interactions between biotic and hydrologic processes. While dams can reduce the erosion and destruction of fluvial islands, they also promote bank attachment by decreasing the sediment supply and reducing the downstream transport capacity which lead to deposition of tributary input sediment. Where this occurs, channels tend to narrow and secondary channels that generally define islands can fill in with sediment.

Dams, however, can also be the cause of island development. The erosional flows downstream of a dam could scour around some centralized topography. Merritt and Cooper [2000] documented the downstream emergence and formation of fluvial islands on the Green River after an initial period of channel narrowing following the installation of Flaming Gorge Dam.

CHAPTER 3 – DEVELOPMENT OF AN ISLAND CLASSIFICATION SCHEME

CAUSES OF ISLAND FORMATION

Research on the formation processes of fluvial islands has been limited. Tooth and Nanson [2000] described the formation of islands in an ephemeral Australian river due to the deposition of sediment behind teatrees. Gurnell et al. [2001] analyzed the influence of riparian vegetation, sediment type, and hydrologic regime on island formation in the Fiume Tagliamento of northeast Italy. They developed a conceptual model for island formation in this region and determined that islands form by either channel avulsion or the vegetation of exposed gravel bars. Osterkamp [1998] considered all the processes involved with islands in more detail. He proposed that islands could be separated into at least eight categories based on their formation process. These are described and elaborated on in the following sections.

AVULSION

During a high flow event, a river may excavate a shorter path, particularly across a bend, thereby leaving two flow channels after the river stage has receded. These avulsive types of islands may form through such mechanisms as toppling of riparian trees and flow diversion by debris dams. One example of this island type was described in the Little River valley in northern Virginia by Kochel et al. [1987], where log jams during a low-frequency storm event trapped gravel within the channel up to an elevation of 1.5 meters higher than the surrounding floodplain, causing the flow to avulse around part of the floodplain to form a new island. Log jams have also been documented on the Morice River in British Columbia that diverted flood flows across the floodplain, creating a nickpoint retreat that resulted in an avulsion and a new island [Gottesfeld and Gottesfeld, 1990]. Avulsions also have significance in law and property definitions. Most State laws maintain that riparian property lines do not change with an avulsion, only with gradual stream migration (e.g., erosion and deposition). Numerous court cases have arisen over the dispute of island ownership after avulsive events (e.g., see Ryles, Larrison, and Maris v. Riffle, Arkansas Appellate Court, 2003, about the ownership of Fourche Island on the

Arkansas River). Figure 3-1 shows an example of an avulsion island that appeared after a flood event on Chase Creek in British Columbia, Canada.

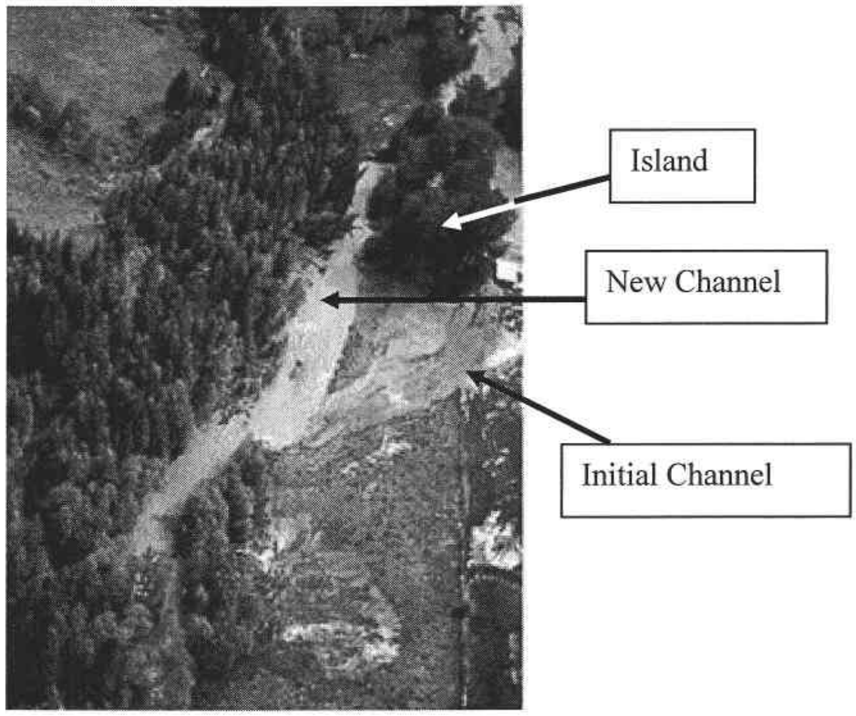

Figure 3-1. Example of an island that formed after a flood-related avulsion on Chase Creek in British Columbia, Canada, June 1997. Flow is towards the bottom of the figure. Photo from Ministry of Water, Land, and Air Protection in British Columbia.

GRADUAL DEGRADATION OF CHANNEL BRANCHES

The gradual-erosion type of island usually results from steady evacuation over years or centuries of sand/gravel flood deposits or glacial outwash sediments, or from other processes of accelerated upland erosion, bank failure, or abundant supply of stored bed sediments. Transport of bed sediments in anabranches by regulated streamflow may lead to the formation of fluvio-deltaic islands, which are formed by the sorting of coarse sediments delivered by high-energy tributaries to low-gradient mainstems that cannot mobilize the incoming coarse material. Divided flow in the mainstem, splitting around the coarse material, may result in the formation of islands through deposition on the coarse material and/or incision of the flanking channels. Examples of this type include islands near Grand Junction, Colorado, that are re-worked glacial debris rarely mobilized by runoff from the Rocky Mountains [Osterkamp, 1998]. Vegetated islands along the Platte River have been documented to aggrade to floodplain level following low-flow dissection of transitional and longitudinal bars [Johnson, 1997]. Figure 3-2 shows an example of a gradual-erosion type of island on the Ohio River.

Figure 3-2. Grape Island on the Ohio River, an example of a gradual erosion island.

LATERAL SHIFTS IN CHANNEL POSITION

Lateral-shift islands are created by channel migration and meander cutoff or by interactions at the confluence of multiple meandering streams. Numerous examples of this type occur along the Mississippi River downstream of Memphis, Tennessee, especially near the confluences of the White and Arkansas Rivers [Osterkamp, 1998]. This type of island is also common in braided channels, such as the Platte River or the Wisconsin River (Figure 3-3). Maser and Sedell [1994] describe islands along the lower Willamette River that were formed by deflected flow around woody debris that may be centuries old. An Indian term, *char*, describes islands in the braided Brahmaputra River formed by sand and silt accreting from a bar cluster to floodplain level [Thorne et al., 1993].

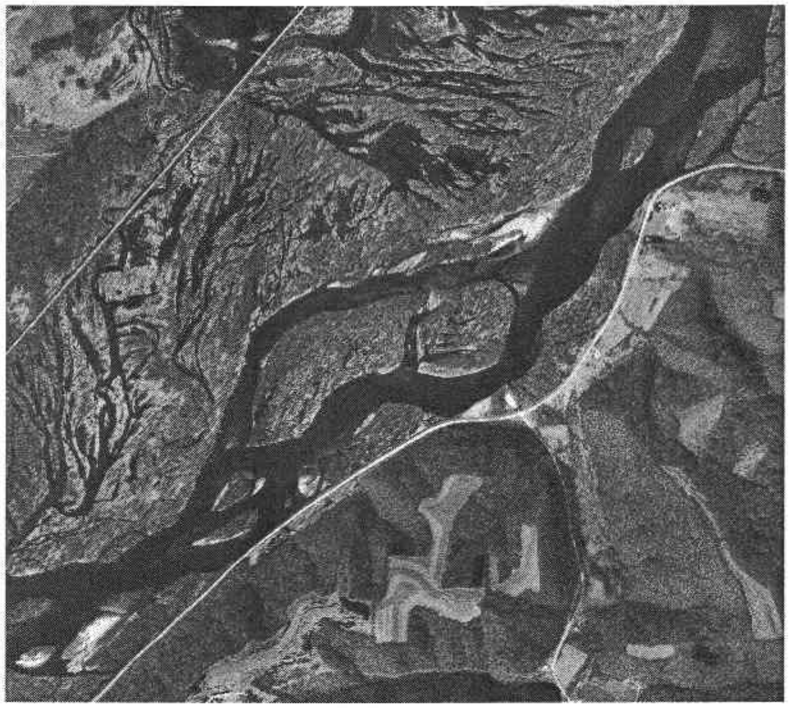

Figure 3-3. Braid islands along the lower Wisconsin River.

STABILIZATION OF A BAR OR RIFFLE

Bar/riffle-stabilization islands form from long term aggradational and sorting processes of coarse bed sediments or by redistribution of sand and gravel in streams having large bedload fluxes. Examples of this type include aggradational islands along the Platte River following a long period of peak flow reduction [Eschner et al., 1983] and emergent islands in the flood-widened channel of the Gila River [Burkham, 1972]. An extended period of low-flow allows for riparian vegetation to encroach onto depositional surfaces. Hooke's [1986] analysis of English rivers concluded that it takes one to three years for vegetation to sufficiently stabilize exposed bars. Graf [1978] documented a 70-year decline in discharge on the Green River in Utah. This resulted in the formation of many new depositional features, islands and bars. A non-native shrub, Tamarisk, invaded these new features and helped anchor the sediment enough that they were not removed by high flows in subsequent years. These islands were shown to restrict the channel width by 13% to 55%. Figure 3-4 shows a streamlined mid-channel sand bar on the Arkansas River. If flows remain low for a long enough period of time, vegetation may accumulate on its surface and stabilize the emergent island against future higher flows.

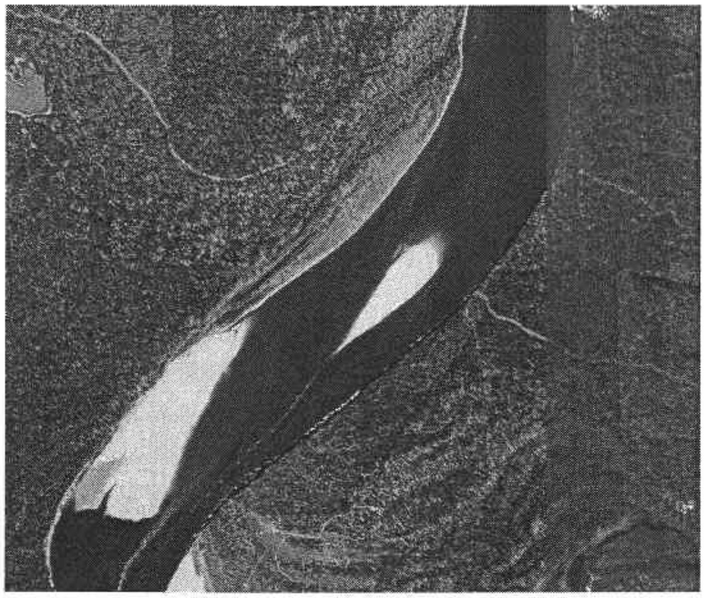

Figure 3-4. Sand bar on the Arkansas River.

Structural Features

The structural-feature type of islands forms almost exclusively in non-alluvial, often bedrock, channels of karstic, glacial, or volcanic ash geology. Structural-islands may emerge as the river preferentially erodes through bedrock fractures. Examples include Goat Island (Figure 3-5), an isolated monocline that separates Niagara Falls and American Falls on the Niagara River [Tessmer, 1981], and islands on the Potomac River upstream of Great Falls, Virginia.

Figure 3-5. Goat Island at Niagara Falls. Island is a structural monocline isolated by the Niagara River.

Rapid Incision of Deposited Sediments during Flood Recession

Flood-deposit islands form during the rapid evacuation of sediment during a flood, mass movement, or general landscape instability. Dewatering and accelerated incision of fresh flood-deposited sediment can cause upstream migration of multiple headcuts during flood-peak recession that may isolate higher central topography. The main difference between these type of islands and avulsion islands is that flood-deposit islands are formed by erosion of newly-deposited sediments, whereas avulsion islands are composed of older-deposited floodplain material. These types of islands are most common along small streams that are substantially altered during short time periods, such as Plum Creek, near Denver, during the 1965 Flood [Friedman et al., 1996]. These types of islands are not restricted by spatial scales, however, as other examples of this case involve islands that are deposited during unique extreme flow events and are made up of material that is unmovable during normal river flows, such as many of the fluvial islands along the Snake River in southern Idaho that were deposited during the Bonneville Flood about 14,500 years ago and have not been overtopped since [O'Connor, 1993]. Figure 3-6 shows a pair of islands on the Snake River that consist of material too coarse for the normal streamflows to transport, and yet are not topped with fluvial deposits.

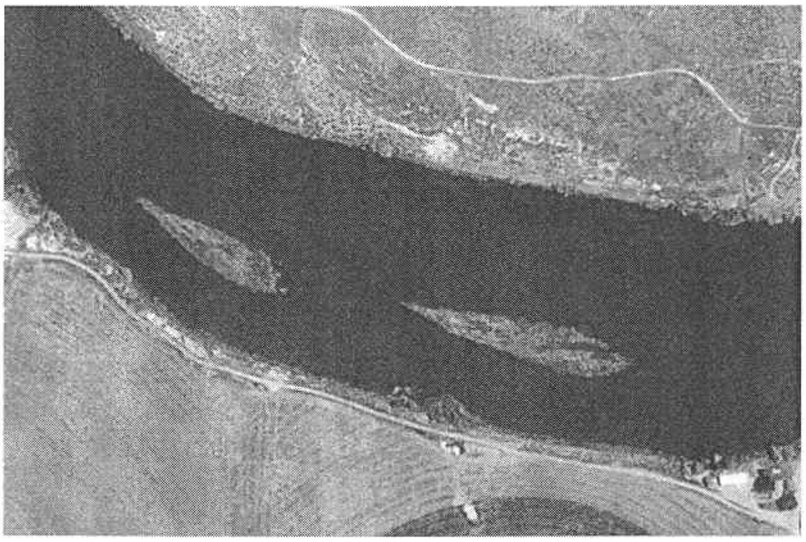

Figure 3-6. Islands along the middle Snake River formed from flood deposits of the Bonneville Flood.

Lee Deposition

Lee-deposition islands are common in widened, braided channels of all sizes where steady sediment evacuation, usually as bedload, occurs. Immediately downstream of a channel obstruction or snag (e.g., see Figure 3-7), a local zone of shallow depth, reduced velocity, and accumulating sediment may develop and quickly become vegetated. In-stream woody debris has been shown to be important in nucleating and maintaining mid-channel islands in Pacific Northwest mountain streams [e.g., Grant et al., 2001; Ward et al., 2002b]. Shull [1922] noted the formation of an island of this type in the Mississippi River near Belmont, Missouri. In March, 1913, unusually high flows capsized a barge, which was subsequently stranded on a mid-river shoal in the receding flows. The barge created a zone of shallow depth and slow velocities in its lee in which sediment began accumulating. By 1919, the deposition had acquired a stand of cottonwood trees and had grown to a length of 3/4 mile, a width of 1/8 mile, and an area of 60 acres. Tooth and Nanson [2000] describe sand accumulations behind tea trees in an ephemeral Australian river that form teardrop-shaped islands. Pre-existing craters in the Martian outwash areas may have accumulated sediments in their lees in this fashion as well (see Chapter 8 for more discussion on Martian islands).

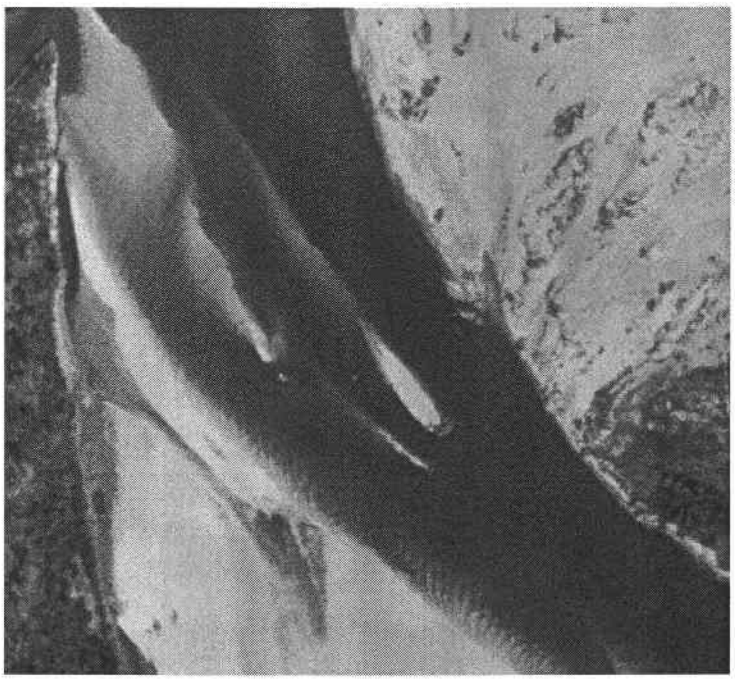

Figure 3-7. Debris snag on the Red River that has collected a silt/sand deposition in its wake.

MASS MOVEMENT

Mass-movement islands usually occur in lowlands that are catastrophically altered by extreme events such as debris avalanches. Other examples that may not be quite so extreme include islands formed by rockfall, soil slump, and bank failure.

RESERVOIR INSTALLATION

When a dam, whether man-made or natural, is emplaced, it ponds water upstream. If there is a sufficient water level rise, high riparian topography may become isolated as the valleys are flooded. These islands may or may not be composed of bedrock. Because the erosive power of rivers are reduced drastically within a reservoir, these types of islands are highly stable and may only cease to be islands if the dam is removed or the water surface elevation is dropped. Figure 3-8 shows an example of a riparian hill that was isolated from the floodplain after Pickwick Dam was built on the Tennessee River.

Figure 3-8. Riparian topography isolated after the installation of Pickwick Dam on the Tennessee River.

COMMENTS ON THE CHANGEABILITY OF ISLAND SHAPE

Because of the nature of an island's sediment composition and its formation, only five of the types of islands discussed above would be able to be shaped or re-shaped by normal streamflow processes into a streamlined shape: Avulsion, Gradual Erosion, Lateral Shifts, Bar/Riffle Stabilization, and Lee Deposition. An island formed by a mass movement (e.g., debris flow) can be significantly affected by peak discharges, but is unlikely to stabilize and become fluvially shaped. Islands that are flood related (Avulsion, Flood Deposits, Lee Deposits, and Mass Movement) are likely to change rapidly, whereas the others could persist for an extended period of time in their present condition.

CAUSES OF ISLAND ELIMINATION

Osterkamp [1998] described several scenarios in which islands could disappear. Perimeter sediment deposition could eliminate an island by several methods. The first method is by preferential in-filling of one of the side channels that effectively raises the bed level in one anabranch but not the other, and thereby shifts the flow into a single path. The second method is by sedimentation around the whole perimeter of the island until it eventually coalesces with other nearby islands or the floodplain, again forcing the flow into a single path. A third method of island elimination is by the flow preferentially incising one of the side channels and leaving the other anabranch 'high and dry'. This is common downstream of dams after peak flows have been reduced. If a low flow regime persists for long enough, vegetation may accumulate between an island and its floodplain. The meandering nature of a river can cause it to laterally migrate and abandon one of the anabranches around an island. Floods can eliminate an island by two methods. The first is by simply increasing the flows to levels high enough that the entire island is eroded away. The second is by changing the main direction of the flow during a flood, thereby altering the angle of attack from the water and gradually wearing away the island by abrasion.

RIVER CLASSIFICATION METHODS

The variable interactions of channel flow and erodible boundaries can produce a wide spectrum of channel forms. Several researchers through the years have attempted to impose some sort of order on this diversity by proposing channel classification schemes. One of the earliest was that of Davis [1899] who distinguished rivers by their age – *youthful*, *mature*, or *old* – according to the stage of development within the cycle of erosion they were in. However, hydrologists found that the age of a channel is difficult to determine. Other researchers have attempted to create a classification scheme based on more readily identifiable properties, such bed material, channel slope, or mean discharge. Schumm [1963] based his classification scheme on the expected dominant mode of sediment transport in the channel, using the percent of silt/clay present in the bed material as the distinguishing criteria – *bed-load channel* ($\% \leq 5$); *mixed-load channel* ($5 < \% < 20$); and *suspended load (or wash load) channel* ($\% \geq 20$). Schumm furthered categorized the channels by their apparent stability – *stable*, *eroding*, or *depositing*. This scheme has been built upon and altered by other hydrologists because most natural channels do not easily fit into these categories, nor does the percent of silt/clay in the bed material necessarily equate to the transport mode of the channel. For a bed material-based classification scheme, simpler distinctions have been used [Knighton, 1998] – *cohesive*, which is separated into either bedrock or silt/clay; and *non-cohesive*, which is separated into sand, gravel, or boulder bed channels. Most natural channels are in the sand or gravel categories [Knighton, 1998].

A river classification devised by Kellerhals et al. [1976] is the only one I have found in the literature that specifically incorporates islands into its scheme. Figure 3-9 shows the island characteristics section of their more detailed river classification scheme. The authors codify islands for their proximity to other islands as (1) *occasional* – no overlapping of islands (i.e. not on the same cross-section) with an average spacing greater than ten river widths, (2) *frequent* – infrequent overlapping with average spacing less than ten river widths, (3) *split* – frequent or continuous overlapping, creating two or three flow paths, and (4) *braided* – many channels divided by islands and bars, which may be washed out in high flows.

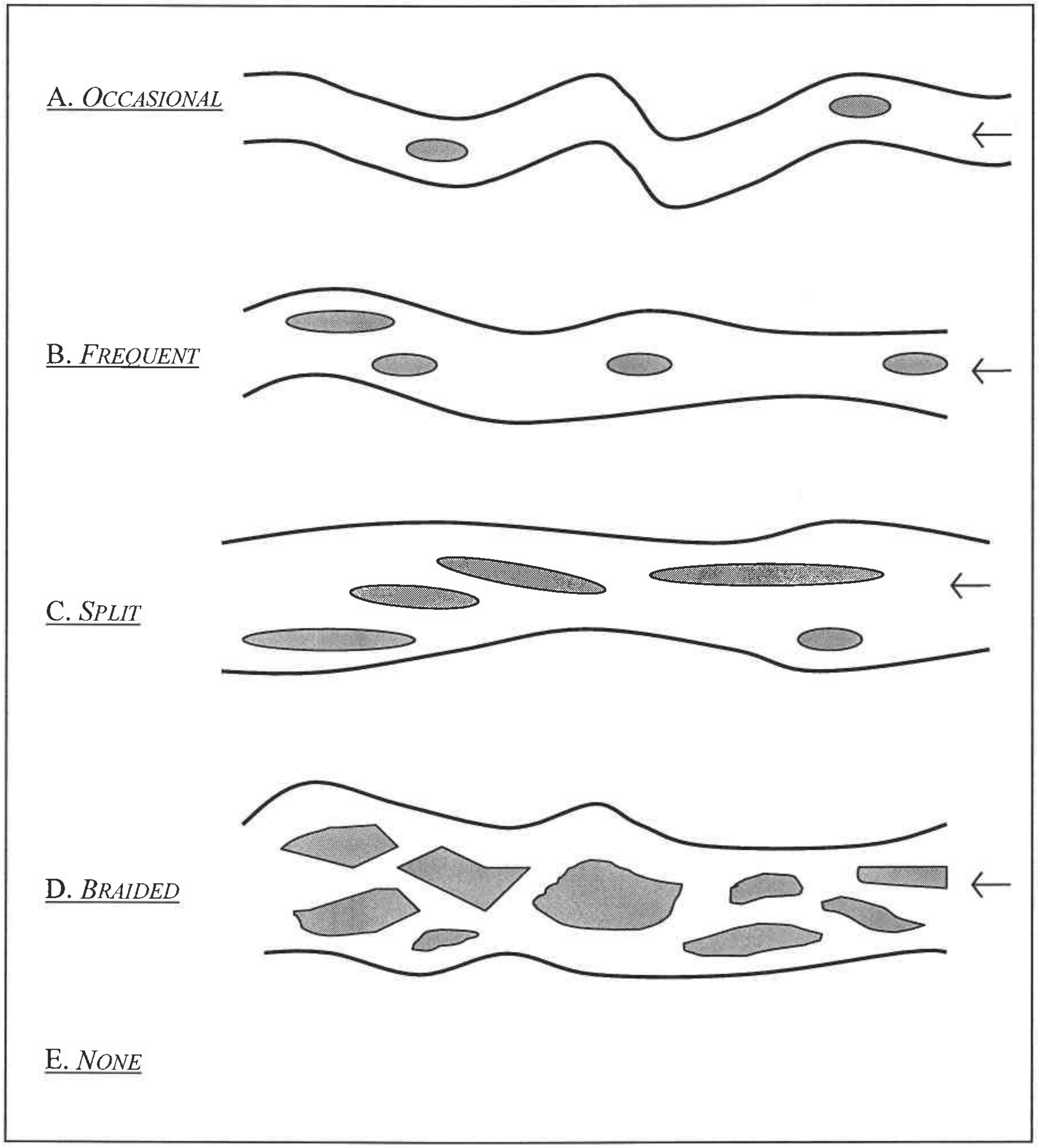

Figure 3-9. Codification of fluvial islands in relation to their proximity to other fluvial islands. Modified from Kellerhals et al. [1976].

The most detailed channel classification scheme to date is that proposed by Rosgen [1994, 1996]. It has been widely used by geomorphologists and hydrologists. Rosgen's scheme describes 41 separate channel types based on combinations of bed material, entrenchment ratio (valley width/channel width), sinuosity, width/depth ratio, and channel slope. To facilitate the use of his scheme, Rosgen designed a table to describe the geomorphic characteristics of streams (Table 3-1).

Table 3-1. Detailed stream classification method. Modified from Rosgen [1996].

Stream Type	Meander width ratio	Entrenchment Ratio	Width/Depth Ratio	Sinuosity	Slope
Aa+	1 to 3	< 1.4	< 12	1.0 to 1.1	> 0.10
Geomorphic Description	Laterally contained, very steep & entrenched, low W/D ratio. Step-Pool morphology with chutes, debris flows, and waterfalls. These channels tend to occur in debris avalanche-prone areas, deep depositional areas such as glacial tills or outwash terraces, or structurally-controlled landforms such as faults or joints. Usually very high stream energy and sediment supply. Usually associated with bedrock or zones of deep deposition and/or deeply incised residual soils.				
A	1 to 3	< 1.4	< 12	1.0 to 1.2	0.04 to 0.10
Geomorphic Description	Similar valley forms and bedforms to Type Aa+. Less steep than Aa+. High sediment transport potential.				
B	2 to 8	1.4 to 2.2	> 12	> 1.4	0.02 to 0.039
Geomorphic Description	Occur in narrow, moderately-sloped basins. Can be influenced by structural contact zones such as faults, joints, colluvial-alluvial deposits. Valley side slopes usually structurally controlled. The narrow valleys limit the development of a wide floodplain. Channels are usually moderately entrenched, and exhibit a high W/D ratio with a low sinuosity. Bed morphology influenced by debris constraints and local confinements that create scour holes and rapids. Relatively low bank erosion.				
C	4 to 20	> 2.2	> 12	> 1.4	< 0.02
Geomorphic Description	Valleys usually occur in alluvial deposits and have well-developed floodplains. Channels usually exhibit low gradients, high W/D ratios, and high sinuosities. Bed morphology consists of pool/riffle sequences. Point bars common within the active channel.				
D	1 to 2	n/a	> 40	n/a	< 0.04
Geomorphic Description	Braided streams with high W/D ratios. Typically found in depositional fans, glacial outwash, and deltas. Usually not deeply incised, but can be laterally confined within narrow valleys. Tend to exhibit high bank erosion rates and low meander width ratios. Unlimited sediment supply, generally fines. Bed features result from convergence/divergence processes of local bed scour and sediment deposition. Channel populated with bars or unvegetated islands that frequently shift positions.				
DA	1 to 2	> 2.2	Wide range	Wide range	< 0.005
Geomorphic Description	Anastomized channels with very low gradient. Banks often consist of fine-grained, cohesive materials and densely vegetated, which lead to high stability. Very low lateral migration rates, with infrequent avulsions. Bed morphology usually riffle/pool sequence. Low bedload contribution to total sediment load. Islands generally very stable and therefore vegetated.				
E	20 to 40	> 2.2	< 12	> 1.5	< 0.02
Geomorphic Description	These types of channels generally represent the 'end-point' of channel stability and fluvial process efficiency for alluvial streams in a naturally dynamic sequence of system evolution. Often develop within the wide, meandering Type F channels following floodplain development and vegetation recovery. Very high sinuosity with low W/D ratio. High-frequency riffle/pool formations. Highly stable channels, but can be sensitive to disturbance.				
F	2 to 10	< 1.4	> 12	> 1.4	< 0.02
Geomorphic Description	The classic entrenched, meandering channel. Typically deeply incised within a low-gradient valley. Banks composed of highly erodible material. Riffle/pool morphology. High lateral extension rates. High sediment supply and storage, exemplified by the significant bar deposition.				
G	2 to 8	< 1.4	< 12	> 1.2	0.02 to 0.039
Geomorphic Description	"Gully" type streams. Entrenched, narrow, deep, step-pool channels. Exhibit low to moderate sinuosity with high bank erosion rates and sediment supply. Moderate to steep slopes and low W/D ratios. High bedload and suspended loads. Occur in a variety of landscapes.				

A detailed hierarchical classification system, such as Rosgen's, allows for other stream classification variables, e.g., fishery or riparian ecology, to be incorporated and helps determine the potential of a given river. Another advantage of Rosgen's classification scheme is that it provides the necessary context for linking the driving forces and the response variables at all scales. Rosgen's objectives for developing such as detailed hierarchy are (1) to predict a river's behavior simply from observation, (2) to further develop the hydraulic and sediment relationships for any type of stream, (3) to provide a system by which unknown streams can be described using characteristics from other similar stream reaches, and (4) to provide a consistent vocabulary for all hydrologic disciplines to discuss stream morphology [Rosgen, 1996].

Rosgen's stream classification scheme does not specifically include islands in its descriptions. However, with some knowledge of the stream processes that are involved in each type of Rosgen's streams and the processes involved with forming each type of fluvial island, a relationship between island type and stream classification can be created (Table 3-2). Table 3-3 shows that each main Rosgen category is capable of providing a setting for one or more Osterkamp island types. Furthermore, most Osterkamp island types appear to fit the Rosgen C, E, F, and G categories. These categories represent sinuous-to-meandering streams that may have wide floodplains or entrenched streams with sufficient channel width for bars and islands to occur.

Table 3-2. Basic comparison of fluvial island type and stream classification. (descriptions based on Osterkamp [1998] and Rosgen [1994])

Island Type	**Stream Classification**
Avulsion (Av)	C, E, F
Gradual Erosion (GE)	C, D/DA, E, F, G
Lateral Shifts (LS)	C, D/DA, E, F, G
Bar/Riffle Stabilization (BS)	C, D
Structural (St)	A, B, G
Flood Deposits (FD)	C, E, F
Lee Deposits (LD)	Bedrock: A,B,C,G Wood: D,E, F
Mass Movement (MM)	A, B, G
Reservoir (Rs)	C, F

Table 3-3. Expanded matrix of the types of fluvial islands that would occur in a given type of stream. (descriptions based on Osterkamp [1998] and Rosgen [1994])

		Stream Classification						
		A/Aa+	B	C	D/DA	E	F	G
Island Type	Av			X		X	X	
	GE			X	X	X	X	X
	LS			X	X	X	X	X
	BS			X	X			
	St	X	X					X
	FD			X		X	X	
	LD	X	X	X	X	X	X	X
	MM	X	X					X
	Rs			X			X	

Proposed Island Classification Scheme

In developing an island classification scheme, the objectives here are similar to those of Rosgen. By observing the islands' characteristics, inductive generalizations may be made about the river's hydrologic and ecologic potential. In the river hierarchy, the distinguishing variables Rosgen chose to describe the streams were characteristics that could easily be discerned from their appearances, i.e. field determinable. A similar approach is sought for island classification.

The distinguishing characteristics of any island can be sorted into three basic categories: (1) those that can be measured from a topographic map or an aerial photograph, (2) those that can be measured *in situ* at the island, and (3) those that can be inferred from either a known history of the island or from the other characteristics of the island.

The characteristics of islands that can be determined from a planview map or aerial photography include: (1) the location of the island with respect to the thalweg, (2) the hydrodynamic shape of the island, (3) the width of the island relative to the flow width, and (4) the abundance of islands in the system. The location of the island in the river can be separated into either (a) in or near the main thread of the flow or (b) away from the main flow. From the island's location, the formation process can usually be inferred.

The hydrodynamic shape of the island refers to its subaerial planform shape. Islands are known to have various shapes, and these shapes can be categorized as either (a) irregular, (b) angular, or (c) streamlined (Table 3-4). The shape of an island may be influenced by its age (see Chapter 7), since islands that have experienced more eroding flows may be more streamlined in shape. The type of island could also be inferred from the shape; for example, bar-stabilization or lee-deposition islands will tend to be streamlined whereas lateral-shift or mass-movement islands will tend to be irregularly shaped. The relative width of the island is the ratio of the island's maximum width to the combined width of the flanking flow channels (Figure 3-10). Islands can be distinguished as (a) wide, having a ratio greater than 1.5, (b) equal, having a ratio between 0.5 and 1.5, and (c) narrow, having a ratio less than 0.5. The abundance of islands is based on Kellerhals et al.'s [1976] classification (Figure 3-9) and similar descriptive terms will be used here.

Table 3-4. Common shapes of fluvial islands and their classifications.

Shape Category	Shape name	Planform Shape
Streamlined	Lemniscate (upstream or downstream)	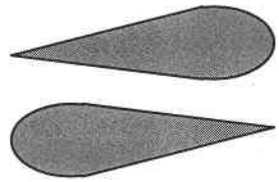
	Elliptical	
	Lenticular	
	Semi-circular or Hemispherical	
Angular	Triangular	
	Rhombic	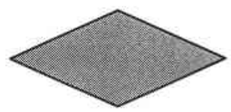
Irregular		

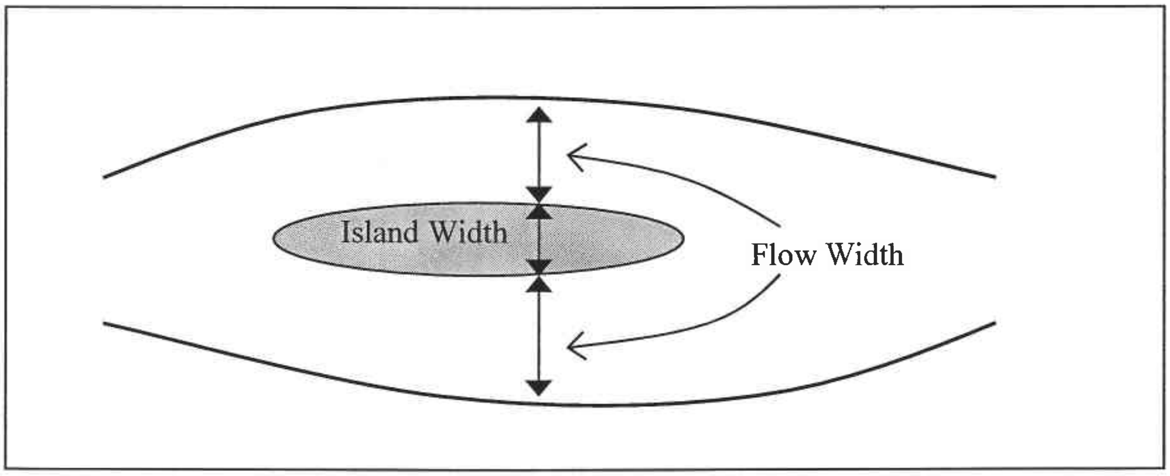

Figure 3-10. Ratio of island width to flow width to determine relative width of island for use in the classification of the island type.

Other useful island characteristics may require *in situ* examination. These include: (1) the evolutionary status of the vegetation on the island, (2) the composition of the sediment, and (3) the likely origin of the sediment. The vegetation on an island can help determine the age of the island, as well as how often it becomes inundated. The vegetation can be categorized as (a) mature/mixed, which means that the island surface has been exposed long enough to accommodate older-growth vegetation, (b) pioneer, which would indicate a young island or one that has recently been scoured by a flood, and (c) none, which could indicate that the island is too young to have recruited vegetation yet, or that it is too rocky to accommodate any vegetation. The sediment composition is categorized as predominately (a) bedrock, (b) boulder/cobble, (c) gravel, (d) sand/silt, or (e) cohesive material. The origin of the sediment can help infer the formation process of the island, and is categorized as (a) in-channel, (b) floodplain, or (c) non-alluvial. Non-alluvial sediment sources include landslides off the valley slopes as well as intrusive bedrock outcrops. An island composed of particles different than the surrounding channel would tend to be created allocthonously (e.g., from a debris flow or a bank slump). If an island's sediment type and size distribution are equivalent to those in the channel, then one could extrapolate that the island was formed in-channel.

Other distinguishing characteristics of an island which can not be directly measured without knowledge of the island's history can be inferred from what is known of the river and from the measurable characteristics. These include: (1) the formation process, (2) the age of the island, (3) the types of changes that are occurring to the island, (4) the factors causing the changes, (5) how much the island could be changed, and (6) the likely persistence of the island. The formation process is separated into two general categories: islands that are formed fluvially or islands that are isolated from the surrounding floodplain. The age of an island is categorized as (a) ancient, older than 100 years, (b) mature, between 15 and 100 years old, or (c) recent, younger than about 10 years. The types of changes occurring at the island are (a) accretion, (b) erosion, or (c) none (i.e., stable). The factors that would cause a change in the island area are categorized as (a) realignment in the flow of the river, (b) incision within the channel, (c) aggradation within the channel, (d) erosion by floods, or (e) none, which would refer to a stable island. How much the island could change in area or shape depends on a combination of its sediment composition and the river's hydrograph. This characteristic is categorized as either (a) stable, meaning it experiences no significant changes, or (b) changeable. The persistence of an island refers to the likelihood that the island will remain as an island in the future, and is characterized as either (a) long-term, (b) intermediate, or (c) short-term. Causes of island elimination have been previously discussed in this chapter. The likely persistence of the island is also related to several other categories, such as the type of vegetation, composition of the sediment, and the changes occurring in the system.

Once all the suitable characteristics are determined, a matrix of island classification can be created and used for other island type determinations. Table 3-5 shows which characteristics are generally expected for each type of island.

Figure 3-11 is a convenient method of tabulating the characteristics of the island of interest to use in conjunction with Table 3-5 to determine the island's classification. Figure 3-11 may be used to either (1) determine the expected characteristics of a given island type or (2) determine the island type from the noted characteristics.

The first method is to determine the island's characteristics if the type of island is already known. Figure 3-12 shows an example of an island that is known to have stabilized from an emergent bar. The directly measurable characteristics (such as location in river, shape, abundance of other islands, relative width, age of vegetation, and composition and origin of the sediment) are then highlighted. The inferable characteristics (such as formation process, age of island, changes, factors for changes, erodibility, and persistence) can then be determined by cross-referencing with Table 3-5.

The second method is to determine the type of island from the measured characteristics. Figure 3-13 shows an example of an unknown type of island that is known to have the characteristics highlighted in the figure. After the known characteristics are recorded, you can use Table 3-5 to determine which type of island could have that set of characteristics. Once the island type is known, the other characteristics can be inferred using the example shown in Figure 3-12 and the classification may be determined.

Table 3-5. Major components of proposed island classification matrix based on physical characteristics of islands.

Island Characteristics	Island Type	Avulsion	Gradual Erosion	Lateral Shifts	Bar/Riffle Stabilization	Structural	Flood Deposits	Lee Deposits	Mass Movement	Reservoir
Location with respect to Thalweg	Away from main flow	X		X					X	X
	In or near main flow		X		X	X	X	X		
Formation Process	Floodplain isolation	X				X				X
	Fluvial		X	X	X		X	X		
Hydrodynamic Shape	Irregular	X	X	X		X	X		X	X
	Angular	X		X					X	
	Streamlined		X		X		X	X		
Abundance of Islands in System	Occasional	X	X	X	X	X	X	X	X	X
	Frequent	?	X	X	X	X	X	X		
	Split			X	X	?				
	Braided			X	X					
Relative Width	Wide	X		X	X		X			
	Equal	X	X	X	X	?	X			
	Narrow		X	X	X	X	X	X	X	X
Age of Island	Ancient		X			X	X		X	
	Mature	X	X		X		X	X	X	X
	Recent	X		X	X		X	X	X	X
Evolutionary Status of Vegetation	Mature-Mixed	X	X	X	X	?	?			X
	Pioneer			X	X		X	X	?	
	None		X			X	X	X	X	X
Sediment Composition	Bedrock					X				X
	Boulder/ Cobble		X	?	X		X	?	X	
	Gravel	X	X	X	X		X	X	X	
	Sand/ Silt	X	X	X	X		X	X		
	Cohesive			X				X		
Sediment Origin	In-Channel		X	X	X		X	X		
	Floodplain	X		X						?
	Non-alluvial					X			X	X
Changes	Stable		X			X	X		X	X
	Accreting		X	X	X			X		
	Eroding	X	X	X			?	X	X	
Factors for Changes	None		X			X	X		X	X
	River flow Realignment	X		X				X	X	
	Channel Incision	X	X				X	X	X	
	Channel Aggradation			X	X			X		
	Flood Erosion	X			X		X	X	X	
Erodibility of Island	Stable	X	X			X	X		X	X
	Changeable	X	X	X	X			X		
Persistence	Long-term		X			X	X		X	X
	Intermediate	X	X		X		X	X	X	
	Short-term	X		X	X			X		

Island Type	Location with respect to thalweg	Formation Process	Hydrodynamic Shape	Abundance of islands in system	Relative Width	Age of Island	Evolutionary Status of Vegetation	Earth Material Composition	Earth Material Origin	Changes	Factors for Change	Erodibility of Island	Persistence	Island Type
Av	Away from main flow	Flood-plain isolation	Irregular	Occasional	Wide	Ancient	Mature/ Mixed	Bedrock	Channel	Stable	None	Stable	Long-term	Av
GE	In or near main flow	Fluvial	Angular	Frequent	Equal	Mature	Pioneer	Boulder/ Cobble	Flood-plain	Accreting	River flow realignment	Changeable	Intermediate	GE
LS			Stream-lined	Split	Narrow	Recent	None	Gravel	Non-alluvial	Eroding	Channel Incision		Short-term	LS
BS				Braided				Sand/ Silt			Channel Aggradation			BS
St								Cohesive			Flood Erosion			St
FD														FD
LD														LD
MM														MM
Rs														Rs

Figure 3-11. Proposed island classification scheme arranged for application to island analysis. Abbreviations used in the Island Type column are explained in Table 3-2.

Island Type	Location with respect to thalweg	Formation Process	Hydrodynamic Shape	Abundance of islands in system	Relative Width	Age of Island	Evolutionary Status of Vegetation	Earth Material Composition	Earth Material Origin	Changes	Factors for Change	Erodibility of Island	Persistence	Island Type
Av				**Occasional**				Bedrock			None			Av
GE	Away from main flow	Flood-plain isolation	Irregular		Wide	Ancient	Mature/ Mixed		**Channel**	Stable			Long-term	GE
LS				Frequent				Boulder/ Cobble			River flow realignment	Stable		LS
BS											Channel Incision			BS
St			Angular		**Equal**	Mature	**Pioneer**		Flood-plain	**Accreting**			**Intermediate**	St
FD				Split				Gravel			**Channel Aggradation**			FD
LD	**In or near main flow**	**Fluvial**						**Sand/ Silt**				**Changeable**		LD
MM			**Stream-lined**	Braided	Narrow	**Recent**	None		Non-alluvial	Eroding	Flood Erosion		**Short-term**	MM
Rs								Cohesive						Rs

Figure 3-12. Island classification scheme application, Example A: Determination of island classification components and physical characteristics when island type is known (in this example, the island is known to have stabilized from an emergent bar). Abbreviations used in the Island Type column are explained in Table 3-2.

Island Type	Location with respect to thalweg	Formation Process	Hydrodynamic Shape	Abundance of islands in system	Relative Width	Age of Island	Evolutionary Status of Vegetation	Earth Material Composition	Earth Material Origin	Changes	Factors for Change	Erodibility of Island	Persistence	Island Type
Av				**Occasional**				Bedrock			None			**Av**
GE	**Away from main flow**	Flood-plain isolation	**Irregular**		Wide	Ancient	**Mature/ Mixed**		Channel	Stable			Long-term	GE
LS				Frequent				Boulder/ Cobble			River flow realignment	Stable		LS
BS														BS
St			Angular	Split	**Equal**	Mature	Pioneer	**Gravel**	**Flood-plain**	Accreting	Channel Incision		Intermediate	St
FD											Channel Aggradation			FD
LD	In or near main flow	Fluvial										Changeable		LD
MM			Stream-lined	Braided	Narrow	Recent	None	Sand/ Silt	Non-alluvial	Eroding			Short-term	MM
Rs								Cohesive			Flood Erosion			Rs

Figure 3-13. Island classification scheme application, Example B: Determination of island type based on known or determinable physical properties. Abbreviations used in the Island Type column are explained in Table 3-2.

CHAPTER 4 – REVIEW OF APPLICABLE RIVER MECHANICS

Fluid flow through an open channel, and its resulting effects (i.e., flow resistance and sediment transport), are governed by three fundamental equations: those for the conservations of mass, momentum, and energy. Conservation of mass states that the mass (M) of a fluid within a closed system will remain constant over time (t), and may be shown numerically as:

$$\frac{dM}{dt} = \frac{d}{dt}\int_x\int_y\int_z \rho dxdydz \qquad (4\text{-}1)$$

For incompressible flow, the density, ρ, is constant. For open channel flow, control volumes with dimensions dx, dy, and dz are often used in analyses. With no flow across the side and bottom boundaries of the control volume, the equation can be applied to a selected length of channel and integrated between the two end cross-sections having areas A_1 and A_2, respectively, to give [e.g., Munson et al., 1990]:

$$Q = \int_{A_1} VdA = \int_{A_2} VdA \quad \rightarrow \quad Q = V_1A_1 = V_2A_2 \qquad (4\text{-}2)$$

Here, Q is the flow discharge and V_1 and V_2 are the mean flow velocities through cross-sections A_1 and A_2. This final form is commonly referred to as the Continuity Equation.

Conservation of Momentum is originally derived from Newton's 2nd Law of Motion to describe the motion of fluid through a control volume. By assuming constant density and viscosity and by integrating Newton's 2nd Law, the equation becomes a non-linear, second-order partial differential equation that has no exact solution [Munson et al., 1990] and was named after its original derivers, Navier-Stokes. As complicated as the Navier-Stokes solution may be, appropriate assumptions can be used to solve for local approximations. Applications of these solutions include Bernoulli's Equation and the analyses of hydraulic jumps.

Conservation of Energy is derived from the first law of thermodynamics, which states that the net energy of a control volume equals the increase of energy into the system plus the energy that leaves. For open channel flow, the energy of a control volume is the sum of its potential energy, kinetic energy, and pressure (or flow) energy. Energy losses (h_L) include losses due to boundary friction, expansions and contractions of the channel, and wake turbulence behind an obstacle in the streamflow. The conservation of energy between two cross-sections in open channel flow can be expressed as [e.g., Chanson, 1999]:

$$\frac{v_1^2}{2g} + z_1 + \frac{P_1}{\rho g} = \frac{v_2^2}{2g} + z_2 + \frac{P_2}{\rho g} + h_L \qquad (4\text{-}3)$$

where v, z, and P are the local fluid velocity, elevation, and pressure, respectively, and each term is expressed in units of length. Hydrostatic principles state that:

$$P = \rho g d \qquad (4\text{-}4)$$

where d is the flow depth. The elevations, z_1 and z_2, can be related to each other by the slope of the channel (S_o) and the distance between the two cross-sections (L). Equation 4-3 can be rewritten as:

$$\frac{v_1^2}{2g} + S_o L + d_1 = \frac{v_2^2}{2g} + d_2 + h_L \qquad (4\text{-}5)$$

If we can assume a relatively horizontal channel (i.e., $S_o \sim 0$) and negligible energy losses (i.e., $h_L = 0$, which is accurate for small distance, L), then we can simplify Equation 4-5 again:

$$\frac{v_1^2}{2g} + d_1 = \frac{v_2^2}{2g} + d_2 \qquad (4\text{-}6)$$

The specific energy (E) of a cross-section in open channel flow is defined as the sum of the flow depth and velocity head:

$$E = d + \frac{v^2}{2g} \qquad (4\text{-}7)$$

FLOW IN A STRAIGHT CHANNEL

Water flowing in an open channel is subject to two dominant forces: (1) gravity, the force driving the flow downslope; and (2) friction, the force opposing the downward flow. The balance of these forces determines the water's ability to erode and transport material. The shear stress, τ, is often used as an indicator of this ability. An expression for shear stress can be derived from a force balance in open-channel flow (Figure 4-1).

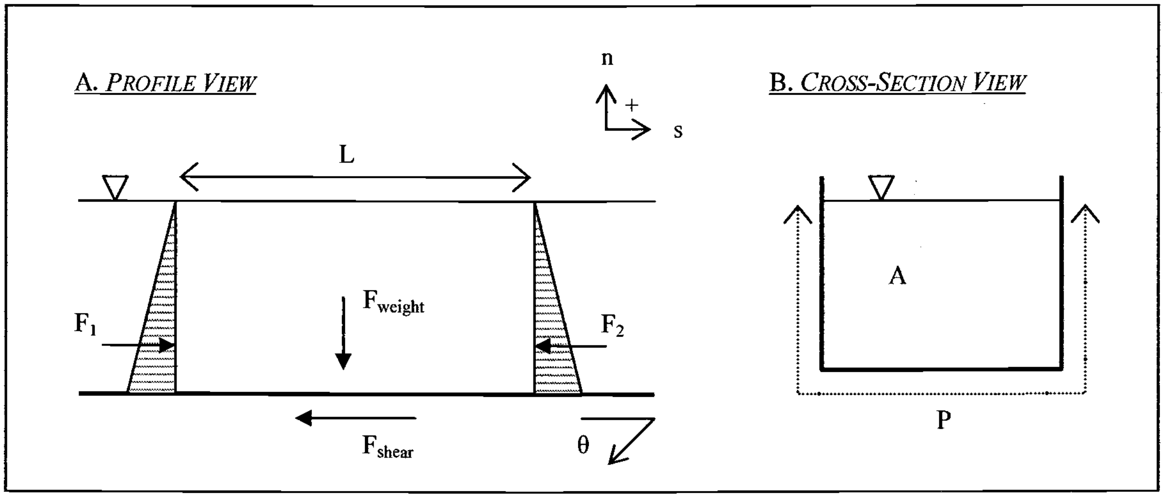

Figure 4-1. Forces associated with open-channel flow.

In Figure 4-1 and the following equations, F_{weight} is the force due to gravity of the volume of fluid, F_1 and F_2 are the hydrostatic forces on the upstream and downstream cross-sections, respectively, of the fluid volume, F_{shear} is the frictional shear force between the moving fluid and the channel boundary, L is the length of the fluid volume in the s-direction, θ is the angle from horizontal of the channel slope, A is the area of the fluid volume normal to the s-direction, and P is the wetted perimeter of the fluid volume.
Using Newton's 2nd Law of Motion,

$$\Sigma F = ma \tag{4-8}$$

the forces on a volume of water (Figure 4-1 A) can be summed in the s-direction:

$$\Sigma F_{s\text{-}dir} = F_1 - F_2 + F_{weight}\sin\theta - F_{shear} = \rho Q(V_2 - V_1) \tag{4-9}$$

If we assume the depths at cross-sections 1 and 2 are equal, then the hydrostatic forces, F_1 and F_2, must be equal and therefore cancel each other out. Equation (4-2) shows that V_1 and V_2 must also equal if the depths are equal, and therefore also cancel each other out. Equation (4-9) then simplifies to:

$$F_{shear} = F_{weight}\sin\theta \tag{4-10}$$

where

$$F_{shear} = (\text{average boundary shear stress})*(\text{surface area}) = \tau PL$$

$$F_{weight}\sin\theta = (\text{weight/unit volume})*(\text{volume})*(\text{direction component}) = \gamma AL\sin\theta$$

Therefore,

$$\tau PL = \gamma AL\sin\theta \quad (4\text{-}11)$$

Rearrange terms to solve for shear stress, τ:

$$\tau = \gamma\,(A/P)\,\sin\theta = \gamma\,R\,\sin\theta \quad (4\text{-}12)$$

where R is the hydraulic radius, equal to the ratio of cross-sectional area to the wetted perimeter. The dimensionless slope of the channel is represented as S_o, and for small channel slopes, $\sin\theta \sim \tan\theta \sim S_o$, therefore:

$$\tau = \gamma\,R\,S_o \quad (4\text{-}13)$$

Open channel flow can be classified based on four main criteria:

Velocity constant/variable with position	→	Uniform/Non-uniform
Velocity constant/variable with time	→	Steady/Unsteady
Reynold's Number < 500, > 2000	→	Laminar/Transitional/Turbulent
Froude Number < 1, = 1, > 1	→	Subcritical/Critical/Supercritical

Reynold's Number (Re) is a dimensionless ratio of the inertial forces and the viscous forces of the flow, and is generally represented as:

$$\mathrm{Re} = \frac{\rho VR}{\mu} \quad (4\text{-}14)$$

Here, ρ is the fluid density, μ is the fluid dynamic viscosity, V is the flow velocity, and R is the hydraulic radius of the channel. The Froude Number (Fr) is a dimensionless ratio of the inertial forces and gravitational forces, and is usually represented as:

$$Fr = \frac{V}{\sqrt{gy_h}} \quad (4\text{-}15)$$

Here, g is the acceleration due to gravity and y_h is a characteristic dimension of the channel equivalent to the mean flow depth in prismatic channels. The simplest form of open channel flow to model is a steady, uniform flow, but natural flow is usually unsteady, non-uniform, and turbulent.

Each of the above criteria depends on the flow velocity, and the flow velocity is strongly related to the flow resistance. Several equations have been developed to determine the relationship between flow resistance and velocity:

Chezy $\qquad V = C\,(RS_o)^{1/2} \qquad (4\text{-}16)$

Manning	$V = (k/n)\, R^{2/3} S_o^{1/2}$	(4-17)
Darcy-Weisbach	$V^2 = 8gRS_o / f$	(4-18)

V is the mean velocity, R is the hydraulic radius of the channel, S_o is the channel slope, g is the acceleration due to gravity, k is a constant dependent on the unit system used, and C, n, and f are the respective resistance coefficients. Each of these equations assumes steady, uniform flow.

Total flow resistance consists of: (1) boundary resistance, consisting of friction with bed material (grain roughness) and bed forms (form roughness); (2) channel resistance, due to bank irregularities and changes in channel alignment; and (3) free surface resistance, due to distortion of the water surface by waves and hydraulic jumps. The grain roughness is a function of the relative roughness of the bed material and is important for shallow flows or for gravel and cobble bed streams. As the flow depth increases, however, the relative effect of the grain roughness decreases and form roughness due to features developed in the bed material is generally dominant. This is particularly true for sand bed streams. The sequence of bed forms are correlated with the flow intensity (Table 4-1). Bed forms can be classified into either a lower or upper flow regime based on their shape, resistance to flow, and mode of sediment transport. In the lower regime, form roughness is dominant, whereas grain roughness is dominant for the upper regime (forms such as antidunes change rapidly through quick erosion and deposition).

Table 4-1. Bed forms and their associated flow regimes.

<table>
<tr><td>Ripples</td><td>Dunes with superimposed ripples</td><td>Dunes</td><td>Plane Bed</td><td>Antidunes with standing waves</td><td>Antidunes with breaking waves</td><td>Chute and pool</td></tr>
<tr><td colspan="3">Lower flow regime
(Subcritical Flow)</td><td colspan="4">Upper flow regime
(Supercritical Flow)</td></tr>
</table>

Dunes generally have the highest flow resistance of the bed forms, but as waves begin breaking over antidunes, the energy loss begins to increase and could have similar flow resistances as dunes. Most calculations tend to include all the applicable roughness factors, since the individual components are difficult to differentiate.

FLOW IN A CURVED CHANNEL

The pattern of the flow around a bend has three main components that are different from flow in a straight channel. These are: (1) superelevation of the water surface against the outer (concave) bank due to inertia of flow entering the bend (Figure 4-2b), (2) transverse secondary currents that are directed towards the outer bank at the surface and towards the inner bank at the bed level (Figure 4-2a), and (3) changing of the maximum velocity (i.e. thalweg) such that it moves from near the inner bank at the bend entrance to near the outer bank at the bend exit, crossing the channel at the zone of greatest curvature.

These effects reflect the interaction between the outwardly-acting centripetal force and the inward-acting pressure gradient force driven by the superelevation of the water surface. The combination of the transverse current and the main downstream-directed flow creates a helical or spiral motion to the flow (Figure 4-2). This helical flow pattern creates variations in boundary shear stress and velocity throughout the bend. The superelevation also gives rise to a locally steep downstream energy gradient and hence a zone of maximum shear stress close to the outer bank just beyond the bend apex.

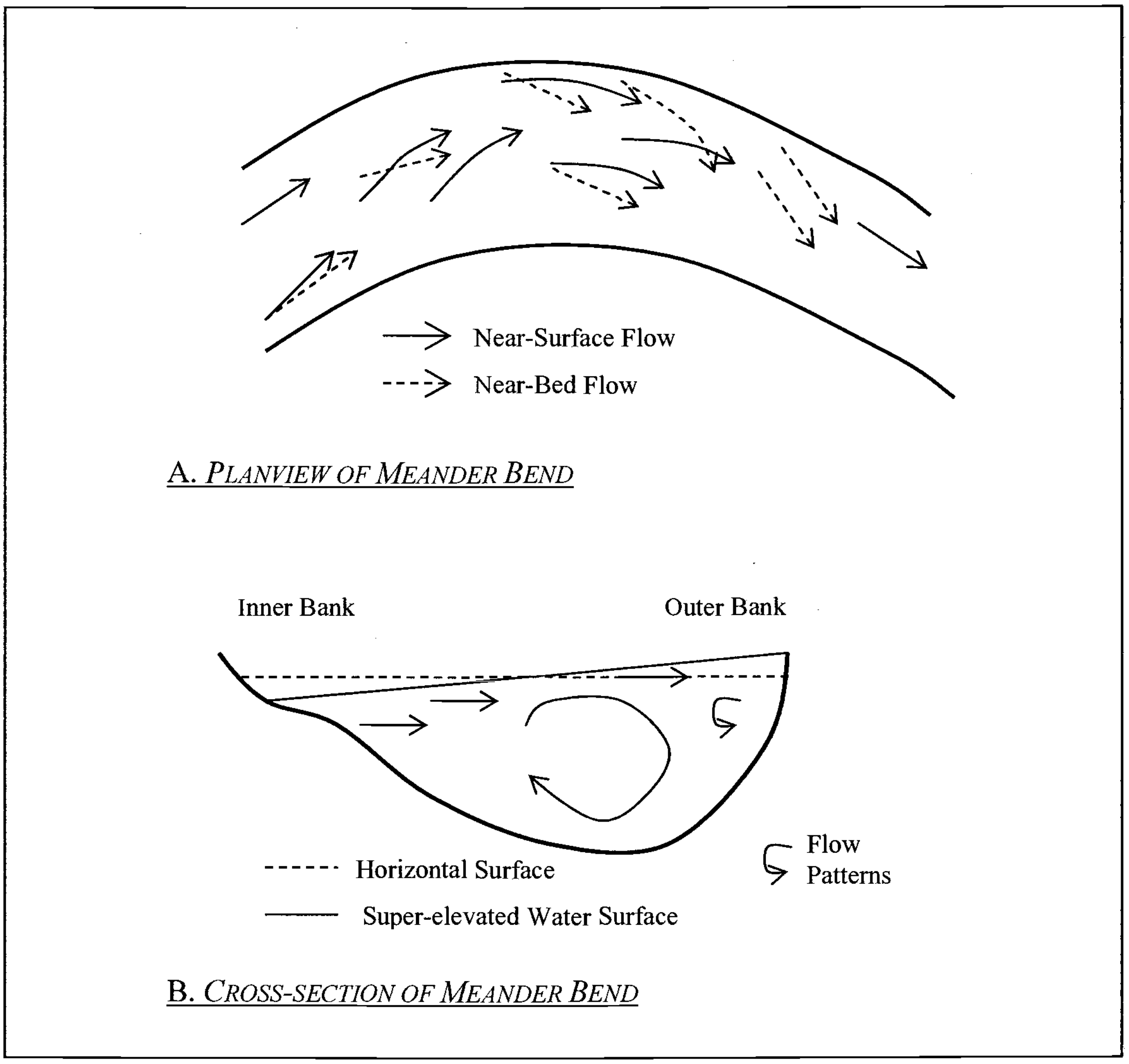

Figure 4-2. Secondary sub-surface currents associated with meander bends. Modified from Dietrich [1987].

Incipient Motion of Sediment Particles

Forces on individual particles

Most natural islands are accumulations of many small particles that are subjected to a drag force (F_d), buoyant force (F_b), lift force (F_L), gravitational force (F_g), and a resisting force (F_R) (Figure 4-3).

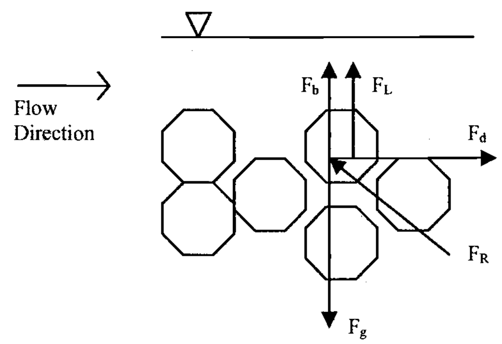

Figure 4-3. Schematic of forces acting on bed particles.

Drag force (F_d) is the net force in the direction of the flow due to the pressure forces and shear forces acting on the surface of the particle. If the distributions of pressure and shear stress are known, then the drag force can be determined analytically; however, these instances are rare. Most of the information known about drag force stems from numerous experiments in wind tunnels, water tunnels, etc. on scale models. These data have been compiled into a dimensionless form [e.g., Munson et al., 1990]:

$$F_d = 0.5 C_d \rho V^2 A \tag{4-19}$$

Here ρ is the fluid density, V is the fluid velocity, A is the cross-sectional area of the object normal to the flow direction, and C_d is a dimensionless drag coefficient that is usually empirically determined and can be a function of such parameters as: Reynold's Number, Mach Number, Froude Number, relative roughness of the object, and the shape of the object.

If we can assume the bed particles are spheres, then the drag coefficient on the particles is a function of the Reynold's Number (Re) of the flow. The drag coefficient can be represented by [Julien, 1995]:

$$C_D = \frac{24}{\mathrm{Re}} + \frac{2\pi He}{\mathrm{Re}^2} + 1.5 \tag{4-20}$$

where He is the Hedstrom number, a dimensionless ratio determined by [Julien, 1995]:

$$He = \frac{\rho_m {d_s}^2 \tau_y}{{\mu_m}^2} \tag{4-21}$$

The fluid mixture density, ρ_m, is related to increasing sediment concentration, C_V, by [Julien, 1995]:

$$\rho_m = \rho_w (1 + (SG_s - 1)C_V) \tag{4-22}$$

Here, ρ_w is the density of pure water and SG_s is the specific gravity of the sediment. The yield stress of the fluid, τ_y, can also be related to sediment concentration by the following equation [Julien, 1995]:

$$\tau_y = 0.1e^{13(C_V - 0.05)} \tag{4-23}$$

The dynamic viscosity, μ_m, similarly is dependent on the sediment concentration as shown by [Julien, 1995]:

$$\mu_m = \mu_w (1 + 2.5C_V + e^{23(C_V - 0.05)}) \tag{4-24}$$

Lift force is similar to drag force, but with a dimensionless lift coefficient (C_L) instead of C_d and it acts on the area parallel to the flow rather then perpendicular. As a first-order approximation, the lift force can be considered proportional to the drag force ($F_L \propto F_D$). Buoyant force is the product of the specific weight of the fluid (or fluid-sediment mixture) and the grain volume. Gravitational force is the product of the specific weight of the grain and its volume. The resisting force is the frictional forces between the grains that would prevent the particle from moving.

If we assume that the slopes of the water surface and bed surface in Figure 4-3 are approximately zero, then the gravitational force and buoyant force act opposite to each other, and can be combined into a submerged weight term, F_S, where

$$F_S = \frac{\pi}{6}(\gamma_s - \gamma_m)d_s^3 \tag{4-25}$$

Incipient Motion Approaches

Incipient motion is a difficult concept to define. Different investigators have used different distinctions in particle movement to define incipient motion, such as when the first particle moves; when several particles are moving; or when there is 'weak' or 'critical' movement [Yang, 1996]. Despite the vagueness of the definition of incipient motion, significant research has been done in this field.

Several researchers have approached the determination of incipient motion by using the bed shear stress, τ, as the dominant factor. White [1940] related the drag force on a particle of a determined size to the shear stress. Shields [1936] created his well-known diagram by relating two dimensionless parameters, a dimensionless shear stress and boundary Reynold's number, which are made up of the important factors in incipient motion. Vanoni [1977] then modified the Shields diagram to relate a dimensionless shear velocity and shear velocity Reynold's number.

The flow velocity has been a common parameter from which to determine incipient motion. Fortier and Scobey [1926] determined permissible velocities for flows of different sediment concentrations to transport particles of various diameters. Hjulstrom [1935] and ASCE related sediment size and average flow velocity to distinguish between erosion, transportation, and sedimentation conditions. Yang [1996] used a balance of velocity-based forces (Figure 4-3) on particles to determine the critical incipient motion velocity.

Other approaches include Meyer-Peter and Muller's [1948] method of relating the diameter of the particle moved to the flow depth, channel slope, and channel roughness. Mavis and Laushey [1948] related the movable sediment size to the competent bed velocity, which they equate to be 70% of the mean flow velocity. The U.S. Bureau of Reclamation (USBR) [1977] related critical shear stress to mean particle diameter.

STREAM POWER

A natural stream tends to move towards dynamic equilibrium by minimizing the rate of energy expenditure. One method of numerically representing this is with the concept of minimum stream power [e.g., Knighton, 1998; Yang, 1996]:

$$\Omega = \gamma Q S_0 = \gamma A V S_0 \tag{4-26}$$

Here, γ is the specific weight of water, Q is the stream discharge, S_o is the channel slope, A is the cross-sectional area, and V is the mean stream velocity. Stream power is defined as the rate of potential energy expenditure per unit length of channel (i.e., the rate of doing work). For a unit width of a wide channel, it can be approximated by:

$$\Omega/b = \gamma(A/b)VS_o \approx \gamma DVS_o = \tau V \tag{4-27}$$

where b is the channel width, and τ is the shear stress of the flow, calculated by γDS_o,. D is the mean flow depth, which can be used as a proxy for hydraulic radius, R, from Equation 4-13 for wide channels (i.e., b>>D). Several sediment transport methods utilize the concept of a minimum unit stream power, which is approximated as VS_o. Hooke [1986] found that mid-channel bars are generally not present in low gradient, straight alluvial sections of a river; therefore, there must be a relation to stream power and bar formation.

SEDIMENT LADEN FLOWS

Variation in flow processes are caused by variations in content and type of entrained sediment. There exists a continuum from low-concentration, clear-water flows to mudflows and dry sediment landslides. The physical properties of each type of flow are easily identifiable, but the defining boundaries between each are vague and often even variable due to sediment characteristics. In general, the continuum between clear-water flows and mudflows involve a transition from Newtonian to non-Newtonian flow behavior, from turbulent to laminar flow, and from a non-uniform to uniform sediment concentration profile [Julien, 1995]. Newtonian behavior is related to particle interactions and can be defined in terms of sediment concentration, but the sediment characteristics are important for determining the concentration limits. The flow regime transforms from turbulent to laminar as other internal forces become more dominant and most of the turbulent energy is consumed in keeping sediment particles suspended. This transition usually accompanies a transition from steady to unsteady flow as well. The sediment concentration profile is also related to the turbulent/laminar transition. Some researchers have shown that the effect on von Karman's constant, which is a function of depth-averaged concentration, particle fall velocities, and bed-shear velocities, can be used to quantify the non-uniformity of concentration profiles [e.g., Ippen, 1971; Wang, 1981], although this effect has been debated throughout the literature [Coleman, 1980; van Rijn, 1983].

CLEAR WATER FLOWS

Most floods in large channels are water floods, which may be regarded as clear-water flows because of the typically low sediment concentrations present. Such flows act like pure water in having a Newtonian behavior; they have viscosities that are constant for a specific temperature. Newtonian behavior is defined as exhibiting no yield strength and a linear relationship between shear strength, τ, and strain rate, dv/dy, with a slope equal to the dynamic viscosity, μ. In numerical form, this may be expressed as:

$$\tau = \mu \frac{dv}{dy} \tag{4-28}$$

where v is the mean velocity and y is the distance from the bed. This relationship best describes shear strength for laminar flow in a smooth-bottomed channel. Floods, however, are turbulent in behavior. For turbulent flow, the ratio of shear strength and strain rate is called 'eddy viscosity' and can be expressed as [Munson et al., 1990]:

$$\tau = \rho L_m \left(\frac{dv}{dy} \right)^2 \tag{4-29}$$

where ρ is the fluid density and L_m is the mixing length of turbulent fluid particles from velocity region to another region of different velocity.

As the sediment concentration increases, the shear strengths necessarily increase as well. Water flows carrying sediment have been shown, however, to sustain small shear strengths, up to 100 dynes/cm^2, and still exhibit Newtonian behavior for sediment concentrations up to 40% by weight (20% by volume) [Mingfu et al., 1983].

For water flows, sediment and water move as two separate phases. The sediment moves by suspension, rolling, or saltating along the bed. The dominant support mechanisms are electrostatic charges for slow water, and turbulence for faster waters. Physical characteristics of such water flows are a non-uniform sediment concentration profile, bulk densities less than 1.33 g/cm^3, viscosities less than 20 poises, and particle fall velocities greater than 33% of that for pure water fall velocities [Costa, 1988]. Standard hydraulic and sediment transport equations, such as Manning's or Einstein's, apply.

HYPERCONCENTRATED FLOWS

Beverage and Culbertson [1964] first defined hyperconcentrated flows (HCF) as those flows carrying a sediment concentration of between 40% and 70% by weight (20% to 47% by volume), with no mention of shear strength as a descriptor. As sediment concentration increases, particle fall velocity decreases, fluid density and viscosity increase, and the flow begins to exhibit small, measurable shear strengths. For HCF, those shear strengths are defined as between 100 and 400 dynes/cm^2 [Costa, 1988]. The shear strength depends on the sizes of the entrained particles. For silts, the flow acquires a measurable shear strength for concentrations of about 53 to 59%. For clays, the concentrations are about 23%. The fall velocities decrease to less than 33% of that for pure water fall velocities, and since fine sediments stay in suspension longer, sediment transport rates generally increase substantially. The sediments and water still flow as separate phases. Vertical fluctuations in turbulence tend to keep sediments in suspension by increasing the viscous drag on the particles, which tends to dampen the overall turbulence of the flow. The effects of buoyancy and dispersive stresses become more dominant in suspending sediments. Since most sediment transport equations are empirically based on pure water conditions (low sediment concentrations), they become less accurate for increasingly higher sediment laden flows [Costa, 1988]. Channel resistance has been shown to be about the same as clear-water values (see Chapter 5). HCF can be approximated as non-Newtonian flow; however, Newtonian behavior can be sustained up to a sediment concentration of 23% by weight for flows with neutrally-buoyant particles with low strain rates [Costa, 1988], and up to 58% by weight for more poorly sorted sediments [Lane, 1940].

DEBRIS FLOWS

Debris flows behave very differently from water flows or hyperconcentrated flows. The phases of sediment and water are indistinguishable as they move at the same velocity as a single visco-plastic unit. The sediment concentrations exceed 70% by weight (47% by volume) and the bulk densities exceed 1.8 g/cm^3 [Costa, 1988]. The shear stress is concentrated at thin boundary zones. There is a distinct yield strength, greater than 400 dynes/cm^2. The strain rate is not constant throughout the flow, and therefore debris flows are approximated as Bingham plastic flow (or viscoplastic flow). The shear strength now depends not only on the strain rate, but also on particle cohesive forces, c, and internal friction [Costa, 1988]:

$$\tau = c + \sigma \tan \alpha + \mu \frac{dv}{dy} \tag{4-30}$$

where σ is the normal stress and α is the angle of internal friction. Cohesion is controlled by the amount of clay present in the fluid. The influence of buoyant forces increases as they can now support 75 – 90% of the particle weight due to the diminished difference in particle and fluid densities. Dispersive stress, which results from the lift force produced by a transmittal of force by particle collision, also increases. Turbulence becomes even more dampened, giving the flow a laminar appearance. Whereas sediment transport in water and hyperconcentrated flows are dominated by turbulence, shear, lift, drag, and dispersive stress, sediment transport in debris flows are dominated by cohesion, buoyancy, grain interactions, structural support, and some turbulence.

COMPARISONS

Table 4-2 summarizes the physical properties of these three types of flows, as defined originally by Beverage and Culbertson [1964] based on sediment concentration distinctions.

Table 4-2. Comparison of characteristics of flows with varying sediment concentrations (modified from Costa [1988]).

Flow Type	Sediment Concentation	Bulk Density (g/cm^3)	Viscosity (poise)	Shear Strength ($dynes/cm^2$)	Sediment Support Mechanisms
Water	0 – 40% by wt. 0 – 20% by vol.	< 1.33	0.01 – 20	< 100	Electrostatic forces, turbulence
HCF	40 – 70% by wt. 20 – 47% by vol.	1.33 – 1.80	20 - ≥ 200	100 – 400	Buoyancy, Dispersive stress, turbulence
Debris	> 70% by wt. > 47% by vol.	> 1.80	>> 200	> 400	Cohesion, buoyancy, dispersive stress

Stream Pattern Continuum

The concept that a continuum exists for stream channel pattern was first set forth by Leopold and Wolman [1957]. Each pattern is composed of the same basic morphologic unit – the pool/riffle unit – just in different spatial arrangements [Knighton, 1998]. The channel pattern reflects the hydrodynamics, sediment transport processes and energy dissipation of the flow within the channel unit. The continuum is a response to the varying potential energy conditions. Although finer distinctions can be made, the general continuum of stream channel patterns runs from straight channels (low energy) to meandering channels (intermediate energy) to braided systems (high energy). The total available energy for the system is the dominant characteristic that determines which pattern will emerge (Figure 4-4). The classification of streams is often dependent on flow stage; e.g., a straight channel with a mid-channel bar may resemble a braided system at low flow. The use of the straight-meandering-braided classification system is convenient for predicting the hydrodynamic and sediment transport processes involved [Richards, 1982].

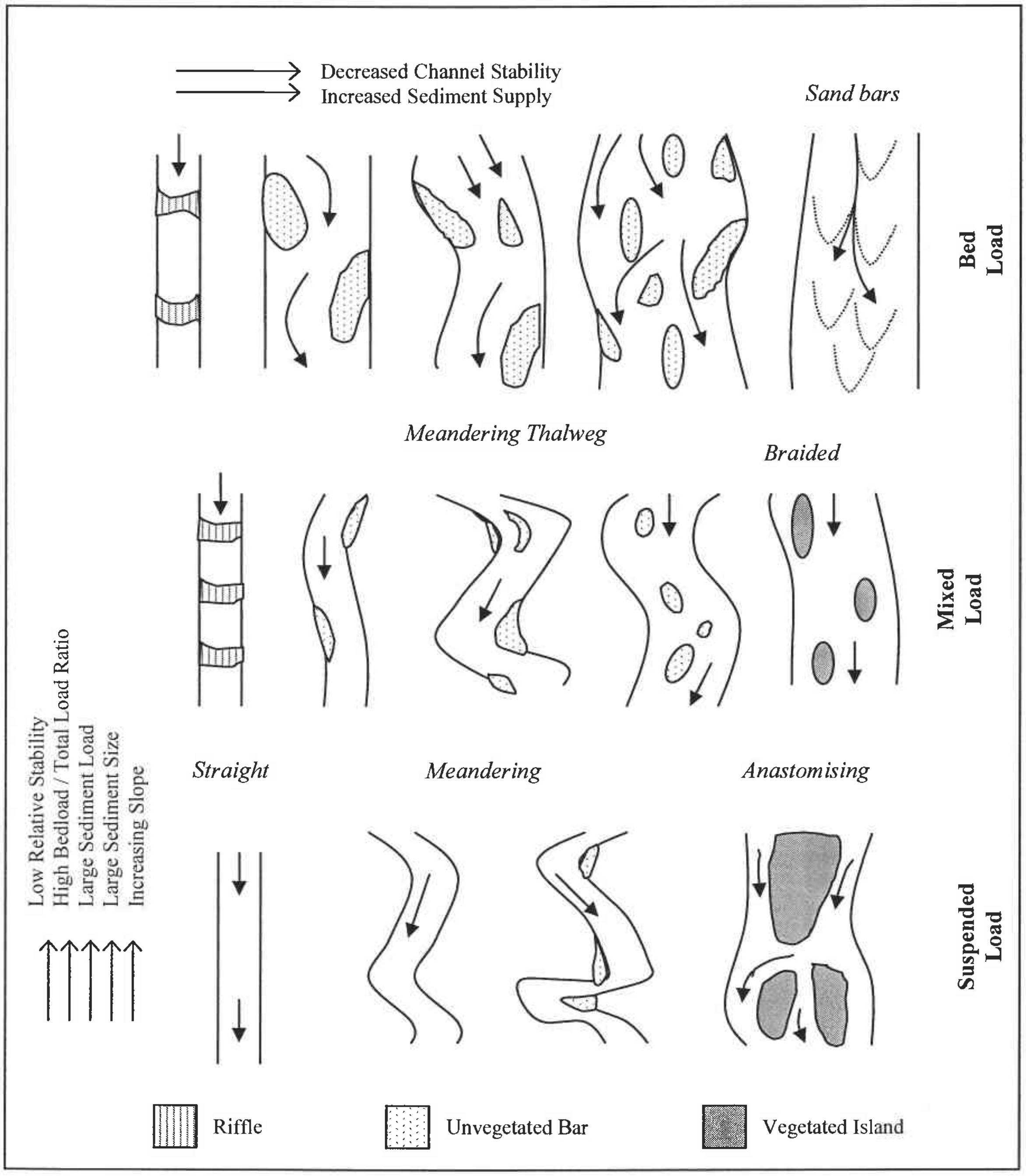

Figure 4-4. Classification of channel patterns. Modified from Schumm [1985].

Scour at Bridge Piers

Many island residuals in the Scablands or in Martian outflow channels exhibit a horseshoe-shaped scour pit at the upstream end [Baker, 1978a]. While these characteristics have been noted in various geomorphic studies, the calculations and predictions of such scour has been dominated by engineering fields in conjunction with the insertion of bridge piers into a stream.

The dominant features of flow patterns at a bridge pier include the downflow ahead of the pier, horseshoe vortex at the base of the pier, a surface roller ahead of the pier, and wake vortices downstream of the pier [Melville and Coleman, 2000]. The downflow is a result of flow deceleration of the flow ahead of the pier. Because streamflow velocities are greatest near the water surface and decrease toward the bed, the stagnation pressure is greatest near the surface and decreases downwards. The resulting downward pressure gradient on the pier face generates a downflow, which impinges on the bed as a vertical jet and erodes it to form a scour hole. The development of the scour hole creates a lee eddy (the horseshoe vortex). The downflow and vortex combine to scour the hole at the pier base. The wake vortices result from the flow separation around the pier.

The magnitude of the scour hole (i.e. the scour depth, D_s) is affected by many variables, such as shown in the computational equation [Melville and Coleman, 2000]:

$$D_s = K_{yb}K_IK_dK_sK_\theta K_GK_t \qquad (4\text{-}31)$$

Each term is described in detail in the following paragraphs.

K_{yb} is the effect of the flow shallowness and is related to the ratio of the flow depth, y, and the effective width of the pier, b. Depending on this ratio, the variable K_{yb} can be defined as [Melville and Coleman, 2000]:

$$2.4b \qquad \text{for } b/y < 0.7 \qquad (4\text{-}32a)$$

$$2*\mathrm{sqrt}(yb) \qquad \text{for } 0.7 < b/y < 5 \qquad (4\text{-}32b)$$

$$4.5y \qquad \text{for } b/y > 5 \qquad (4\text{-}32c)$$

As seen by the above equations, the scour depth is dependent only on the pier width for wide channels, but dependent only flow depth for wide pier intrusions.

K_I is the effect of the flow intensity and is related to the critical velocity for incipient bedload transport, V_c. For stream velocities less than the critical velocity, clear-water conditions exist. Live bed conditions prevail for velocities greater than the critical velocity, which means bedload transport occurs and the scour hole receives a continuous supply of sediment. The flow intensity variable is set to a value of 1.0 for clear-water conditions, but is otherwise equal to the ratio of stream velocity to critical velocity.

K_d is the sediment size factor. It may be calculated by [Melville and Coleman, 2000]:

$$0.57 \log (2.24\ B/d_{50}) \qquad \text{for } B/d_{50} \leq 25 \tag{4-33}$$

$$1.0 \qquad \text{for } B/d_{50} > 25$$

where B is the channel width and d_{50} is mean particle diameter.

K_s is the shape factor and K_θ is the pier alignment factor. These two are usually combined into one factor, values of which can be found in tables in the literature.

K_G is the approach channel geometry factor. Scour around piers is not affected by the upstream geometry, however. This factor is only used for scour near abutments; therefore this factor is set to a value of one.

K_t is the time factor. The scour hole depth will not remain constant over time and researchers have derived an empirical equation to determine this effect [Melville and Coleman, 2000]:

$$\exp \{-0.03\ [V_c/V \ln (t/t_e)]^{1.6}\} \tag{4-34a}$$

where t is the time of interest since installation and t_e is computed by:

$$48.26\ D/V\ (V/V_c - 0.4) \qquad \text{for } y/D > 6 \text{ and } V/V_c > 0.4 \tag{4-34b}$$

$$30.89\ D/V\ (V/V_c - 0.4)\ (y/D)^{0.25} \qquad \text{for } y/D < 6 \text{ and } V/V_c > 0.4 \tag{4-34c}$$

and D is the effective diameter of the pier.

CHAPTER 5 – INFLUENCE OF ISLANDS ON CHANNEL FLOW PROCESSES

Based on the concepts reviewed in the previous chapter, something can be said about how and why and island might form in a natural channel. This chapter will discuss island genesis as well as how islands affect the streamflow patterns and the flow energy.

BAR FORMATION AND ISLAND GENESIS

Bars are larger-scale features than the bedform classifications discussed in Table 4-1, having lengths on the order of the channel width or greater, and are generally classified based on their shape and position within the channel [Knighton, 1998]. Bars have heights comparable to the mean depth stage of the channel flow and are therefore usually exposed at low flow stages. The most common types of bars are: (1) point bars, which form on the inner bank of meander bends (Figure 5-1a); (2) alternate bars, which are distributed alternately along each bank due to the internal meander structure of the flow (Figure 5-1b); (3) tributary bars, which form at the junctions of a river and its tributaries due to a change in the sediment transport capabilities (Figure 5-1c); (4) transverse or diagonal bars, which form diagonal to the flow (Figure 5-1c); and (5) mid-channel bars, which form in the middle of the channel bisecting the flow around both sides (Figure 5-1e).

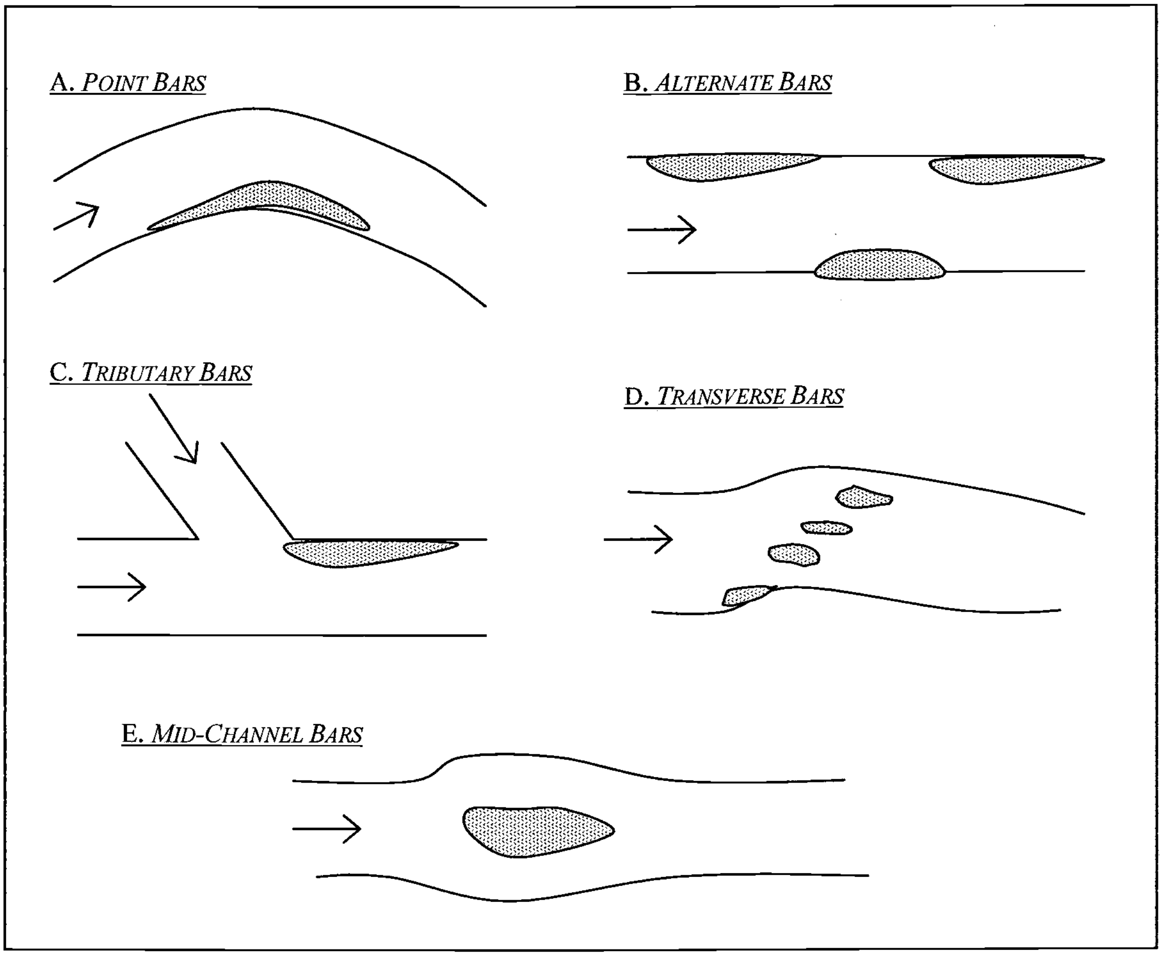

Figure 5-1. Classification of fluvial bars.

The types of bars I will discuss in this section are mid-channel bars, alternately known in the literature as braid, medial, longitudinal, crescentic bars, or sandflats. The differences between mid-channel bars and islands are that bars are unvegetated or have limited vegetation (pioneer species) and are submerged at bankfull flows, whereas islands are usually vegetated with advanced species composition and remain exposed at bankfull flows (bankfull flows having an estimated return frequency of about 1-2 years). Bars also exhibit some transience or instability, whereas islands are stable over longer time periods, although no objective definition of 'stable' can be found in the geomorphology literature. Simply put, though, islands are often considered to be 'permanent' features.

Hooke [1986] studied bar formation on the River Dane in England ($w=15m$, $Q_{bf}=30m^3/s$) and found that the dominant cause of bar formation was the rapid erosion of low-resistance banks in steep sections. Hooke [1986] also described several other formation processes, including: (1) an alteration in flow patterns and sediment loads at tributary junctions (isolated tributary bars, see Figure 5-1c); (2) lee deposition behind fallen trees; (3) chute formation as the river cut through a point bar; and (4) deposition due to low shear stress and diverging flow in a widened meander zone.

Bar formation is usually discussed in the literature in conjunction with initiation of braided rivers [e.g., Petts and Foster, 1985; Yalin, 1992; Bridge, 1993]. Yalin [1992] describes the development sequence for bars in the following manner. Consider an initially straight channel with a flat mobile bed as shown in Figure 5-2a. Some discontinuity at the upstream end of the section, either a change in the planform or in the slope, or an obstacle in the flowpath, causes converging turbulent flows. Further downstream, the maximum velocities will diverge from the centerline and sediment deposition will occur (Figure 5-2b).

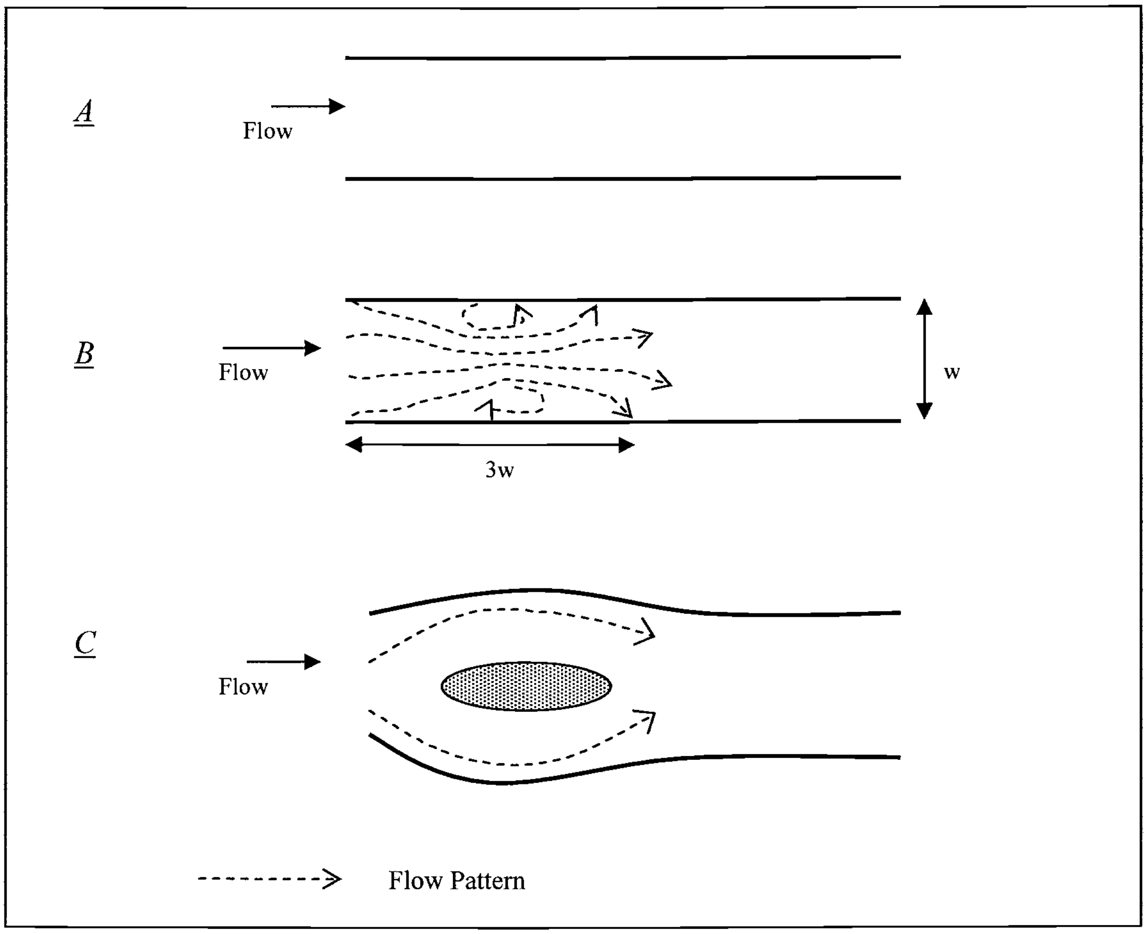

Figure 5-2. Possible mechanism for mid-channel island development, modified from Yalin [1992].

If the channels are rigid enough, then the flow sequence would create episodic bars, or scroll bars. If the banks are not rigid, then convective flow acceleration patterns will cause the sediment to converge towards the centerline. Downstream velocities at the centerline will decelerate, causing coarse sediment deposition, initiating a central bar. The initial shape is likely to be diamond, or rhombic, extending slightly downstream. As the bar grows, it may separate the water nearly equally into the flanking channels, which will deepen and laterally cut into the outer banks (Figure 5-2c). As deepening continues, the water level will lower, which will expose the emergent deposition as an island. Fine sediment will accumulate at the downstream end and small vegetation may appear on the exposed surface.

The widening of the channel around the island alters the plan geometry of the flow and alluvial formation. If the resulting flanking flows are unable to subsequently carry the sediment load, then similar erosion/deposition patterns will emerge downstream and braiding will occur. As non-overtopping flows persist, the island may stabilize by such processes as woody debris accumulation at its head or vegetation recruitment along the flanks. As the island persists, vegetation density will increase and the inherent meander structure in streams may cause the flow to preferentially divert to one side, thus attaching the bar to the floodplain. Hooke [1986] found the time scale for the full cycle of bar development and disappearance to be about 5 to 15 years on a medium-sized meandering river in western England.

Another developmental sequence of fluvial islands could stem from the initiation of river meanders (Figure 5-3). Several researchers have attempted to explain why an initially straight channel will develop into a meandering pattern [e.g., Richard, 1982; Carling, 1996]. The regularity of the natural bends suggests something other than random flow disturbances. Most explanations fall into two basic categories. The first type of explanation is that meanders are a result of the interaction of the flow and the mobile channel bed and that sediment transport is the dominant characteristic. The second type of explanation is that oscillations are inherent properties of turbulent flow. Secondary flow currents may develop as a result of vortices that are generated at the boundary walls. These vortices are due to inequalities in bank roughness along the channel, which can cause disturbances in the flow pattern and periodic reversals of the dominant flow cells, thereby resulting in a meandering thalweg with alternating bars.

Transverse bars and riffles can initiate and accelerate bank erosion in a straight channel by causing the thalweg to meander, thereby increasing sinuosity and point bar accretion. Braid development in sinuous flows require bank erosion, channel widening, and the formation of mid-channel bars [Petts and Foster, 1985].

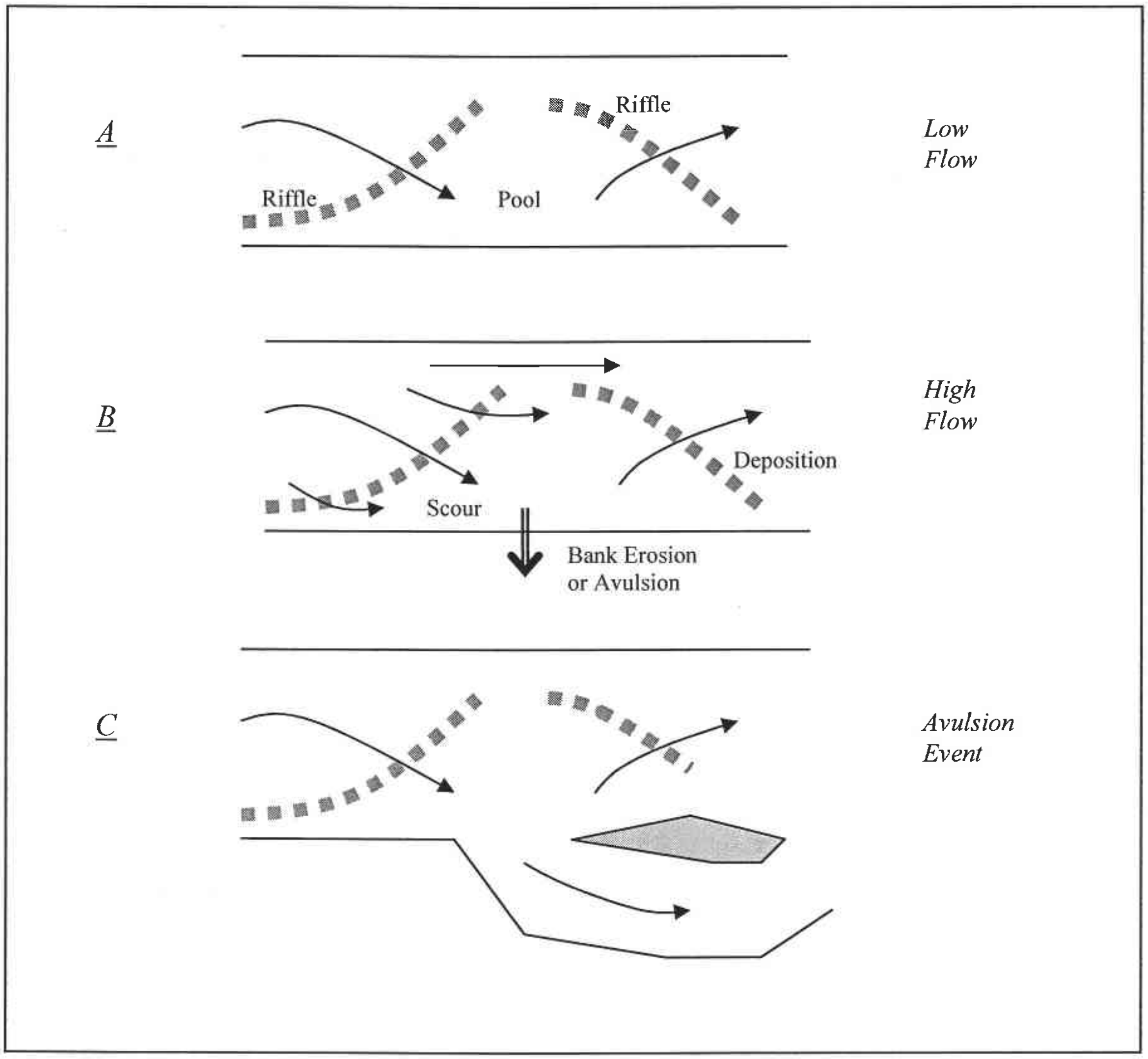

Figure 5-3. Natural river meander creating a fluvial island, modified from Petts and Foster [1985].

Flow Patterns around Islands

Flow in an individual curved branch around an island or bar can be regarded as similar to flow in a single-channel sinuous river [Bridge, 1993]. Curved flow around an island results in a transverse flow component of the water surface slope towards the inner convex bank, a helical flow pattern, and convective accelerations and decelerations of depth-averaged velocities (Figure 5-4). The spiral flow patterns arise because of an imbalance through the flow depth of curve-induced centrifugal forces and pressure gradients associated with transverse-sloping water surface. The convective patterns are associated with spatially-varying bed topography and channel curvature and, to some extent, spiral flow. These flow patterns combine to cause the maximum depth-averaged velocity to transgress from the inner, convex bank at the bend to the outer, concave bank with a progression around the bend. This pattern results in a net outward flow in the upstream segments of the bend and a net inward flow at the downstream segments.

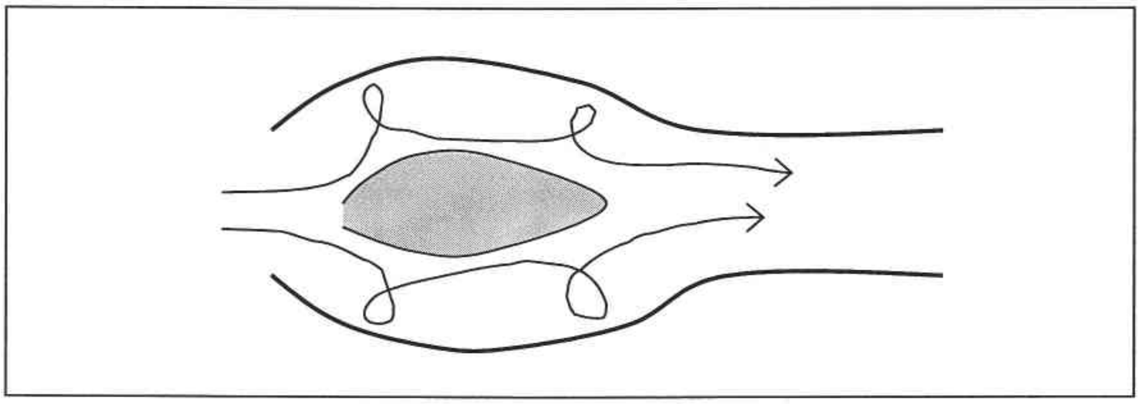

Figure 5-4. Flow pattern around a mid-channel island.

Bridge and Gabel [1992] determined the vertically-averaged velocity vectors associated with a mid-channel bar on the Calamus River in Nebraska (Figure 5-5). Their measurements, taken at high, low, and intermediate flow stages, show an outward bending of the flow field near the upstream section of the bar, and a convergence of flow at the downstream end. The furthest upstream transect experiences flow divergence as well, showing the influence of the submerged nose of the bar.

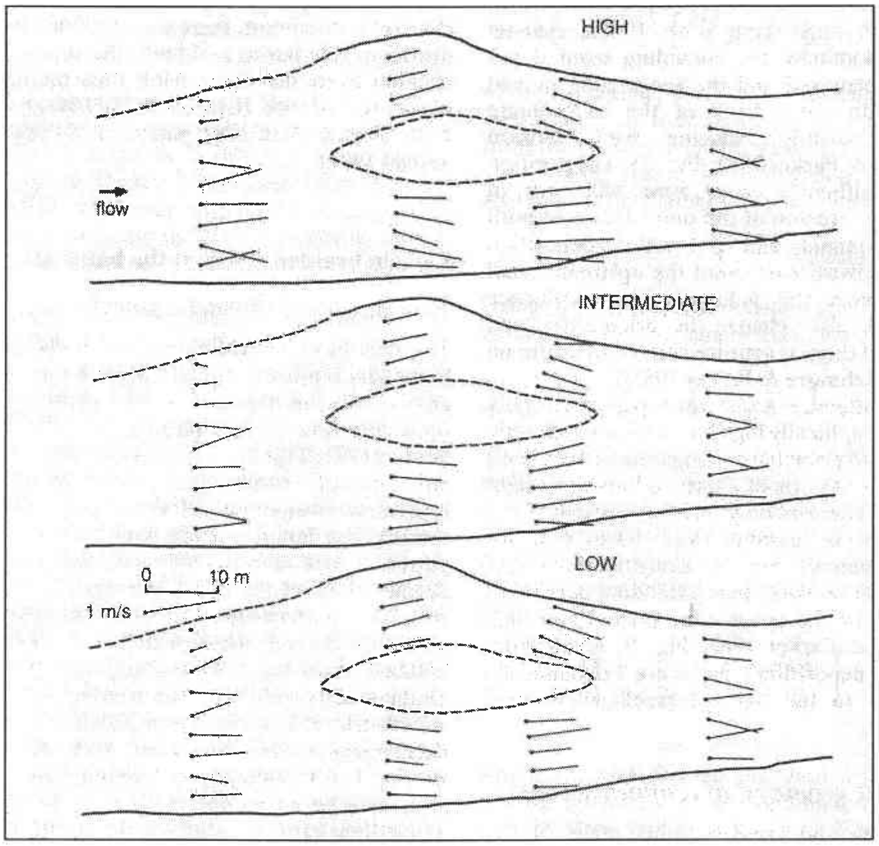

Figure 5-5. Depth-averaged velocity vectors near a mid-channel bar, Calamus River, Nebraska. Taken from Bridge [1993].

Sediment Transport around Islands

Maximum bedload transport will tend to occur at the locations of maximum velocity and maximum bed shear stress. As flow diverges around an island, the thalweg (line of maximum channel velocity) will divide into two thalwegs and will diverge towards the outer banks of each channel around the island. In general, there is a small net bedload transport towards the outer banks. However, for streams with a substantial gravel fraction, the location of maximum bedload transport will stay close to the center of the channel. The reason for the difference between transport in sandy and gravelly streams is that both the mean grain size and bedload transport rate are dependent on the proportion of the total bed shear stress available for bedload transport relative to that associated with the immobile bed fraction and bedform drag [Bridge, 1993]. In a mixed sand and gravel stream, shear stresses will allow the flow to clear away the sand from the gravel, so that a coarser bed (larger fraction of gravel) will exist at the location of maximum velocity and shear stress, reducing the total bedload transport rate there. In sand-bed streams, an increase in bed shear stress may result in an increase or decrease in bedform height and length (i.e. form drag) such that the effective bed shear stress for bedload transport may subsequently decrease or increase [Bridge, 1993].

FLOW RESISTANCE AGAINST ISLANDS

DRAG FORCES ON THE ISLAND AS A WHOLE

An object interfering with the relative velocity pattern of a fluid induces a drag force that is proportional to that velocity. Drag force consists of two components: friction and pressure forces. The friction drag force is due to the shear stress exerted on the object by the fluid. It is a function of the magnitude of the wall shear stress and the sine of the orientation angle of the surface on which it acts. If the surface is parallel to the upstream fluid velocity, then the entire shear force contributes to the drag. If the surface is perpendicular, then the shear stress does not contribute at all. The pressure drag force, otherwise known as the form drag because of its high dependency on shape, is due to the pressure exerted on the object by the fluid and is proportional to the cosine of the orientation angle of the object's surface. The more perpendicular the surface is the upstream fluid velocity, the more the pressure force contributes to the drag force. These two components are rarely analyzed separately, but together as a total drag force.

The total drag force (F_d) is the product of the dynamic pressure of the flow, the cross-sectional area of the object, and a dimensionless shape coefficient. A conventional way of expressing it is [Munson et al., 1990]:

$$F_d = C_d PA = C_d (\frac{1}{2}\rho V^2)(BH) \qquad (5\text{-}1)$$

where B is the width of the object normal to the flow, and H is the height of the object. The drag coefficient (C_d) is a descriptor of how much the object disrupts the flow lines.

Eisner [1929] performed experiments on the drag force of various shapes submerged in water. With all other parameters equal, a blunter object will have a greater drag force than a streamlined object due to their representative drag coefficients (Figure 5-6). The drag coefficient can be considered relatively constant for a given Reynold's Number.

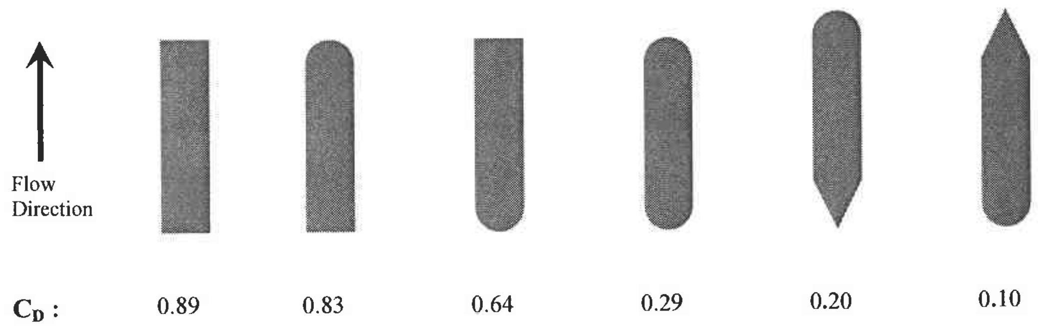

Figure 5-6. Effect of obstacle shape on drag force coefficient. All shapes have length/width ratios of about 6. Values for velocity = 12 ft/sec, L/W = 6, and Re = 10^6. Modified from Hoerner [1965].

FLOW RESISTANCE OF OBJECTS IN VARYING SEDIMENT CONCENTRATIONS

Consider the island as a solid, cohesive object, such as a crater rim in the Martian channels or a PVC pipe installed in a laboratory flume. How does the flow resistance of sediment-laden water compare to that of clear water?

It is unreasonable to compare flows of the same Reynold's number because the sediment-laden flows must exhibit higher velocities to achieve equivalent Reynold's numbers, and therefore would represent a different flow regime. We must, therefore, compare conditions with the same velocities.

For laminar flows, the friction factor is dependent on the Reynold's number:

$$f = \frac{64}{\mathrm{Re}_1} \tag{5-2}$$

where the Reynolds number has the following form for sediment-laden flows [Wan and Wang, 1994]:

$$\mathrm{Re}_1 = \frac{4\rho_m VD}{\eta\left(1 + \frac{2}{3}\frac{\tau_B D}{\eta V}\right)} \tag{5-3}$$

where ρ_m is the fluid density, V is the mean fluid velocity, D is the fluid depth, η is the plastic viscosity, and τ_b is the Bingham yield stress of the fluid, which has been found empirically to be exponentially proportional to sediment concentration:

$$\tau_b = KC_V^m \tag{5-4}$$

where m is generally taken to equal 3 [e.g., Thomas, 1961] and K is dependent on sediment type.

Laminar sediment-laden flows would exhibit lower Reynolds numbers than clear water flows, and therefore have a greater friction factor. However, laminar flow regimes are rare in natural rivers. We must instead look at the turbulent flow regime, which is more common in large natural rivers. As an example, consider a flow that has the following parameters: depth (y) of 1-meter, mean velocity (V) of 1 m/s, sediment concentration (C_V) of 10%, and temperature of 15°C. Equation 4-22 shows that the density (ρ) of the water-sediment mixture would be 1165 kg/m^3, and Equation 4-24 shows that the dynamic viscosity (μ) would be 4.4×10^{-3} kg/m-s. The hydraulic radius, R, can be calculated as:

$$R = \frac{A}{P_w} = \frac{By}{B+2y} \approx y \qquad \text{(for B >> y)} \tag{5-5}$$

where A is the cross-sectional area, P_w is the wetted perimeter, and B is the channel width. By solving Equation 4-14, we get:

$$\text{Re} = \frac{\rho VR}{\mu} = \frac{(1165)(1)(1)}{4.4 \times 10^{-3}} = 2.6 \times 10^5$$

For a Reynolds number greater than about 8,000 to 10,000, the friction factor becomes independent of the Reynolds number, and is only proportional to the boundary roughness (K_S). Since the effective viscosity of hyperconcentrated flow is higher than clear water flow, the boundary roughness is usually too small compared to the viscous sublayer to effect the friction factor. Yang and Zhao [1983] experimented with bed roughness and sediment concentration, and found that for fully developed turbulent flow, the relationship between friction factor and relative roughness is the same in hyperconcentrated flow and clear water flow (Figure 5-7).

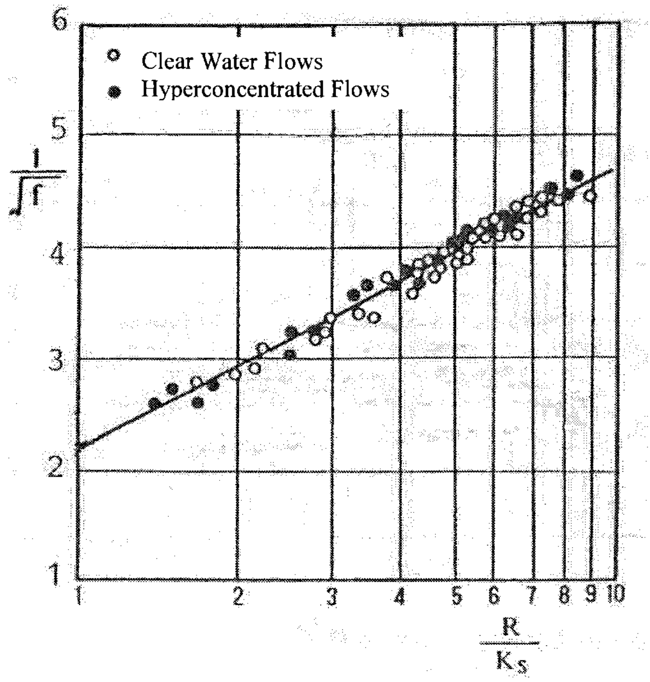

Figure 5-7. Relationship of bed roughness (K_S) and friction factor (f) and sediment concentration, as taken from Yang and Zhao [1983]. Open circles represent clear water experiments, dark circles represent hyperconcentrated water experiments.

Pressure loss, however, can be reduced by increasing the sediment concentration of the flow. Toms [1948] was the first to observe that the frictional drag was reduced when he added polymers to turbulent flow. Subsequent researchers have found the same effect by adding clay particles in suspension. Hou and Yang [1983] found that the friction factor of a disk rotating in a hyperconcentrated flow was larger for laminar flow, but smaller for turbulent than that in clear water flow. Pierson and Scott [1985] found that both the Manning's roughness factor and the Darcy friction factor were reduced during a hyperconcentrated flow on the North Fork Toutle River near Mt. St. Helens as compared to a normally concentrated flow of similar discharge.

CHAPTER 6 – PHYSICAL EXPERIMENTS ON ISLAND PROCESSES

Field and flume experiments were conducted to learn more about the formation of islands and to test ideas developed from observations discussed in Chapter 5.

FIELD EXPERIMENTS ON ISLAND FORMATION

To simulate all nine processes of island formation discussed in Chapter 3 is beyond the scope of this research. However, we did experiment with creating flow conditions that would allow for a lee-deposition type of island to form. The formation of such islands has been well documented in the literature (see Chapter 3), so the purpose of these types of physical experiments was to describe the flow processes associated with such an island formation.

This analysis could be relevant for discussions of extreme, unique flood events that leave behind streamlined residuals, sometimes associated with resistant bedrock. In Martian megaflood channels, many streamlined shaped islands occur in the lee of impact craters within the channel (Figure 6-1). Scientists are unsure of the exact process by which these islands formed. Some say that the erosive power of the flows was deflected outward and away from the crater, thereby leaving an undisturbed area in the leeward zone while eroding the surrounding soil away. Others think that the crater disrupted the flow such that a wake zone of slower, non-erosive waters formed behind the crater, and the suspended material simply deposited there. One application of this research could be to assess which theory is correct. While it is known that both processes can form some kind of an island, which process is more likely to form a streamlined shape conforming to the observed aspect ratios of those in the Martian channels?

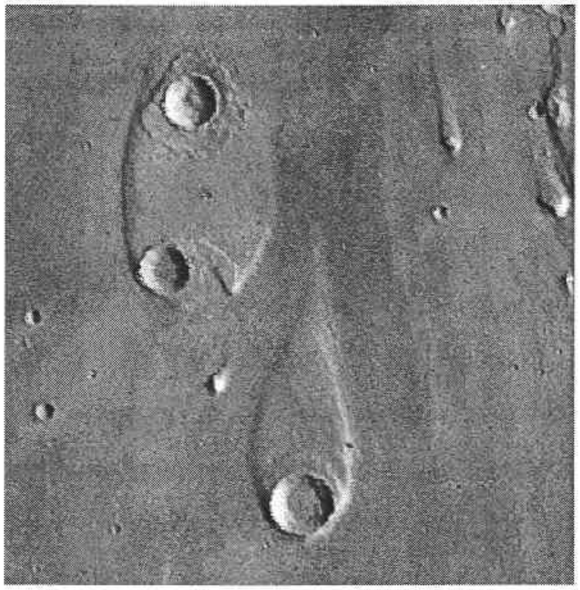

Figure 6-1. Example of residual islands formed downstream of craters on Mars. Craters are 8-10 kilometers in diameter. Topmost crater occurred after the floods (note surrounding ejecta).

LEE DEPOSITION IN OREGON COASTAL STREAMS

We attempted to use a natural stream as an experimental flume to test the ideas of island creation. Experiments were performed on two beach streams on the central Oregon coast – Lost Creek and Driftwood Creek. Lost Creek is located 7 miles south of Newport on the Oregon coast of the Pacific Ocean. Its hydraulic parameters at the time of observations in March, 2004 were: discharge (Q) = 2.6 cfs, width (W) = 7 feet, and maximum depth (D_{max}) = 0.3 feet. Driftwood Creek is located 6 miles south of Lost Creek and 3 miles north of the town of Waldport, Oregon. Its hydraulic parameters at the time of observation were: Q = 3.6 cfs, W = 10 feet, and D_{max} = 0.35 feet. Both streambeds consist of non-cohesive sand.

These small streams drain the local topography near the coast and traverse the sandy beaches before they reach the Pacific Ocean. The steep slopes of the beaches allow for high local shear stresses along the channels. This condition, combined with the inherent non-cohesiveness of sand, allows for continuous fluvial transport of sand particles and rapid changes of bed features. The high sediment transport rates were expected to offer ideal opportunities to experiment with lee deposition as a mechanism for island creation.

The experiments consisted of inserting an object into the flow and measuring the sand deposition in its wake. The object in this case was a PVC (poly-vinyl chloride) pipe with gravel glued to the outside to provide some roughness. Pipes of various diameters were used. They were individually installed into what appeared to be the thalweg of the stream, and were then monitored over several minutes to document any lee deposition (Figure 6-2).

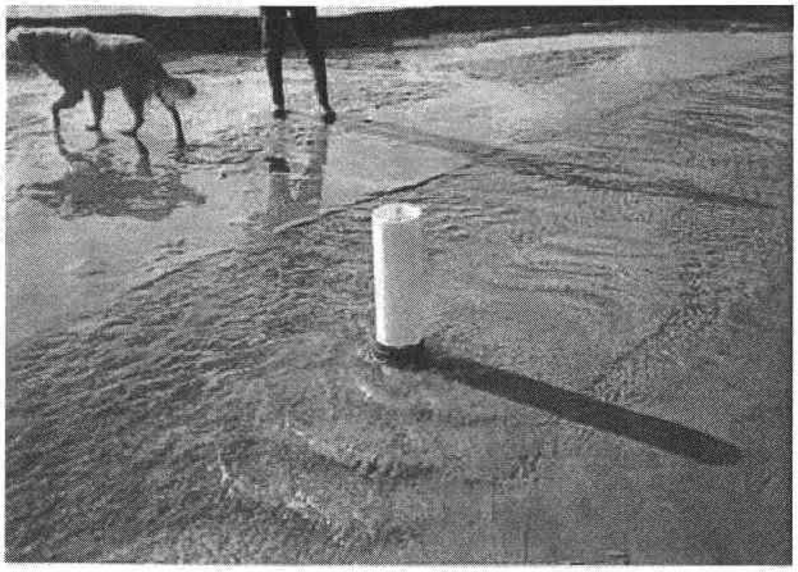

Figure 6-2. PVC pipe in Lost Creek, December 2004.
Flow direction is towards the top right of the photograph.

During these experiments, the flows were unable to form islands, however. There are several possible reasons as to why. (1) We could not control the discharge. In order to form islands in the short experimental time necessary for flume work, we must be able to simulate island-forming conditions over an abbreviated time scale. For a lee-deposition type of island, a fluctuating discharge is imperative. For this kind of island to stabilize, a key ingredient in formation processes is the recruitment of vegetation. For this, we need bar emergence. At high flows, the sediment transport rate increases and deposition behind an obstacle builds up. As those flows recede, the deposition emerges as an unvegetated bar. If it is exposed long enough, vegetation or even woody debris will accumulate onto its surface and stabilize the island. (2) Another problem could be the mobile sandy bed. A deep, horseshoe-shaped scour hole typically forms upstream of and around small, compact obstacles, creating enough local turbulence to prevent some lee deposition. Natural streams surely create some scour at obstacles, but the scour depth would be governed by the depth to the immobile sub-layers. The scour holes created here had depths on the order of the flow depth. (3) The highly mobile bed also made it easy for the flow to migrate away from the obstacle. Since the beach streams do not have rigid banks to contain the flow, the thalweg would usually divert away from the pipe before any significant deposition in its lee could occur.

OAK CREEK VELOCITY PATTERNS

The Oak Creek watershed is located in western Oregon, approximately 5 miles northwest of Corvallis and Oregon State University (OSU). Its headwaters begin in a steep forested area contained in MacDonald State Forest, a research forest managed by OSU's Department of Forestry to serve a variety of research needs for scientists and engineers. The stream then flattens out as it courses through agricultural land and an urban area near the OSU campus before emptying into Marys River near its confluence with the Willamette River. The site of my experiment is located in the forested area, approximately 37.5 feet upstream of the previous site of the Oak Creek vortex bedload sampling system [Milhous, 1973]. The upstream drainage area is 7 km^2 (2.7 mi^2). The mean annual flow is about 0.1 m^3/s (3.5 cfs), with mean summer flows of 0.03 m^3/s (1 cfs), mean winter flows of 0.3 m^3/s (10.5 cfs), and peak flows ranging from 5 – 8 m^3/s (175-280 cfs) [Klingeman, 1979]. The bed material is predominately gravel. Streamflow and sediment concentration are measured routinely by a digital recorder at the site of the former vortex sampler as part of ongoing OSU studies.

The purpose of the experiment was to determine whether an object in a streamflow would create velocity patterns conducive to the formation of a streamlined-shaped depositional zone. This was done by inserting a concrete cinderblock in the middle of a gravel-bed stream using rebar to hold the block in place (Figure 6-3). The cinderblock has a width of one foot normal to the flow, and a width of 0.5 feet parallel to the flow. Velocities were measured using a flowmeter (Marsh-McBirney) that uses pressure differences and Bernoulli's Law to calculate and digitally display an average velocity. Measurements were taken every 0.25 feet across the stream up to one foot away from either edge of the cinderblock, beginning near the upstream end of the block and progressing downstream at every 0.5-foot cross section until there was no discernible flow disruption. A bendable sheet of metal could be added at the upstream end to create a more rounded nose that extended another foot upstream.

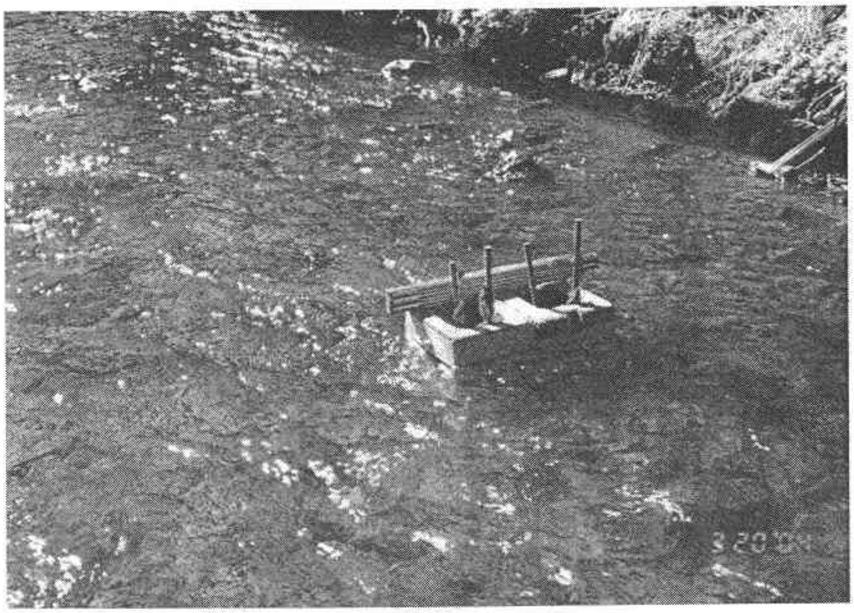

Figure 6-3. Cinderblock acting as obstacle to flow in Oak Creek. Flow is towards the left of the photograph.

The experiment was performed once with just the blunt-nosed cinderblock and again with the rounded nose. The maximum width (one foot) remained the same for both situations. The downstream velocity pattern of each object was similar (Figure 6-4a for the blunt object; Figure 6-4b for the rounded object). For both cases, the zone of small velocities (shown as the smaller diamonds in the figures) can be seen tapering off downstream. If we consider just the negative eddy velocities as those capable of depositing sediment, then the blunt object created a depositional zone with a length of 2.5 feet. Including the extra 0.5 feet upstream length of the object, the total length of the presumed future island would be 3.0 feet and the aspect ratio would be 3:1. The length of the eddy zone for the rounded object was 1.5 feet. Add to that length the 1.5 feet of upstream length of the object, and again we have a total length of 3.0 feet and an aspect ratio of 3:1.

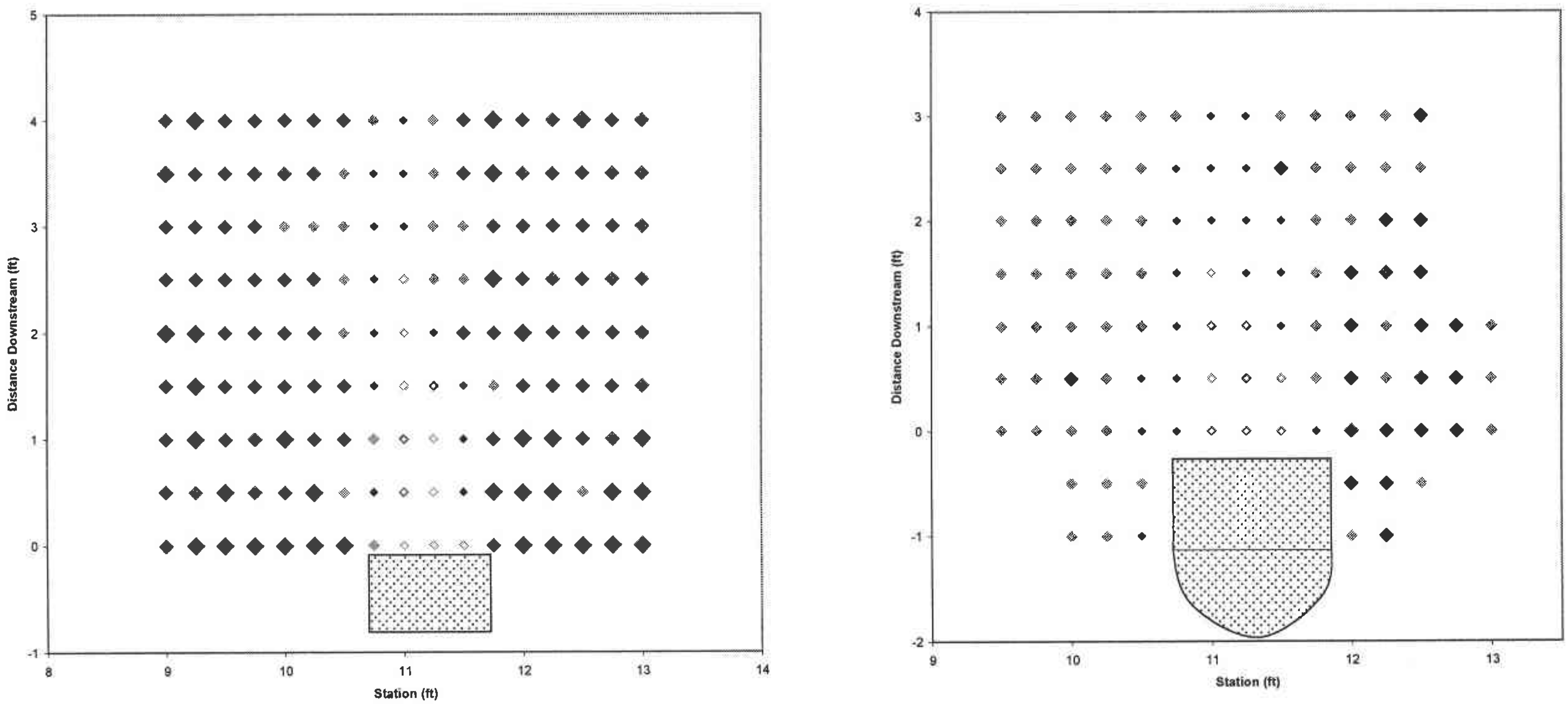

Figure 6-4. A) Velocity pattern behind square obstacle in streamflow on March 23, 2004 (Q = 4.3 cfs). B) Velocity behind rounded obstacle in streamflow on May 23, 2004 (Q = 3.0 cfs). The largest dots indicate velocities greater than 1.5 fps. The velocity decreases by 0.5 fps for each size reduction of the dot. Open dots indicate negative, or upstream, velocities. Gray objects in the figure represent approximate location of cinderblocks with respect to flow pattern. Flow direction is towards the top of the figure.

EXPERIMENTS ON EFFECTS OF ISLANDS ON FLUVIAL PROCESSES

FLUME EXPERIMENTS ON THE EFFECTS OF ISLAND SHAPE ON FLOW PROCESSES

To measure the effects islands have on flow processes, I installed islands of various sizes in a laboratory flume and measured the total head and shear stress upstream and downstream of each island. The flume is 24-foot (7.32-meter) long, 1.47-foot (0.448-meter) wide, equipped with a recirculating pump (optimum flowrate 350 gpm (22 L/s), optimum head 59 ft (18 m)), and set at a slope (S_o) of 0.32%.

The experiments consisted of creating artificial "islands" made up of sections of PVC pipes and placing them into the flume and measuring the induced drag force and the total head loss across a given length of channel as compared to the frictional drag and head loss for the flume without any obstructions in the flow. Each PVC pipe section had a diameter of 169 millimeters (6.65 inches), except for the downstream-most pipe in all the multi-pipe islands, which had a diameter of 127 millimeters (5 inches). For each experiment, the discharge was kept as constant as possible (~0.5 ft^3/s ~ 0.014 m^3/s) and average flow depths were measured three feet (0.91 m) upstream and five feet (1.52 m) downstream from the upstream nose of the island. The location of the upstream nose of each island was kept constant for each run, and each subsequent island was built upon in the downstream direction (Figure 6-5). Weights were placed on top of each pipe section, and above the water surface, to prevent the islands from being washed downstream (square objects in Figure 6-5).

The first 'island' consisted of one 169-mm diameter pipe section (Figure 6-5a). The next test island was made up of one 169-mm diameter pipe section and one 127-mm diameter pipe section placed directly downstream (Figure 6-5b). The subsequent test islands had two, three, and four 169-mm diameter pipe sections and one 127-mm diameter pipe section (Figures 6-5c, d, and e). Each island had the same width of 169 mm (0.554 ft), thereby eliminating any effect a change in width may have on the flow processes. Any effect in flow processes must, therefore, be due to the change in length of the test islands.

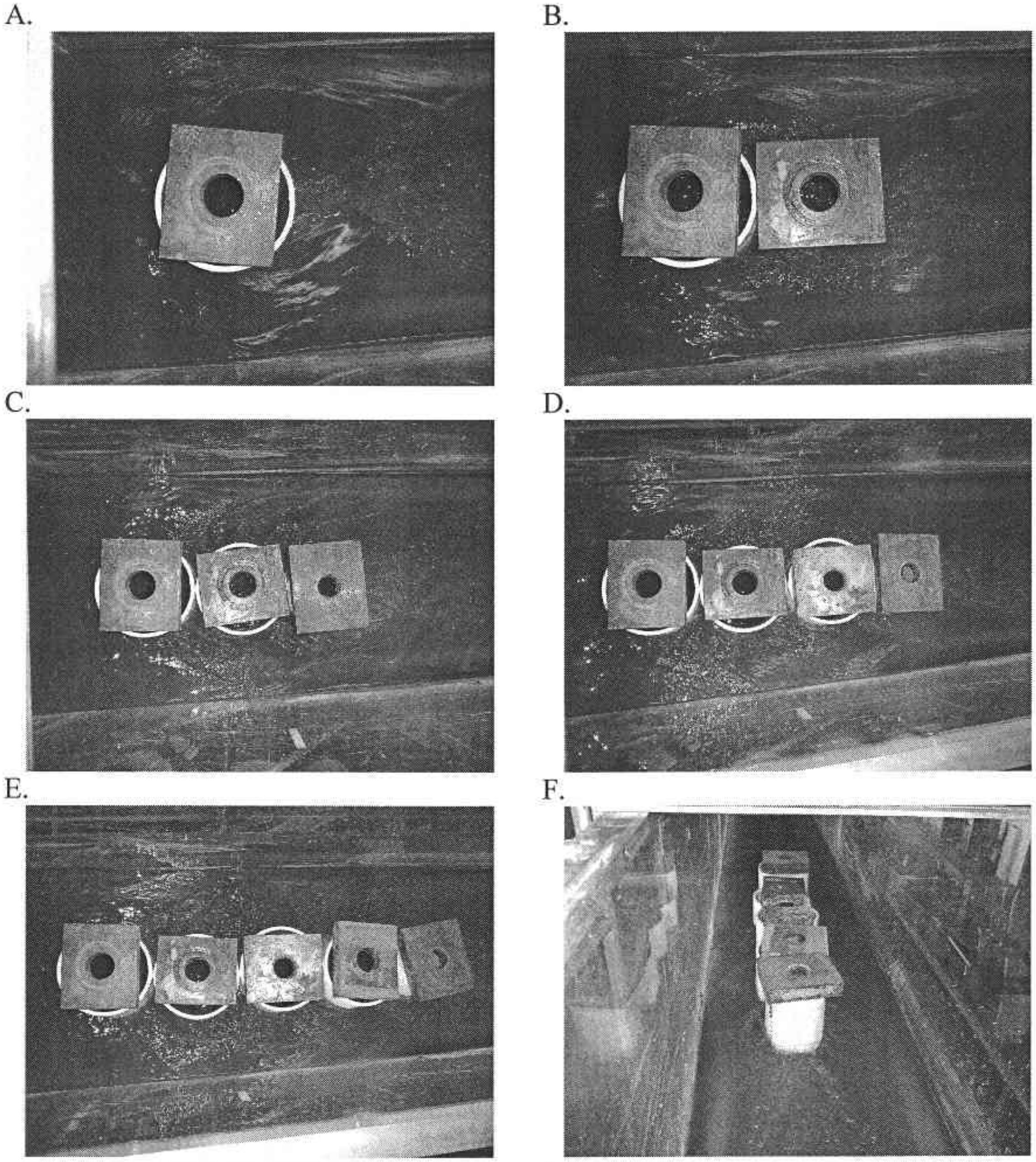

Figure 6-5. Overhead views of PVC pipe setups for flume experiments. Note: square objects in photos are weights applied above water line to hold pipes in place. Photo F is oblique view of 5-pipe run (E) showing relations of pipes, weights, and water level.

By maintaining a constant discharge for each run and changing only the island size, I can calculate the effect that the island's shape has on head loss, shear stress, and drag force. To measure the discharge (Q), a differential manometer was attached to the inflow pipe. The difference between the heads of each manometer tube (Δh) is correlated to the discharge with a Q-Δh relationship that has been calibrated for this flume:

$$Q = 0.522\Delta h^{0.353} \quad (6\text{-}1)$$

Thereafter, I could calculate the velocity at any cross-section by measuring the flow depth and using a ratio based on Equation 4-2:

$$V = \frac{Q}{BD} \quad (6\text{-}2)$$

where B is the flume width, and D is the average flow depth measured at a given cross-section. From the velocity at each cross-section, a velocity head was calculated:

$$\text{Velocity Head} = V^2/2g \quad (6\text{-}3)$$

From the channel slope, S_o, the change in channel elevation (Δz) can be calculated by:

$$\Delta z = S_o L \quad (6\text{-}4)$$

The length (L) of the channel between the upstream and downstream measurements remained constant at 8 ft (2.44 m). The Δz between the measurements, therefore, remained constant at 0.0257 feet (7.83 mm). The total head at each cross-section is calculated as:

$$H = z + D + \frac{V^2}{2g} \quad (6\text{-}5)$$

The total head loss (h_L) across each island was calculated as the difference between the total head upstream of the island and the total head downstream of the island:

$$h_L = H_{u/s} - H_{d/s} \quad (6\text{-}6)$$

From the measured flow depth (D), we also calculated the flow area (A) and the wetted perimeter (P). The hydraulic radius (R) is the ratio of the flow area and the wetted perimeter. Assuming a fluid specific weight of 62.4 lb/ft^3 (1.0 g/cm^3), we calculated the shear stress (τ) each cross-section using Equation 4-13. Since the channel slope and fluid specific weight did not change in the series of experiments, the shear stress became a function only of the hydraulic radius, which itself is a function of flow depth (i.e., $\tau \sim R \sim D$).

The frictional force (F) on each island was calculated using an equation based on the conservation of momentum, commonly known as the Belanger Equation (a form of Equation 4-9) [Chanson, 1999]:

$$F = \left(\frac{1}{2}\rho g B\right)\left(D_1^2 - D_2^2\right) - \rho Q\left(V_2 - V_1\right) \qquad (6\text{-}7)$$

where ρ is the fluid density and B is the channel width. If we can assume that this force minus the frictional force calculated for the "no island" setup is the effective drag force (F_D) on the island, then we can calculate the drag coefficient (C_D) of the island by rearranging Equation 5-1:

$$C_D = \frac{F_D}{\frac{1}{2}\rho V^2 A} \qquad (6\text{-}8)$$

where A, in this case, is the effective area of the island normal to the flow. From these values, I found a relationship between drag coefficient (C_D) and head loss (h_L) to aspect ratio (R_A) (Figure 6-6). The results from each flume experiment are shown in Table 6-1.

Table 6-1. Effect of Island Size on Flow Parameters in Flume Experiments.

	No island	**1 pipe Fig. 6-5a**	**2 pipes Fig. 6-5b**	**3 pipes Fig. 6-5c**	**4 pipes Fig. 6-5d**	**5 pipes Fig. 6-5e**
Island Length (ft)	n/a	0.554	0.971	1.53	2.08	2.64
Island Width (ft)	n/a	0.554	0.554	0.554	0.554	0.554
Aspect Ratio	n/a	1.0	1.75	2.75	3.75	4.75
Head Loss (% of $H_{u/s}$)	4.14	18.2	16.5	9.71	11.7	15.7
Shear stress u/s of island (lb/ft^3)	0.019	0.035	0.035	0.035	0.036	0.037
Shear stress d/s of island	0.022	0.020	0.019	0.017	0.017	0.017
Reynold's Number	2.09×10^4	1.76×10^4	1.75×10^4	1.75×10^4	1.75×10^4	1.72×10^4
Drag force on island (lb)	0.098*	0.752**	0.721**	0.565**	0.658**	0.842**
Drag Coefficient	n/a	4.12	3.98	3.12	3.68	4.94

* - force calculated for 'no island' scenario represents frictional drag due to the flume.
** - drag forces on islands calculated by subtracting 'no island' frictional drag from total measured drag force for each scenario.

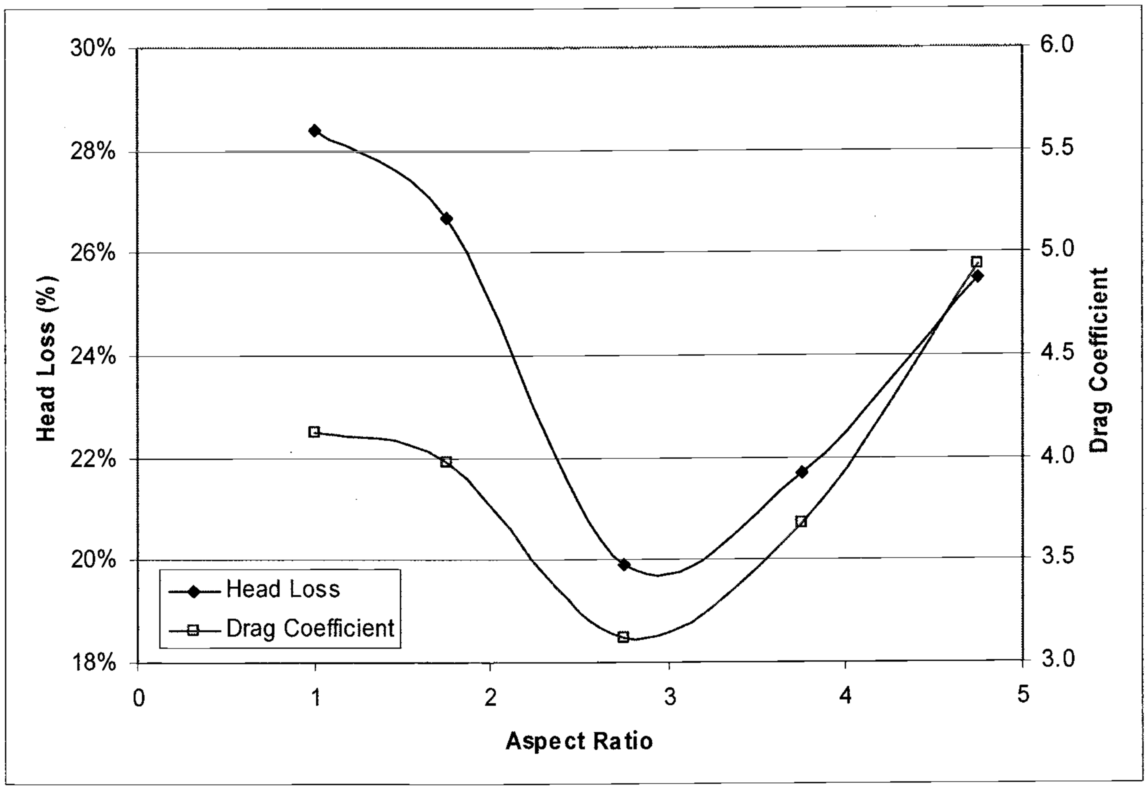

Figure 6-6. Relationship of island aspect ratio to drag coefficient and channel head loss. Reynold's Number for each test equal to about 1.75×10^4.

The minimum head loss and drag coefficient for the flume experiments described above appear to correspond to an aspect ratio of about 3.0 (Figure 6-6). This might mean that a natural fluvial island would tend to reshape itself to exhibit an aspect ratio of about 3.0 in order to minimize the energy loss of the river system.

Effects of Islands on Flow Processes in Oak Creek

To simulate the effects of islands on flow processes in a natural channel, we set up an experiment in Oak Creek similar to the experiments in the flume study. We installed 10 stilling pipes along the banks to measure water elevations (to determine slopes) (Figure 6-7) and seven transects across the channel for measuring depth-averaged, cross-sectional velocities (Figure 6-8). To understand what the flow was like without any islands, we measured the water surface slope and cross-sectional velocities before any island object was placed in the stream. The velocities were measured with a Marsh-McBirney flowmeter every foot along each transect. For subsequent measurements that included an island in the stream, the upstream nose of each island was placed at the third transect. The averaged discharge during the experiments was about 2.3 ft^3/s (0.065 m^3/s).

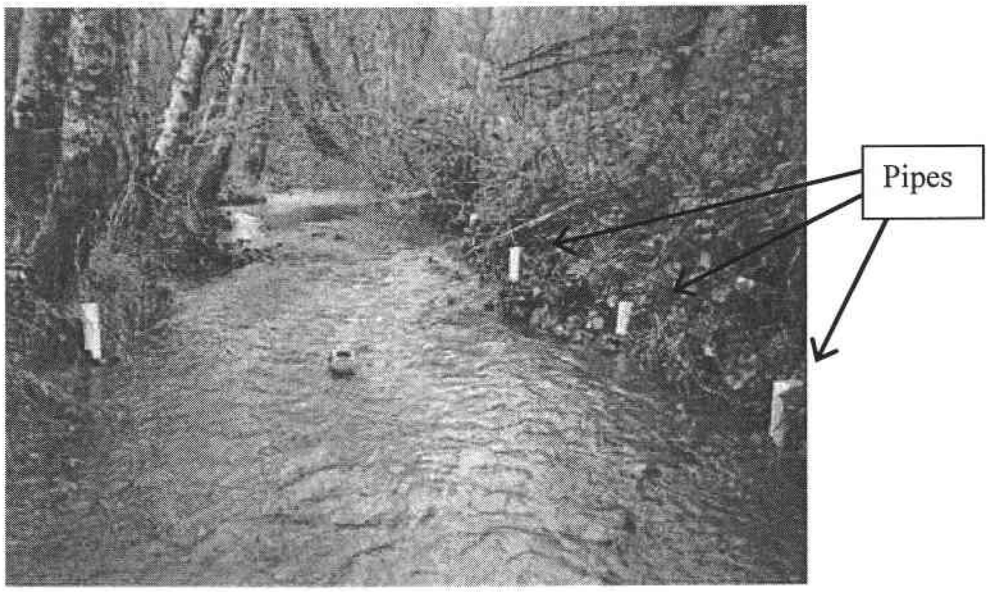

Figure 6-7. Stilling pipes installed along banks of Oak Creek. View is upstream.

The 'islands' were made of 0.3-meter (1.0-foot) diameter plastic buckets (Figure 6-9). Two island sizes were analyzed in these experiments. The small island (Figure 6-9a) consisted of four buckets set in a diamond pattern with the long axis parallel to the stream flow. The large island (Figure 6-9b) consisted of ten buckets. Each island had a width of two buckets (0.6-meter ~ 2.0-feet).

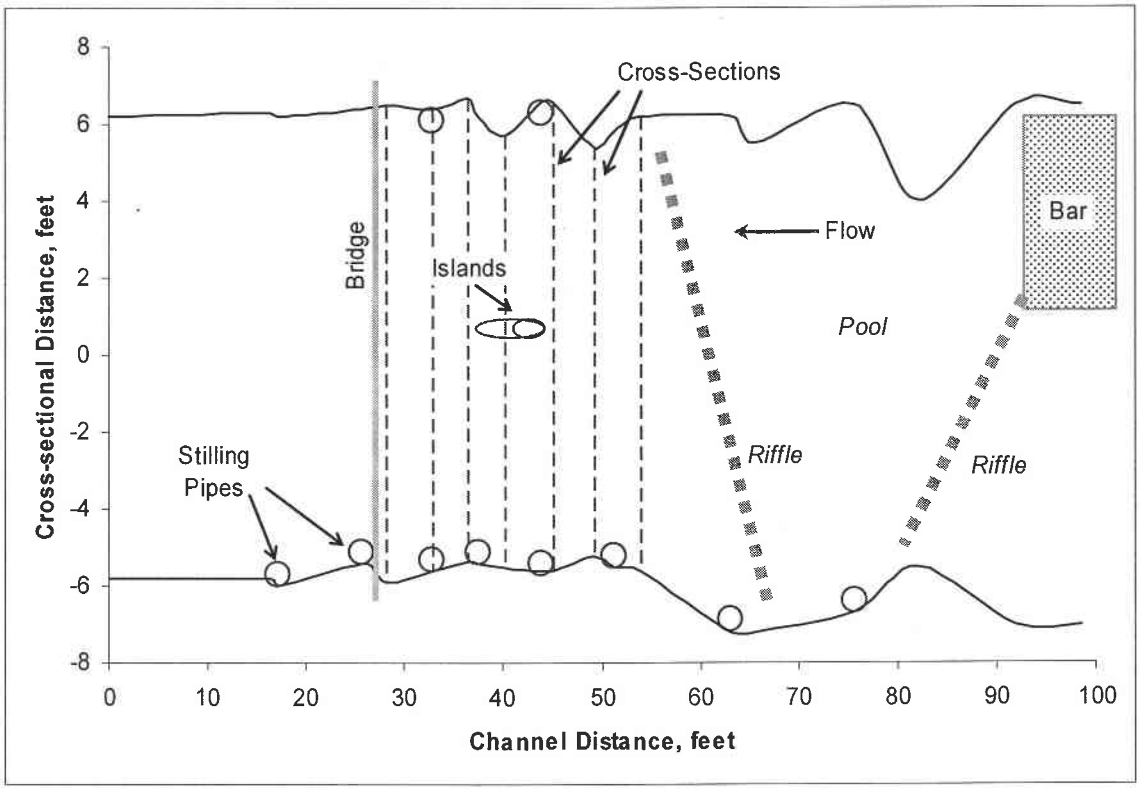

Figure 6-8. Sketch of setup in Oak Creek. Distance measured in feet upstream from concrete edge of vortex sampler. Figure has 4:1 vertical distortion.

A: Small island (4 buckets)

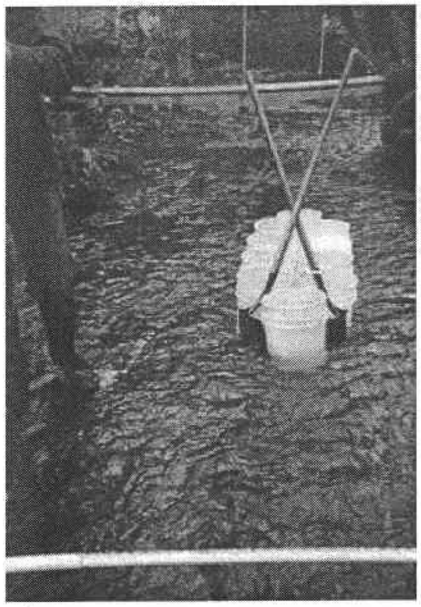

B: Large island (10 buckets)

Figure 6-9. Setup of two artificial islands in Oak Creek. View is downstream.

For each island setup, we measured the water elevation and profile along the channel and the depth-averaged velocity profiles across each transect. From these data, we determined the average depth and velocity head (Equation 6-3) for each cross-section. Using Equation 4-7, we determined the specific energy, E, for each cross-section. The energy grade line for each experiment is shown in Figure 6-10. The total head loss (h_L) through the study reach is equal to the difference in head between the upstream and downstream transects using Equation 4-5. For the measured channel slope of about 0.011, the difference in channel elevations ($\Delta z=S_0L$) between transects 2 and 6 is 0.18 feet (0.055 m). The total head loss for the no-island run was 0.224 feet (0.068 m). The total head losses for the runs with the small and large island setups were 0.256 and 0.287 feet, respectively (0.078 and 0.0874 meter). The large island created about twice as much more head loss than the small island.

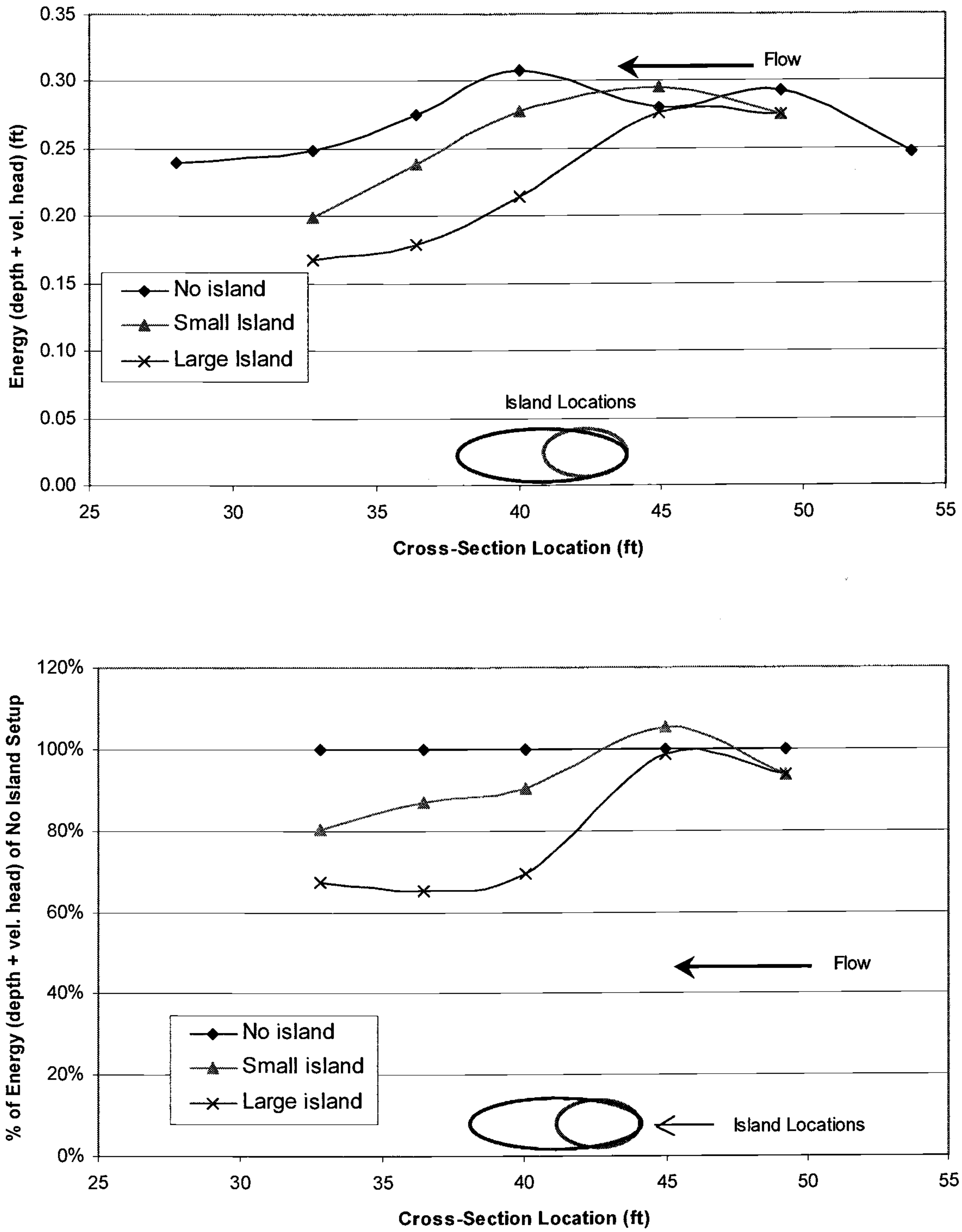

Figure 6-10. Absolute and percent changes in specific energy for different size islands in Oak Creek.

Using Equation 6-7, I calculated the frictional drag force between the upstream and downstream transects for each experiment. For the run without any island, the difference in flow forces upstream and downstream should represent the sum of the frictional forces due to the channel. For the experiments with islands, the additional drag force calculated must then be due to the island. The frictional drag without any island was calculated to be about 8 lbs (35.6 N). The additional drag forces calculated for the small and large island setup were about 4 and 8 lbs, respectively (17.8 and 35.6 N). The large island, again, created twice the frictional drag force as that for the small island. Prevailing low flow conditions during the time period of this study prevented extended analysis of more island sizes or for different flow regimes; however, these experiments do show the effects islands have on the flow processes in a natural river.

VELOCITY PATTERNS NEAR AN ISLAND IN THE CALAPOOIA RIVER

To show that the effects islands have on flow processes are scale independent, we analyzed the flows around an island in a medium-sized river: The Calapooia. The Calapooia River drains a long, narrow watershed off the western flanks of the Cascade Mountains in central Oregon and empties its flow into the Willamette River at Albany. Its drainage area is 370 square miles (958 km^2) and its mean daily discharge at the mouth is 897 ft^3/s (25.4 m^3/s) (as measured by the USGS from 10/1/1940 through 12/10/1981), and is therefore a river of intermediate size and discharge between Oak Creek and the Willamette River (analyzed in the next section).

The island of interest (Figure 6-11), located in the upper portion of the watershed at river mile 75, had a maximum length of 72 feet (22 m) and a maximum width of 16.5 feet (5 m) at the time of measurement. The channel bed material is composed mostly of bedrock, with some boulders and cobbles. The local landowners claim that the island has been present for at least ten years, which is corroborated by aerial photos. The island is probably an exposed section of a transverse riffle, as submerged riffles extend diagonally toward the banks from both the upstream and downstream ends of the island (Figure 6-12).

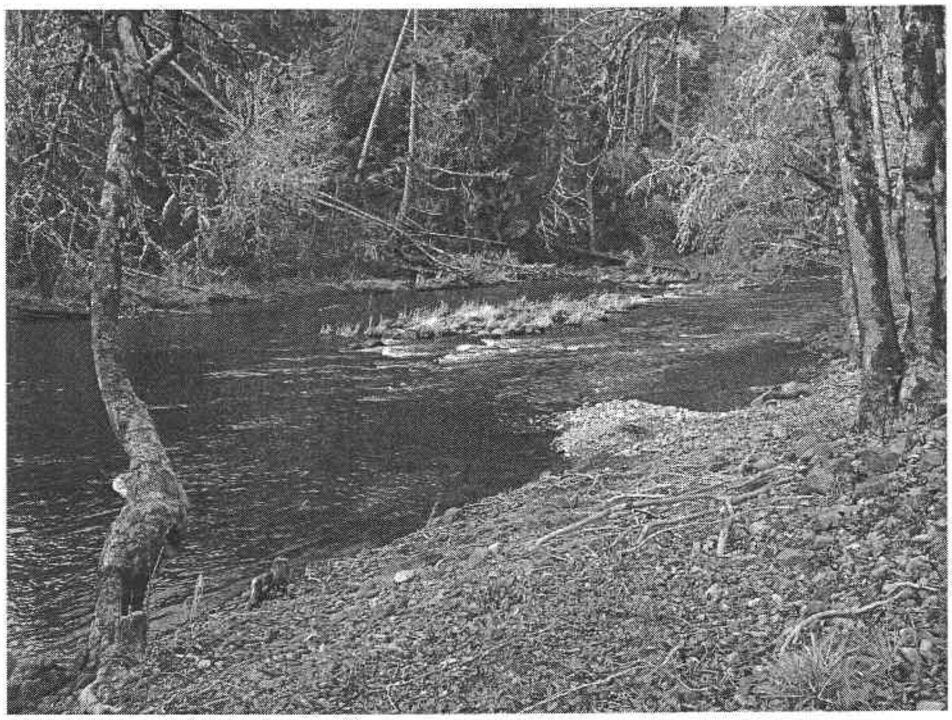

Figure 6-11. Oblique view of small cobble island on the Calapooia River. Flow is to the right of the figure.

Depth-averaged velocities were measured with a Marsh-McBirney flowmeter every two feet along four transects (dash-dot lines in Figure 6-12). The locations of each transect were: one far enough upstream of the island to show 'unaffected' flows, one just upstream of the island, one across the middle of the island, and one downstream. The relative direction of the surface velocities were also recorded for each measurement location, as well as sketched for the inter-transect areas. The directional vectors of the surface flow are sketched in Figure 6-12. The presence of the island in the normally straight flow stream (see vectors at the upstream transect in Figure 6-12) are bent outwards and around the island. The flows then converge again downstream of the island.

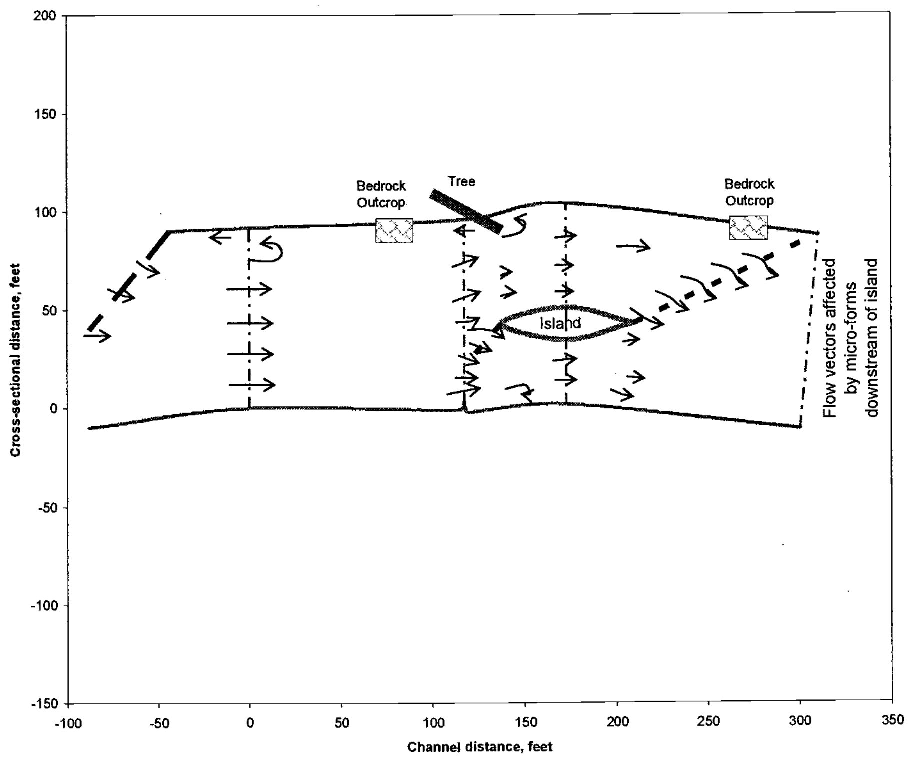

Figure 6-12. Sketch of flow patterns near cobble island on Calapooia River. Dashed lines represent riffles. Dot-dash lines represent locations of transects.

The depth and velocity profiles for each transect are shown in Figure 6-13. The centralized thalweg (location of maximum velocity) in the upstream transect has begun to diverge by the second transect. At the island transect, the maximum velocities have moved towards the outer banks. The downstream transect shows the irregularity of the velocity pattern as the flows converge upon each other.

From the average depths and velocities for each cross-section, I used to Equation 4-7 to calculate the specific energy at each transect (Figure 6-13). There is a head loss between the transects upstream and downstream of the island of 0.88 feet (0.27 m). This head loss cannot be totally attributed to the island, however, as the river contains several other channel roughening agents, but the results are similar to those from the experiments in Oak Creek and the laboratory flume.

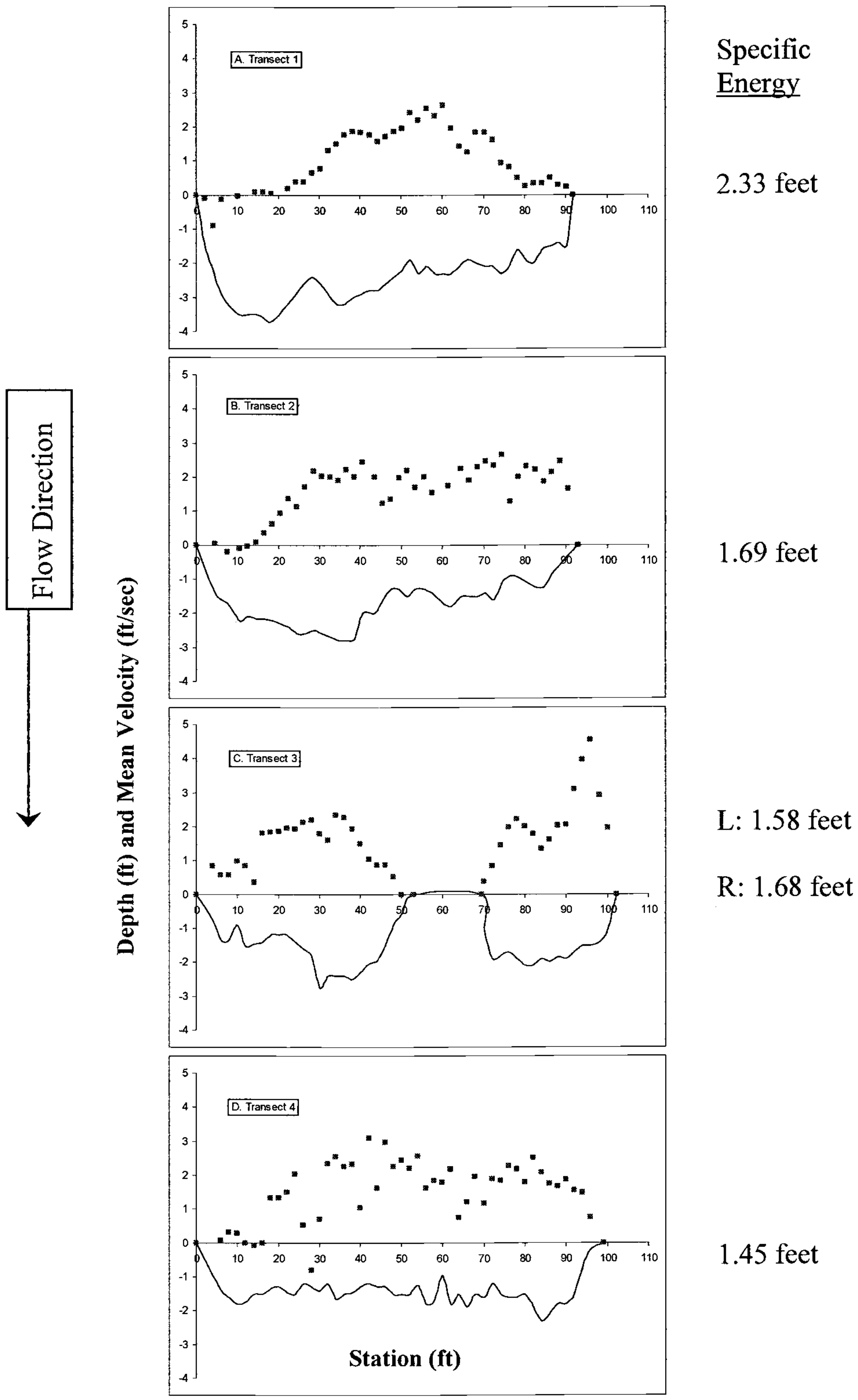

Figure 6-13. Profile of bed (solid line) and depth-averaged velocities (square dots) at many points along four transects near a cobble island on the Calapooia River.

VELOCITY PATTERNS NEAR AN ISLAND IN THE WILLAMETTE RIVER

To show the effects of an island in a large-scale river, we analyzed the flow patterns around an island at river mile 137 on the Willamette River. This island is fairly young compared to other islands on the Willamette. Aerial photo analysis shows that it was not present in 1961 (Figure 6-14A). By 1972, an unvegetated, irregularly-shaped gravel bar is visible (Figure 6-14B). The channel width at that location has also increased, mostly due to erosion of the left bank, which may have precipitated the emergence of the bar. In 1974, the Danis Revetment was installed along the left bank to prevent further erosion. By 1981 (Figure 6-14C), the bar recruited vegetation and increased in size, thus becoming an 'island'. It has also become somewhat streamlined in shape, although the downstream end is still dissected with overflow chutes. In 1984, the Cannon Revetment was installed along the right bank, thus permanently eradicating any possible future channel widening at this site. By 1986, the downstream chutes have become smaller and the vegetation cover has increased (Figure 6-14D). By 1994, the entire streamlined diamond shape has become subaerial and a side bar has emerged downstream of the island (Figure 6-14E). By the 1999 aerial photo, the island has become fully elliptical (Figure 6-14F). As seen in this aerial photo sequence, the location of the island has not changed significantly throughout these years.

To analyze the flow around this island, we set up several transects upstream of the island and along the right channel (Figure 6-15). Using a SonTek acoustic-doppler profiler (ADP), we measured velocity profiles at each cross-section. An ADP measures the 3-D velocity profile at a user-specified number of depth cells as well as the directional vector for each cell (for more information on the ADP, see http://www.sontek.com). To minimize errors, multiple repetitions were made for each cross-section and the results were averaged.

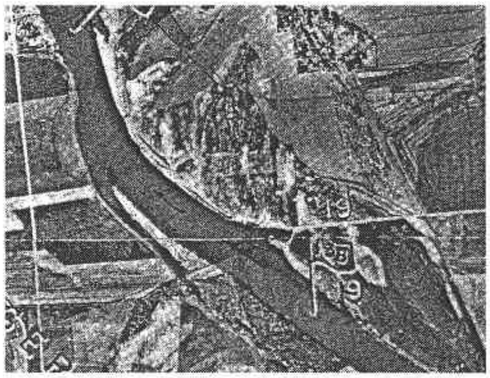

A: 1961

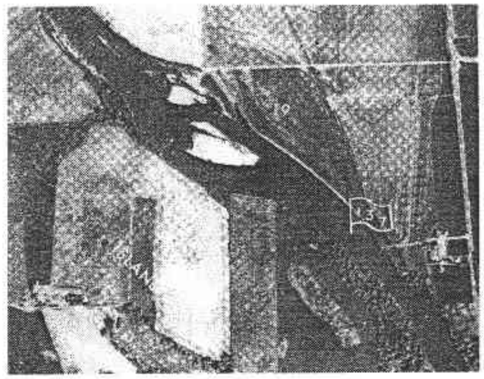

B: 1972

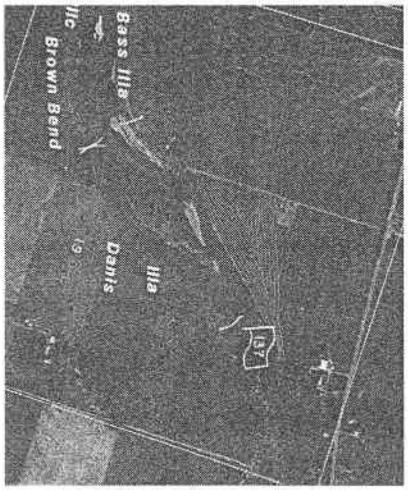

C: 1981

D: 1986

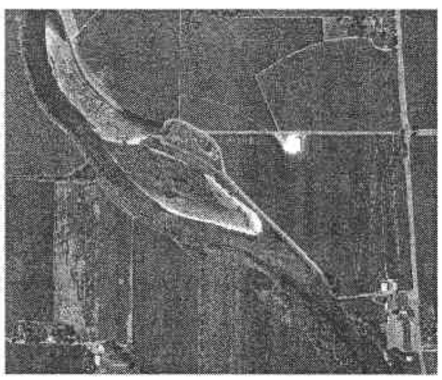

E: 1994

F: 1999

Figure 6-14. Aerial photo sequence showing emergence and stabilization of island on Willamette River from 1961 through 1999. Flow is towards the top of each figure.

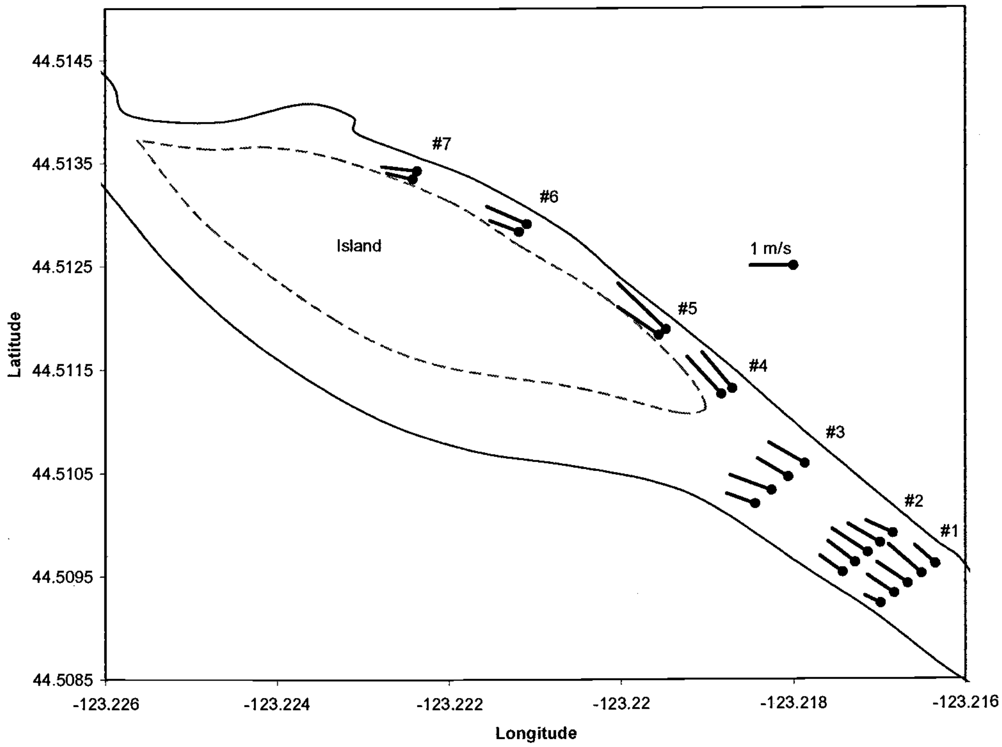

Figure 6-15. Flow patterns near island on the Willamette River. Transect numbers are labeled on the right bank. Flow in right channel is about 25% of total upstream flow. Access difficulties hindered left channel measurements.

Figure 6-15 shows the velocity directional vector patterns around the Willamette island, as well as the relative magnitude of the depth-averaged velocities. Transects #1 and #2 show an expected velocity pattern with a thalweg velocity near the center of the channel. By Transect #3, the divergence of the flow around the island is becoming apparent. As the flow enters the right channel, the depths decrease significantly (from over 3-meters deep to under 1-meter deep) and the velocities increase. Because the values expressed in Figure 6-15 are depth-averaged velocities, they do not show the helical flow pattern described in Figure 4-2, but by the two downstream transects it is apparent that the flow is exhibiting some inward directional patterns. Note that the right channel carries about 25% of the mainstem flow. Difficulties in gaining access to the left channel hindered any detailed analysis of that flow.

More detailed cross-sectional velocity patterns are shown in Figure 6-16. Only four of the seven transects are shown in Figure 6-16, but the general flow pattern from upstream of the island to the right channel is represented. Fairly uniform velocities are evident in the upstream transect, while the right channel transects exhibit greater average velocities closer to the right bank. These results are similar to the velocity patterns shown for the Calapooia River in Figure 6-13.

DISCUSSION OF RESULTS

Islands create a measurable decrease in flow energy. The extent of this energy loss is affected by the shape of the island. Experiments describe herein and in previous research [e.g. Komar, 1983] have shown that the energy loss can be minimized with an island length/width ratio of about three. A centralized thalweg is known to move towards the outer bank in a meander curve of a river [e.g. Dietrich, 1987]. Analyses of flow patterns around fluvial islands show similar processes with the centralized thalweg splitting around an island and moving closer to both outer banks. The flow vectors begin to diverge upstream of the island, creating a shoaling effect at the upstream nose of the island. Flanking channels around an island also exhibit the characteristic triangular cross-sectional shape previously described for meander bends of a river.

The experiments described in this chapter have a wide range of scale, yet similar flow processes were observed for all of them. The flows for each experiment were subcritical and turbulent. The comparable characteristics for the experiments are listed in Table 6-2.

Table 6-2. Comparison of physical experiment parameters.

Experiment	Island Length/Width	Froude Number	Reynold's Number	Channel Slope	Flow Discharge (cfs)
Flume	1.0 – 4.75	0.44	1.75×10^4	0.32%	0.5
Oak Creek	1.5 – 3.5	0.20	1.42×10^4	1.1%	2.0
Calapooia	4.36	0.21	1.63×10^5	unknown	220
Willamette	3.5	0.22	1.69×10^6	0.05%	9,200

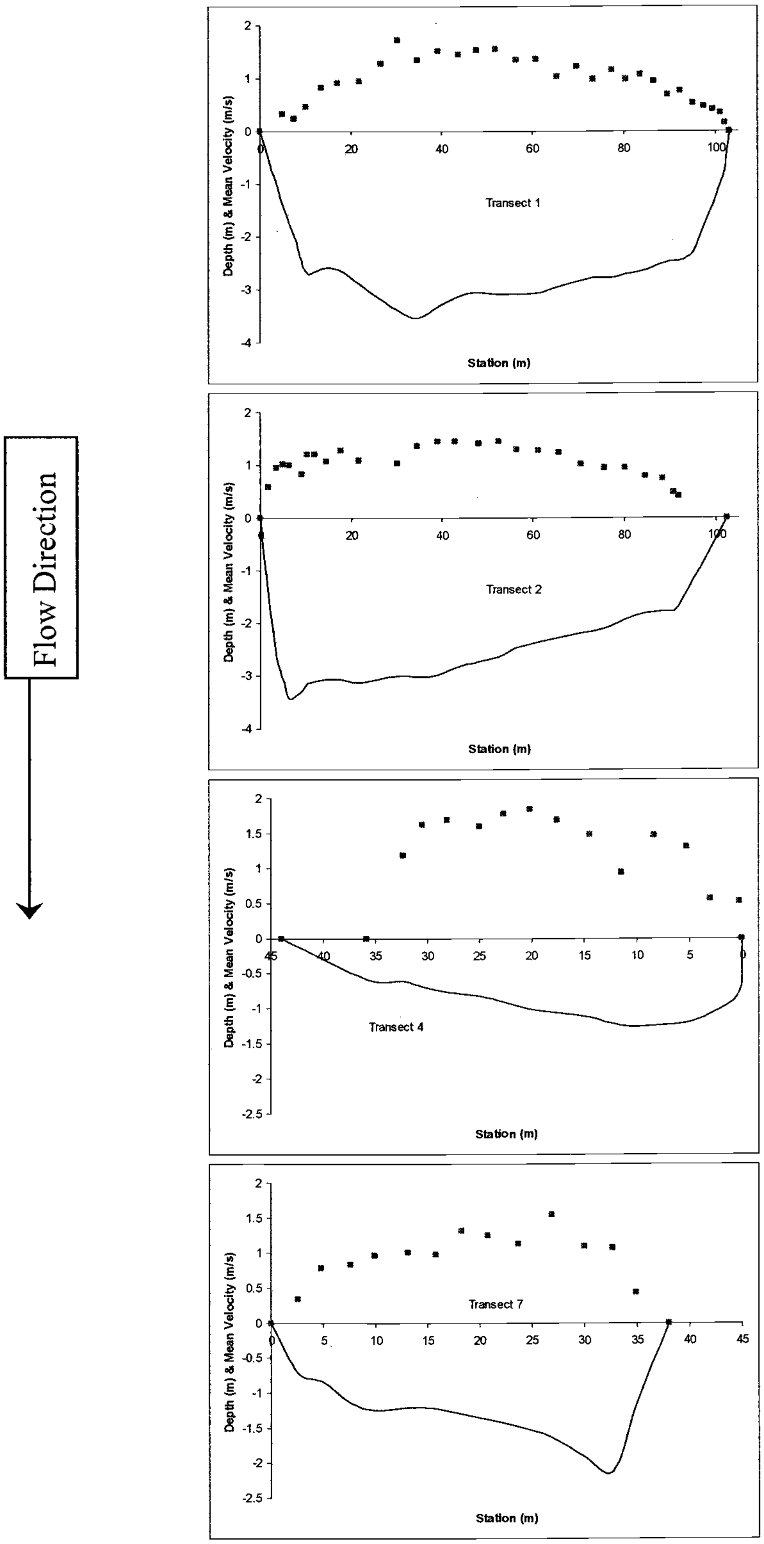

Figure 6-16. Profile of bed (solid line) and depth-averaged velocities (square dots) at many points along four transects near an island on the Willamette River.

CHAPTER 7– ANALYSIS OF ISLAND SHAPES AND SHAPE EVOLUTION

GEOMETRIC ANALYSIS OF ISLAND SHAPE

In this chapter, I will examine the geometries of fluvial islands in terrestrial rivers, with particular focus on how their length-to-width ratios compare intra-basin and inter-basin. Also analyzed are the effects on these ratios by such fluvial characteristics as the channel width, river discharge, and sediment concentration. Because we are analyzing islands with dimensions ranging over several orders of magnitudes, especially when including those in the Channeled Scablands and on Mars, the best method to compare the islands is with the use of dimensionless properties.

As discussed in Chapter 5, the minimum drag shape is that of a streamlined teardrop tapered downstream. This shape can be approximated as a half-lemniscate (Figure 7-1) and represents an equilibrium of fluvial processes. Streamlined islands have been compared to the lemniscate shape in various environments such as American rivers [Komar, 1984], Northeastern drumlins [Komar, 1984], Channeled Scablands [Baker, 1978a], ephemeral Australian rivers [Tooth and Nanson, 2000], Lake Agassiz drainage paths [Kehew and Lord, 1986], and Martian outflow channels [Baker, 1979].

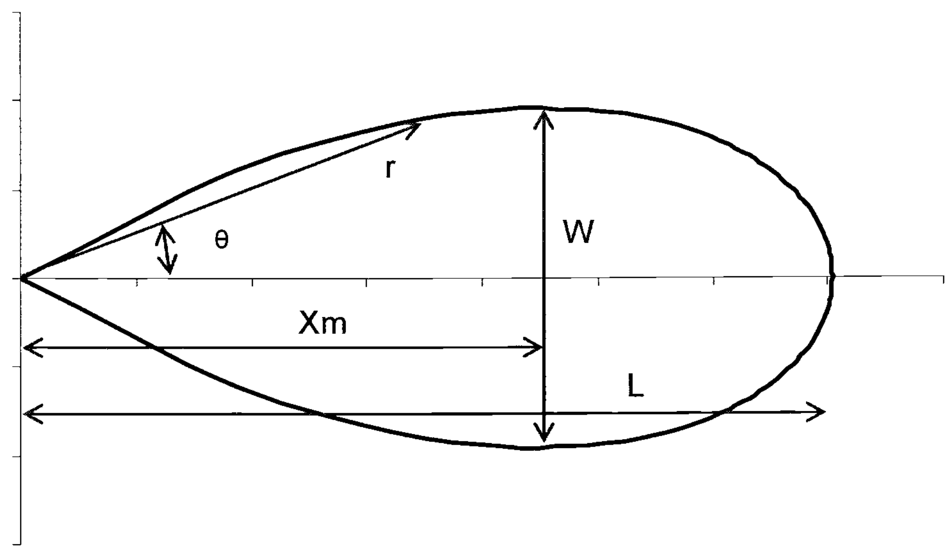

Figure 7-1. Dimensions of the lemniscate shape.

Using a lemniscate as a comparison is a simple method to compare the dimensions of fluvial islands, approximating them in two-dimensional form. Mathematically, a lemniscate can be expressed as an equation with the form, in polar coordinates:

$$r = L\cos(k\theta) \qquad (7\text{-}1)$$

where k is the degree of elongation, calculated by:

$$k = \frac{\pi L^2}{4A} \qquad (7\text{-}2)$$

and L is the maximum length of the shape and A is the planform area. As k approaches unity, Equation 7-2 becomes the definition of a circle. These terms are shown in Figure 7-32. The maximum width (W) of the streamlined shape occurs at x_m where $dy/dx = 0$. Integrating this with the equation for a lemniscate, we can derive a relationship between k and θ_m [Komar, 1984]:

$$k\tan(\theta_m)\tan(k\,\theta_m) = 1 \qquad (7\text{-}3)$$

where θ_m is the angle between the length vector of the island and the point of maximum width. θ_m can also be defined as the maximum angle, θ, achievable by Equation 7-1 for a given lemniscate shape.

The degree of elongation can represent the skin friction of the object. By minimizing k, an object minimizes its frictional drag. The pressure drag can be minimized by increasing the elongation of the object. The balance of these two drag forces dictates the object's k value.

Using the lemniscate shape as a basis of comparison, I can then determine dimensionless properties of fluvial islands, including: (1) aspect ratio (length/width, denoted as R_A), (2) degree of elongation (k), and (3) location of maximum width (x_m/L). The location of maximum width can be calculated in the field or from aerial photographs as well as mathematically determined for that of an equivalent lemniscate form by [Komar, 1984]:

$$x_m/L = k\sin(\theta_m)\sin(k\,\theta_m) \qquad (7\text{-}4)$$

The ratio, x_m/L, generally lies between 0.60 and 0.70 for equivalent lemniscate forms [Komar, 1984]. Therefore, if an island's natural x_m/L ratio is not in this range, using lemniscate parameters to characterize the island may not be accurate.

Other dimensionless characteristics involve the island's relation to the river itself, including the island's relative location in the river (percent of width from a given bank) and the ratio of island width to channel flow width at three transects: (1) at the location of the island, (2) upstream one channel width from the island, and (3) downstream one channel width from the island (Figure 7-2).

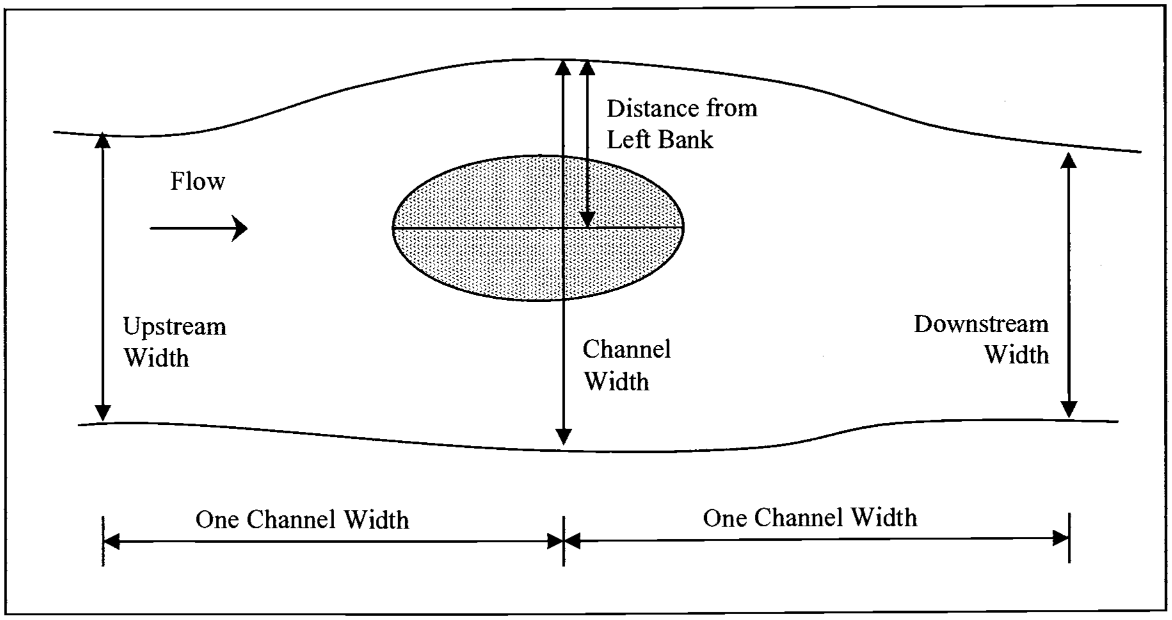

Figure 7-2. Characteristics of surrounding channel dimensions.

As an example of how to calculate these characteristics, consider Skamania Island at river mile 136 on the Columbia River, shown in Figure 7-3. The measurements made from this figure and calculations based on those measurements are shown in Table 7-1. Measurements were made using distance and area calculation tools available on www.mapcard.com. With a measured maximum length of 704 meters and a subaerial planform area of 0.095 km^2, the degree of elongation is calculated to be 4.1 using Equation 7-2. Because the island's x_m/L ratio is equal to a value of 0.63, which is between 0.6 and 0.7, the island can be considered comparable to a lemniscate shape. Using Equation 7-1, we can determine the equivalent lemniscate shape for Skamania Island, shown in Figure 7-4. Visually, the island's actual shape and its equivalent lemniscate compare favorably to each other.

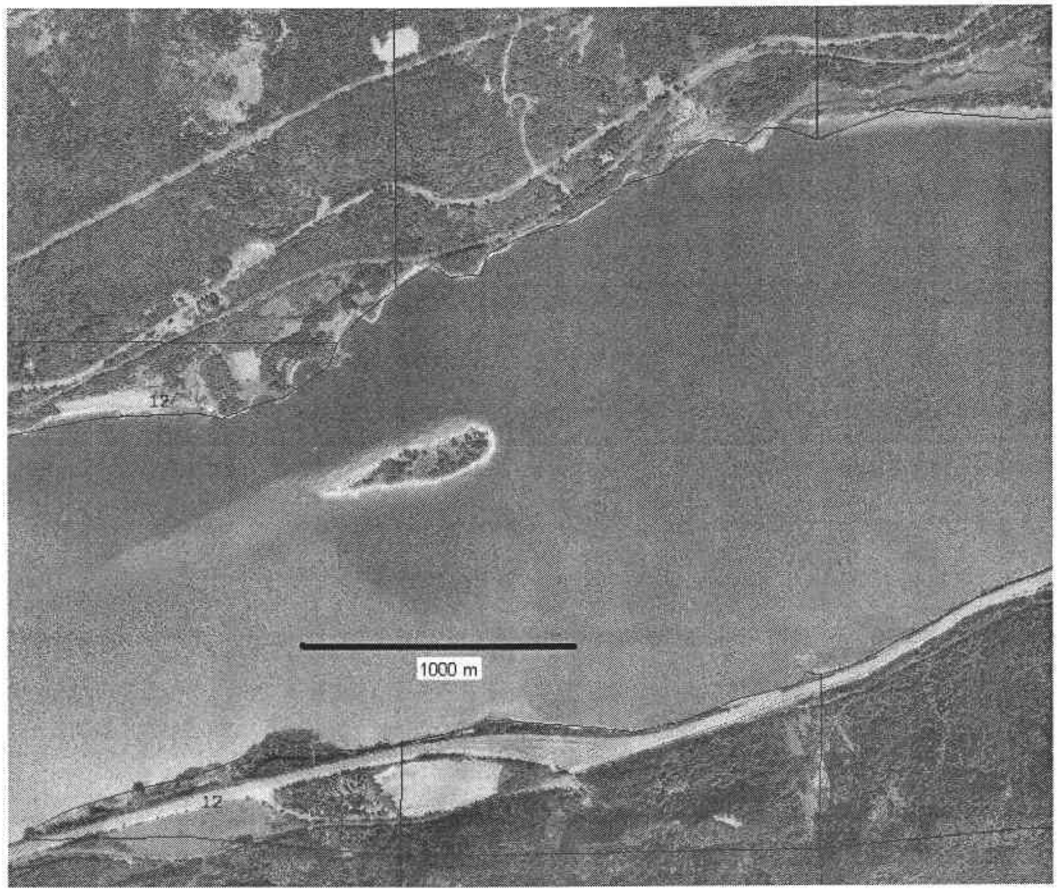

Figure 7-3. Skamania Island at River Mile 136 on the Columbia River. Flow is towards the left of the figure.

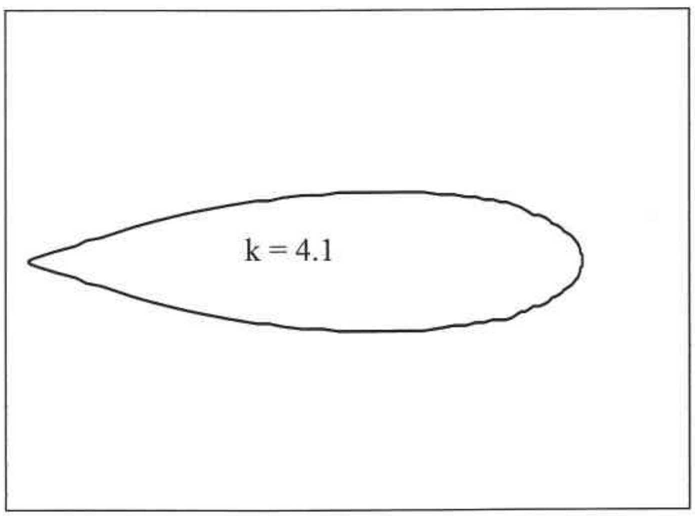

Figure 7-4. Equivalent lemniscate for Skamania Island.

Table 7-1. Measured and calculated properties of Skamania Island.

Measured Property	Value
Island Length (L)	704 m
Island Width (W)	192 m
Island Planform Area (A)	0.095 km^2
Location of Maximum Width (x_m)	441 m
Distance to Left Bank	900 m
Distance to Right Bank	472 m
Channel Width (CW)	1550 m
Upstream Channel Width	1895 m
Downstream Channel Width	1395 m
Island Shape	Lemniscate
Vegetation	Trees & Shrubs
Proximity to Other Islands	Isolated
Calculated Property	**Value**
Aspect Ratio (R_A)	3.68
x_m / L	0.63
Degree of Elongation (k)	4.1
Flow Width (CW – W)	1358 m
Ratio of Island Width to Flow Width	0.14
Relative Distance to Left Bank	0.64
Ratio of Upstream Width to Channel Width	1.22
Ratio of Downstream Width to Channel Width	0.90

Similar analyses were performed on fluvial islands in thirteen rivers throughout the United States. Descriptions of the rivers and analyses their islands are presented in detail in the following section.

ANALYSIS OF ISLANDS WITHIN EACH RIVER SYSTEM

With the availability of topographic maps and aerial photographs on the Internet (e.g., see http://www.mapcard.com), I can analyze islands located in rivers across all climates of the United States (Figure 7-5). I have access to continuous aerial photographs for the lower 48 states, and topographic maps of all 50 states. The finest resolution I can acquire of the aerial photographs is 1:6000; therefore I must restrict this analysis to only the largest rivers. Detailed measurements are compiled in Appendix II and are summarized graphically in the following sections. All streamflow and sediment concentration data summarized here are based on U.S. Geologic Survey (USGS) data available on the web at http://waterdata.usgs.gov/nwis/sw and //co.water.usgs.gov/sediment/seddatabase.cfm.

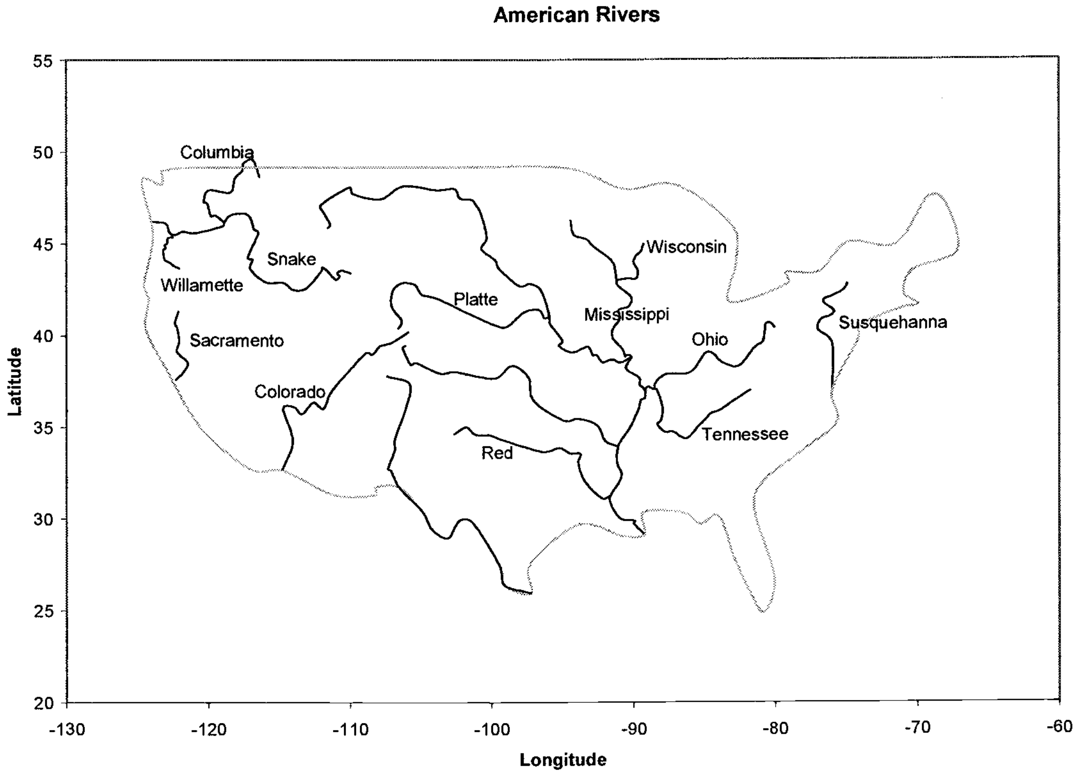

Figure 7-5. Map of the rivers containing fluvial islands used for this analysis. Only the labeled rivers are used in this analysis. Other lines on the map are large rivers without significant fluvial islands. The outline of the lower 48 states is also given. Not shown in the figure, but used in the analysis, is the Yukon River in Alaska.

For each river basin described below, the maximum lengths and widths of their fluvial islands are compared to the two-dimensional plan areas. The average length/width ratio (aspect ratio) is calculated and compared to the power law trendline fit of the width versus length plots. For the set of islands whose natural x_m/L ratios lie between 0.6 and 0.7, the average degree of elongation (k) is calculated and used to plot the average equivalent lemniscate shape for the fluvial islands.

SUSQUEHANNA RIVER

The Susquehanna, the largest river on the Eastern Seaboard, begins its nearly 450 mile trek at Otsego Lake in central New York State. By the time it flows into the Chesapeake Bay, the Susquehanna has have drained 27,000 square miles. Its location on the east coast of the United States has exposed the river to almost four centuries of European settler influences. The Susquehanna used to be shallow, swift-flowing, and difficult to navigate. Now, it is a chain of locks and dams, including Conowingo Dam, the largest nonfederal power station in the country. Due to the humid climate and dense urbanization in the valley, flooding is a continuous problem; devastating floods occur every few decades, the latest in 1972 was caused by heavy rainfall from Hurricane Agnes [Penn, 2001].

The fluvial islands analyzed in this paper are located within the river stretch from the Conowingo Dam to upstream near the junction with the Juniata River. One dam, York Haven, separates the majority of the island dataset. Most of the islands are centered about Harrisburg, Pennsylvania (Figure 7-6), where the USGS has operated a streamflow gaging station since October 1, 1890, and operated a daily continuous sediment gaging station from March 13, 1962 to March 31, 1981. Other relevant streamflow gaging stations include sites at Conowingo, Marietta, and Sunbury (Table 7-2).

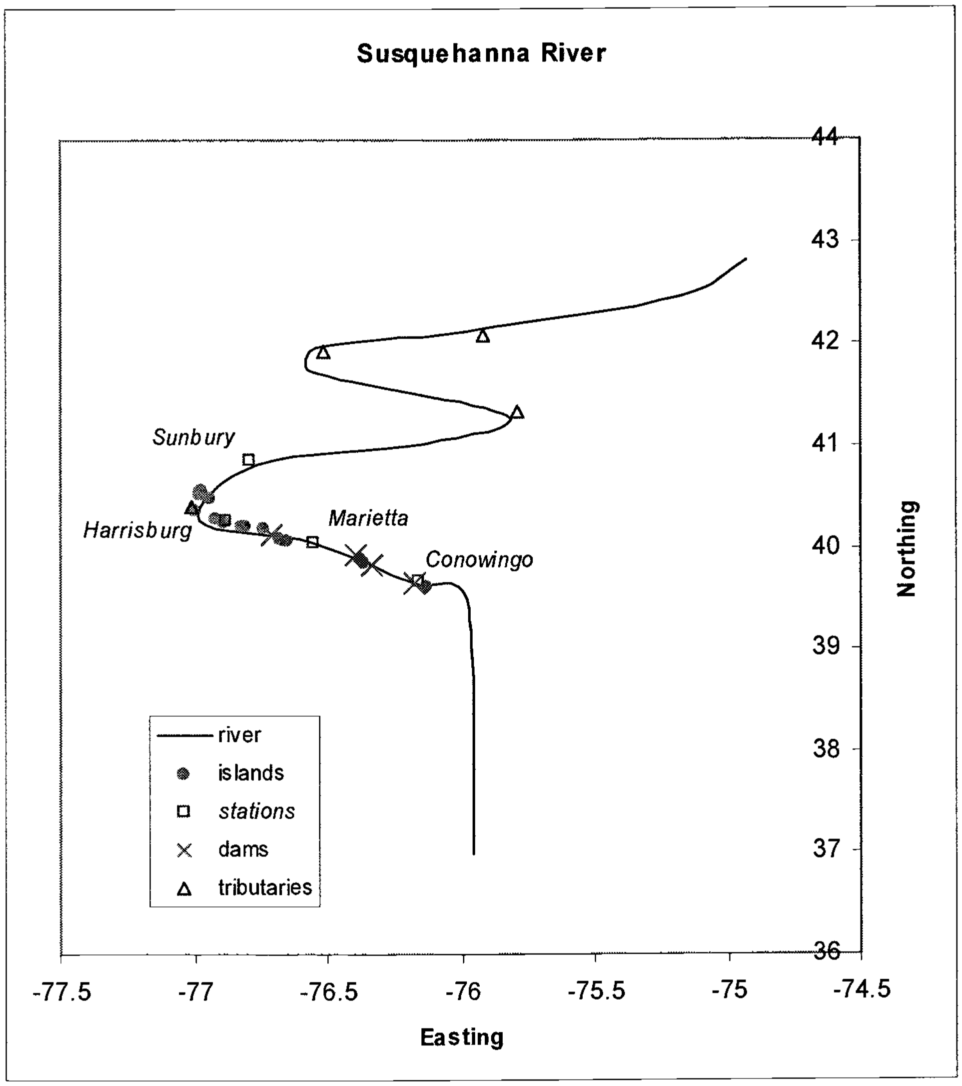

Figure 7-6. Sketch of Susquehanna River. Flow is to the south.

Table 7-2. Gaging station records along the Susquehanna River.

Gaging Station	Dates of Record	Number of Measurements	Average Daily Discharge (cfs)	Upstream Drainage Area (sq mi)
Conowingo, MD	10/1/1967 – present	13149	40,182	27,100
Marietta, PA	10/1/1931 – present	26298	37,203	25,990
Harrisburg, PA	10/1/1890 – present	41272	34,252	24,100
Sunbury, PA	10/1/1937 – present	24106	26,849	18,300

A total of 28 fluvial islands were analyzed on the Susquehanna River. Twelve of these islands were located in island clusters near Burgers Run and Berry Mountain. Most of the islands have a much smaller width than the surrounding flow channel. The channel width ranged from about 1000 to 1500 meters, whereas the islands' widths ranged from about 30 to 500 meters (Figure 7-7). Figure 7-7 shows the correlation between island length and island area, and between island width and island area.

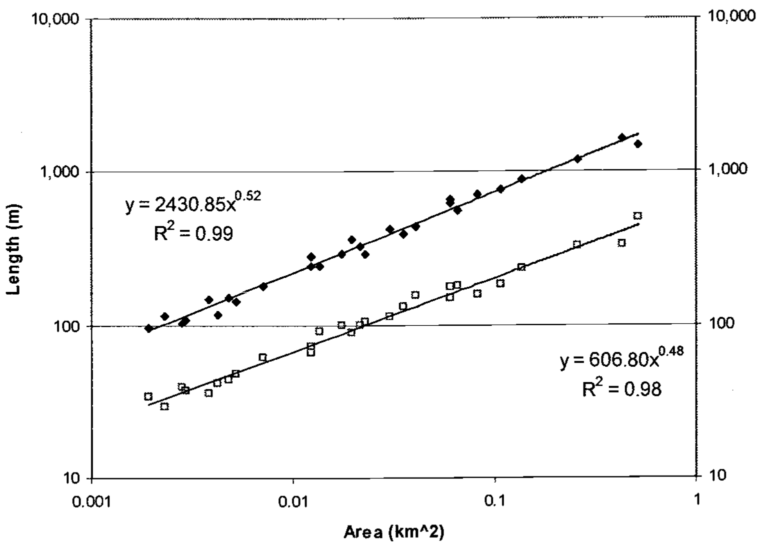

Figure 7-7. Size characteristics of Susquehanna River islands. Solid diamonds represent the island lengths; open squares the island widths.

The length/width ratio (aspect ratio) of the islands ranged between 2.7 and 4.9, with a mean value of 3.44. Figure 7-8 shows the relationship between the maximum lengths and widths of islands on the Susquehanna River.

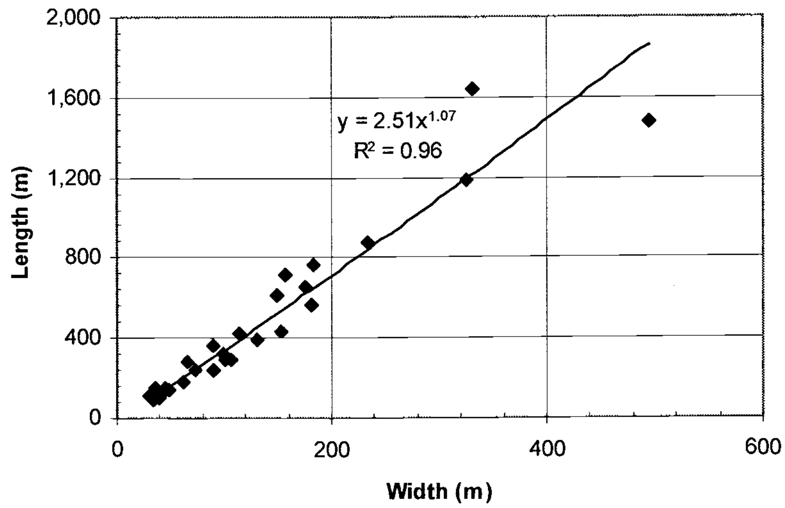

Figure 7-8. Length versus width comparisons of fluvial islands in the Susquehanna River.

Of the 28 analyzed islands on the Susquehanna, only 11 exhibit an x_m/L ratio between 0.6 and 0.7, and are therefore naturally comparable to the lemniscate shape. For these lemniscate islands, the average degree of elongation, k, was equal to 4.1 (Figure 7-9).

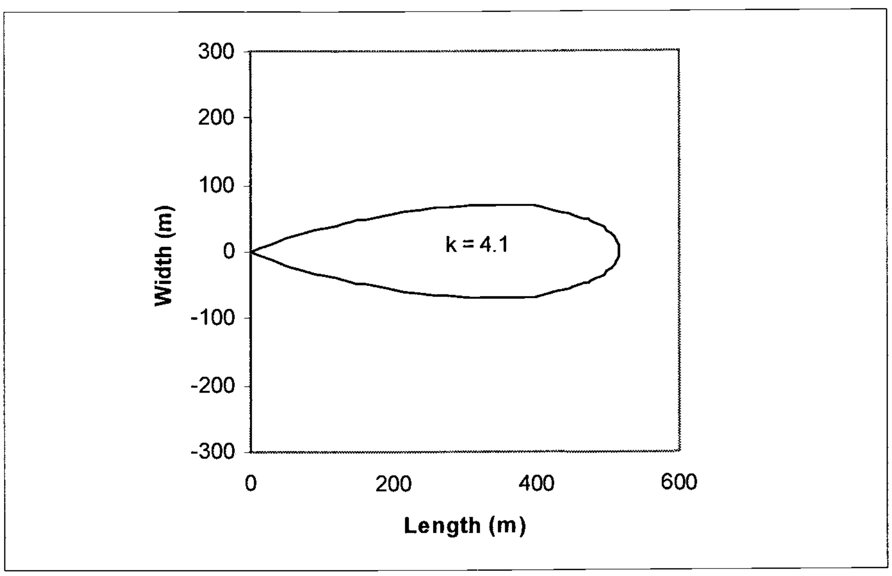

Figure 7-9. Equivalent average lemniscate for Susquehanna River islands.

<u>OHIO RIVER</u>

The Ohio River officially begins at the confluence of the Allegheny and Menongahela Rivers at Pittsburgh, Pennsylvania. It then flows 981 miles and drains 204,000 square miles before joining the Mississippi River near Cairo, Illinois. Except for the first few miles, the river drops with a fairly even gradient. The Ohio River was once narrow and winding, and studded with islands. However, a set of 50 locks and dams were built by 1929 (replaced by only 21 in the mid-1980's) transforming it into a stair-step cascade providing a minimum navigational depth of 9 feet throughout its length [Penn, 2001].

The suite of islands stretches the length of the river (river miles 932 – 35), which includes several large tributaries and dams (Figure 7-10). Several gaging stations with long-term records are located within the clusters of islands analyzed for this research (Table 7-3). Only one, however, operated a daily continuous sediment gaging station – Louisville. That gage collected sediment concentration data from October 1, 1979 through September 30, 1983.

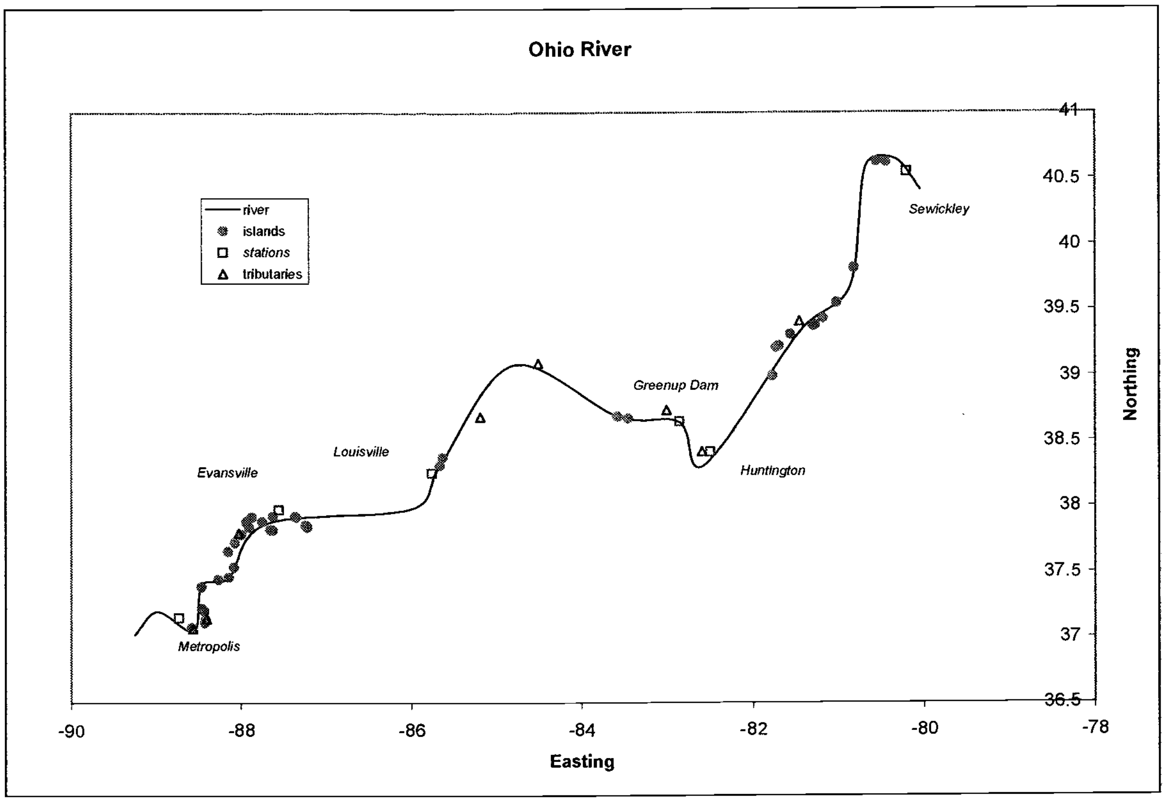

Figure 7-10. Sketch of Ohio River. Flow is to the west.

Table 7-3. Gaging station records along the Ohio River.

Gaging Station	Dates of Record	Number of Measurements	Average Daily Discharge (cfs)	Upstream Drainage Area (sq mi)
Metropolis, IL	4/1/1928 – present	27576	277,372	203,00
Evansville, IN	10/1/1940 – 9/30/1997	17096	166,480	Not given
Louisville, KY	1/1/1928 – present	27667	115,738	91,170
Greenup Dam	10/1/1968 – present	12783	88,348	62,000
Huntington, WV	9/1/1934 – 9/29/1986	16139	85,985	55,850
Sewickley, PA	10/1/1933 – present	25567	33,269	19,500

A total of 46 fluvial islands were analyzed on the Ohio River. Most of the islands are elongated in shape (i.e. lemniscate, elliptical, or lenticular), and have widths only somewhat less than the channel widths. The island lengths and widths span almost two orders of magnitude (Figure 7-11). There is good correlation between the islands' lengths and widths and their areas (Figure 7-11).

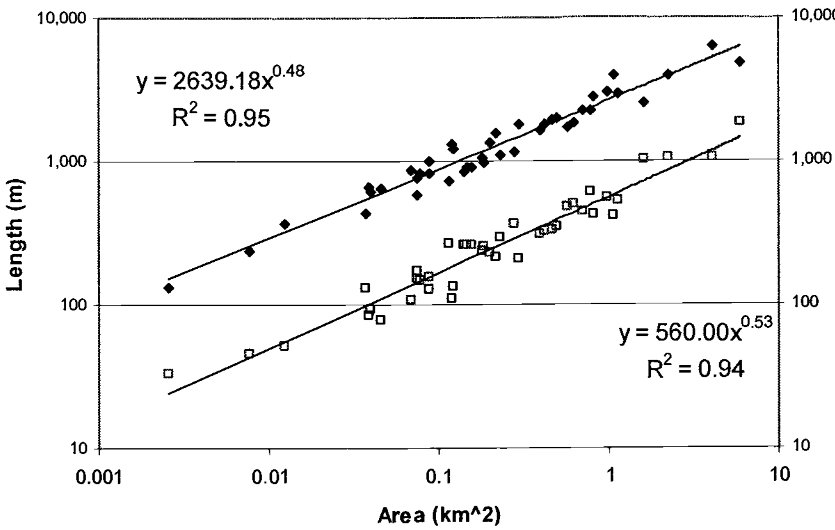

Figure 7-11. Size characteristics of Ohio River islands. Solid diamonds represent the island lengths; open squares the island widths.

The aspect ratios range from 2.5 to 9.4, with a mean value of 5.44. Figure 7-12 shows the relationship between the maximum lengths and widths of islands on the Ohio River.

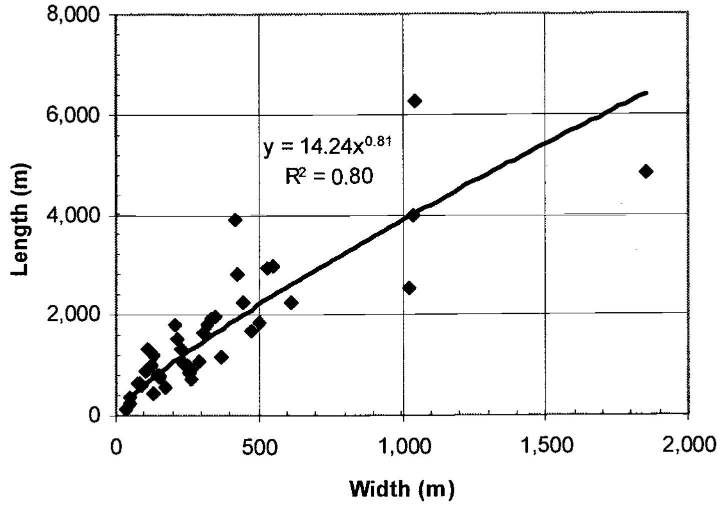

Figure 7-12. Length versus width comparisons of fluvial islands in the Ohio River.

Of the 46 analyzed islands on the Ohio, only 16 exhibit an x_m/L ratio between 0.6 and 0.7, and are therefore naturally comparable to the lemniscate shape. For these lemniscate islands, the average degree of elongation, k, was equal to 5.1 (Figure 7-13).

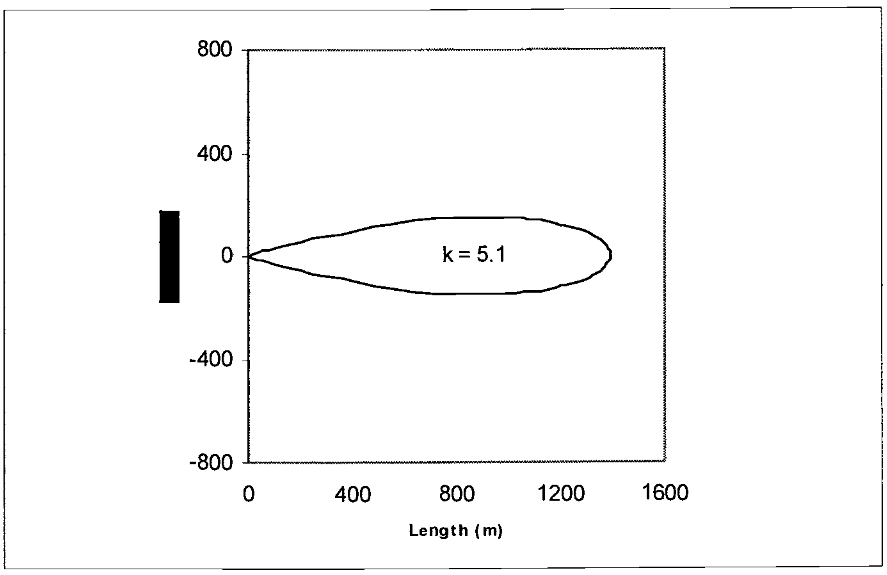

Figure 7-13. Equivalent average lemniscate for Ohio River islands.

TENNESSEE RIVER

The Tennessee River begins at the confluence of the French Broad and Holston creeks near Knoxville, Tennessee, and flows 650 miles to its confluence with the Ohio River at Paducah, Kentucky (Figure 7-14). When the Tennessee Valley Act (TVA) was passed by Congress in 1933, the once free-flowing river became "less a river than a chain of lakes" [Bartlett, 1984] by installing 25 dams along its length.

Most of the analyzed islands are located along a non-dammed stretch of the river near Savannah, Tennessee downstream of Pickwick Dam. A gaging station at Savannah has measured daily streamflow since October 1, 1930 (Table 7-4), and measured daily sediment concentration from December 1, 1934 through February 28, 1942.

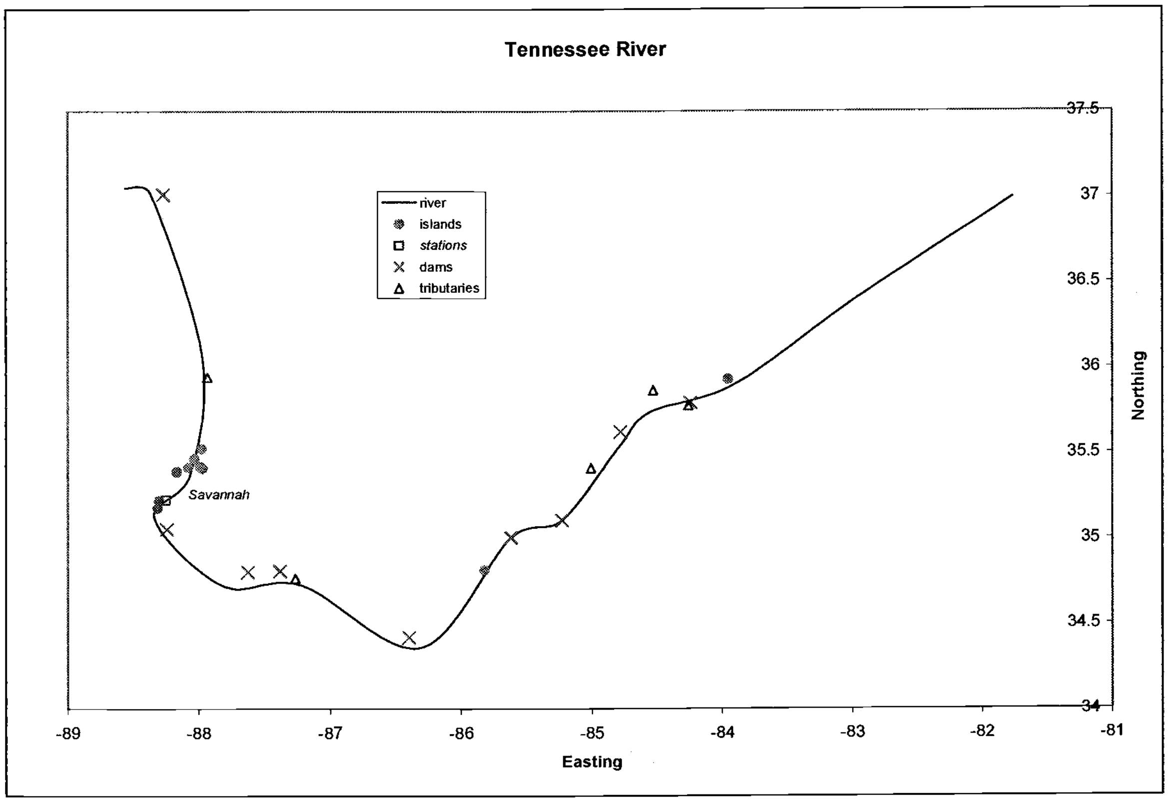

Figure 7-14. Sketch of Tennessee River. Flow is to the west.

Table 7-4. Gaging stations along the Tennessee River.

Gaging Station	Dates of Record	Number of Measurements	Average Daily Discharge (cfs)	Upstream Drainage Area (sq mi)
Savannah, TN	10/1/1930 – present	26663	54,630	33,140

A total of 12 fluvial islands were analyzed on the Tennessee River. The channel width ranged from about 600 to 1000 meters. Figure 7-15 shows the good correlation between the islands' lengths and widths and their areas.

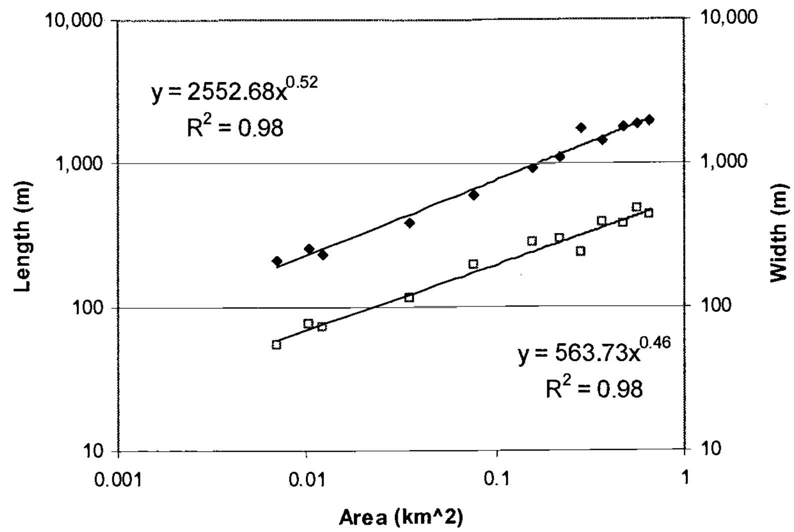

Figure 7-15. Size characteristics of Tennessee River islands. Solid diamonds represent the island lengths; open squares the island widths.

The aspect ratios of the islands ranged from 3.17 to 4.63, with a mean value of 3.8. Figure 7-16 shows the relationship between the maximum lengths and widths of islands on the Tennessee River.

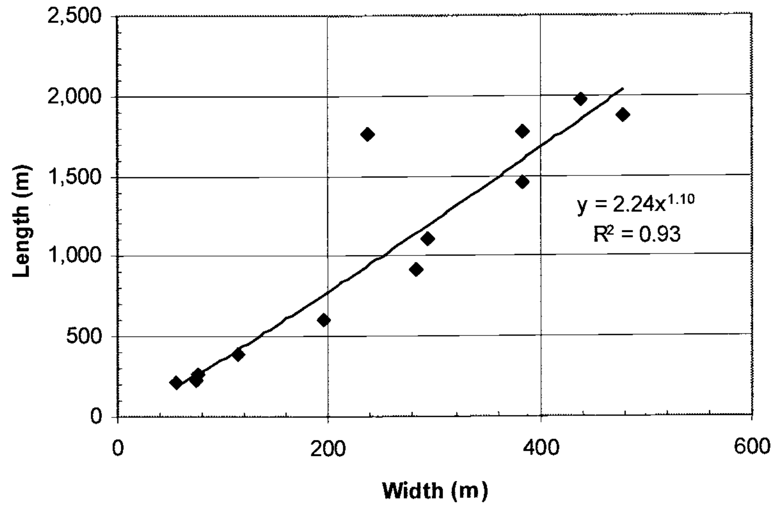

Figure 7-16. Length versus width comparisons of fluvial islands in the Tennessee River.

Of the 12 analyzed islands on the Ohio, only 5 exhibit an x_m/L ratio between 0.6 and 0.7, and are therefore naturally comparable to the lemniscate shape. For these lemniscate islands, the average degree of elongation, k, was equal to 4.0 (Figure 7-17).

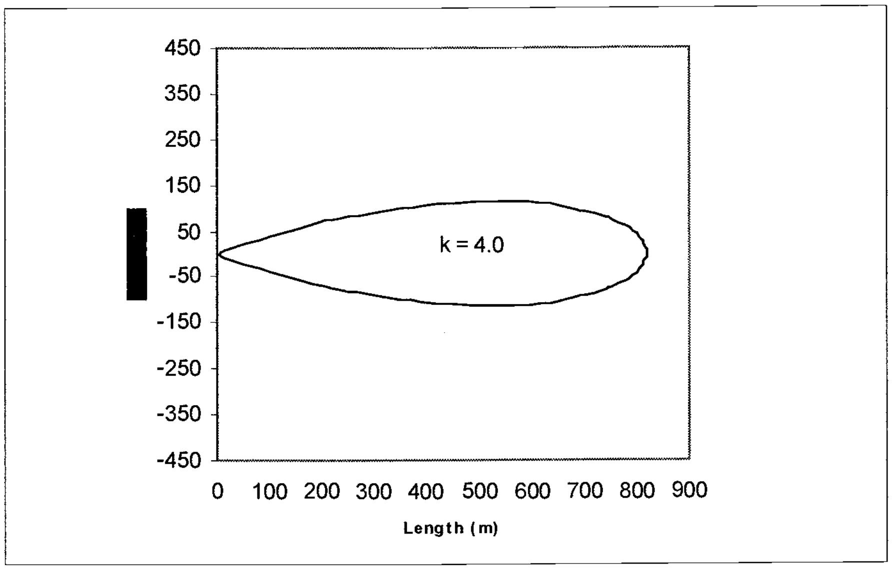

Figure 7-17. Equivalent average lemniscate for Tennessee River islands.

WISCONSIN RIVER

The Wisconsin River begins near the Wisconsin-Upper Michigan border at the Lac Vieux Desert (actually a shallow lake, not a desert). It then flows south/southwest for 430 miles until it joins the Mississippi River near Prairie du Chien, Wisconsin. The river has more than 50 hydroelectric power installations, but runs free, except for a dam at Sauk City, downstream of Portage, Wisconsin. Early lumbermen described the river as many-islanded and full of sharp twists and turns. An early explorer, Father Marquette, reported it as a wide, sandy river with numerous shoals and vine-covered small islands [Penn, 2001].

The islands on the Wisconsin River analyzed for this research all lie along the low-gradient, braided section downstream of Sauk City Dam (Figure 7-18). A gaging station is located at Muscoda, Wisconsin which has recorded daily streamflow measurements since October 1, 1913 (Table 7-5), and also measured daily sediment concentration values from July 1, 1975 through September 30, 1979.

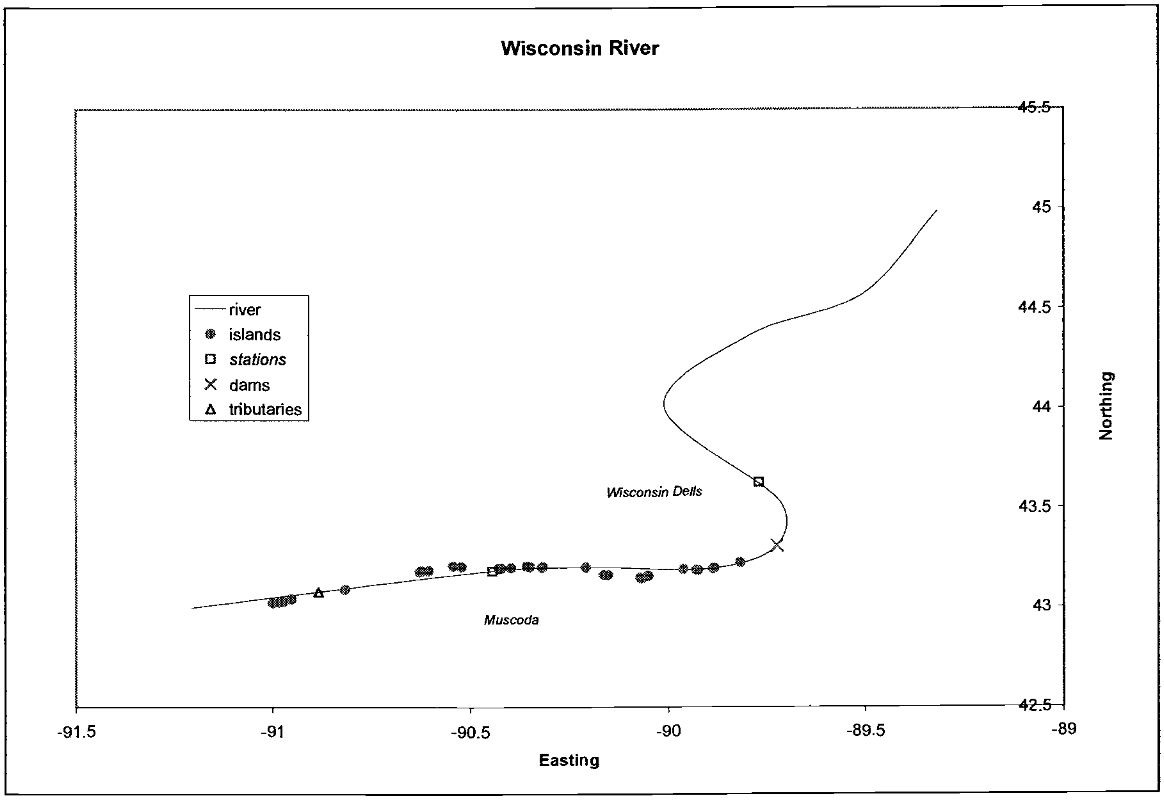

Figure 7-18. Sketch of Wisconsin River. Flow is to the west.

Table 7-5. Gaging station records along the Wisconsin River.

Gaging Station	Dates of Record	Number of Measurements	Average Daily Discharge (cfs)	Upstream Drainage Area (sq mi)
Muscoda, WI	10/1/1913 – present	32872	8,743	10,400
Wisconsin Dells, WI	10/1/1934 – present	25202	6,826	8,090

Thirty-three fluvial islands were analyzed along the Wisconsin River (Figure 7-19). All of the islands are vegetated.

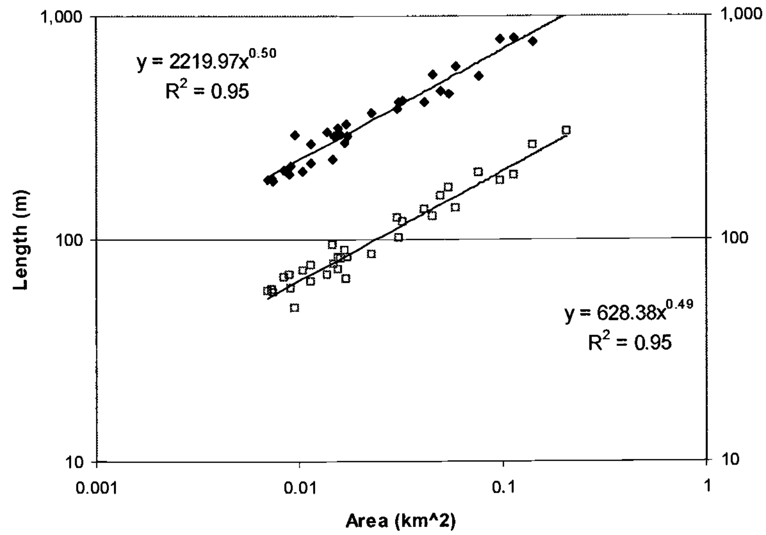

Figure 7-19. Size characteristics of Wisconsin River islands. Solid diamonds represent the island lengths; open squares the island widths.

The aspect ratios range from 2.41 to 5.96 with a mean value of 3.58. Figure 7-20 shows the relationship between the maximum lengths and widths of islands on the Wisconsin River.

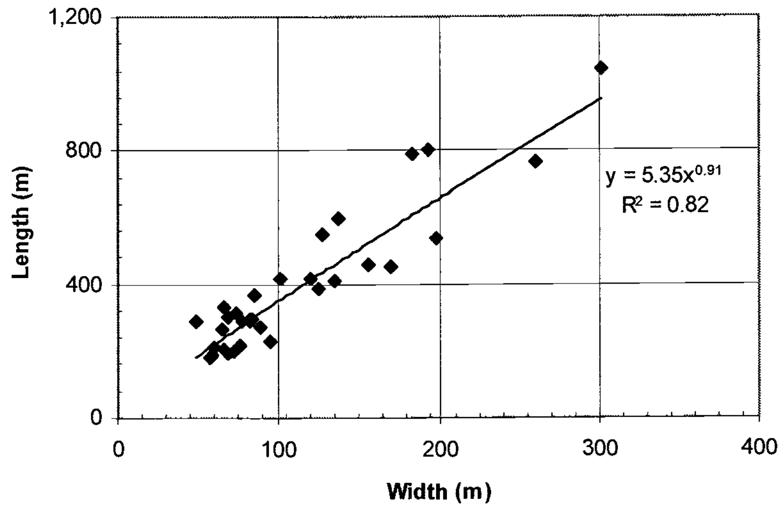

Figure 7-20. Length versus width comparisons of fluvial islands in the Wisconsin River.

Of the 33 analyzed islands on the Ohio, only 7 exhibit an x_m/L ratio between 0.6 and 0.7, and are therefore naturally comparable to the lemniscate shape. The low percentage of lemniscate-shaped islands is probably due to the braided nature of the river in the analyzed section. Islands in braided systems tend to exhibit more irregular shapes due to the effects of resulting asymmetrical flows [Komar, 1984]. For the lemniscate islands, the average degree of elongation, k, was equal to 3.8 (Figure 7-21).

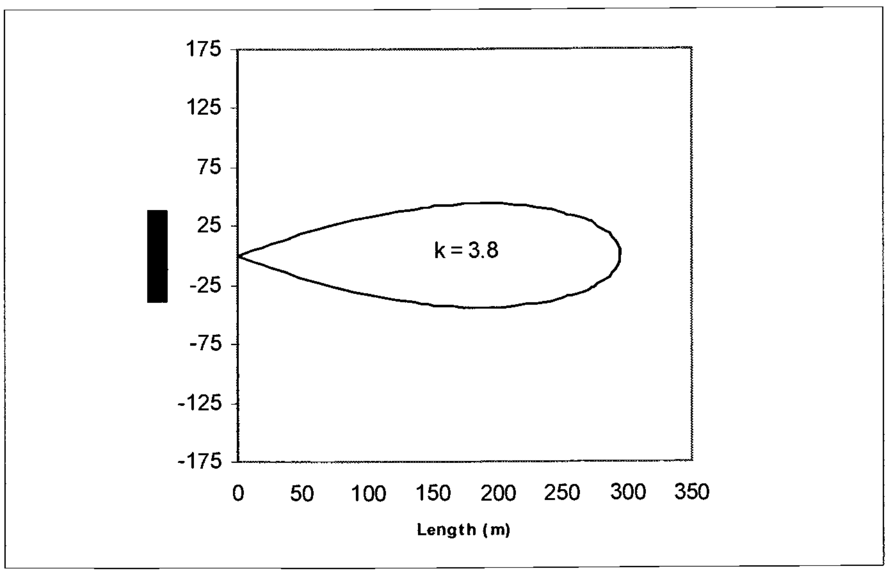

Figure 7-21. Equivalent average lemniscate for Wisconsin River islands.

Mississippi River

Even though the Ohio River adds more total streamflow and the Missouri River is longer, the Mississippi River is defined as the stream that starts at Lake Itasca in northwest Minnesota, and flows generally southward for 2,350 miles until it disgorges its massive volume into the Gulf of Mexico near New Orleans, Louisiana. In all, the total watershed encompasses an area over 1.2 million square miles. Officially, the U.S. Army Corps of Engineers (USACE) defines the mouth of the Ohio River as the division point between the upper and lower Mississippi valleys. The lower valley meanders through a vast alluvial plain that is heavily altered by humans. An immense levee system, which contains the river in its current course, was installed to prevent flooding of the growing population centers along the floodplain. In 1811, a massive earthquake struck near the town of New Madrid, Missouri and resulted in the reshaping of the Mississippi River by creating new fluvial island and destroying others [Penn, 2001].

Along the lower Mississippi River, downstream of the Ohio River, the islands in my dataset span the length of the river from its confluence with the Ohio to near its mouth – a stretch of 750 miles (Figure 7-22). Two long-term streamflow gaging stations operated at Vicksburg, Mississippi and Red River Landing, Louisiana (Table 7-6). The USGS also operated a long-term sediment gaging station at Red River Landing, Louisiana from October 1, 1949 through September 30, 1975. Two historically silty rivers join with the Mississippi in this stretch, the Arkansas and the Yazoo. Therefore, the sediment concentration data from Red River Landing may not accurately describe the conditions for the upper islands.

Along the middle Mississippi, between the Missouri and Ohio Rivers, most of the islands are located near Thebes and Chester, Illinois (Figure 7-22). Three islands are located in the upstream stretch near St. Louis, Missouri. All three of these cities have operated a streamflow gaging station (Table 7-5), as well as measuring daily sediment concentration values at sometime. No major tributaries or dams are located along this section of the river; however, numerous spur dikes have been installed on its banks, which may have an effect on sediment transport. The downstream trend in sediment concentration through this section of river seems to be decreasing. The gaging station at St. Louis recorded an average daily sediment concentration of 513 mg/L, the station at Chester, Illinois had an average of 423 mg/L, and the station at Thebes had a value of 404 mg/L for similar time periods. This is most likely due to the sediment trapping effects of the spur dikes along the river banks.

Along the upper Mississippi River, upstream of the Missouri River, all of the islands for this section are upstream of the Alton, Illinois gage and are centered around the Grafton, Illinois gage (Figure 7-22). These two gages are separated by 17 river miles and both began measuring daily streamflow on April 1, 1933 (Table 7-6). Both of these sites have also measured daily sediment concentration values, but the Grafton gage began collecting data the day after the Alton gage stopped. This leads me to believe that the USGS simply moved their operations to Grafton. Since there are no major tributaries or dams between these stations, I can combine the datasets into one. The combined time period for the sediment dataset ran from October 20, 1980 through September 30, 1992.

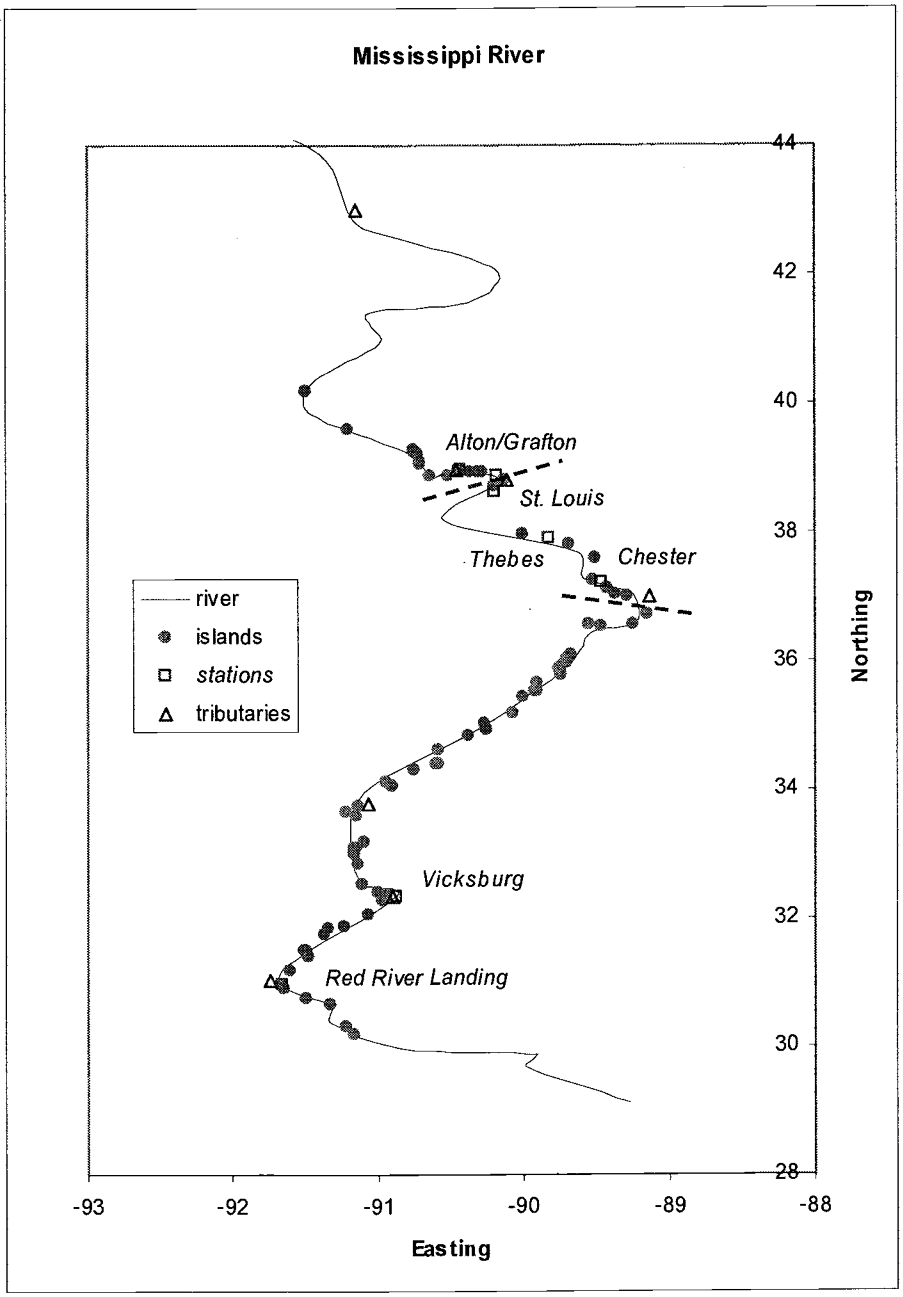

Figure 7-22. Sketch of Mississippi River. Flow is to the south. Red dashed lines represent distinctions between the Upper, Middle, and Lower sections of the river.

Table 7-6. Gaging station records along the Mississippi River.

Gaging Station	Dates of Record	Number of Measurements	Average Daily Discharge (cfs)	Upstream Drainage Area (sq mi)
Red River Landing	10/1/1928 – 11/25/1986	21240	1,520,000	Not given
Vicksburg, MS	10/1/1931 – 9/30/1998	24469	602,309	1,144,500
Thebes, IL	4/1/1930 – present	25020	206,662	713,200
Chester, IL	7/1/1942 – present	22372	206,627	708,600
St. Louis, MO	4/1/1933 – present	25750	189,930	697,000
Alton, IL	4/1/1933 – 9/30/1987	19207	105,058	171,500
Grafton, IL	4/1/1933 – present	25051	109,104	171,300

Along the upper Mississippi River, a total of 21 fluvial islands were analyzed over a stretch of almost 100 river miles. All of the islands have a smaller width than the channel width. The size characteristics of these islands are shown in Figure 7-23.

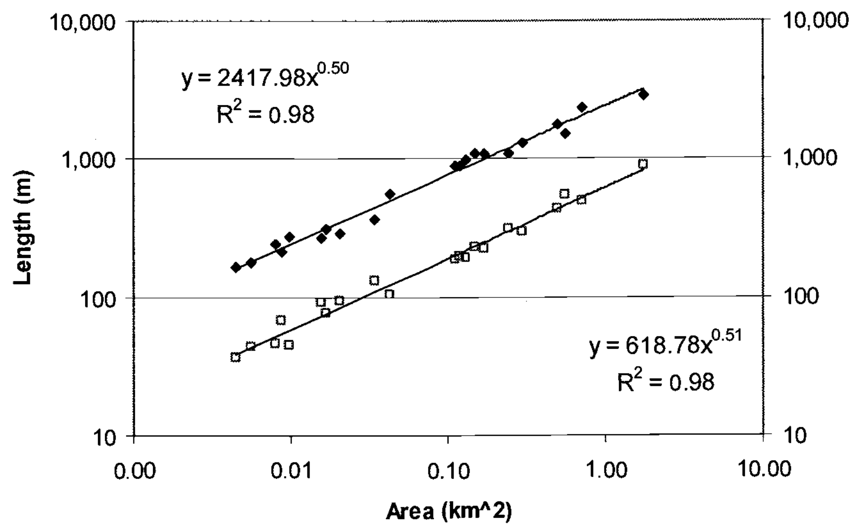

Figure 7-23. Size characteristics of Upper Mississippi River islands. Solid diamonds represent the island lengths; open squares the island widths.

The aspect ratios of the islands ranged from 2.7 to 6.1 with a mean value of 4.18. Figure 7-24 shows the relationship between the maximum lengths and widths of islands on the upper section of the Mississippi River.

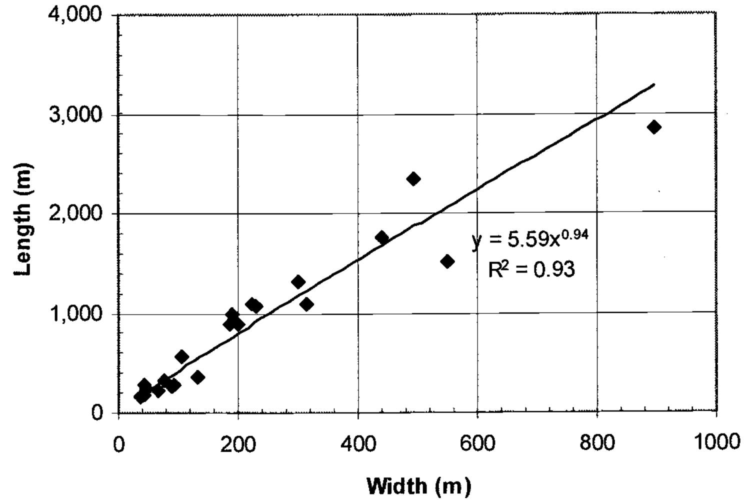

Figure 7-24. Length versus width comparisons of fluvial islands in the upper Mississippi River.

Within the middle section of the Mississippi River, only 10 fluvial islands were analyzed. Several of these islands exhibit a width greater than the normal channel width. The size characteristics for each of the islands are shown in Figure 7-25.

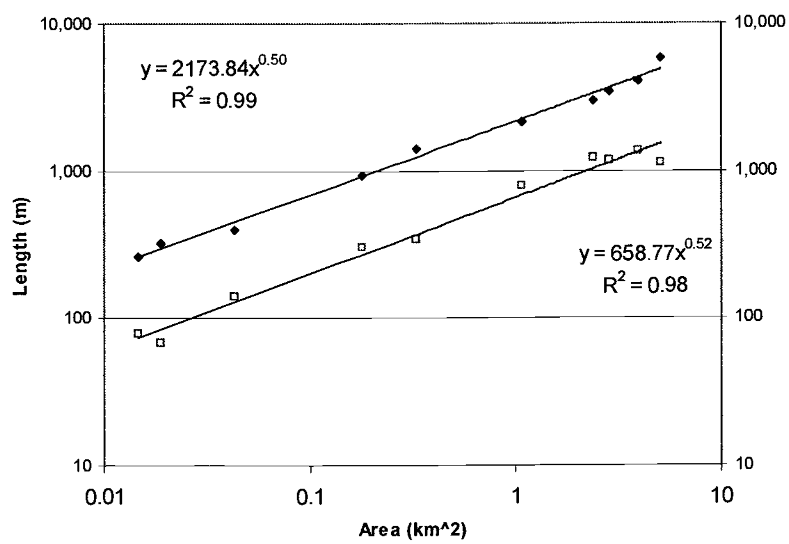

Figure 7-25. Size characteristics of Middle Mississippi River islands. Solid diamonds represent the island lengths; open squares the island widths.

The aspect ratios ranged from 2.5 to 5.3 with a mean value of 3.45, appreciably less than the mean value for the upper section of the river. Figure 7-26 shows the relationship between the maximum lengths and widths of islands on the middle section of the Mississippi River.

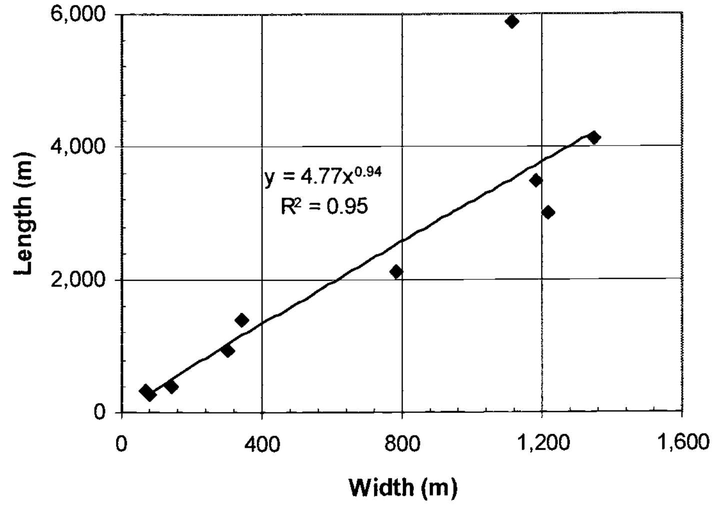

Figure 7-26. Length versus width comparisons of fluvial islands in the middle Mississippi River.

Figure 7-27 shows the size characteristics for the 52 fluvial islands analyzed along the lower Mississippi River. Most of these islands exhibit smaller widths than the channel width.

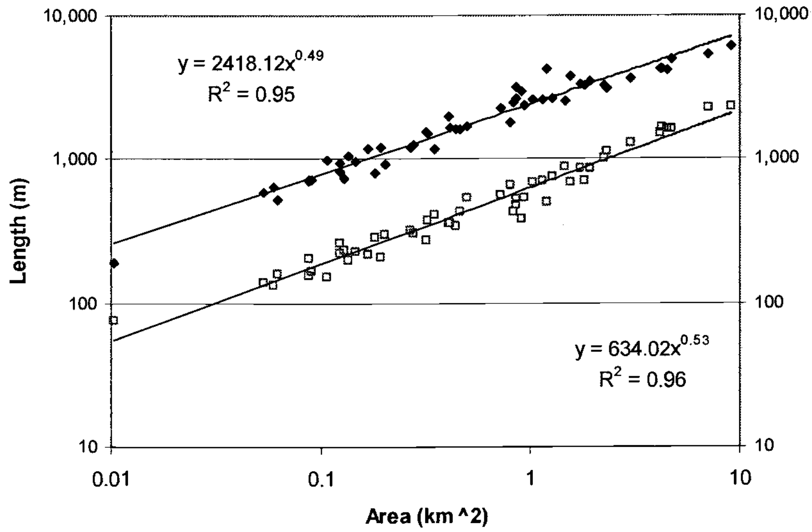

Figure 7-27. Size characteristics of Lower Mississippi River islands. Solid diamonds represent the island lengths; open squares the island widths.

The mean aspect ratio of these islands is quite similar to that of the upper section (mean value of 4.13, with a range between 2.6 and 8.6). Figure 7-28 shows the relationship between the maximum lengths and widths of islands on the lower section of the Mississippi River.

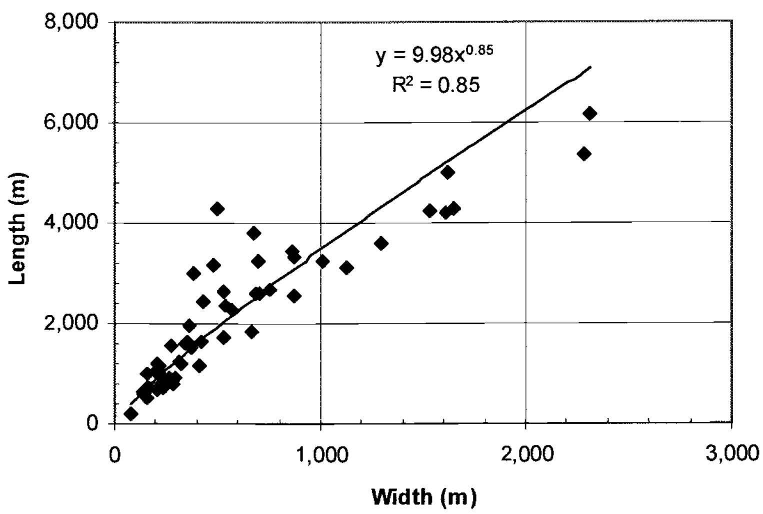

Figure 7-28. Length versus width comparisons of fluvial islands in the lower Mississippi River.

Of the 83 total analyzed islands on the Mississippi, only 30 exhibit an x_m/L ratio between 0.6 and 0.7, and are therefore naturally comparable to the lemniscate shape. For these lemniscate islands, the average degree of elongation, k, was equal to 4.4 (Figure 7-29).

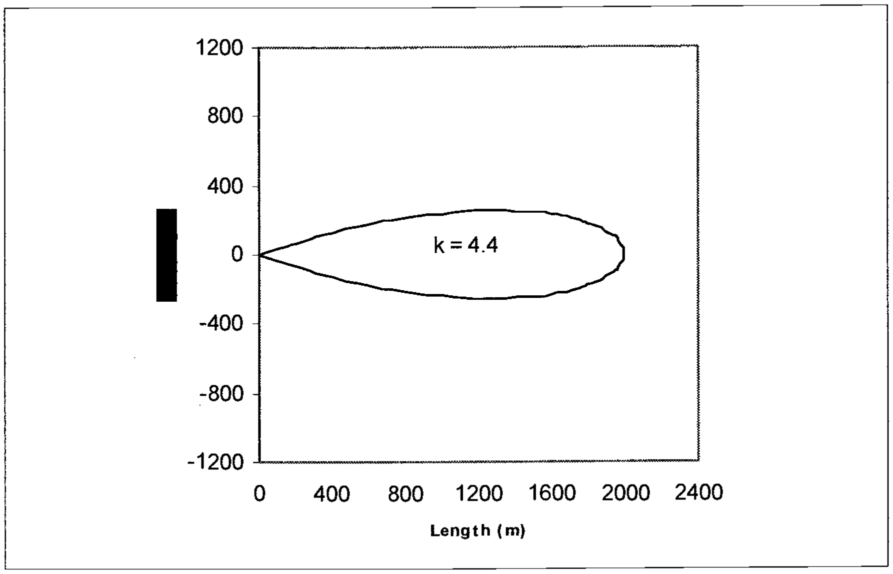

Figure 7-29. Equivalent average lemniscate for Mississippi River islands.

PLATTE RIVER

The main channel of the Platte River is only 310 miles long from the junction of the north and south branches to its confluence with the Missouri River, near Plattsmouth, Nebraska. The North Platte River adds another 600 miles of river, while the South Platte River is 450 miles long. The river's name comes from the French word for 'flat', which is a good descriptor of this muddy, braided stream [Bartlett, 1984]. Early travelers referred to it as the mile-wide, inch-deep river. No dams exist on the mainstem, but many have been installed on the North and South branches, which heavily control the discharge of the mainstem. The Platte River is an important stopover for migratory fowl, including Sandhill and whooping cranes, Canadian geese, and several species of duck. Spits of land form bars and islands on which these birds rest, feed, and mate. The upstream dams reduce the discharge enough that the total island area, and hence migratory bird habitat, has been decreasing [Penn, 2001].

The islands on the Platte River analyzed in this research are located in the low-gradient, braided section downstream of the Loup River (Figure 7-30). There are three gaging stations located in this section that have recorded daily streamflows through the present time (Table 7-7). No gaging station along the Platte River has ever collected daily continuous sediment concentration values. However, the USGS collected 418 instantaneous sediment concentration measurements near Louisville, Nebraska, which is located near the analyzed islands, from between January 15, 1973 and September 19, 2003.

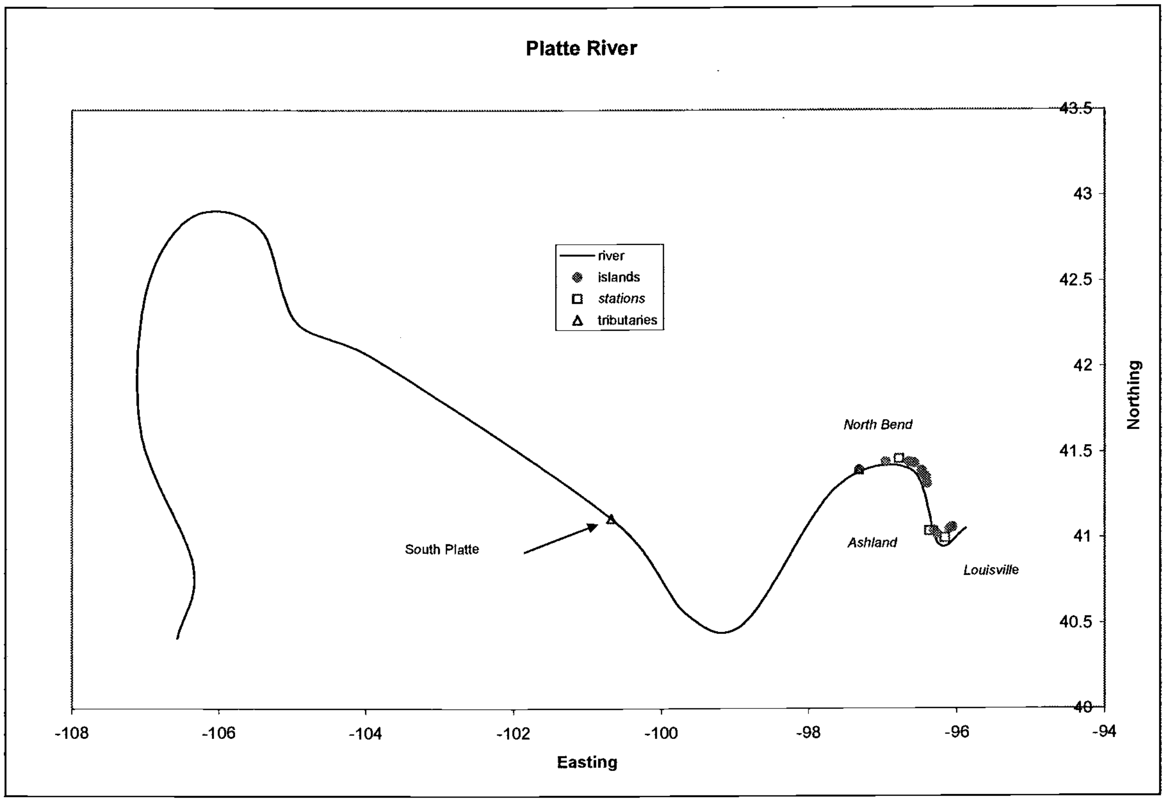

Figure 7-30. Sketch of Platte River. Flow is to the east.

Table 7-7. Gaging station records along the Platte River

Gaging Station	Dates of Record	Number of Measurements	Average Daily Discharge (cfs)	Upstream Drainage Area (sq mi)
Louisville, NE	6/1/1953 – present	18394	7,026	85,329
Ashland, NE	9/1/1928 – present	17266	5,612	84,200
North Bend, NE	4/1/1949 – present	19906	4,610	70,400

The size characteristics for the 15 fluvial islands analyzed along the Platte River are shown in Figure 7-31. All the islands are vegetated and are much less wider than the channel widths. The aspect ratios range from 2.9 to 5.7 with a mean value of 4.09.

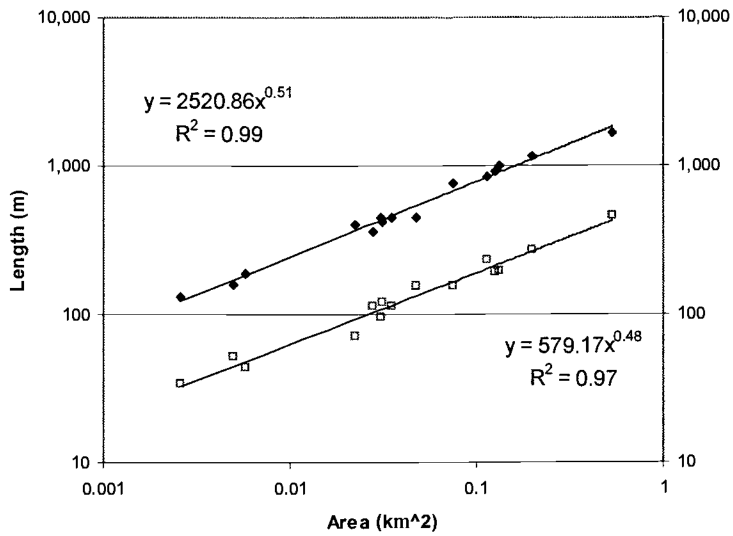

Figure 7-31. Size characteristics of Platte River islands. Solid diamonds represent the island lengths; open squares the island widths.

The aspect ratios range from 2.9 to 5.7 with a mean value of 4.09. Figure 7-32 shows the relationship between the maximum lengths and widths of islands on the Platte River.

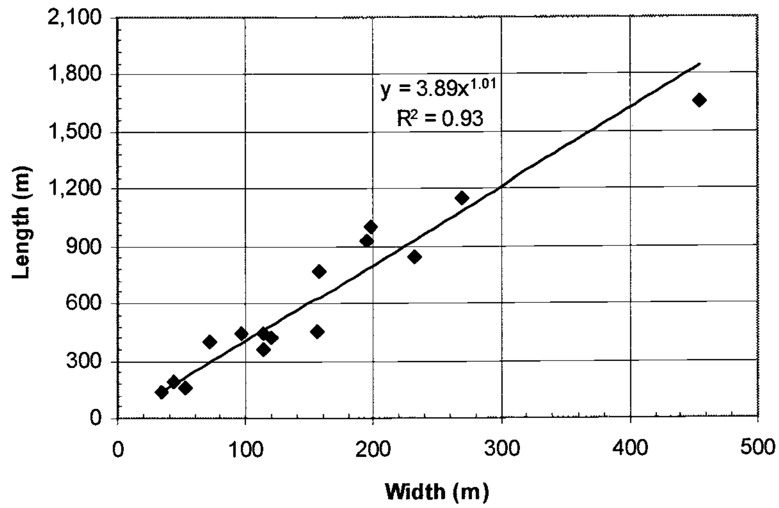

Figure 7-32. Length versus width comparisons of fluvial islands in the Platte River.

Of the 15 total analyzed islands on the Platte, only 5 exhibit an x_m/L ratio between 0.6 and 0.7, and are therefore naturally comparable to the lemniscate shape. For these lemniscate islands, the average degree of elongation, k, was equal to 4.2 (Figure 7-33).

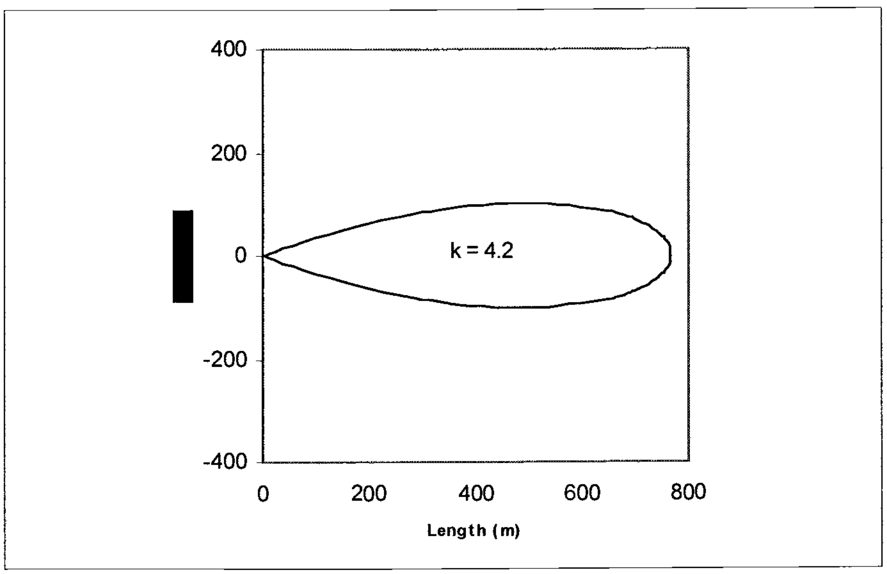

Figure 7-33. Equivalent average lemniscate for Platte River islands.

RED RIVER OF THE SOUTH

The Red River officially starts at the confluence of the North Fork and Prairie Dog Town Creek near Vernon, Texas. After flowing generally east-southeast for 1,300 miles, the flow then splits at its mouth between the Atchafalaya and the Mississippi rivers. The name comes from the color it acquires as it erodes silt from the red sandstone hills in its upper reaches. Many dams cross its pathway, including Denison Dam, which creates Lake Texoma, one of the largest reservoirs in the country. For much of its upper reach, it forms the border between Oklahoma and Texas, and in one the rare cases of this, the south bank, not some median distance, is the official border [Bartlett, 1984]. As the river enters Louisiana, it becomes a swampy, hummocky, slow-moving stream, which is dredged by the USACE to provide navigation as far upstream as Shreveport, Louisiana [Penn, 2001].

All but one of the analyzed islands are located upstream of Shreveport, Louisiana and downstream of the Washita River confluence (Figure 7-34). Several dams are also located through this section. Three relevant gaging stations have recorded daily streamflows (Table 7-8), and the gage at Shreveport also measured daily continuous sediment concentration from October 1, 1979 through August 18, 1982.

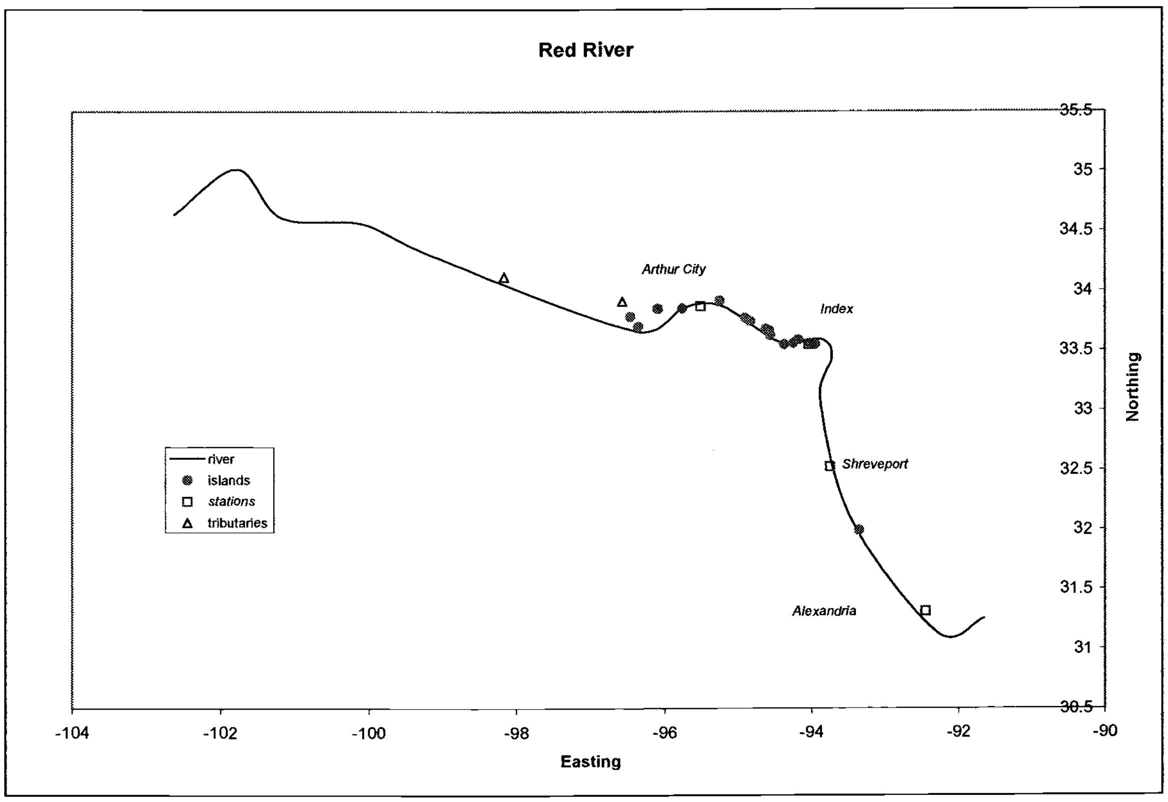

Figure 7-34. Sketch of the Red River of the South. Flow is to the east.

Table 7-8. Gaging station records along the Red River.

Gaging Station	Dates of Record	Number of Measurements	Average Daily Discharge (cfs)	Upstream Drainage Area (sq mi)
Alexandria, LA	10/1/1928 – 9/30/1983	20088	30,868	67,500
Shreveport, LA	8/1/1928 – 9/30/1983	20149	24,156	60,613
Index, AR	10/1/1936 – present	24471	13,134	48,030
Arthur City, TX	10/1/1905 – present	26642	9,196	44,531

A total of 19 fluvial islands were analyzed along the Red River, and most of these are unvegetated mid-channel sandbars. The size relationships (Figure 7-35) and aspect ratios, however, agree well with relationships of the vegetated island datasets on other rivers.

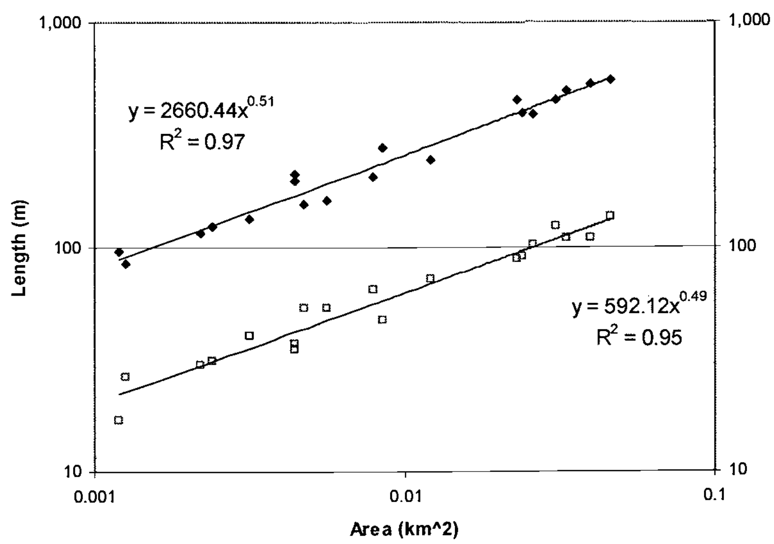

Figure 7-35. Size characteristics of Red River islands. Solid diamonds represent the island lengths; open squares the island widths.

The aspect ratios range from 2.9 to 6.0 with a mean value of 4.22. Figure 7-36 shows the relationship between the maximum lengths and widths of islands on the Red River.

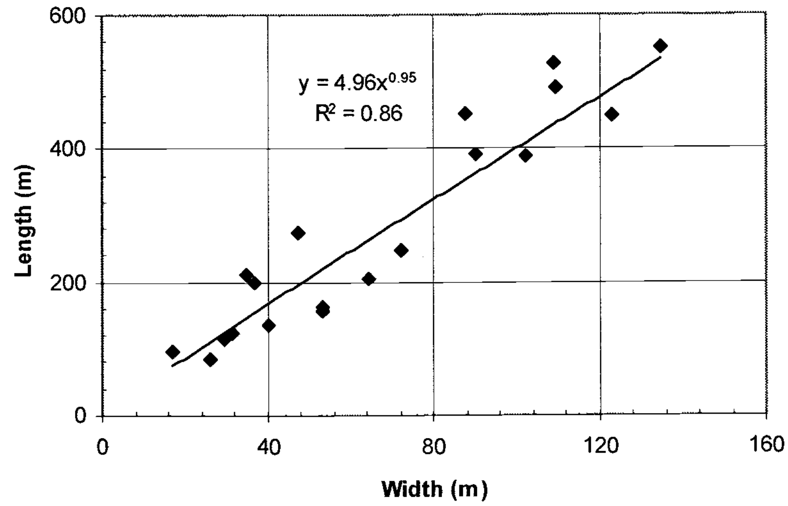

Figure 7-36. Length versus width comparisons of fluvial islands in the Red River.

Of the 19 total analyzed islands on the Red River, only 5 exhibit an x_m/L ratio between 0.6 and 0.7, and are therefore naturally comparable to the lemniscate shape. For these lemniscate islands, the average degree of elongation, k, was equal to 4.7 (Figure 7-37).

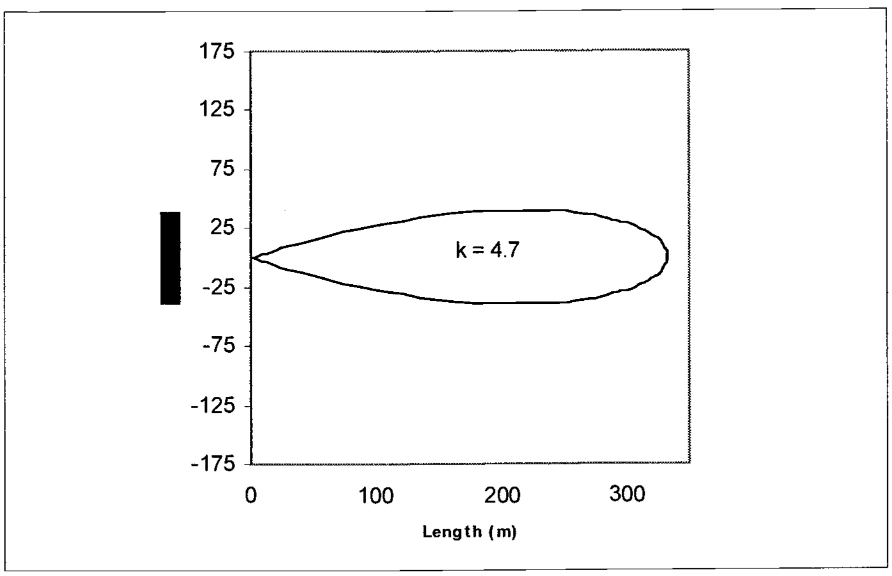

Figure 7-37. Equivalent average lemniscate for Red River islands.

COLORADO RIVER

Although the Green River carries the most flow, the Colorado is designated as the stream that starts at Grand Lake in northwest Colorado before it joins with the Green River and courses 1,400 miles through six states and empties into the Gulf of Lower Mexico. The river is heavily silt-laden, giving it a reddish color and hence its name from the Spanish word for 'red'. The Colorado is the lifeline for an arid section of the country [Bartlett, 1984]. Many dams, including the two largest reservoirs in the nation – Lake Mead and Lake Powell, trap water for irrigation and drinking purposes for the surrounding large cities, such as Las Vegas, Phoenix, and Los Angeles. In fact, so much of the flow is dammed up that after it flows past the Morelos Dam in Mexico, it is a tiny braided trickle [Penn, 2001].

Most of the islands in my data set are located downstream of Headrock Gate Dam, while another set is located upstream of Lake Powell (Figure 7-38). Two dams, Laguna and Imperial, interrupt the lower suite of islands. There are no long-term streamflow gaging stations located upstream of Imperial Dam and downstream of Headrock Gate Dam to give accurate flow characteristics for the islands located within this section. Streamflow gaging stations, however, are located near the downstream set of islands (Table 7-9). The Topock station gathered daily sediment concentration data for between October 1, 1934 and March 31, 1939; however two dams are located between the Topock station and the furthest upstream analyzed island.

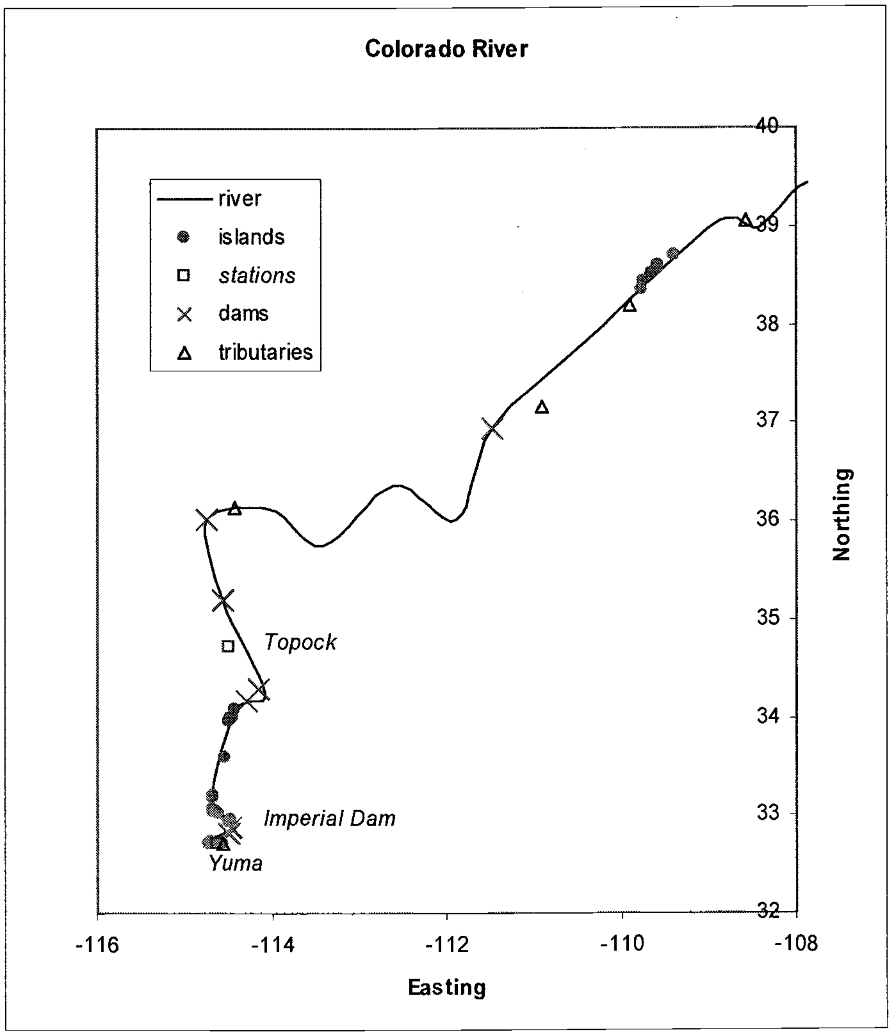

Figure 7-38. Sketch of Colorado River. Flow is to the southwest.

Table 7-9. Gaging station records along the Colorado River.

Gaging Station	Dates of Record	Number of Measurements	Average Daily Discharge (cfs)	Upstream Drainage Area (sq mi)
Yuma, AZ	1/1/1904 – 11/1/1983	22322	13,844	242,900
ab. Imperial Dam	7/13/1934 – present	12863	10,799	188,500
Topock, AZ	2/1/1917 – 9/30/1982	23983	14,878	176,300

The size characteristics of all 32 fluvial islands analyzed on the Colorado River are shown in Figure 7-39. The channel width ranges from less than 100 meters downstream of Laguna Dam to almost 300 meters upstream of Glen Canyon Dam. Most of the islands have a width much less than the channel width.

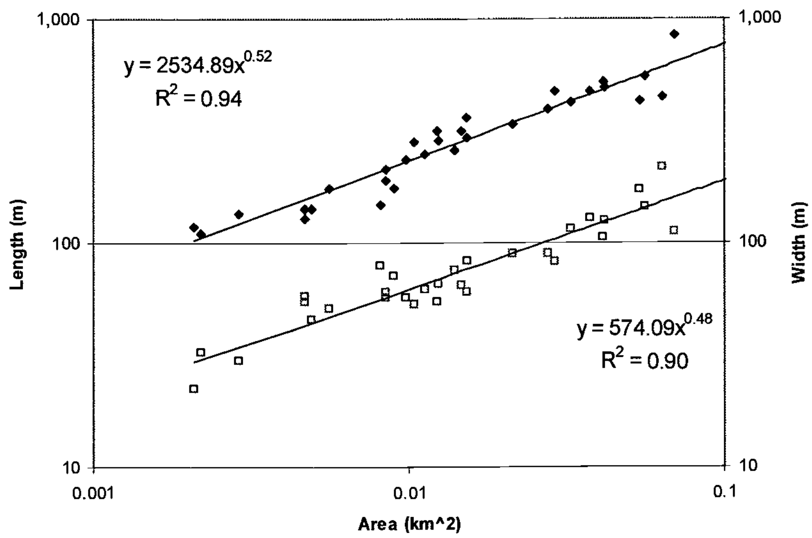

Figure 7-39. Size characteristics of Colorado River islands. Solid diamonds represent the island lengths; open squares the island widths.

The aspect ratios range from 1.9 to 7.6 with a mean value of 3.98. Figure 7-40 shows the relationship between the maximum lengths and widths of islands on the Colorado River.

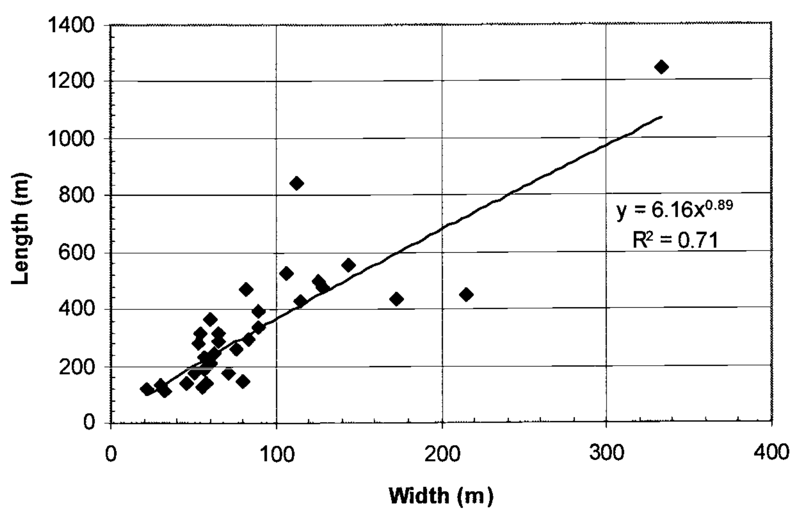

Figure 7-40. Length versus width comparisons of fluvial islands in the Colorado River.

Of the 32 total analyzed islands on the Colorado, only 13 exhibit an x_m/L ratio between 0.6 and 0.7, and are therefore naturally comparable to the lemniscate shape. For these lemniscate islands, the average degree of elongation, k, was equal to 4.8 (Figure 7-41).

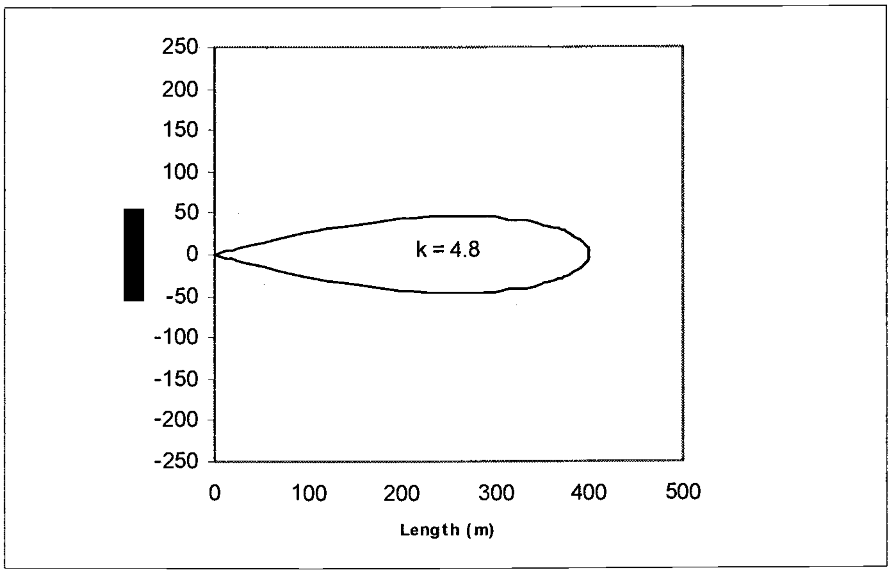

Figure 7-41. Equivalent average lemniscate for Colorado River islands.

<u>SACRAMENTO RIVER</u>

The Sacramento River starts at a small lake on Mt. Eddy in the Sierra Nevadas. It then flows 320 miles southward, until it joins the San Joaquin River at Suisan Bay, an eastward extension of San Francisco Bay. Several dams have been built in its channels, including Oroville Dam, the largest earth-fill dam in the country. The lower section of the river is not naturally navigable; hence, the Sacramento Deep Water Channel was built parallel to the mainstem [Penn, 2001].

All of the analyzed islands on the Sacramento River are located between the towns of Red Bluff and Colusa, California (Figure 7-42). No major tributaries or dams are present in this section. Within this section, there have been four long-term streamflow gaging stations (Table 7-10), each of which have also recorded daily sediment concentration values for some span of time.

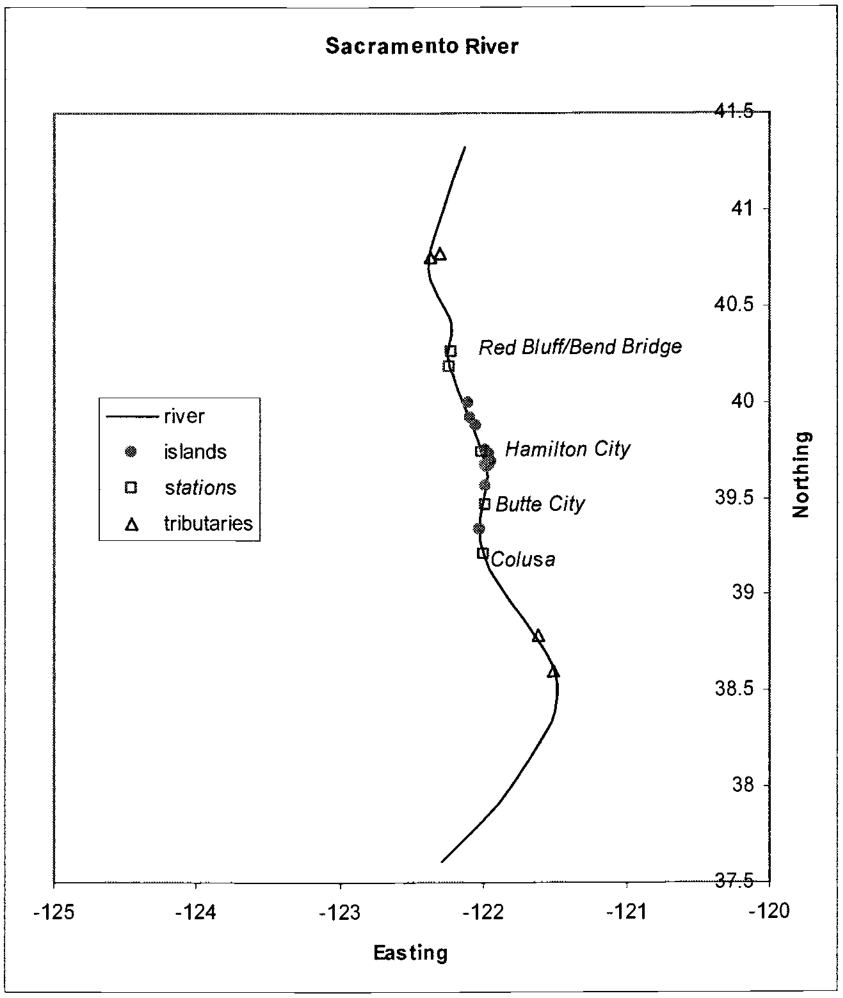

Figure 7-42. Sketch of Sacramento River. Flow is to the south.

Table 7-10. Gaging station records along the Sacramento River.

Gaging Station	Dates of Record	Number of Measurements	Average Daily Discharge (cfs)	Upstream Drainage Area (sq mi)
Colusa, CA	4/11/1921 – present	26541	10,517	12,090
Butte City, CA	10/1/1933 – 6/30/1995	20727	13,128	12,075
Hamilton City, CA	4/21/1945 – 10/2/1980	12793	12,409	10,833
Bend Bridge nr Red Bluff, CA	10/1/1891 – present	40907	12,003	8,900

A total of 12 fluvial islands were analyzed on the Sacramento River, most of them non-vegetated. They all exhibit smaller widths than the channel width. The relationships between each island's area and its length and width are shown in Figure 7-43.

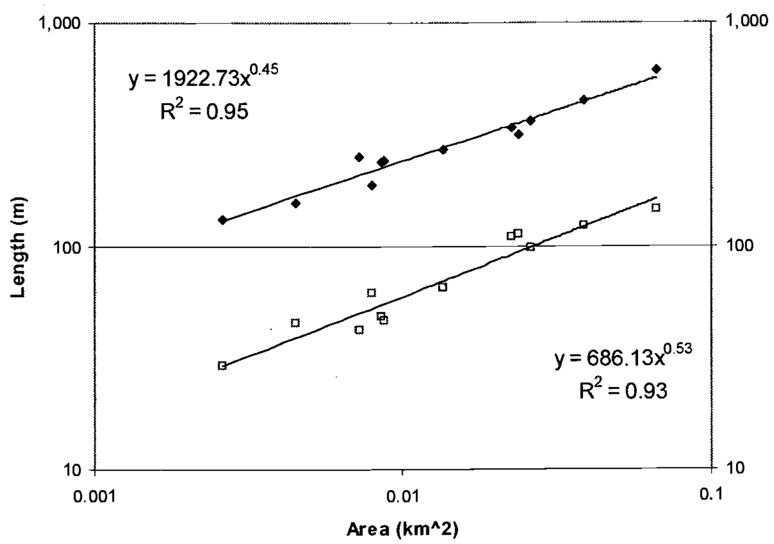

Figure 7-43. Size characteristics of Sacramento River islands. Solid diamonds represent the island lengths; open squares the island widths.

The aspect ratios ranged from 2.8 to 6.0 with a mean value of 4.07. Figure 7-44 shows the relationship between the maximum lengths and widths of islands on the Sacramento River.

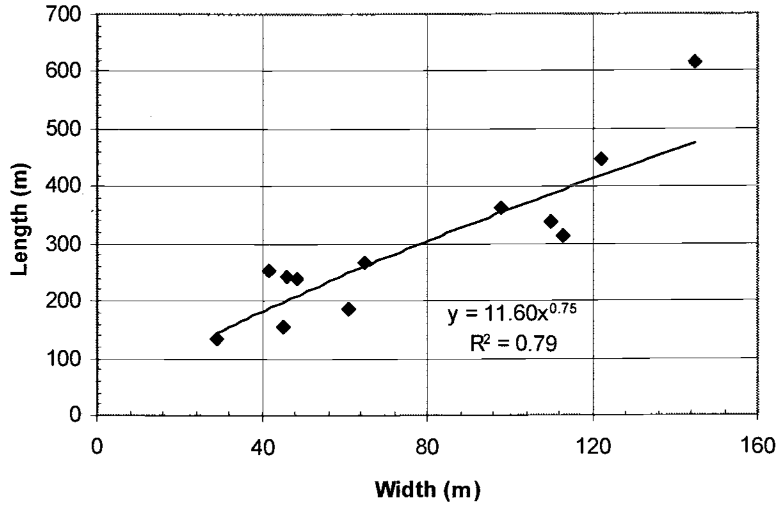

Figure 7-44. Length versus width comparisons for fluvial islands in the Sacramento River.

Of the 12 total analyzed islands on the Sacramento, only 3 exhibit an x_m/L ratio between 0.6 and 0.7, and are therefore naturally comparable to the lemniscate shape. For these lemniscate islands, the average degree of elongation, k, was equal to 4.0 (Figure 7-45).

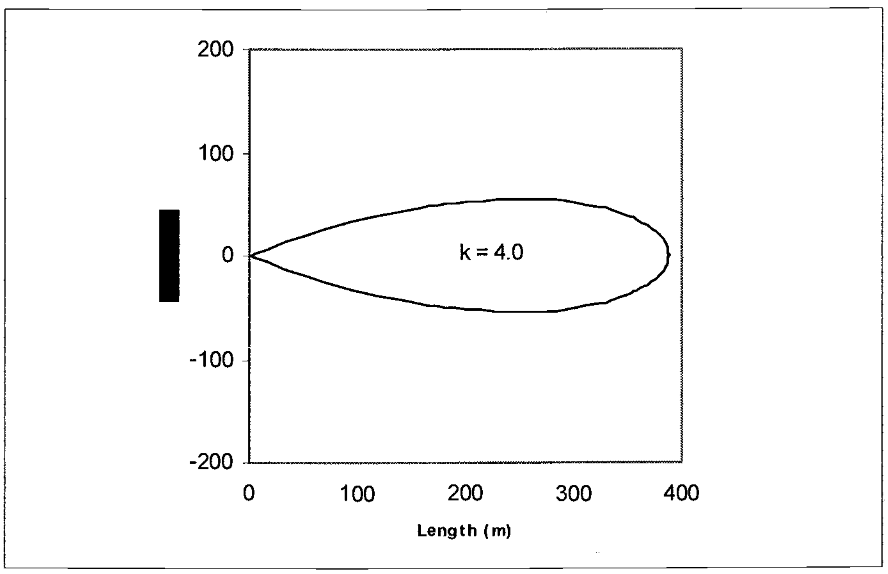

Figure 7-45. Equivalent average lemniscate for Sacramento River islands.

SNAKE RIVER

The Snake River's headwater can be traced up to a plain in Yellowstone Park that provides water to both the west-flowing Snake River and the east-flowing Yellowstone River. It has a total length of 1,038 miles and drains over 100,000 square miles. It joins the Columbia River, of which it is the largest tributary, near Pasco, Washington. Even for all the 25 dams that are emplaced along the river, it still runs free for about half of its length. These dams, however, are excellent sediment traps, so much so that the release flows are "hungry" and erode downstream beaches, islands, and pool-riffle systems [Penn, 2001]. About 14,500 years ago, a vast inland sea centered on present-day Utah, broke one of its northern banks and catastrophically emptied some of its waters through the Snake River Valley. This extreme flood event created islands made up of very coarse material that is not erodible by contemporary flood levels [O'Connor, 1993].

Most of the analyzed islands along the Snake River are located between the Brownlee and the CJ Strike Dams, but a handful of other islands are located downstream of Hells Canyon Dam (Figure 7-46). Long-term streamflow records exist for several gaging stations along this section (Table 7-11). The USGS has not operated a sediment gaging station anywhere on the Snake River; however, it has collected 97 instantaneous sediment concentration measurements from August 1, 1969 through September 3, 2003 at Weiser, Idaho, which is located near most of the analyzed islands.

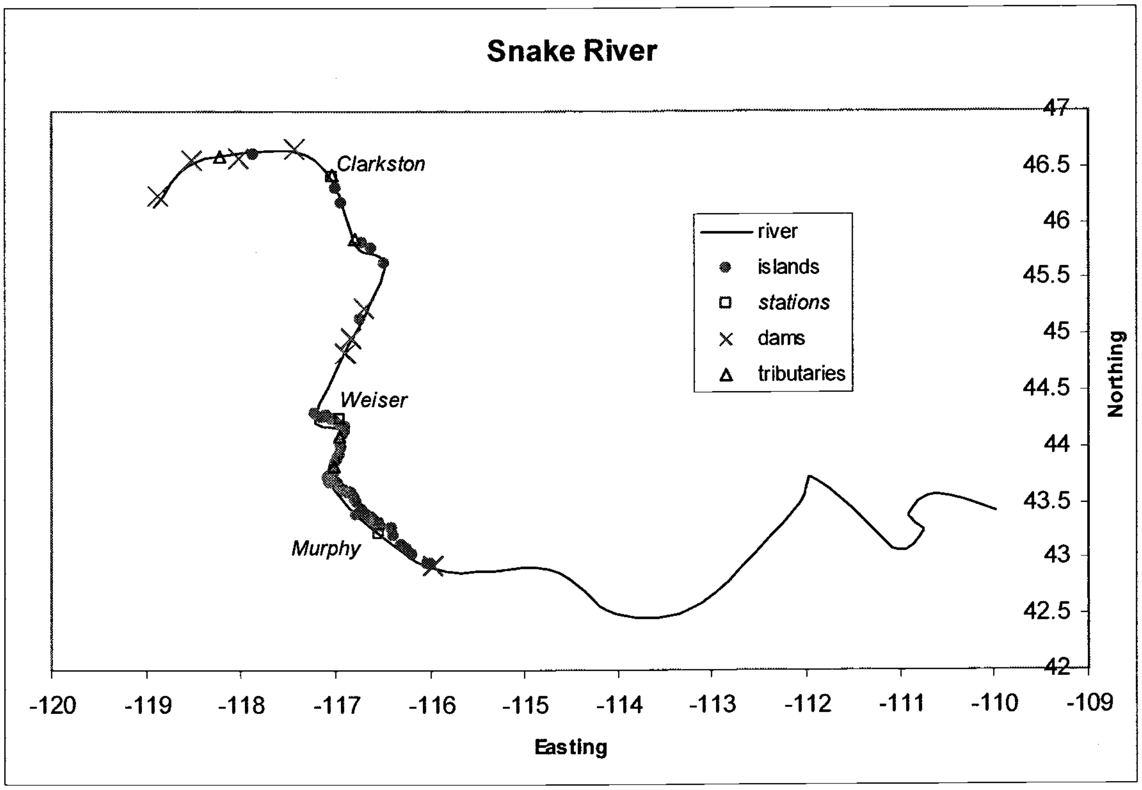

Figure 7-46. Sketch of Snake River. Flow is to the west.

Table 7-11. Gaging station records along the Snake River.

Gaging Station	Dates of Record	Number of Measurements	Average Daily Discharge (cfs)	Upstream Drainage Area (sq mi)
Clarkston, ID	10/1/1915 – 1/10/1973	18791	50,094	103,200
Weiser, ID	10/1/1910 – present	33968	18,057	69,200
Murphy, ID	8/29/1912 – present	32977	10,979	41,900

The dataset for the Snake River includes the greatest number of fluvial islands, 80, than other river sections. There still exist strong correlations between the island's area and its length and width (Figure 7-47).

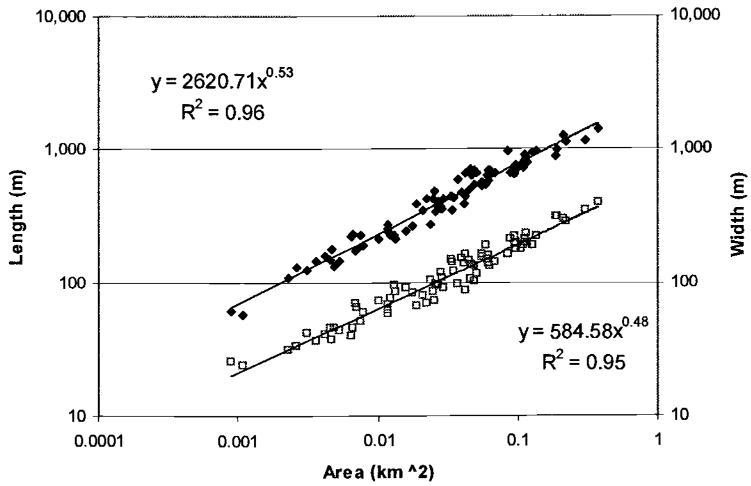

Figure 7-47. Size characteristics of Snake River islands. Solid diamonds represent the island lengths; open squares the island widths.

The aspect ratios ranged from 2.4 to 7.6 with a mean value of 3.94. Figure 7-48 shows the relationship between the maximum lengths and widths of islands on the Snake River.

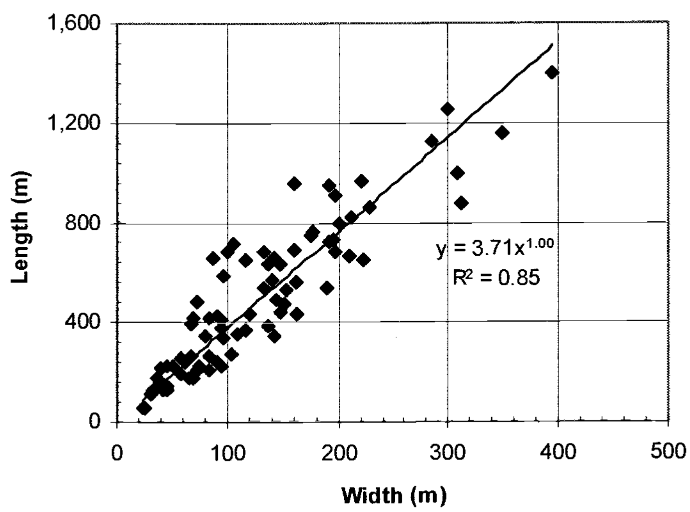

Figure 7-48. Length versus width comparisons for fluvial islands in the Snake River.

Of the 80 total analyzed islands on the Snake, only 27 exhibit an x_m/L ratio between 0.6 and 0.7, and are therefore naturally comparable to the lemniscate shape. For these lemniscate islands, the average degree of elongation, k, was equal to 4.4 (Figure 7-49).

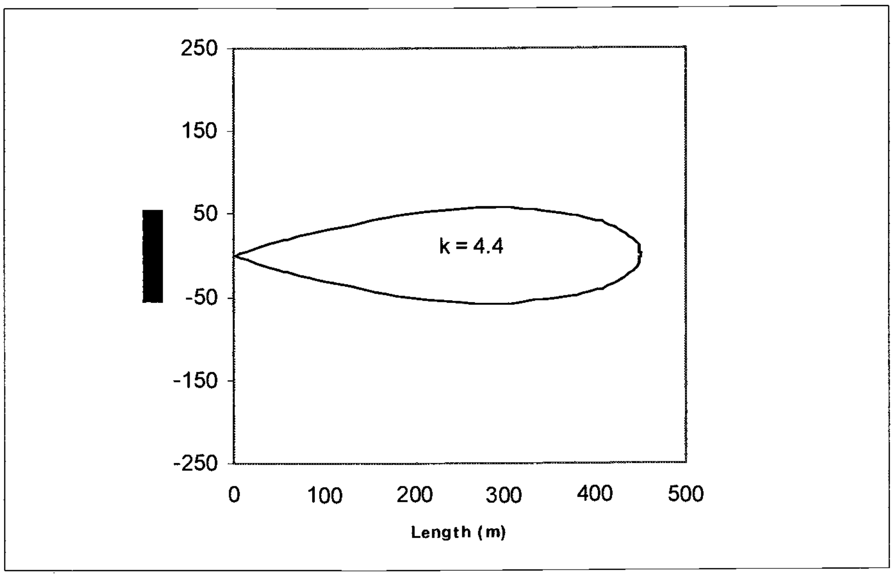

Figure 7-49. Equivalent average lemniscate for Snake River islands.

<u>WILLAMETTE RIVER</u>

Near Springfield, Oregon, the Coast and Middle Forks join together to become the Willamette River, which then flows northward 189 miles to its confluence with the Columbia River near Portland, Oregon. This meandering, locally-braided river carries a heavy sediment load over a small gradient and has historically swathed over 2-3 miles east to west. Although no dams have been constructed on the mainstem, fourteen have been built on its tributaries. In the 1850's, steamboat navigation was assisted by clearing out rocks and debris throughout the lower section of the river.

Most of the analyzed islands on the Willamette River are spread out from Salem to Eugene, with a few located in the tidally-influenced section downstream of Willamette Falls (Figure 7-50). Several long-term streamflow gaging stations are located along the Willamette River (Table 7-12). The USGS has not operated any daily sediment gaging station along the Willamette River; however, they did collect 273 instantaneous sediment concentration measurements near Portland, Oregon between October 25, 1974 and September 10, 2003. Thirteen discreet measurements were also collected near Salem.

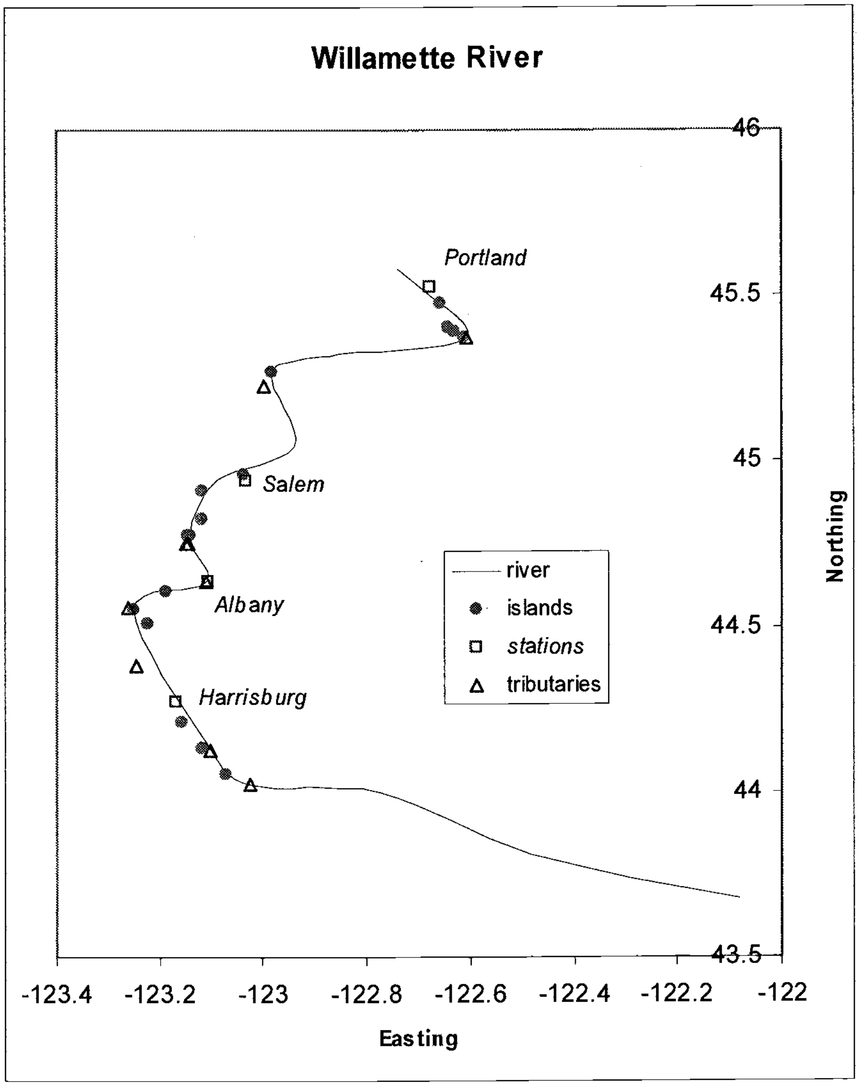

Figure 7-50. Sketch of Willamette River. Flow is to the north.

Table 7-12. Gaging station records along the Willamette River.

Gaging Station	Dates of Record	Number of Measurements	Average Daily Discharge (cfs)	Upstream Drainage Area (sq mi)
Salem, OR	10/1/1909 – present	32050	23,432	7,280
Albany, OR	11/1/1892 – present	40387	14,266	4,840
Harrisburg, OR	10/1/1944	21549	11,727	3,420

A total of 16 fluvial islands were analyzed along the Willamette River, 12 of which are located upstream of Willamette Falls. The size characteristics are shown in Figure 7-51.

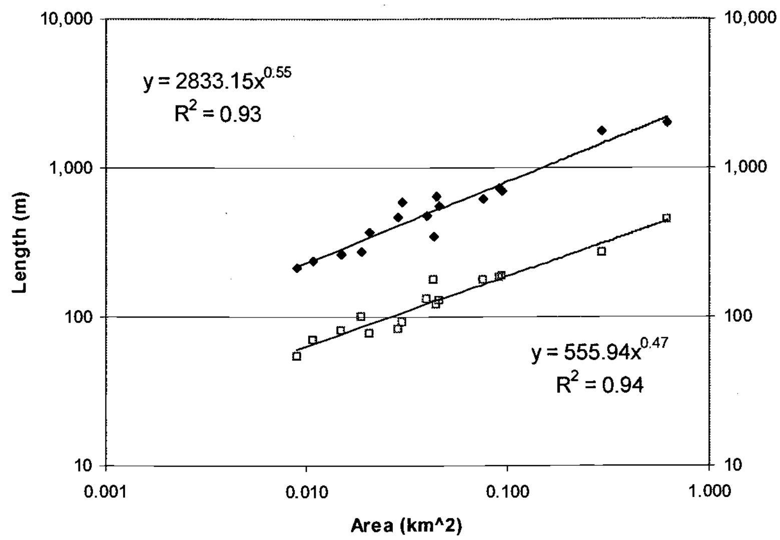

Figure 7-51. Size characteristics of Willamette River islands. Solid diamonds represent the island lengths; open squares the island widths.

The aspect ratios ranged from 2.8 to 6.5 with a mean value of 4.23. Figure 7-52 shows the relationship between the maximum lengths and widths of islands on the Willamette River.

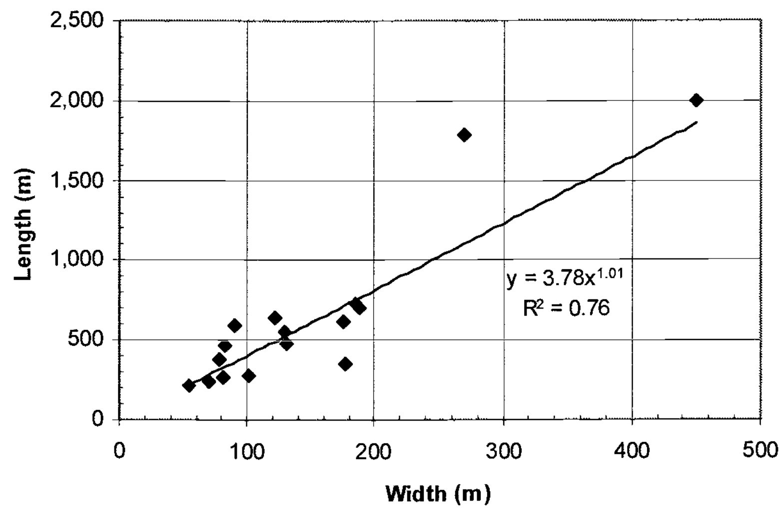

Figure 7-52. Length versus width comparisons for fluvial islands in the Willamette River.

Of the 16 total analyzed islands on the Willamette, only 5 exhibit an x_m/L ratio between 0.6 and 0.7, and are therefore naturally comparable to the lemniscate shape. For these lemniscate islands, the average degree of elongation, k, was equal to 5.7 (Figure 7-53).

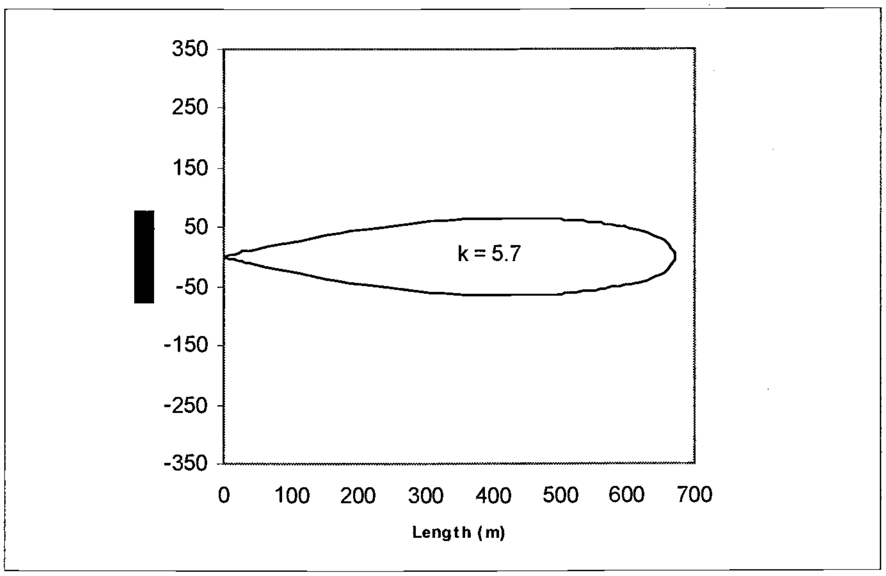

Figure 7-53. Equivalent average lemniscate for Willamette River islands.

<u>COLUMBIA RIVER</u>

Columbia Lake in southwest British Columbia, Canada is the source for the Columbia River, the second-largest river system in terms of discharge to an ocean in North America. The mainstem is 1,210 miles long and drains almost 260,000 square miles before it empties into the Pacific Ocean at Astoria, Oregon. Nearly a dozen dams (six federal, five non-federal) have been built along its length. The only 'natural' sections left are the Hanford reach and the lower river from Bonneville Dam downstream to the Pacific Ocean [Penn, 2001]. The section of river downstream of the Bonneville Dam, however, is continually dredged to accommodate shipping traffic.

All but five islands of my dataset are located downstream of Bonneville Dam (Figure 7-54). No long-term streamflow gaging station is located near these islands; however, a station at Quincy, Oregon, located downstream of the islands, has recorded streamflows since 1968 (Table 7-13). A gage at Vancouver, Washington recorded daily sediment concentration values from October 1, 1963 through September 30, 1969.

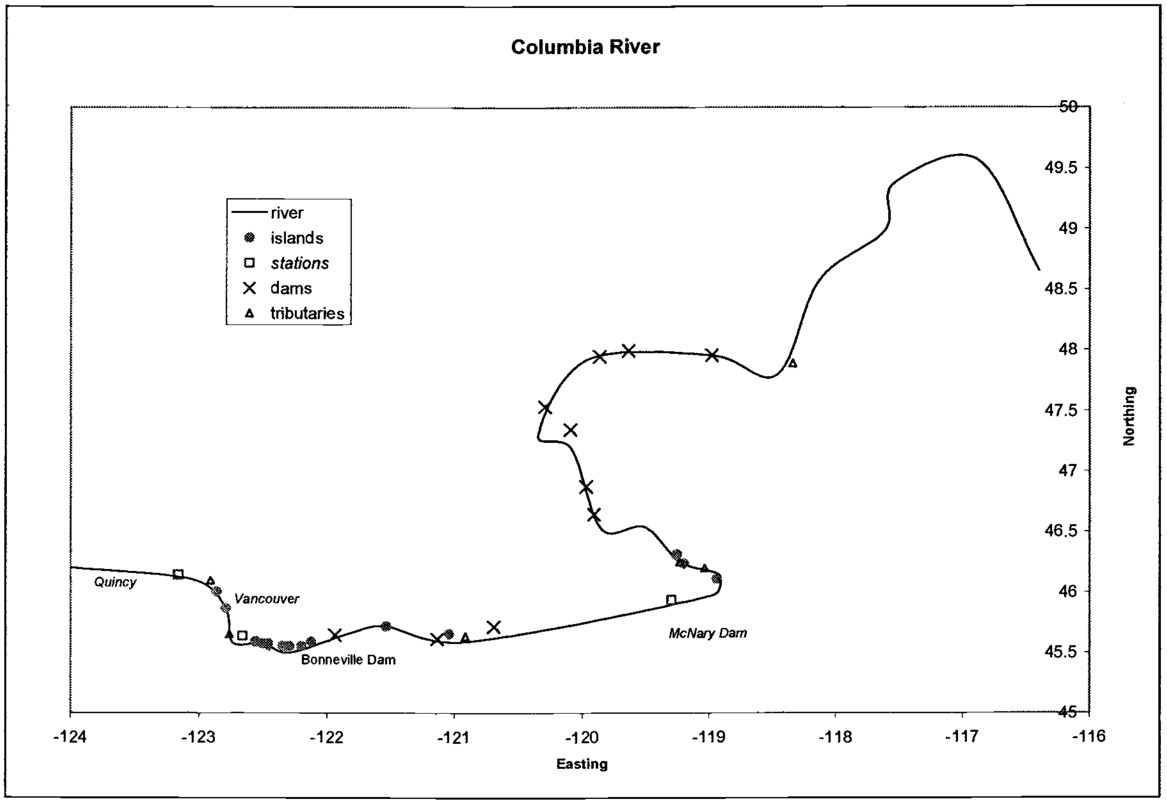

Figure 7-54. Sketch of Columbia River. Flow is to the west.

Table 7-13. Gaging station records along the Columbia River.

Gaging Station	Dates of Record	Number of Measurements	Average Daily Discharge (cfs)	Upstream Drainage Area (sq mi)
Quincy, OR	5/1/1968 – present	5269	236,528	256,900
The Dalles, OR	6/1/1878 – present	45777	191,068	237,000
McNary Dam	10/1/1950 – present	11323	182,384	214,000

Fourteen fluvial islands were analyzed downstream of Bonneville Dam on the Columbia River, and another five upstream of the dam. The size characteristics of the islands are shown in Figure 7-55.

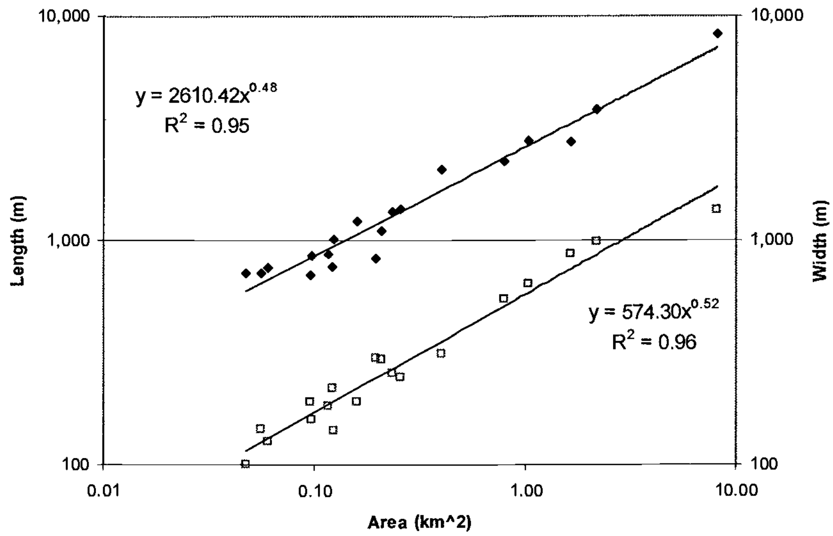

Figure 7-55. Size characteristics of Columbia River islands. Solid diamonds represent the island lengths; open squares the island widths.

For the islands downstream of Bonneville Dam, the aspect ratios ranged from 3.7 to 7.1 with a mean value of 4.97. Figure 7-56 shows the relationship between the maximum lengths and widths of islands on the Columbia River.

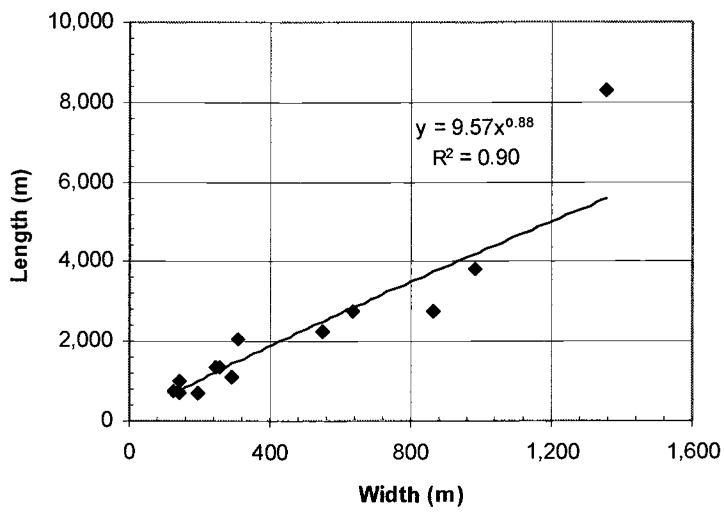

Figure 7-56. Length versus width comparisons for fluvial islands in the Columbia River.

Of the 14 total analyzed islands on the Columbia, only 6 exhibit an x_m/L ratio between 0.6 and 0.7, and are therefore naturally comparable to the lemniscate shape. For these lemniscate islands, the average degree of elongation, k, was equal to 5.1 (Figure 7-57).

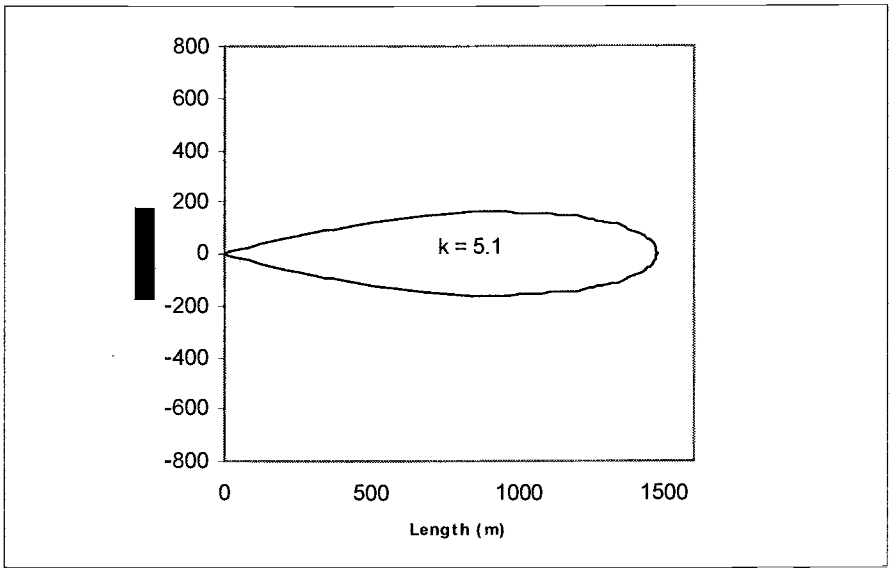

Figure 7-57. Equivalent average lemniscate for Columbia River islands.

YUKON RIVER

The Yukon River has its source in the Coastal Range of northwest British Columbia. It then traverses 2,300 miles before entering the Bering Sea in western Alaska near Kotlik. It is the fourth largest river in the United States, and one of the few un-dammed great rivers remaining. The river generally becomes frozen over between October and June. Before the fall freeze, the discharge drops and the river becomes braided with a multitude of channels that weave around hundreds of islands and sandbars that clog the riverbed [Penn, 2001]. After incising through the Yukon Plateau, it widens out into a broad, meandering, braided system that includes a myriad of island and extensive marshes. This area is an important destination for migratory fowl, and includes the Yukon Flats Wildlife Refuge.

The analyzed islands on the Yukon River are located downstream of Rampart, Alaska to near the river mouth (Figure 7-58). There have been four daily streamflow gaging stations operating at one time in this section (Table 7-14). The only station along the

Yukon River that collected daily sediment concentration values is at Eagle, Alaska near the Canadian border, which is many miles upstream from these islands. The USGS, however, did collect 164 instantaneous sediment concentration measurements near Pilot Station, Alaska between September 18, 1954 and September 23, 2003. Pilot Station is located among the set of islands in the dataset, and would therefore be more applicable to the analysis.

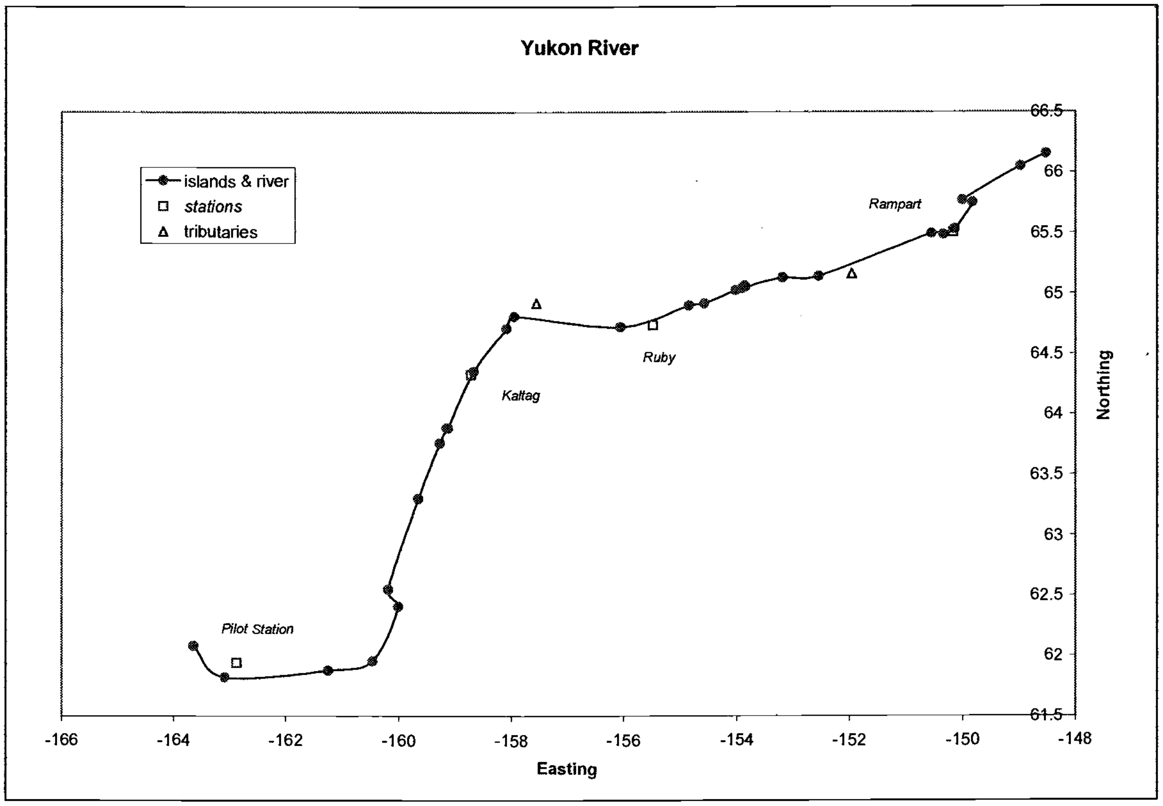

Figure 7-58. Sketch of Yukon River. Flow is to the west.

Table 7-14. Gaging station records along the Yukon River.

Gaging Station	Dates of Record	Number of Measurements	Average Daily Discharge (cfs)	Upstream Drainage Area (sq mi)
Pilot Station, AK	10/1/1975 – present	8584	230,742	321,000
Kaltag, AK	10/1/1956 – 9/30/1966	3652	216,484	296,000
Ruby, AK	10/1/1956 – 9/30/1978	8035	166,868	259,000
Rampart, AK	10/9/1954 – 9/30/1967	4508	131,401	199,400

A total of 29 fluvial islands were analyzed along the Yukon River. Unlike the previous datasets that were analyzed from aerial photographs, these islands were analyzed from the most recent topographic maps. The measured size characteristics are shown in Figure 7-59.

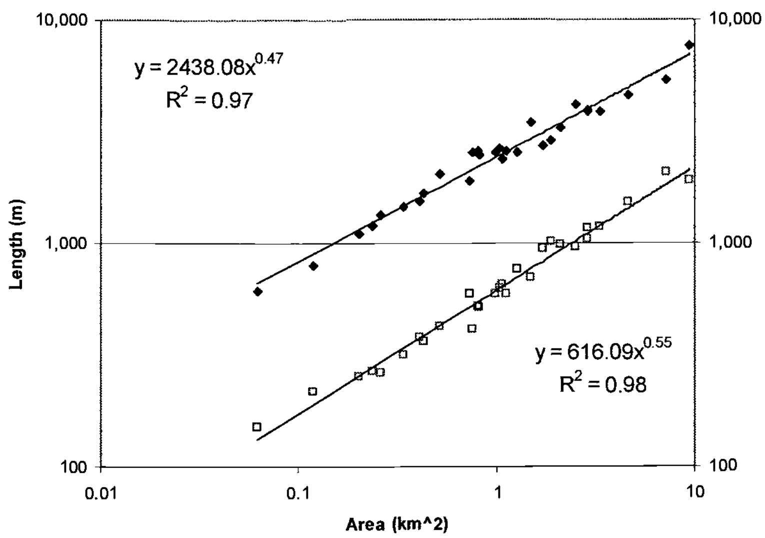

Figure 7-59. Size characteristics of Yukon River islands. Solid diamonds represent the island lengths; open squares the island widths.

The aspect ratios ranged from 2.6 to 6.2 with a mean value of 4.05. Figure 7-60 shows the relationship between the maximum lengths and widths of islands on the Yukon River.

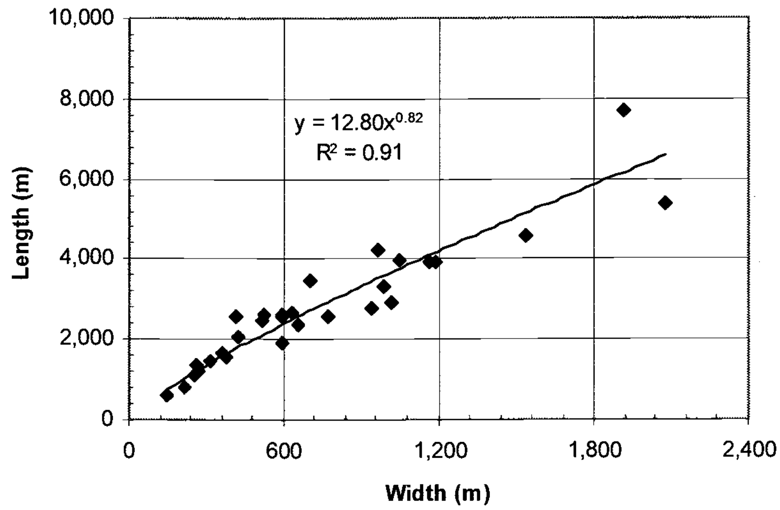

Figure 7-60. Length versus width comparisons for fluvial islands in the Yukon River.

Of the 29 total analyzed islands on the Yukon, only 7 exhibit an x_m/L ratio between 0.6 and 0.7, and are therefore naturally comparable to the lemniscate shape. For these lemniscate islands, the average degree of elongation, k, was equal to 4.9 (Figure 7-61).

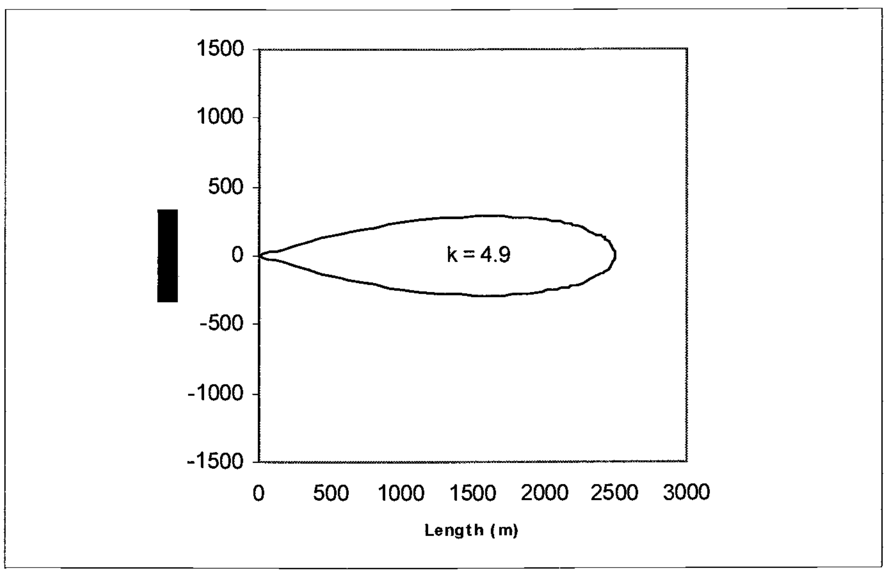

Figure 7-61. Equivalent average lemniscate for Yukon River islands.

COMPARISONS OF ALL RIVER ISLANDS

The lengths (L) and widths (W) of fluvial islands within each river have been analyzed and graphed in the form of:

$$W = aL^b \qquad (7\text{-}5)$$

where a and b are empirical constants. If the exponent, b, is equal to one, then the relation between island length and width is 'isometric', which means here that the lengths and widths vary at equal rates. If the exponent, b, is not equal to one, then the relationship is 'allometric', which means here that the lengths and widths vary at different rates [Graf, 1978]. An allometric effect can be due to bank stability.

The islands within each individual watershed have been shown to exhibit strong correlations between the lengths and widths of the islands to the areas of the islands. This strong correlation, however, is not watershed dependent. As Figure 7-62 shows, the overall correlation of all island size parameters is very strong as well. This means that the same type of flow processes dictate the islands' size parameters. Figure 7-63 shows that is no notable of consistent difference in the ratios of island lengths and areas between fluvial systems. There exists some limiting shape factor for streamlined fluvial islands.

The relationship for the lengths and widths of islands in all the rivers is shown in Figure 7-64. The average aspect ratio for all islands is 4.14. While I was analyzing the islands in each river, I tried to select only somewhat streamlined islands. Further analysis, however, showed that not all of the islands exhibited a natural x_m/L ratio of between 0.6 and 0.7. Non-lemniscate shaped islands could represent a wide range of flow energy conditions. Islands that are lemniscate, however, may represent similar flow regimes. The lengths and widths of only the islands whose x_m/L ratios lie between 0.6 and 0.7 are compared graphically in Figure 7-65.

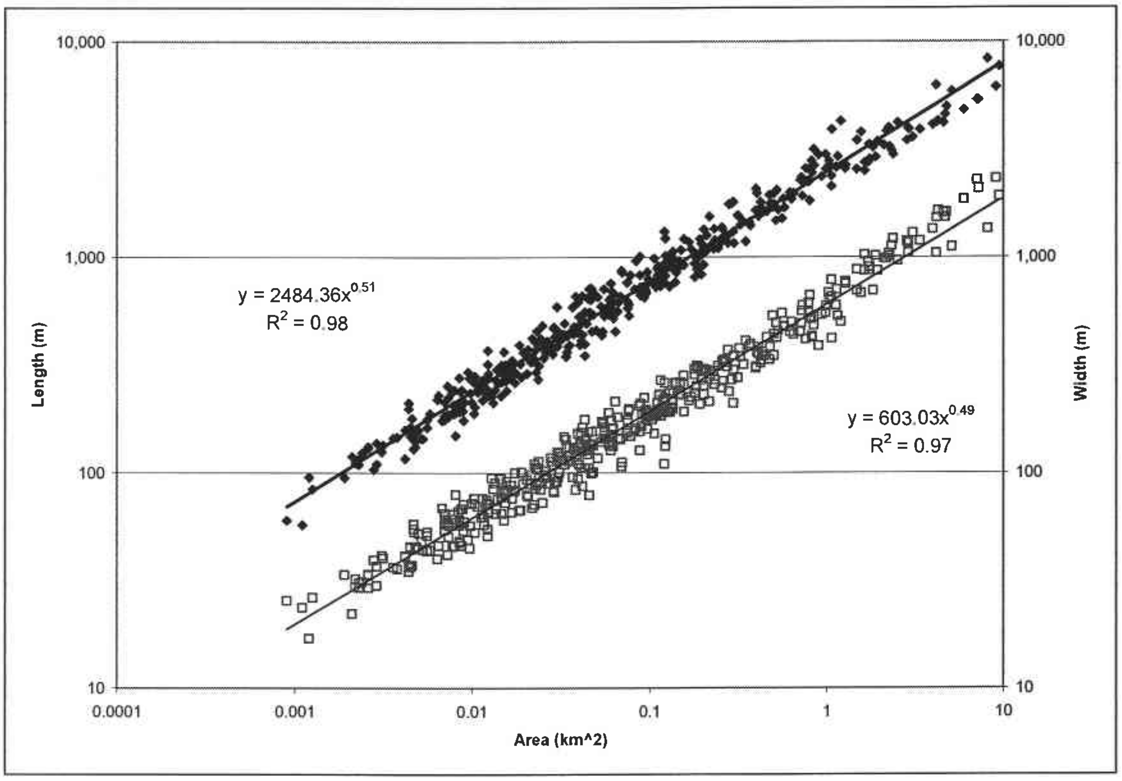

Figure 7-62. Comparison of lengths and widths to areas of fluvial islands in all rivers. Solid diamonds are the islands' lengths. Open squares are the islands' widths.

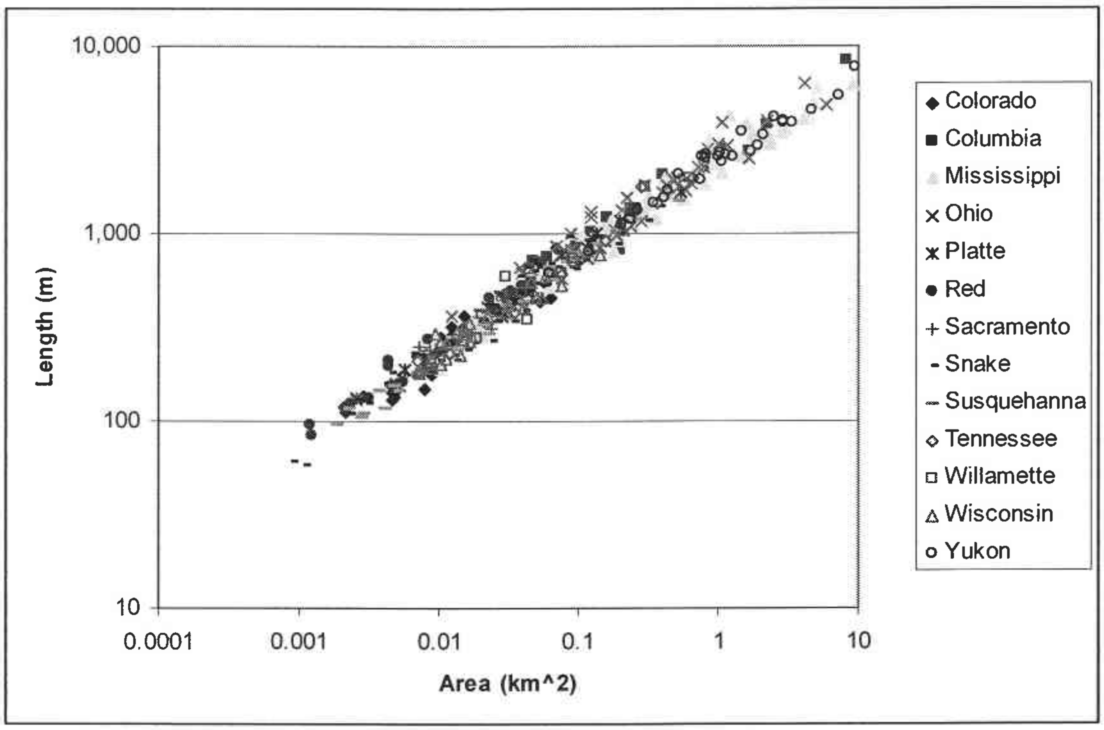

Figure 7-63. Comparison of island lengths and areas between basins.

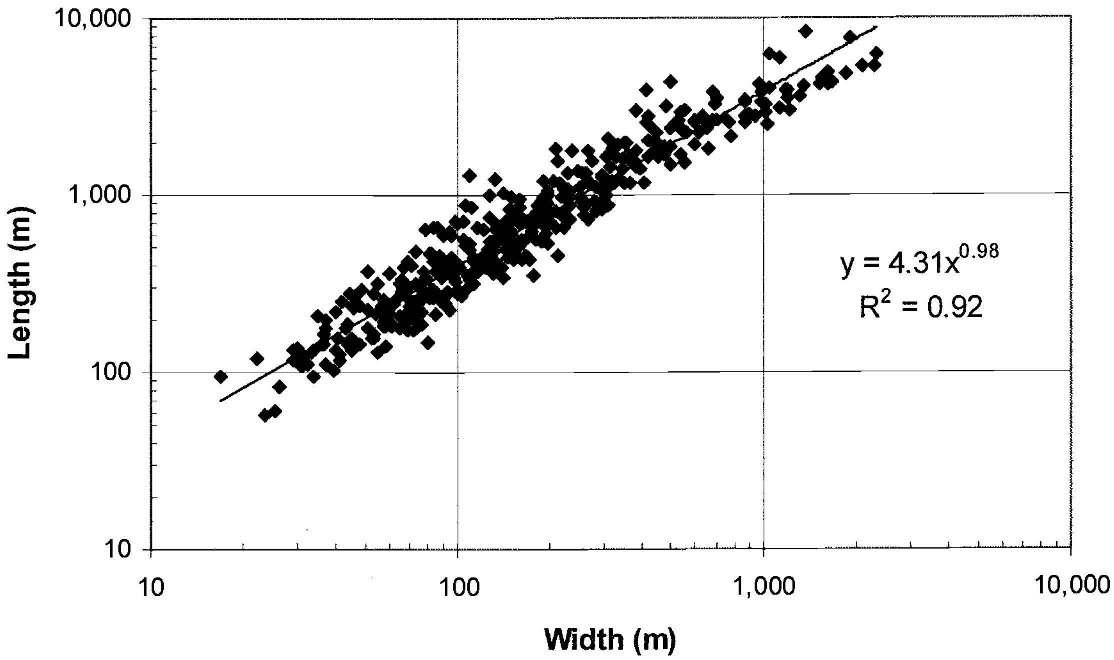

Figure 7-64. Length versus width relationships of islands in all rivers used in this research.

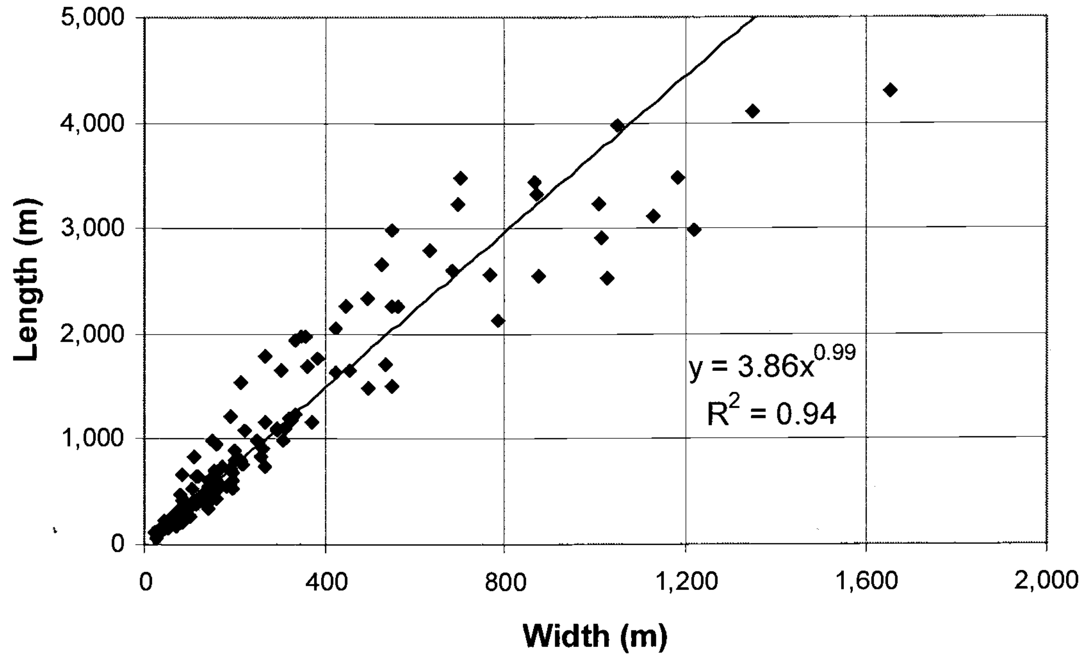

Figure 7-65. Length versus width relationships for all lemniscate-shaped islands.

A summary of the characteristics of each river's set of islands from the previous sections is shown in Table 7-15 (more detailed tables given in Appendix II). The average aspect ratios for each river range from 3.44 (Susquehanna) to 5.44 (Ohio). The differences in these ratios could be due to the differences in the available energy for each river. If we could measure the river discharge (Q) and channel slope (S) at each island location, we should expect a positive relationship between aspect ratio, which represents the potential energy loss, and the product QS, which represents the potential energy, or stream power, of the system. I could determine the slopes from topographic maps of only five of the analyzed rivers – the Columbia, Mississippi, Snake, Willamette, and Wisconsin Rivers. For these rivers, I calculated the QS values and compared them to the average aspect ratios of the fluvial islands (Figure 7-66). Even though the dataset is small, there is an apparent positive trend of increasing island aspect ratio with increasing stream power. The slope values used are the average slope for the whole river channel. The discharge values used are the mean annual average discharges nearest the mouth of each river.

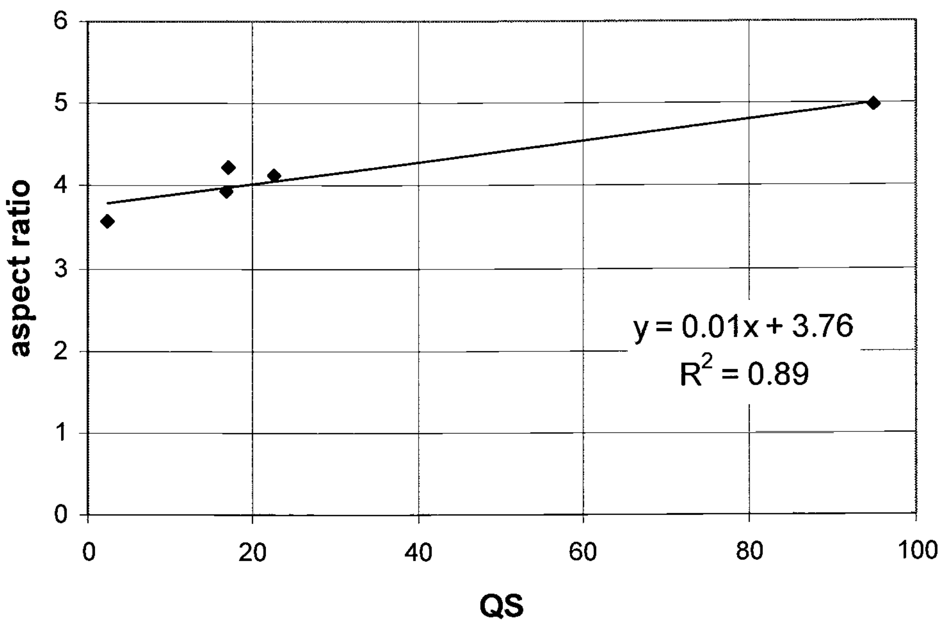

Figure 7-66. Comparison of stream power, QS, and average aspect ratio for five rivers.

Table 7-15. Characteristics of islands in researched rivers.

			$L = aW^b$		
River	**# of Islands**	**Mean R_A**	**a**	**b**	**R^2**
Colorado – Total	32	3.98	6.16	0.89	0.71
Below Laguna Dam	*5*	*3.97*	*25.97*	*0.47*	*0.67*
Below Headrock Gate Dam	*20*	*3.69*	*3.30*	*1.02*	*0.72*
Above Lake Powell	*7*	*4.81*	*59.40*	*0.43*	*0.32*
Columbia – Total	19	4.97	10.61	0.86	0.86
Below Bonneville Dam	*13*	*4.97*	*9.37*	*0.88*	*0.90*
Mississippi – Total	83	4.06	6.81	0.90	0.92
Above Missouri River	*21*	*4.18*	*5.59*	*0.94*	*0.93*
Above Ohio River	*10*	*3.45*	*4.77*	*0.94*	*0.95*
Below Ohio River	*52*	*4.13*	*9.98*	*0.85*	*0.85*
Ohio – Total	42	5.44	14.24	0.81	0.80
Platte – Total	15	4.09	3.89	1.01	0.93
Red – Total	19	4.22	4.96	0.95	0.86
Sacramento – Total	12	4.07	11.60	0.75	0.79
Snake – Total	80	3.94	3.71	1.0	0.85
Above Brownlee Dam	*73*	*4.04*	*4.23*	*0.98*	*0.85*
Susquehanna – Total	28	3.44	2.51	1.07	0.96
Tennessee – Total	12	4.01	2.24	1.10	0.93
Below Pickwick Dam	*10*	*3.76*	*2.38*	*1.09*	*0.99*
Willamette – Total	16	4.23	3.78	1.01	0.76
Above Willamette Falls	*12*	*4.59*	*3.24*	*1.07*	*0.86*
Wisconsin -- Total	33	3.58	5.35	0.91	0.82
Yukon – Total	29	4.05	12.80	0.82	0.91
All Rivers	420	4.14	4.31	0.98	0.92
Lemniscate Equiv Only *	140	3.87	3.86	0.99	0.94
Other Published Analyses of Streamlined Fluvial Islands					
Combined Columbia, Mississippi, & Missouri Islands [Komar, 1984]	38	4.30	0.235	1.04	0.98
Marshall River, Australia [Tooth & Nanson, 2000]	25	3.25	0.288	1.03	0.856
Channeled Scablands [Baker, 1979]	135	3.15	0.340	0.980	0.87
Northern Great Plains (lemniscate only *) [Kehew & Lord, 1986]	34	2.88	0.364	1.02	0.76
Martian Outflow Channels [Baker, 1979]	47	3.25	0.230	1.05	0.85

* Islands whose natural x_m/L ratios lie between 0.6 and 0.7.

EFFECTS OF CHANNEL PROCESSES ON ISLAND FORMATION

In general, we can consider the shape of fluvial islands to be independent of watershed based on figures 7-62 and 7-63. But further analysis of the fourth column in Table 7-15 shows varying values between each river system. To determine what might account for these differences, the following sections analyze the relationships between island shapes and river-specific flow characteristics.

EFFECT OF SEDIMENT CONCENTRATION ON ISLAND SHAPE

To determine the effect that the average daily sediment concentration of a river has on the shape of its islands, I have gathered sediment data for the 15 stretches of rivers in the dataset (Table 7-16). Most of the rivers have (or had at one time) a gaging station that measured continuous daily sediment concentration by the USGS. All the rivers have at least one set of instantaneous sediment concentration measurements taken by USGS. Where feasible, I used the daily continuous data. Where these databases do not exist or where the gaging stations are too far away from the island locations, I used the instantaneous data. For the continuous datasets, I also determined the maximum daily sediment concentration, the average of the sediment concentration peaks, the average sediment discharge, and the average water discharge for that time period. The period of record for each river has been discussed previously in this chapter.

Table 7-16. Summary of sediment concentration measurements on analyzed rivers.

River	Average Sediment Conc. (mg/L)	Max Daily Sediment Conc. (mg/L)	Avg of Conc. Peaks (mg/L)	Avg Sediment Discharge (kg/sec)	Avg Water Discharge (m^3/sec)
Colorado	2,260	27,030	2,797	46,215	235
Columbia	34	2,660	116	29,294	5,716
Lower Mississippi	442	2,400	521	629,976	12,840
Middle Mississippi	404	3,890	480	4,525	6,586
Upper Mississippi	165	2,120	231	72,738	3,779
Ohio	103	955	231	66,860	3,367
Platte	1,058	n/a	n/a	39,004	n/a
Red	703	42,543	865	76,538	612
Sacramento	82	1,480	256	8,915	370
Snake	59.4	n/a	n/a	2,230	n/a
Susquehanna	32	879	75	8,779	1,028
Tennessee	52	770	102	11,159	1,347
Willamette	22.4	n/a	n/a	7,296	n/a
Wisconsin	21	218	37	570	235
Yukon	236	n/a	n/a	206,148	n/a

Does sediment concentration affect island shape, at least empirically? Figure 7-67 shows the relationship between the average daily sediment concentration and the average island aspect ratio for each river. The scatter shows that there is no correlation between a river's sediment concentration and its islands' shapes, which contradicts previously published data of Wyrick [2003]. The data from Wyrick [2003] were preliminary and only used four rivers in the analysis. Comparing the aspect ratios to other parameters, such as maximum concentration or sediment discharge, also gives a similar "shotgun-blast" relationship.

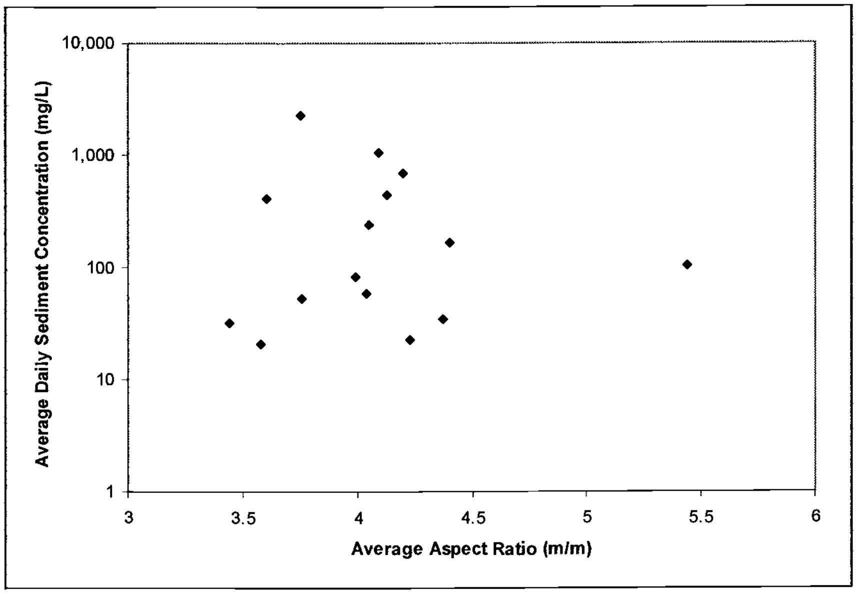

Figure 7-67. Effect of sediment concentration on the average aspect ratio of islands in studied rivers.

From a physical point of view, should we expect sediment concentration to affect the island shape? If we consider the drag coefficient, C_d, from Equation 4-18 as a proxy for the aspect ratio, and the fluid density, ρ, from Equation 4-18 as a proxy for sediment concentration, then the drag coefficient and fluid density should adjust with each other in order to maintain the other variables (drag force and stream velocity) of equation 4-18 as constants. As the sediment concentration increases (and therefore the fluid density increases), the turbulence of the flow has been shown to decrease [Costa, 1988]. As the intensity of the turbulence is decreased, the pressure drag on an object in the flow also decreases. This decrease in pressure drag would affect the shape of the island. Therefore, one could expect an inverse relationship between sediment concentration and island shape (i.e. as sediment concentration increases, island aspect ratio decreases), but perhaps the data used in this analysis are not detailed enough to tease out that balance.

EFFECT OF BOUNDARY WIDTH ON ISLAND SHAPE

Perhaps a limiting factor in an island's shape parameters is the ability of the channel banks to accommodate an expansion in total channel width with the growth of a mid-channel island. As a river encounters a fluvial island, its flow must split into the two flanking anabranches (see Figure 5-4). As the flow bends around the island, it impinges more directly on the banks. Soft, erodible banks can accommodate an expansion in the total channel width. Harder banks will deflect the flows back towards the center of the channel sooner, thereby not allowing as much downstream deposition on the island. Figure 7-68 shows the relationship between an island's length and the ratio of the channel widths upstream of the island and at the island. The exact equation for the envelope curve (dashed line) shown in Figure 7-68 is not the same for each river system, but the shape of it is. The regression equation for the limit curve is in the shape of a decaying power function, with a power of about -1.

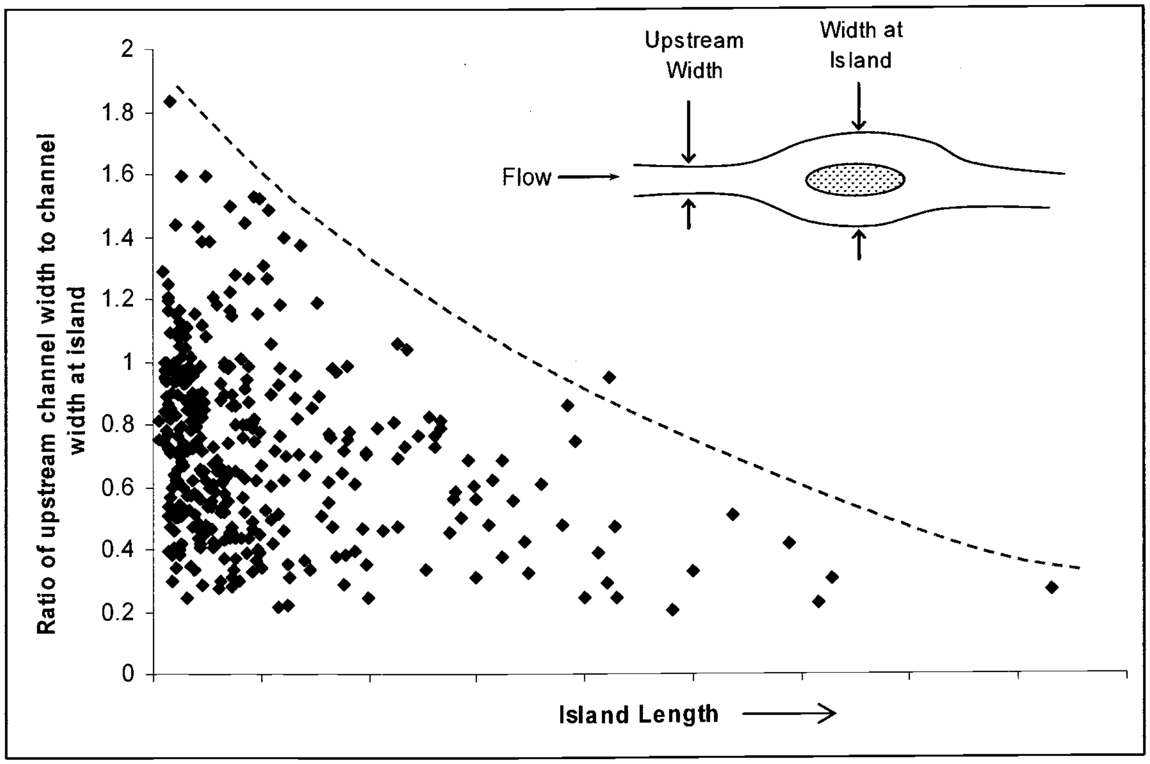

Figure 7-68. Relationship of island length to the ratio of upstream channel width and channel width at the island. The dashed line shows the approximate limit in island length for a given width ratio.

Channels that do not expand to accommodate an island will also not accommodate an increase in the island length. The flow patterns within a channel will not allow for a very long island within a uniform-width channel. The longer an island grows, the wider the channel will expand around it. This may also be a factor in the optimum aspect ratios of islands. If a river will optimize an island's aspect ratio to be near three, then as the island increases in length, it will also increase in width, thus expanding the channel around it.

EVOLUTION AND OPTIMIZATION OF ISLAND SHAPE

To minimize drag force for a given fluid velocity, the drag coefficient, which depends on the shape of the object, must be a minimum. Hoerner [1965] showed experimentally that for teardrop-shaped objects in water flow, the drag coefficient (and therefore the drag force) is a minimum for a length/width ratio between 3 and 4 (Figure 7-69). In his experiments, the width was kept constant and the length was varied. He found that as the length/width ratio of an object decreased, the frictional drag due to shear also decreased, but the pressure drag increased. The reverse situation was found true as the length/width ratio was increased. The optimum aspect ratio of between 3 and 4 was corroborated by the flume experiments discussed in the previous chapter (e.g., Figure 6-6)

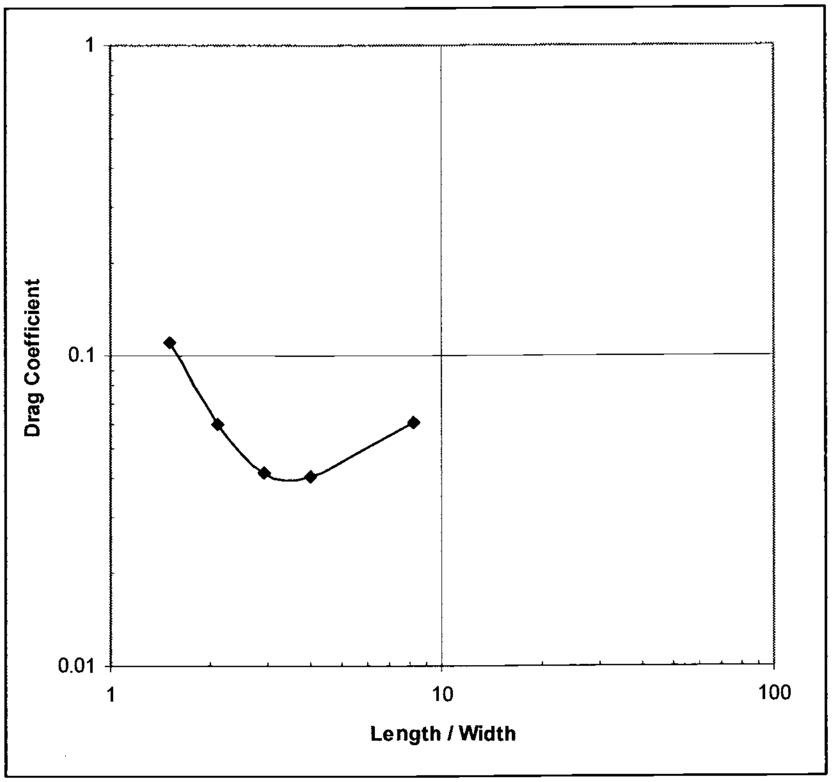

Figure 7-69. Relationship between drag coefficient and length/width ratio for objects in water flow. Based on data from Hoerner [1965] as analyzed by Komar [1983].

If a river tends to seek the least amount of resistance in flowing to its downhill destination, then minimizing the drag force on its islands would be desirable. One might then ask: do islands evolve to some equilibrium aspect ratio? As an example, consider Skamania Island downstream of Bonneville Dam on the Columbia River (Figure 7-70). In 1956, this island (Figure 7-70a) had a length of 2570 m, a width of 500 m, and an area of 0.86 km^2. By 1993, the same island had decreased its length to 700 m, its width to 190m, and its area to 0.10 km^2 (Figure 7-70b). This change in physical proportions, however, also constituted a change in its aspect ratio from 5.14 to 3.68.

Other islands in this same stretch of river have also experienced a change in aspect ratios, but not all of them have experienced a decrease in plan area. The comparisons are shown in Table 7-17. (Note: any impacts of maintenance dredging in nearby navigation channels have not been separately analyzed.)

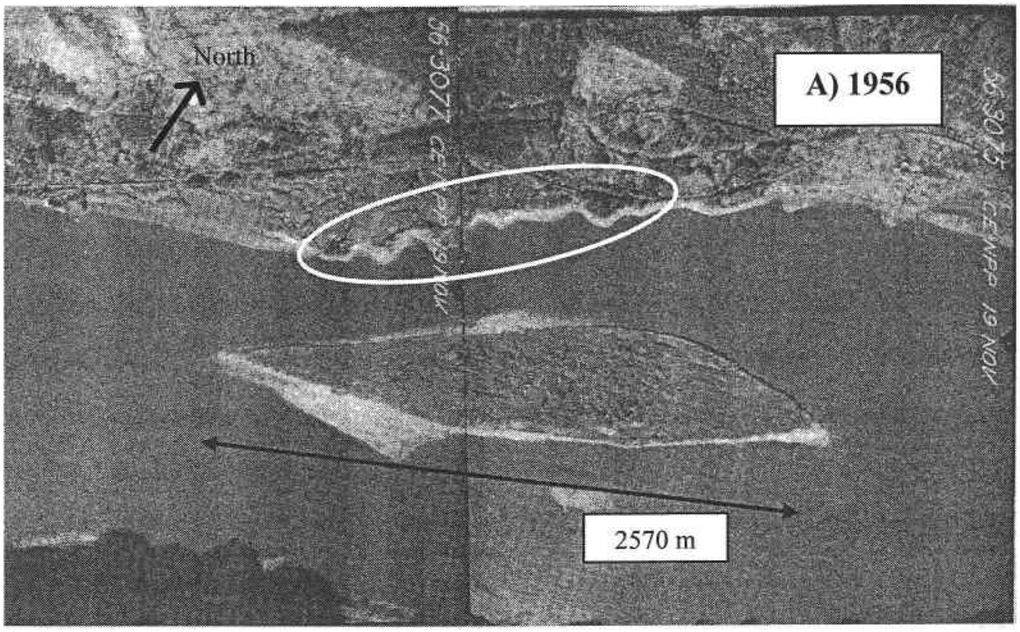

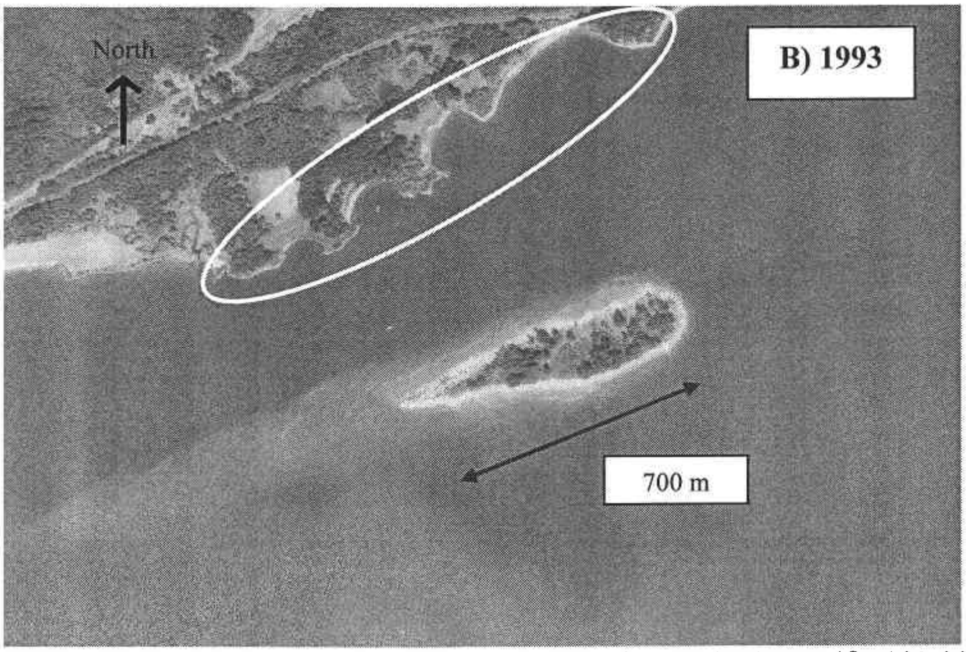

Figure 7-70. A) Aerial photograph of Skamania Island on 11/19/1956 (Q=102,000 cfs). B) Aerial photograph of Skamania Island in 8/1/1993 (Q=114,000 cfs). Note nearly unchanged shore pattern circled on north bank.

Table 7-17. Comparison of evolving aspect ratios of Columbia River islands.

Island Name	River Mile	1930's	1950's	1990's
Sandy	76	2.2		3.2
St. Helens	85.5		4.9	4.3
McGuire	118	4.4	4.1	3.8
Sand	130	4.1		4.1
Reed	127	6.8	6.1	3.9
Skamania	136		5.1	3.7

From this small sample of islands, there seems to be some trend towards this equilibrium aspect ratio that would minimize the drag coefficient. One might ask, however, if this is really a kind of equilibrium. At the beginning of this section, I stated that the drag coefficient became a minimum for a constant velocity. Certainly, the mean velocity of the Columbia River at any given location has not remained constant for 60 years. The earliest aerial photographs I analyzed for these islands were taken in 1935 by the U.S. Army Corps of Engineers. Bonneville Dam was constructed in 1938, followed by many upstream dams, which have collectively regulated the downstream flow in the Columbia River by maintaining a fairly constant minimum flow and reducing the severity of the peak flows through flood control. Perhaps the variability within the flows has been reduced enough to allow for equilibrium development of the island shapes. The only USGS streamflow gaging station on the Columbia River below Bonneville Dam is located near Quincy, Oregon, but it only has daily data from two years in the late-1960's and continually since 1991. There are not enough data to show any kind of dampening trend in peak flows. One piece of information about each of these islands that is missing, however, is how long ago each island formed.

CHAPTER 8 – MEGAFLOODS AND THEIR RELATION TO ISLANDS

Some fluvial islands have derived their origin from extraordinary past events that provided both erosional and depositional conditions not commonly experienced. To provide comparisons with the smaller scale islands discussed in previous chapters, extreme events are considered here for: megafloods on Earth and evidence of megafloods on Mars. Although many cases of extreme flow events on Earth have been discussed in the literature, only a few include discussion of the formation of streamlined residual islands. Islands have been mentioned, but not analyzed in detail, in research on megafloods in the Snake River valley (The Bonneville Flood) [O'Connor, 1993], Strait of Dover (The English Channel) [Smith, 1985], and the Jordan River valley [Inbar, 1987]. There are two cases of terrestrial megafloods in which the shapes of the residual islands were analyzed by previous researchers – The Missoula Floods in eastern Washington [Baker, 1979] and the Souris spillway in northern North Dakota [Kehew and Lord, 1986]. Extreme floods on Mars, likewise, have occurred in several locations on that planet's surface with some analyses having been undertaken of the streamlined residual islands. Each of these events and their respective residual islands are discussed in more detail in the following sections.

EXTREME TERRESTRIAL FLOODS

Unlike most scientific procedures, there is no general theory of megafloods that can be tested, either verified or falsified [Baker, 2002a]. In the study of megafloods, observation usually precedes theory. Residual human memories of gigantic paleofloods occasionally remain in our society, exampled by cultural legends of floods such as the biblical Noah's Flood. A divergence from this kind of thinking began in the early nineteenth century with the idea of uniformitarianism set forth by Hutton, Playfair, and Lyell, mostly because floods of immense proportions just were not observed historically [Knighton, 1998]. The largest recorded flood in the United States was on the Mississippi River at Vicksburg, Mississippi in 1927 with a discharge of 7 x 10^4 m^3/s [data from http://water.usgs.gov], and the largest recorded flood in the world was on the Amazon River in 1953 with a discharge of 3.85 x 10^5 m^3/s [Rodier and Roche, 1984].

Over the last half-century or so, many examples of immense pre-historic floods have been discovered around the world, even on Venus and Mars [Baker et al., 1992b]. Since then, fluvial geomorphologists have returned to the concept of consilience, first described by William Whewell in 1840, which is the confirmation of theories through unexpected connections and explanatory surprises [Baker, 2002a]. The following section is a compilation of contemporary research on various megafloods that have occurred on Earth and their corresponding remnant islands.

THE MISSOULA FLOODS, NORTHWEST UNITED STATES

J. Harlan Bretz, a geology professor at the University of Chicago, began field studies in the Channeled Scablands of eastern Washington during the summer of 1922. While there, he observed surface features that he could only ascribe to catastrophic flood processes due to their immense scale. Bretz first presented his evidence in a 1923 paper, which was received with considerable doubt and criticism [Baker, 1978a]. Most geologists of that time subscribed to the theory of uniformitarianism [Komar, 1996]. This theory was a departure from the catastrophism made popular by the biblical Noah's Flood, and describes geologic processes as being slow and within the constraints of normal, every-day observations. Bretz's flood (termed the Spokane Flood) called for a flowrate greater than anything ever measured on Earth. In 1927, the Geologic Society of Washington invited Bretz to present his research at a conference that was preferentially loaded with anti-catastrophe scientists [Baker, 1978a]. Bretz [1927] calmly outlined the significant geomorphic features within the Channeled Scablands (summarized in Table 8-1). Many alternatives were proposed by other scientists at the conference (during sometimes heated discussions) for the creation of the features. W.C. Alden [1927] suggested that collapsed lava tubes and small volumes of glacial melt could explain the features. O.E. Meizner [1927] claimed that the Columbia River carried significant flows at flood stage, and probably was even larger during the Pleistocene, that could create the erosional features. E.T. McKnight [1927] suggested a glacially-diverted Columbia River at normal flows as an alternative. J. Gilluly [1927] claimed that long, continued erosion of normal streams could create the same features. Bretz embraced the debate, but criticized his opponents for wholly dismissing his hypothesis without their own field work, and wrote [Bretz, 1928]:

> "Ideas without precedent are generally looked on with disfavor and men are shocked if their conceptions of an orderly world are challenged."

Table 8-1. Geomorphic features in Channeled Scablands as described by Bretz (modified from Baker [1978b])

Geomorphic Feature	Descriptions
Channel Morphology	Scale: valleys are really the channels for conveyance of flows Rock Basins: lengths up to 14 km, depths up to 60 m Plexus grouping of channels Cataracts: several more than 5 km wide and 120 m high
Inter-channel Areas	Aligned loess scarps facing the channels: slopes eroded to 30 - 35° Streamlined residual loess hills
Divides	Deeply entrenched by multiple channels at approximately equal elevation
Depositional Features	Gravel, commonly boulders several meters in diameter High gravels up to 120 m above canyon floors contemporaneous with floor deposits Bar morphology: bars up to 30 m high Great fan deposit in northern Quincy Basin
Regional Anastomosis	Results from the abrupt introduction of a huge volume of water flooding a multitude of minor valleys and crossing a multitude of minor pre-flood divides
Downstream Continuity of Flood Features	Flood bars along Columbia Gorge through Cascade Mountains, downstream of Wallula Gap Huge fan delta developed at Portland, Oregon

One of the main discrepancies of Bretz's theory was his lack of a source for the immense volumes of water he proposed for his megaflood. Initially, he thought that the melting of the Cordilleran ice sheet during the last glacial period was the source. However, his initial estimate of discharge through the Wallula Gap was 1.9 x 10^6 m^3/s [Bretz, 1925], which would require 42 $mile^3$/day of melting ice. Even Bretz, himself, thought this to be too extreme. J.T. Pardee [1910] had studied ancient shorelines on hillsides near Missoula, Montana formed by a Pleistocene-era lake that impounded over 2000 km^3 of water. In 1928, after discussions with Pardee, Bretz announced that Lake Missoula was source for his Spokane Flood [Baker, 1978b]. In 1932, Bretz published the last of his research in the Channeled Scabland [Bretz, 1932] and moved on to other research areas.

The debate, however, did not cease. Allison [1933] modified Bretz's theory by describing an ice jam within the Columbia Gorge that ponded water all the way back through Washington, thus creating deposits at the observed high water elevations. Flint [1938], one of Bretz's main opponents, described the features as remnants of leisurely streams from proglacial outwash with discharges about half of present-day Snake River. Flint described in detail large amplitude ripples within the Cheney-Palouse tract, which Bretz et al. [1956] visited afterwards and used as indisputable evidence for an immense flood. The opposition began to fail in 1940, when J.T. Pardee presented at the American Association for the Advancement of Science in Seattle, Washington on his research at Lake Missoula [Baker, 1978a]. Pardee described ripples that measured 15-m in height and 150-m in spacing [Pardee, 1942]. He calculated the total volume of the glacial lake had been 2,167 km^3, which was impounded behind a lobe of the Cordilleran Ice Sheet that must have failed suddenly in order to create these ripples [Pardee, 1942]. Although Pardee did not specifically link his research to the Spokane Flood, others did and the renaissance began. In 1965, the Field Conference of the 7th Congress of International Association of Quaternary Research held a field trip that began at Lake Missoula and traversed the Channeled Scablands. Afterwards, they sent Bretz a long letter that ended with: "We are now all catastrophists" [Baker, 1978a].

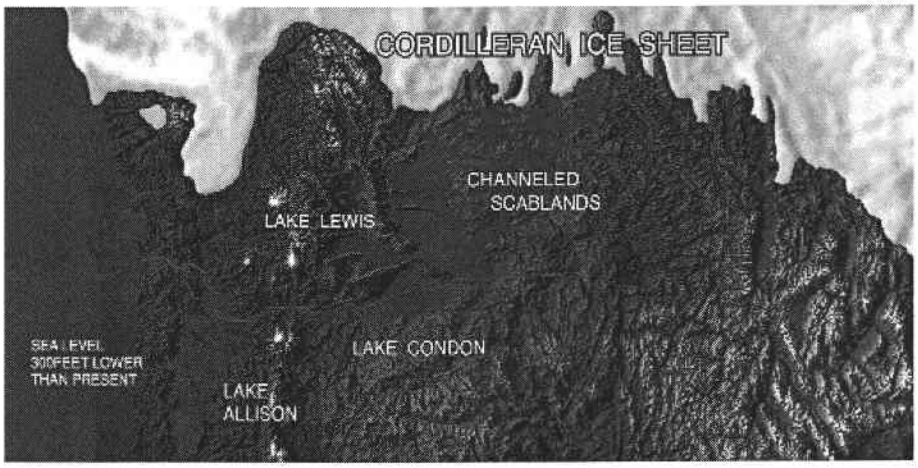

Figure 8-1. Location of Missoula Floods.

Acceptance of the cataclysmic flood theory opened the door for the recognition of similar features in other regions, including on the surface of Mars. Acceptance of Bretz's theory also allowed for more detailed analysis of the flows. Using the Chezy equation (Equation 4-15), Bretz [1923] was the first to estimate the discharge of the Spokane Floods at the Wallula Gap (see Figure 8-2). This location is a prime spot for computation because all the multiple courses the flows followed through eastern Washington had to converge at Wallula to enter the Columbia Gorge. The gap becomes a simple constricted weir with backwater ponding. Several researchers have estimated flowrates of the flood by using a form of the Manning's Equation in a step-backwater process, using observed features such as ice-rafted erratics, gravel deposits, and eroded terraces as maximum stage indicators. Baker [1973] concluded that the discharge was 9×10^6 m^3/s at Wallula Gap. O'Connor and Baker [1992] modified Baker's coefficients of contraction and expansion using a HEC-2 computer program to arrive at a maximum discharge of 10×10^6 m^3/s. These estimates assumed subcritical flow through the gap, based on evidence downstream that the flow was also ponded at various constrictions through the Gorge. If, however, critical flow through Wallula Gap was attained, O'Connor and Baker's estimate increases to 15×10^6 m^3/s. Closer to the outlet of Lake Missoula, the Rathdrum Prairie just east of Spokane is supposed to have conveyed most of the flow. Using the same analysis techniques, Baker [1973] estimated a maximum discharge of 21×10^6 m^3/s, and O'Connor and Baker's [1992] modifications yield a flowrate of at least 17×10^6 m^3/s. Estimates of flow through several pathways within the Channeled Scabland have been made by Waitt et al. [2000]. Near the present-day Grand Coulee Dam, the discharge was at least 15.5×10^6 m^3/s, split between the northwest Columbia Valley (10×10^6 m^3/s), the Grand Coulee (5.5×10^6 m^3/s), and sometimes the Moses Coulee ($5.5 - 11 \times 10^6$ m^3/s). Waitt [1994] estimated that flows through the Cheney-Palouse tract in eastern Washington had discharges of about $7.7 - 11 \times 10^6$ m^3/s.

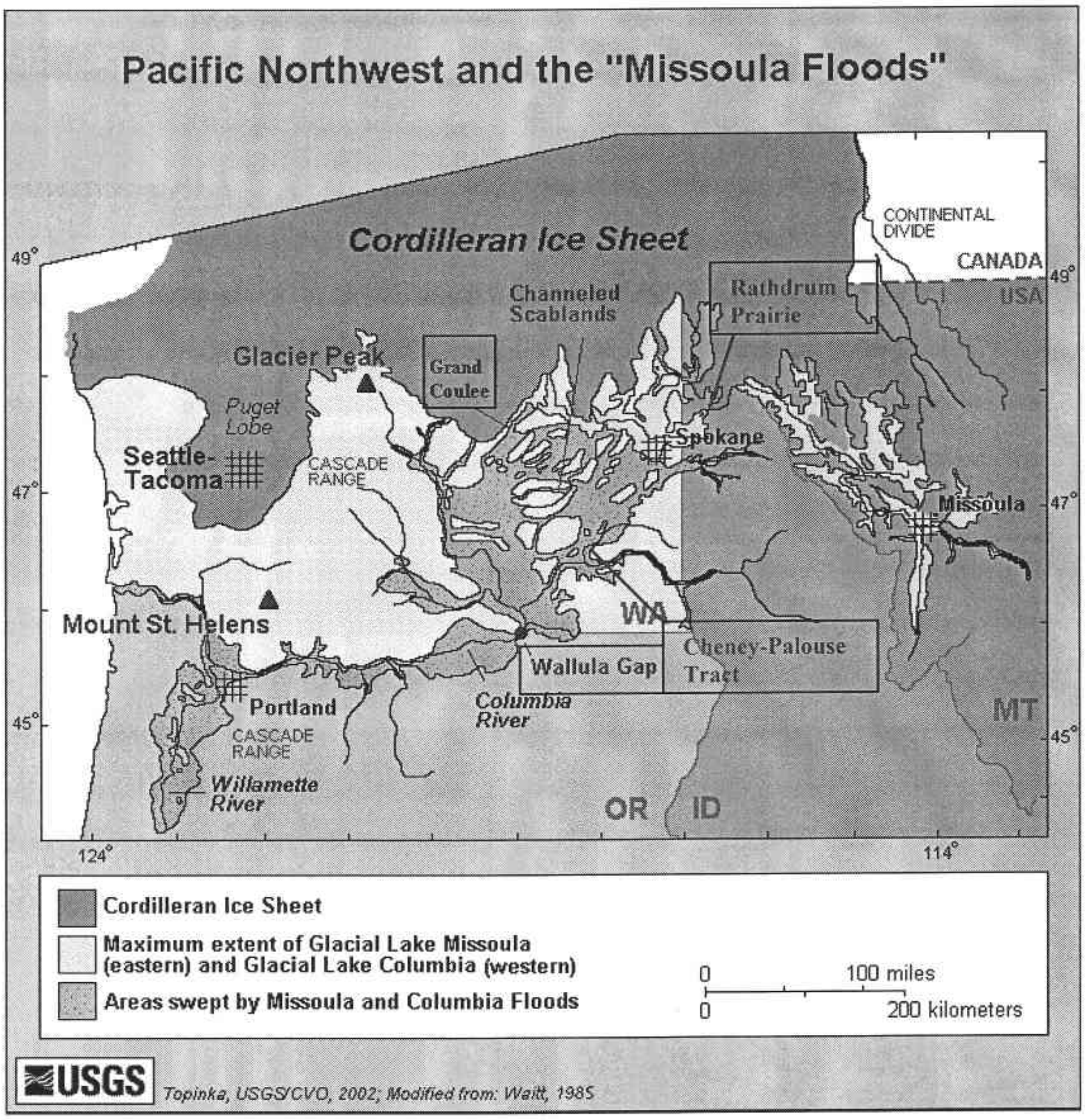

Figure 8-2. Map of Channeled Scablands showing locations of discharge estimates (shown in boxes).

A debate now exists as to how many flood events actually occurred in the Scablands. Initially, Bretz [1923] imagined only one large flood, but by 1969, he amended his number to about seven or eight floods. Allison [1978] decided that there had to be at least several tens of floods based on the number of sediment beds in the Willamette River valley. Benito and O'Connor [2003] mapped all the stage indicators they found within the Columbia River Gorge and used the HEC-2 step-backwater program to calculate the number and value of the discharges. Their analysis showed that at least one flood reached a peak discharge of 10^7 m^3/s, which is consistent with previous studies at Wallula

Gap [O'Connor and Baker, 1992]. Based on radio-carbon dating of Mt. St. Helens tephra, this largest flood is younger than 19,000 years old. Benito and O'Connor's [2003] model also showed that, based on depositional sequences on high terraces, there were at least 25 floods of 10^6 m^3/s or greater.

Shaw et al. [1999] made quite a stir when they announced that they could ascribe all the scabland features to a single flood event with multiple pulses and multiple meltwater sources off the Cordilleran Ice Sheet. They claim a source volume of 10^5 km^3 released over 100 days as the cause of the Scabland features.

Flooding of the Channeled Scablands may not be contained to just the late Pleistocene (younger than 130 thousand years ago (abbreviated as kya)). Radiometric dating and sediment polarity testing by Bjornstad et al. [2001] show that there was at least two episodes of pre-Wisconsin flooding (Wisconsin refers to the last glacial period). They analyzed a depositional bar sequence in the Pasco Basin and found evidence for at least one middle-Pleistocene (780 – 130 kya) flooding episode. Based on the reversed polarity of some of the sediments, there also had to be at least one flood episode in the early-Pleistocene (>780 kya). In fact, Bjornstad et al. [2001] claim this layer to have been deposited during the Olduvai polarity period (1.77 – 1.95 million years ago (Mya)). Many of the erosional features, such as coulees, scablands, and streamlined hills, could have been formed during the pre-Wisconsin flooding episodes and only modified during subsequent late-Pleistocene floods. Since the later floods eroded most of the older evidence away, it is difficult to estimate a value for the discharge of these early-Pleistocene floods.

GLACIAL LAKE REGINA, UNITED STATES-CANADA BORDER

Lake Regina was a giant Pleistocene lake in present-day Saskatchewan created by the damming of local rivers by the Cordilleran Ice Sheet. Several smaller proglacial lakes in present-day North Dakota and Minnesota were connected to form a spillway system (Figure 8-3). Kehew [1982] analyzed the Souris spillway channels and used the Manning's equation to estimate a maximum discharge of 2.7 x 10^5 m^3/s. The channel was estimated to be up to 8-km wide and 100-m deep that carried a flow velocity of up to 4.8 m/s. Kehew and Lord [1986] further analyzed the erosional residuals within the remnant Souris channel by comparing the shapes of the residuals to the lemniscate form.

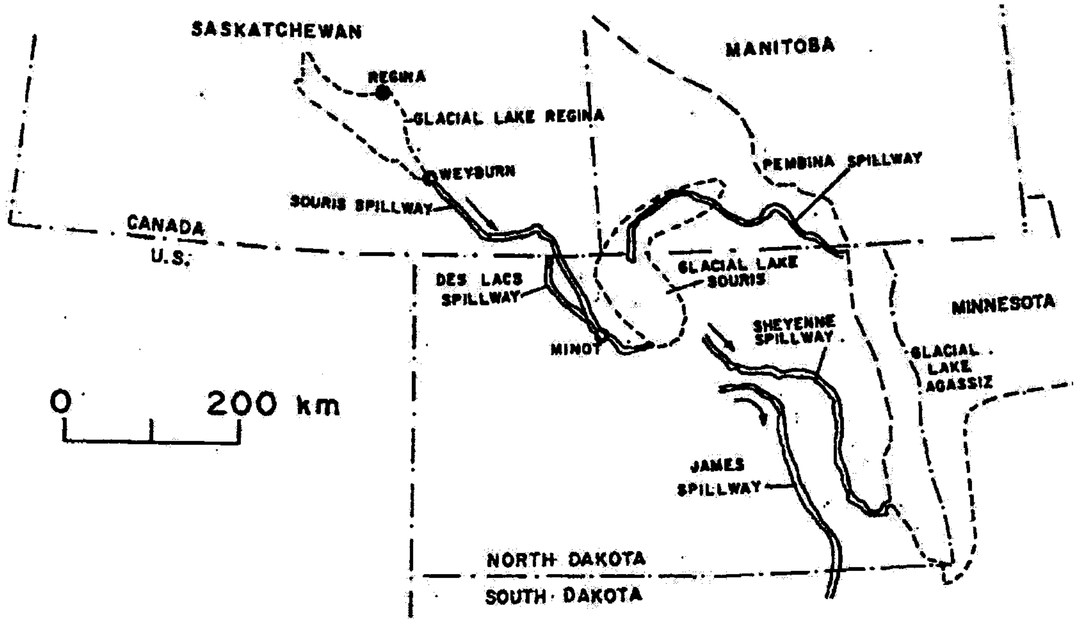

Figure 8-3. Map of spillways from pro-glacial lakes. From Kehew [1982].

<u>COMPARISONS OF HYDRAULIC PARAMETERS</u>

Figure 8-4 compares the magnitude of the extreme flows discussed herein to other known or hypothesized immense flow events on Earth and Mars. The other flow events included in the figure have not been shown to exhibit streamlined residuals in their flood channels, except for Mars which is discussed later in this chapter, although they are of comparable size to the Missoula and Souris floods. The other extreme flow events include ocean currents [Gross, 1987], marine basin overflows [Smith, 1987; Ryan et al., 1997; Baker, 2002b], Altai Mountain floods [Baker et al., 1993], and jökulhlaups of Iceland [Maizels, 1989; Snorrason et al., 2002; Waitt, 2002]. Table 8-2 summarizes the estimated hydraulic parameters of the megafloods described herein, and compares them to other immense flows estimated on Earth and Mars.

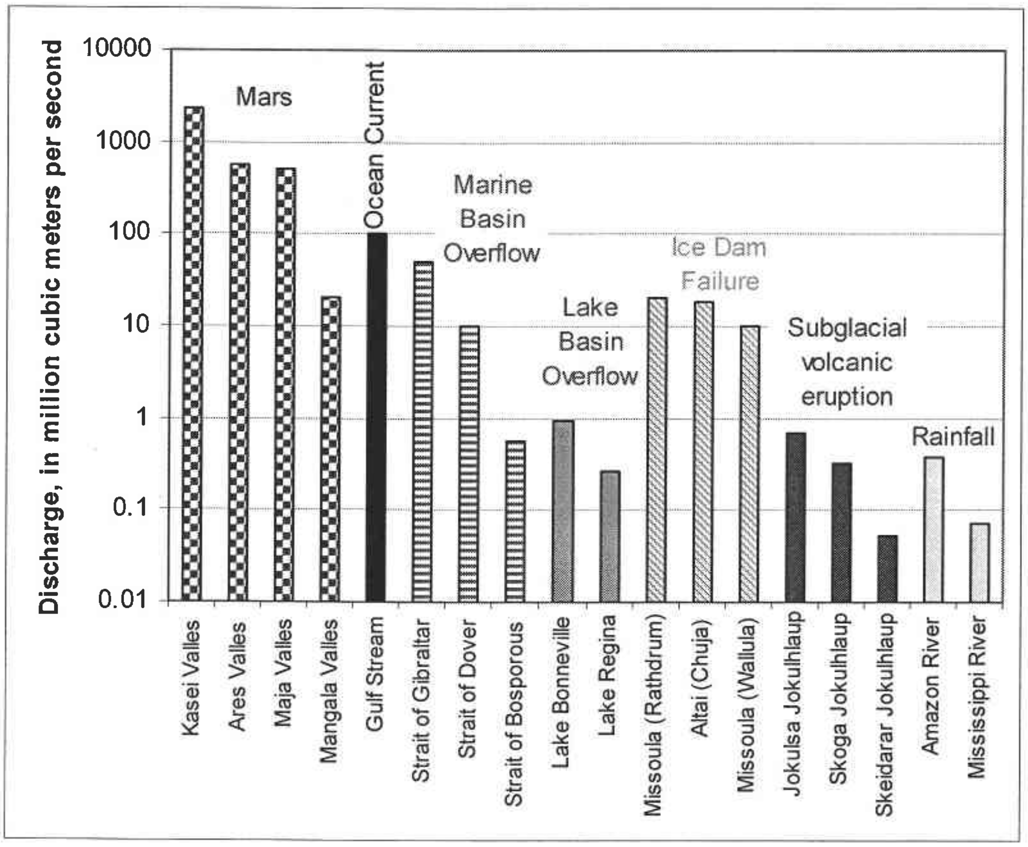

Figure 8-4. Comparison of discharge estimates for extreme flow events.

Table 8-2: Comparison of hydraulic parameters of megafloods, modified from Baker [2002b].

Location	Age (ybp)	W (km)	D (m)	V (m/s)	Q (m^3/s)	τ (N/m^2)	ω (W/m^2)	Slope	Source
Missoula (Rathdrum)	< 19,000	6	150	25	2×10^7	1×10^4	2×10^5	0.01	O'Connor & Baker [1992]
Missoula (Wallula)		1.5	250	27	1×10^7				
Altai (Chuja)	47,200 – 23,000	2.5	400	20 – 45	1.8×10^7	5000 – 20,000	10^5 - 10^6	0.01	Baker et al. [1993]
Bonneville	14,500	0.5	100	26	9.35×10^5	2.5×10^3	7.5×10^4	.0041	Jarrett & Malde [1987]
Souris (Lake Regina)		8	100	4.8	2.7×10^5			0.00019	Kehew [1982]
Dover		20	50	13	1×10^7				Smith [1985]
Gibraltar		6	300	30	5×10^7				Baker [2002b]
Bosporous	7,550	1	100	6	5.78×10^5				Ryan et al. [1997]
Gulf Stream		50 – 75	1000	1-3	1×10^8				Gross [1987]
Skoga Jökulhlaup	1500			4 – 18	3.3×10^5				Maizels [1989]
Jökulsa	2,500 – 2,000	5 – 10	10	10	7×10^5				Waitt [2002]
Skeiðarár jökulhlaup	8			2 – 3	5.2×10^4				Snorrason et al. [2002]
Amazon River (peak flow)	52				3.85×10^5				Rodier & Roche [1984]
Mississippi River (annual average)			12	2 – 3	4×10^4	5	10	.0005	Komar [1979]
Mars									
Mangala	?	15	750	14	2×10^7	3×10^3	6×10^4	0.003	Komar [1979]
Maja	?	80	100	38	5×10^8	2×10^4	8×10^5	0.02	Carr [1979]
Ares	?	25	400	25 – 100	5.7×10^8	1×10^5	3×10^6	0.02	Komatsu & Baker [1997]
Kasei	?	300	500 – 1000	30 – 75	$0.9 – 2.3 \times 10^9$	1×10^5	3×10^6	.001	Robinson & Tanaka [1990]

Island Shape Analysis in Terrestrial Megaflood Areas

One of the distinguishing features of the Channeled Scablands described by Bretz [1923] was the presence of fluvially-shaped streamlined loess hills. Streamlined residuals are known to form under moving glacial ice (known as drumlins) and by aeolian processes (yardangs), as well as in flowing rivers. Using aerial photographs, I measured the lengths, widths, and areas of 20 streamlined residuals near the town of Marengo, Washington. An example of a streamlined Scabland residual is shown in Figure 8-5. Figure 8-6 shows the power functions that describes the correlations between the islands' lengths and widths to their areas. The sizes of the residuals analyzed here are comparable to island sizes on the larger rivers, such as the Columbia, Mississippi and Yukon Rivers (Figure 8-7). Streamlined residuals in the Scablands can be one to two magnitudes greater in size than river islands, however [Baker, 1979].

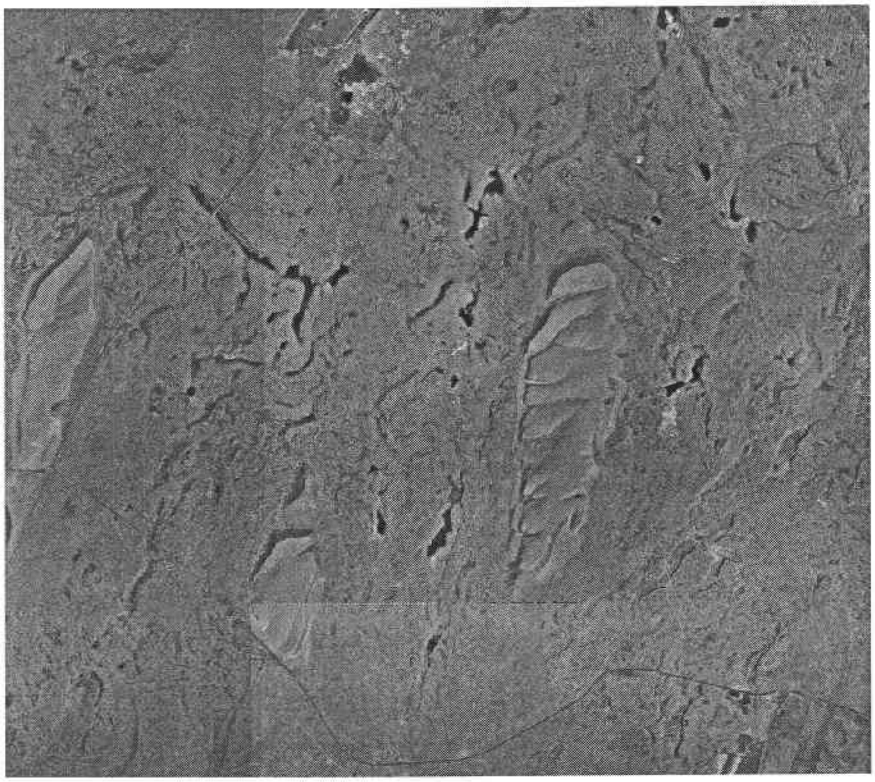

Figure 8-5. Examples of streamlined hills in eastern Washington state (Marengo Quad). Flow is presumed to be towards the bottom of the photograph.

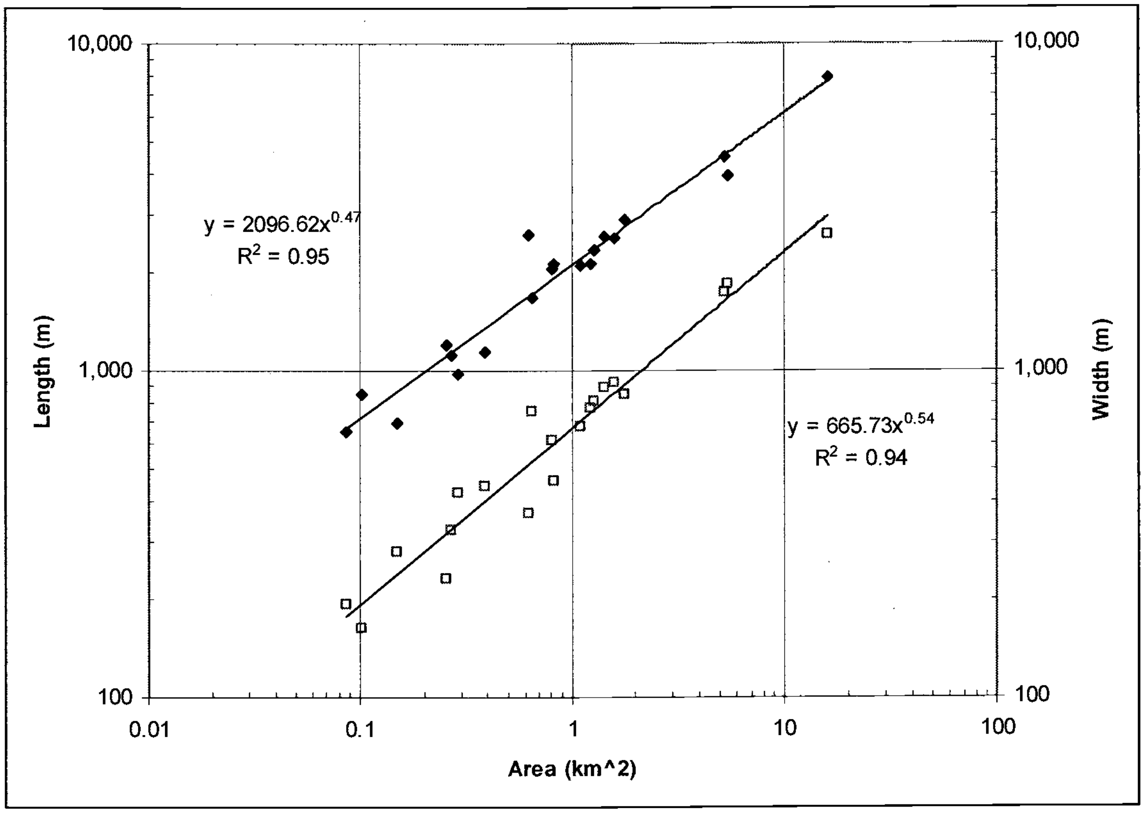

Figure 8-6. Relationship between Scabland residual islands' length and width to area.

Baker [1979] used topographic maps to analyze the planform shape of 137 streamlined residuals in the Scablands. He found a good length-to-width correlation, $W=0.34L^{0.98}$ ($R^2=0.87$), and even a slight increase in streamlining (increase in elongation factor, k [see Chapter 6 for definition]) with increasing Reynold's Number. Kehew and Lord [1986] used topographic maps and aerial photographs to analyze the shapes of streamlined residuals in the Souris spillway that drained Glacial Lake Regina near Minot, North Dakota. The comparisons of each of these megaflood areas are shown in Table 8-3.

Figure 8-7 shows the comparison of length/width ratios of Scabland residuals to those in the rivers discussed in Chapter 7. The correlation of lengths and widths match favorably to the correlation of river islands.

Table 8-3. Comparison of aspect ratios for islands formed by megafloods.

Source	Location	Number of Islands	Average Aspect Ratio	Length v. Area*	Width v. Area*
Baker [1979]	Channeled Scablands	135	3.15	$1.93A^{0.48}$ R^2=0.88	$0.66A^{0.50}$ R^2=0.86
Wyrick [2003]	Channeled Scablands	20	3.37	$2.1A^{0.47}$ R^2=0.95	$0.67A^{0.54}$ R^2=0.94
Kehew & Lord [1986]	Souris Spillway	34	2.88	$2.11A^{0.54}$ R^2=0.94	$0.68A^{0.47}$ R^2=0.92
This paper	American rivers	420	4.14	$2.48A^{0.51}$ R^2=0.98	$0.60A^{0.49}$ R^2=0.97

* Units for lengths and widths are in kilometers, areas in square kilometers

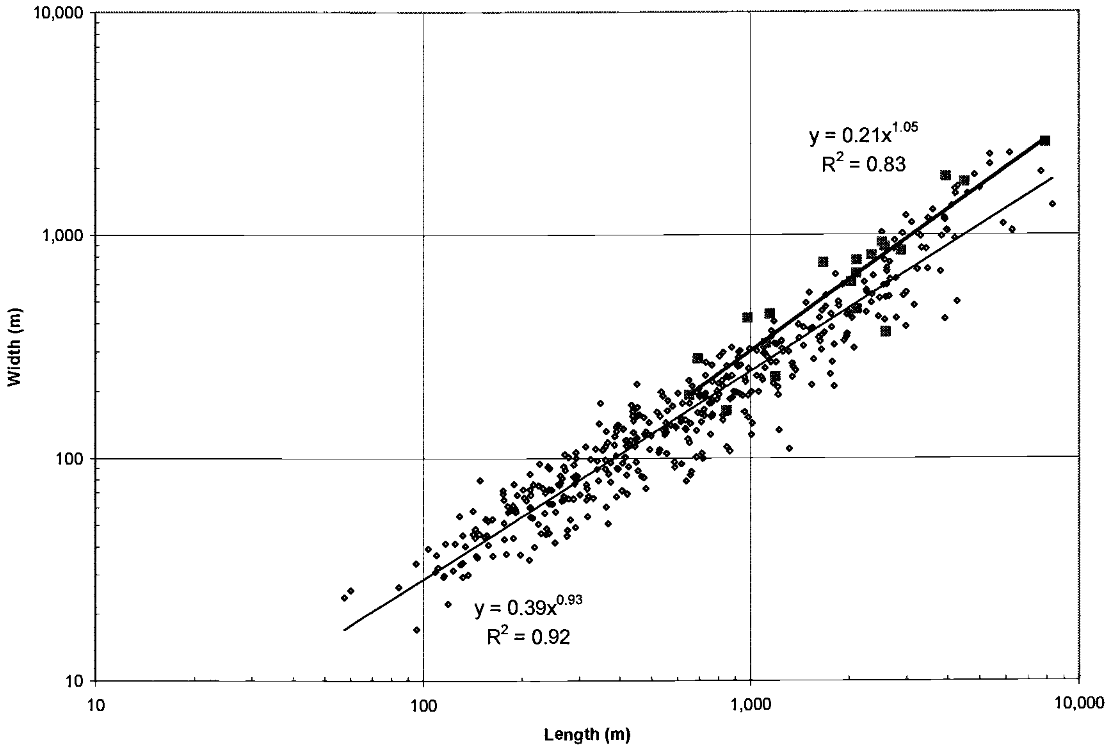

Figure 8-7. Length-Width relationship for residual islands in the Channeled Scablands (solid squares) and fluvial islands in American Rivers (open diamonds).

EXTREME MARTIAN FLOODS

When early civilizations first began observing Mars, its prominent blood-red color caused people to name the planet after their respective gods of war. This association created a sense of fear and awe about the planet, and Mars became a symbol of war and aggression for thousands of years; in fact, panic ensued in 1719 when Mars was in opposition and closer to Earth than it would be until 2003.

In the 17th century, Galileo Galilei was the first to observe Mars through a telescope. Since then, the question of water on the planet has been forefront on many astronomers' minds [Carr, 1996]. Other 17th and 18th century astronomers, notably Christiaan Huygens, Giovanni Cassini, Giancomo Miraldi, and William Herschel, made accurate measurements of the Martian day, the advance and retreat of the polar icecaps, and the movement of dust and water clouds. Most scientists observed large dark areas on the surface and incorrectly assumed them to be oceans. 19th century maps of Mars even included continents and oceans.

In 1877, Giovanni Schiaparelli mapped a suite of long, straight lines on the surface, claiming them to be 'canali' [Flammarion, 1892]. If translated correctly, 'canali' means 'channels', but his announcement instead was interpreted to be 'canals' (perhaps because of the concurrent construction and excitement of the Suez Canal). Canals, as opposed to channels, imply that these features are artificially made, rather than being natural, which led everyone to further suspect intelligent alien life and the presence of flowing water on Mars. Schiaparelli's findings were further corroborated by Percival Lowell in his book *Mars* [1895]. (For more information on the history on the pop culture of Mars, see http://mars.jpl.nasa.gov/mystique/history/.)

Despite other astronomers' claims to the contrary, the notion that Mars had canals persisted well into the 20th century. In fact, prior to the Mariner missions of the 1960's and 1970's, canals were prominent features on the pre-mission planning charts [Carr, 1996]. When Mariner 4 flew by Mars in 1965, it took 22 fuzzy, low-contrast photographs of the planet's surface. Even with the poor resolution of the pictures, no evidence of canals could be found, no oceans, no vegetation, nothing but what appeared to be a cold, dry planet [Leighton et al., 1965]. Flybys by Mariners 6 and 7 in 1969 seemed to confirm this impression of a geologically and biologically dead planet [Leighton et al., 1969]. It was, therefore, a surprise when, in 1971, Mariner 9 returned pictures that showed a planet of geologic diversity and biologic potential. As Mars' first artificial satellite, Mariner 9 compiled a complete mosaic of the surface, including images of huge volcanoes, deep canyons, dune fields, and dry riverbeds. The orbiters of Viking 1 and 2 reached Mars in 1976 and returned more images of the Martian landscape which showed features that strongly suggest erosion by flowing water, such as V-shaped valleys, dendritic channel patterns, and streamlined islands. Twenty years later, the higher resolution mapping technology of the Mars Global Surveyor showed gullies and debris flow features that suggest the presence of liquid water at or near the surface. (For a summary of all NASA missions to Mars, see http://mars.jpl.nasa.gov/missions/.)

The current surface conditions on Mars, however, include a global mean temperature of 218 K (-55 °C) and a mean surface atmospheric pressure of 7 mbar [Squyres and Kasting, 1994]. Liquid water cannot exist in those conditions. The question then arises as to how these apparently fluvial geomorphic characteristics could have formed.

FLUVIAL FEATURES

The valley networks are the most abundant fluvial feature on the Martian surface. Their resemblance to terrestrial drainage patterns have been noted by several researchers [e.g., Milton, 1973; Trevena and Picard, 1978; Komar, 1979; Rakonczai et al., 2001]. If these valleys were fluvially eroded, they suggest a warm, wet climate, since water at these shallow depths (100-200 m) [Goldspiel et al., 1993] would freeze at the current temperatures and pressures before any network could be developed.

Most researchers, therefore, conclude that Mars was not always the cold desert planet it seems today [e.g., Baker et al., 1991; Squyres and Kasting, 1994; Clifford and Parker, 2001]. In the early days of planet formation, Mars could have had an atmosphere [Baker et al., 1991], but due to its low mass and gravity, the atmosphere would have been easily blasted into space as meteors bombarded the planet [Squyres and Kasting, 1994]. But during that early period (about the first half-billion years), climatic conditions could have occurred that would have allowed for flowing liquid surface water. Aging techniques (from crater counts) have determined that most of the small valley systems formed during those first half-billion years.

Whether these channels were formed from precipitation falling and converging or from groundwater sapping (or, indeed, from non-hydrologic means) is unknown. Since most terrestrial rivers combine these two events, the same could be true of the Martian valleys. One difficulty, however, with concluding that these channels were completely fluvially formed is the lack of inner channels [Carr, 1996]. If we are to simply compare the planiforms of these valleys with those of terrestrial valleys, we must compare all aspects. While it is true that the drainage densities and the overall form of the channel networks match terrestrial examples, the inner workings of the valleys do not always match. Inner river channels are expected in terrestrial valleys, but are unseen on Mars. This discrepancy, however, has not prevented most researchers to claim a fluvial origin for these channels.

Other features of possible fluvial erosion on Mars are the large outflow channels (Figure 8-4), some as wide as 100 km and as long as 2000 km. Most of these channels originate in chaotic terrain (an area of jumbled blocks that seems as if the ground collapsed), or grabens (tectonic fractures or elongated depressions), or other features that would suggest a subterranean water source. These large channels generally exhibit low sinuosities, high width-to-depth ratios, transected divides, scour marks around flow obstacles, longitudinal grooves, and streamlined features [e.g., Baker and Milton, 1974; Baker, 1979; Baker et al., 1992a; Carr and Malin, 2000]. From crater counts, we can deduce that the outflow channels have formed during the last half-billion years, possibly up to present day. Since a weather-inducing atmosphere is theorized to have disappeared by this time, the genesis for these outflow channels must be different than for the smaller drainage networks.

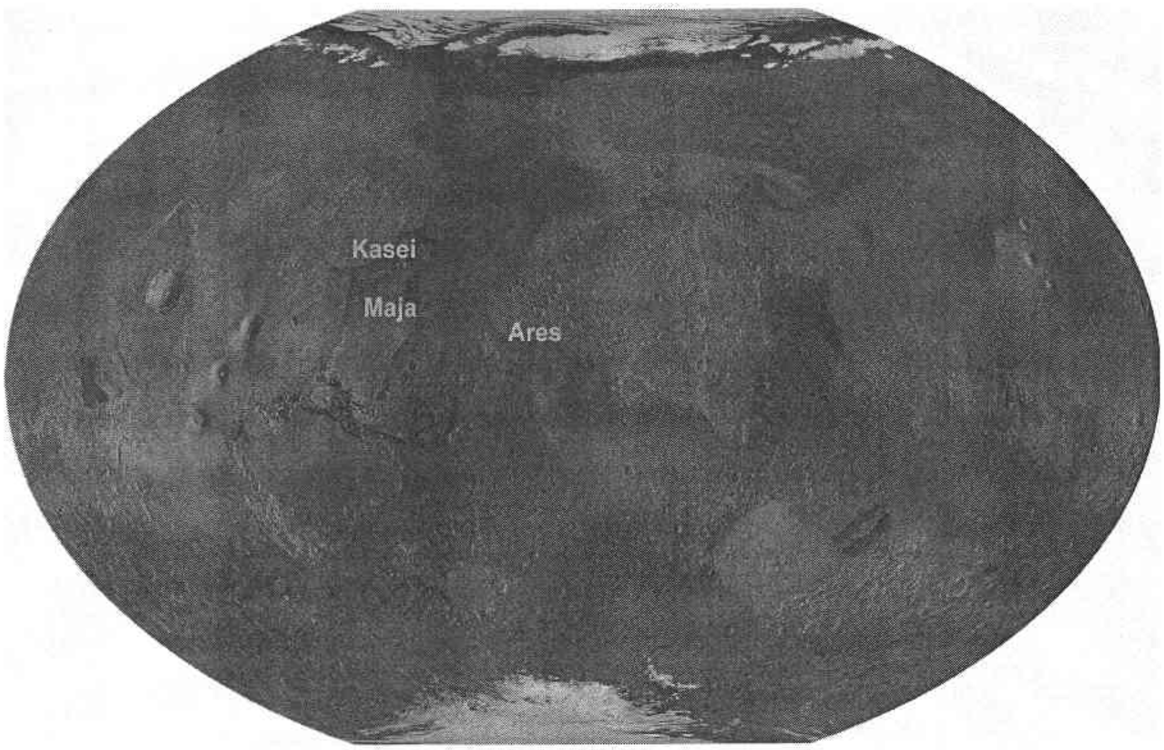

Figure 8-8. Map of Martian surface. Highlighted areas indicate hypothesized areas of cataclysmic flooding.

The dominant theory is that of formation by cataclysmic, short-lived fluvial outbursts similar to the Missoula Floods in northwest U.S. and the Altai Mountains in southern Russia [e.g., Baker and Milton, 1974; Carr, 1979; Tanaka and Chapman, 1990]. The source water for these outburst floods was most likely subsurface water or melted ground ice (see below for discussion). The accepted theory is this catastrophic flood model, mainly because all of the outflow channel features can be found in analogous terrestrial flood examples [Baker and Milton, 1974; Komar, 1979]. Again, however, some problems arise with this theory. The major discrepancies are the instability of liquid water at the surface under the climatic conditions during the time that these channels were formed, and the lack of depositional features at the channels' termini [Baker et al., 1992a].

Because of the problems with the theory of liquid water as the erosional agent, several other hypotheses have been advanced. It is generally accepted that these channels were carved by some kind of fluid flow; the debate is what type of fluid, though. Other fluids that have been suggested are: lavas [Carr, 1974], liquid hydrocarbons [Yung and Pinto, 1978], mudflows [Nummedal, 1978], winds [Blasius and Cutts, 1979], glaciers [Lucchitta, 1982], and liquid carbon dioxide [Hoffman, 2000]. While it has been shown that each of these alternative fluids can create some of the features of the Martian channels, the only theory that can account for the entire suite of features is that of liquid water floods [Baker, 1982; Baker, 2002b].

SOURCE OF WATER

If these features were formed by water, then we must explore the question of the genesis of the valleys, i.e., 'where is the water?' Because of the prevailing surface conditions, liquid water cannot exist on the surface. Water is known to exist, however, on Mars, either as water vapor in the atmosphere or frozen at the poles. Neither of these seems likely candidates for the creation of outflow channels since there is not nearly enough water vapor available to condense for such flows and the origins of the channels are near the equator, not the poles. Therefore, researchers have guessed at the existence of a third reservoir of water – beneath the surface. How possible is this idea?

The upper layer of the Martian geosphere is mostly blocky, brecciated, and impact-dominated, creating a porous zone referred to as the megaregolith. This layer must grade downward to a depth of self-compaction of the pore spaces (< 1% porosity). Researchers, notably Clifford [1993], have defined this depth using Athy's Law [e.g., Ingebritsen and Sanford, 1998]:

$$n_z = n_o \exp(-z / K) \qquad (8\text{-}1)$$

where n_z is the porosity at depth z, n_0 is the porosity at the surface, and K is a decay constant. A decay constant of 6.5 km has been calculated for the Moon, and Clifford [1993] derived a Martian decay constant of 2.82 km based on a ratio of the gravities – $K_{mars} = K_{moon}(g_{moon} / g_{mars})$. The surface porosity is unknown, but the range of values can be estimated. The surface porosity of the Moon has been estimated to be about 20%. Measurements from the Viking Landers showed porosities nearing 50%. Clifford [1993] uses both values for reference. For a surface porosity of 20%, the total storage capacity would be about 8 x 10^7 km^3, which is equivalent to a constant 540 m of water covering the planet. For a surface porosity of 50%, the volume increases to 2 x 10^8 km^3 and the depth to 1400 m.

Under current climatic conditions, part of the water that would fill this potential reservoir must be frozen. Researchers have applied several terms to this zone, including ground ice, cryosphere, and (incorrectly) permafrost [Carr, 1996]. I will use the term 'cryolithosphere', long used by the Russians to denote permanently frozen ground. Evidence for a cryolithosphere is substantial in the literature [e.g., Carr and Schaber, 1977; Soderblom and Wenner, 1978]. Most of the evidence stems from mass-wasting features, thermokarst topography, and the morphology of crater ejecta. The depth of the cryolithosphere can be calculated from the equation:

$$z_c = K\,(T_{mb} - T_{ms})\,Q_h \qquad (8\text{-}2)$$

where K is the thermal conductivity, T_{mb} and T_{ms} are the melting temperature of ice at the base of the cryolithosphere and the surface respectively, and Q_h is the geothermal heat flux. The thermal conductivity on Earth for frozen soils and basalts is 2.0 W m^{-1} K^{-1}. We can assume similar properties on Mars [Clifford, 1993]. The melting temperature at the base of the cryolithosphere is estimated be about 252 K, based on recent evidence from the Mars Rovers that any water present on Mars would be fairly saline. The heat flux for Mars has been estimated to be about 30 mW m^{-2}, compared to a terrestrial value of 82 mW m^{-2}. Since the latitudinal surface of Mars is not flat, the surface melting temperatures vary. From these depths, we can infer a storage capacity of the ground ice. For a porosity of 20%, the capacity is equivalent to 374 m of water covering the surface. Comparing this depth to the total storage capacity of the megaregolith of 540 m, there is 177 m of remaining equivalent depth that could be occupied by liquid water. A porosity of 50%, gives a cryolithic storage capacity of 940 m equivalent depth, which leaves 460 m of equivalent depth for liquid water.

GEOTHERMAL ASPECTS

If the fluvial channels were formed by precipitation and runoff, then the prevailing climate would control them. If the channels were formed by groundwater outflow, then geothermal heat would control them. In the earlier stages of its development, Mars had a higher mantle heat flux and thinner lithosphere [Schubert et al., 1992], which would allow for more liquid groundwater to come to the surface. The geothermal gradient depends on heat flow and the thermal conductivity of the regolith. It is difficult to determine the conductivity of the Martian regolith, but conductivities in terrestrial permafrost areas are in the range of 0.5 – 1.0 W m^{-1} K^{-1} [Clifford and Fanale, 1985]. Using these values, we can estimate that the present geothermal gradient on Mars is between 0.03 – 0.06 K/m. Researchers have modeled the evolution of the gradient through time, and have found that before about 4 billion years ago, the geothermal gradient was in the range of 0.18 – 0.36 K/m [Schubert et al., 1992]. With present climatic conditions and these high gradient values, liquid water would exist within 150 – 300 m below the surface. If the water is more saline (which is probable), then this depth would be even shallower. Areas of concentrated magmatic activity and large impacts create high localized heat gradients, which would decrease the melt depth and produce water temperatures well above freezing near the surface.

Most evidence of channel formation points to origins due to groundwater sapping. However, most sapping valleys are well developed, which requires more than one flow event. Therefore, there must have been aquifer recharging. There are two main methods for aquifer recharge – precipitation or hydrothermal convection. Hydrothermal convection is caused by density gradients that are created by non-uniform heating of the aquifer that will cause a buoyancy-driven flow. The primary mechanism for hydrothermal convection is magmatic activity and impact heating. Areas of either pronounced magma activity or dense crater impacts would have rocks of high permeability (lava rocks and impact-brecciated regolith), which is necessary for high convection rates, and high porosities that allow for quick recharging and head differentials sufficient to maintain the groundwater flow. A magma plug of 100 km^3 could have continuously circulated fluids for about 10^5 years [Squyres and Kasting, 1994]. The widespread distribution of valley networks on Mars requires a planet-wide repetition of local endogenic heating [Baker et al., 1991].

As hydrothermal activity decreased, so did fluvial activity. Hydrothermal convection seems to be linked with meteor impact density, since most valley networks are ancient, occurring during the first 1.5 billion years – a time of heavy bombardment. After the impacts decreased, most of the channels were carved by cataclysmic outflows that are usually localized on volcanic flanks. This change also coincides with a change from volcanism in the cratered terrain to volcanism in the Tharsis and Elysium zones [Tanaka and Chapman, 1990]. The post-Noachian (after the first 1.5 billion years) climate became very cold and dry, disrupted by brief intervals of very large floods. The disruption mechanism was mainly volcanism. Anomalously hot mantle would gradually build up to a critical threshold for decompressive melting. For comparison numbers, Baker et al. [1991] described how a magma plug of 10^7 km^3 would have added 10^{32} ergs of thermal energy, about doubling the geothermal heat flux from 25 to 50 erg cm^{-2} s^{-1} and doubled the geothermal gradient from 25 to 50 K/km. This energy increase would have melted huge amounts of ground ice (~5 x 10^6 km^3) and set up a large thermal convection system that would tend to attract groundwater from adjacent areas. The energy increase would also have driven the now liquid water out through the permeable rocks to the surface.

Hydrogeology

Many of the outflow channels appear to originate from cratered or faulted terrain. Hydrothermal heat probably did not act alone in creating the floods. A high discharge of groundwater requires a high hydraulic head [Carr, 1979]. Since there is no atmosphere to produce precipitation to recharge the aquifers, the head must be provided by elevation or overpressuring the existing groundwater. Mechanisms for these scenarios include tectonic compression or uplift, hydrothermal circulation, and sediment compaction.

Flood-sized flows require large interstitial voids in the rock. These voids may be created by jointing along a fault or by increasing the pore water pressure (hydrofracture), which can occur during faulting and quaking. Hydrofracturing would also occur if the lithostatic pressure is surpassed (about 11 MPa/km, compared to 25.5 MPa/km on Earth). As the surface became colder, the base level of the cryolithosphere would drop, thereby increasing the pore pressure, eventually to lithostatic pressure and beyond. If a graben is deep enough (~ 2 km), it may connect with tension cracks that would provide a conduit for the groundwater to reach the surface. On Earth, tension cracks are common outlets for groundwater [e.g., Laity and Malin, 1985]. If this is also the case on Mars, then rocks with really high permeabilities are not necessary to produce the discharge rates evidenced on the surface.

Tanaka and Chapman [1990] studied the catastrophic flooding that originated at Memnonia Fossae (graben) and carved out the Mangala Valles. They note that the Memnonia graben cuts through lava and cratered terrain, both of which are potential aquifers due to their high porosities (~ 20%) and permeabilities (~ 10^{-2} darcies). Magmatism may have melted ground ice and circulated the water to peripheral areas, which would have saturated the rocks, thus increasing the pore pressures. Radial faulting is evident at Memnonia Fossae, which would create isostatic uplift, which would increase the hydraulic head and fracture any groundwater barriers, thus resulting in groundwater discharge. Flow would cease if the drawdown reduced the flow enough to freeze and reseal the aquifer or when the hydraulic head in the aquifer equaled the depth of burial.

By calculating reasonable estimates for surface discharges and excavated channel volumes (see below for more discussion), we can estimate the total volume of water that was expelled from the aquifer. Tanaka and Chapman [1990] estimated the flood volume for the Mangala Vallis to be about 5×10^{12} m^3. Determining the size of the aquifer below Memnonia Fossae is difficult. The total length of the graben is about 2000 km. By making reasonable assumptions for the depth (1 km) and the width (25 km), then the outflow events would have only emptied about 5% of the pore volume [Tanaka and Chapman, 1990].

After the floodwaters left the subsurface, there was no reentry into the groundwater system because the permafrost layer is too thick [Carr, 1979]. During the early warmer climates, the water could have pooled in a large northern ocean [Baker et al., 1991]. This ocean could have also been the recharge for the extensive aquifer system. During the recent, cataclysmic events, the water probably sublimated and was either lost to space or circulated in the atmosphere as water vapor until it refroze at the poles. This means, however, that there has probably been no recharge to the groundwater since the Noachian period. Each time an outburst flood event would occur, it would drain a little more water from the subsurface, until there would be not enough remaining to produce the pressures necessary for release. This could be a preemptive reason as to why we would not find liquid water if we were to drill on Mars now.

Magnitude of Flows

Could the discharge from a subsurface outburst be sufficient for the discharge necessary to create the surface features we observe? Most researchers have used a modified form of the Manning's Equation [Carr, 1979; Komar, 1979] or computer simulations such as HEC-RAS [Burr, 2003] and FLOWMASTER [Komatsu and Baker, 1997] to calculate the surface discharges based on the observed channel dimensions. Komar [1979] derived a flow velocity (v) by equating shear stress equations that describe the driving force of the flow and the opposing frictional force to obtain the expression:

$$v = (ghS / C_f)^{0.5} \qquad (8\text{-}3)$$

where g is the gravitational constant, h is the flow depth, S is the channel slope, and C_f is a dimensionless friction coefficient. This expression is similar to the Chezy equation applied to one-dimensional flow. If we compare this equation to the empirically-derived Manning's equation for one-dimensional flow:

$$v = n^{-1} h^{2/3} S^{1/2} \qquad (8\text{-}4)$$

where n is Manning's roughness coefficient, we can derive a relationship between Manning's n and the friction coefficient:

$$C_f = g_m (n^2 / h^{1/3}) \qquad (8\text{-}5)$$

Since the values of Manning's n are not unitless and were derived empirically, we must use a conversion factor based on the gravities of Mars (g_M=3.72 m^2/s) and Earth (g_E=9.81 m^2/s) [Komatsu and Baker, 1997]:

$$n_M = n_E (g_E / g_M)^{0.5} = 1.62\, n_E \qquad (8\text{-}6)$$

Once the velocity has been calculated, the discharge (Q) can be calculated by measuring the channel depth (h) and width (w):

$$Q = vhw \tag{8-7}$$

The channel slopes and widths are fairly simple to measure from satellite imagery. The observable depths of the valleys really only give maximum flow depths, and if multiple floods occurred, individual flood depths could have been significantly less than the observed valley depth. Several early researchers used a range of depths to produce a range of possible discharges [Komar, 1979; Baker, 1982]. Recent Mars Orbital Camera (MOC) imagery is detailed enough to show ridgelines within the channels, so that now researchers can better estimate the actual flow depths, and hence discharge [e.g., Burr et al., 2002].

Manga [2004] manipulated the original Manning's equation to derive an expression that includes a gravity term:

$$Q = 0.32\, n^{-1}\, g^{1/2}\, S^{1/2}\, R^{5/3} \tag{8-8}$$

where R is the hydraulic radius of the channel, for which the flow depth, h, is usually taken as a proxy when the channels exhibit a large width/depth ratio (i.e., for relatively wide channels).

For the smaller, meandering channels on Mars, Weihaupt [1974] used empirical terrestrial equations to relate meander length (L) and channel width (w) with discharge:

$$L = 168\, Q^{0.46} \tag{8-9}$$

$$w = 4.88\, Q^{0.8} \tag{8-10}$$

Groundwater discharge was calculated for the Chryse Region by Carr [1979] by solving the groundwater flow equation:

$$\nabla^2 H = \frac{1}{\kappa}\frac{\partial h}{\partial t} \tag{8-11}$$

where h is the hydrostatic head and κ is the hydraulic diffusivity – a ratio of transmissivity (T) and storage coefficient (s). The transmissivity is calculated by:

$$T = k\rho g b / \mu \tag{8-12}$$

where k is the permeability, ρ the fluid density, b the aquifer thickness, and μ is the viscosity. The storage coefficient is calculated by:

$$s = \rho g b\,(\alpha + n\beta) \tag{8-13}$$

where α is the vertical compressibility of the aquifer, n is the porosity, and β is the fluid compressibility. From this, the discharge becomes a function of time, diameter of outlet, aquifer depth, and permeability.

Head et al. [2003] derived an expression for fissure discharge by calculating the vertical rise speed of water in a fracture that involves the fissure geometry and friction.

Manga [2004] used Darcy's equation to describe flow from an aquifer to a fracture:

$$Q = \frac{k_h \rho g H}{\mu} \frac{\partial h}{\partial x} \tag{8-14}$$

where k_h is the horizontal permeability. Manga then characterized the flow through the fracture as flow between two rough plates, described by:

$$Q = \sqrt{\frac{2h_o g w^3}{fD}} \tag{8-15}$$

where h_o is the hydraulic head at the bottom of the fracture, w is the fracture width, f is the friction factor of the fracture, and D is the fracture length.

The surface and subsurface discharges calculated by previous researchers for specific channel regions on Mars are summarized in Table 8-4.

Table 8-4. Summary of surface and sub-surface discharge estimates for specific channels on Mars.

Channel	Maximum Discharge (cms)	Source	Groundwater Discharge (cms)	Source
Area Vallis	10^8 5.7×10^8	Carr [1979] Komatsu & Baker [1997]	10^7	Carr [1979]
Maja Vallis	5×10^8 3×10^7	Carr [1979] Baker [1982]	10^7	Carr [1979]
Kasei Vallis	$0.9 - 2.3 \times 10^9$	Robinson & Tanaka [1990]		
Mangala Vallis	2×10^7	Komar [1979]	10^7	Tanaka & Chapman [1990]
Athabasca Vallis	$1 - 2 \times 10^6$	Burr [2003]	10^6 4.4×10^6	Manga [2004] Head, et al. [2003]
Marte Vallis	$2 - 5 \times 10^7$	Burr & McEwen [2002]		
Meandering channel in Mare Eythraeum	2700 (based on L) 10^5 (based on w)	Weihaupt [1974]	No GW theorized	

It seems that, in most cases, the available groundwater discharge could match the necessary surface discharge. Carr's [1979] estimations for the Ares and Maja regions fall short of his own surface calculations by an order of magnitude, but he claims that these values are fairly close considering that he had to guess at most of the variables used in his calculations.

The duration of these floods can be calculated from the discharges and excavated channel volumes. Ares Vallis drains the Margaritifier, Iani, and Aram Chaos regions. Carr [1996] estimated the total excavated volume of the Ares channel and the associated Chaos Terrain to be 2×10^5 km^3, and assumed that all this volume was eroded out by the flood. If the resulting flow was hyperconcentrated (40% sediment by volume), then the total volume of water expunged in the flood was about 3×10^5 km^3. Using Komatsu and Baker's [1997] estimate for the discharge in Ares Vallis, the flow duration would only be about 6 days. However, Komatsu and Baker's discharge estimate was for a maximum stage of between 400 and 985 meters. It is unlikely that the flow sustained such a depth for the entire time, and therefore the total duration of the flood could be longer.

The main region for the outburst flows are near the Chryse Planitia, which collects the drainage of Kasei, Maja, Tiu, and Ares Valles, among others. These channels seem to originate from Chaotic Terrain. Other locations of possible outburst flows are from grabens, such as Cerberus Fossae, which germinates the Athabasca and Marte Valles, and Memnonia Fossae, the origin of Mangala Vallis. Kasei Vallis is the largest channel with depths between 500 and 1000 meters and widths up to 300 kilometers across, and it exhibits the largest possible discharge as well at 10^9 m^3/s. By comparison, the largest floods thought to have occurred on Earth are associated with glacial outbreak flows during the last Ice Age (Missoula Floods and Altai Mountains Floods) and peak at about $1 - 2 \times 10^7$ m^3/s. The largest estimated *flows* on Earth, associated with spills between marine basins through straits, such as Gibraltar and Dover, peak around $2 - 6 \times 10^7$ m^3/s [Baker, 2001]. Present-day terrestrial rivers have flows that are merely a fraction of these discharges, e.g., Amazon River (3×10^5 m^3/s) and Mississippi River (3×10^4 m^3/s).

SEDIMENT TRANSPORT IN MARTIAN FLOODS

There are several parameters necessary to calculate sediment transport in flows. These parameters would not necessarily be the same on Mars due to gravitational differences ($g_m = 3.72$ m/s^2). Table 8-5 is modified from Rossbacher and Rhodes [1987] and summarizes the effect of the Martian gravity for flow in a channel of the same geometry as on Earth.

Table 8-5. Effect of Martian gravity on sediment transport parameters.

Sediment Transport Parameter	Proportionality to gravity	Mars relative to Earth
Stream velocity, v	$g^{1/2}$	smaller
Froude number, Fr	v^2 / g (= 1)	equal
Potential energy, P_E	g	smaller
Shear stress, τ	g	smaller
Shear velocity, u_*	$\tau^{1/2} = g^{1/2}$	smaller
Darcy friction factor, f	τ / v^2 (= 1)	equal
Chezy coefficient, C	$g^{1/2}$	smaller
Stream power, ω	$\tau v = g^{3/2}$	smaller
Settling velocity, w_s	$g^{1/2}$	smaller

If we also assume that the velocity is equal between the flows on Mars and Earth (as Rossbacher and Rhodes [1987] did), then the Froude number would be greater and the Darcy friction factor would be smaller on Mars than on Earth.

Komar [1979] used the research of Bagnold [1966] to estimate the sediment transport rate for Mangala Vallis. Komar [1979] shows that the sediment transport rate is equivalent to within an order of magnitude of the stream power. The sediment transport rate per unit width, i, can be expressed as:

$$i = \omega\left(\frac{e_b}{\tan\alpha} + 0.01\frac{v}{w_s}\right) \tag{8-16}$$

where e_b is the bedload transport efficiency, v is the mean velocity, and w_s is the settling velocity of the suspended particles. Tan α is the coefficient of solid friction, and is related to the particle diameter and Shield's relative stress by the dimensionless parameter:

$$\theta = \tau / (\rho_s - \rho)gh \tag{8-17}$$

For a flow depth of 10 m, Komar [1979] showed that i is equal to 4 x 10^5 dyn/cm-sec. When this value is multiplied by the average channel width of 15 km and converted to a volumetric transport rate (Q_s), the result is $Q_s = 6 \times 10^2$ m^3/s. Komar went on to calculate the time necessary to erode the channel by estimating the channel volume to be 2×10^{12} m^3 (L = 18 km, W = 15 km, D = 750 m), and estimated that a flow of 10 m would need about 100 years to erode all of that sediment. A flow depth of 100 m would require only about 500 days. If Komatsu and Baker's [1997] estimate of flow duration from above is correct, then multiple flood events are obviously necessary to excavate the entire channel.

The particle sizes that make up the wash loads, suspended loads, and bedloads can be determined from the settling velocity equation [Komar, 1980]. The wash load consists of the suspended particle sizes that exhibit no distribution gradient throughout the flow depth. The distinction between the particle sizes that make up the suspended load and the bedload can be calculated using the dimensionless k, a ratio of the settling velocity and shear velocity. Komar [1980] found that a particle was bedload for a k value > 1.25. Combing terms, we can solve for settling velocity:

$$w_s = k\,(ghS)^{1/2} \qquad (8\text{-}18)$$

A particle is considered to be wash load (as opposed to suspended load) if $w_s < vS$. Komar [1980] estimated that for a flow depth of 100 m, the wash load included particles up to 1-2 mm in diameter, the suspended load 200 – 1000 mm, and bedload 3500 – 9400 mm.

Most researchers have assumed that the flows on Mars were hyperconcentrated. However, it is unlikely that the uplands where the channels originated contained enough fine material to allow for hyperconcentrations to occur [Carr, 1996]. The flows, though, were powerful enough to create their own material by cavitating the surrounding bedrock [Baker, 1979]. The critical velocity for cavitation in terrestrial flows can be calculated by:

$$v_E = \left(\frac{2g}{3}\right)^{1/2}\left(\frac{P_a - P_v}{\gamma} + h\right)^{1/2} \qquad (8\text{-}19)$$

where P_a and P_V are the atmospheric and vapor pressures, respectively, and γ is the specific weight of water. For present-day surface conditions on Mars, the ($P_a - P_V$) term is negligible [Baker, 1979]. By substituting the Martian gravitational constant into the above equation, the critical cavitation velocity on Mars is:

$$v_M = 1.6\ h^{1/2} \tag{8-20}$$

For a depth of 100 m, the critical cavitation velocity would be 16 m/s, which would more than be surpassed by the flow estimates shown in Table 8-4.

Summary of Martian Floods

The most probable theory for the origin of the large channel formations on the surface of Mars is the liquification of subsurface ground ice and its subsequent expulsion onto the outer surface. Geothermal heat is one cause of the melting and circulation of the ground ice. Geothermal heat is created by magmatic activity in the Tharis and Elysium zones. Heat and tectonic faulting probably worked together in some cases of the outburst flooding. However, even in the absence of geothermal heat, floods can occur due to an increase in the hydraulic head by elevation or overpressuring due to tectonic uplift or fracture. Fracturing of rock crust produced outbreaks that tapped confined aquifers under pressure, due to increased pore pressure, hydrothermal circulation, uplift, or compressional loading from above. Grabens may have connected with subsurface tension cracks, thereby creating conduits for groundwater discharge. Multiple flow events most likely occurred, thus the groundwater barriers must have resealed after each discharge by either decreasing the artesian pressures or clogging the outlet path and the aquifers were re-saturated by continuing magmatic activity. Flow discharges within the various channels range from $10^6 - 10^9$ m^3/s for the large outburst floods. Discharge rates from subsurface aquifers have been shown to be capable of producing the necessary volumes estimated from the surface features.

Island Shape Analysis in Martian Megaflood Areas

Satellite imagery from the Viking orbiters was used to digitally record the lengths, widths, and planform areas of streamlined residual islands within the outwash plain of Ares Vallis (part of which is shown in Figure 8-9). Figure 8-10 shows the relationships between the islands' lengths and widths to their respective areas. Baker [1979] performed a similar analysis on streamlined residuals in Maja and Kasei Valles (Figure 8-8). Baker's analyses included more islands and were located in a different channel, but his regression equations are similar to the regression equations I found for the Ares Vallis islands (Table 8-6).

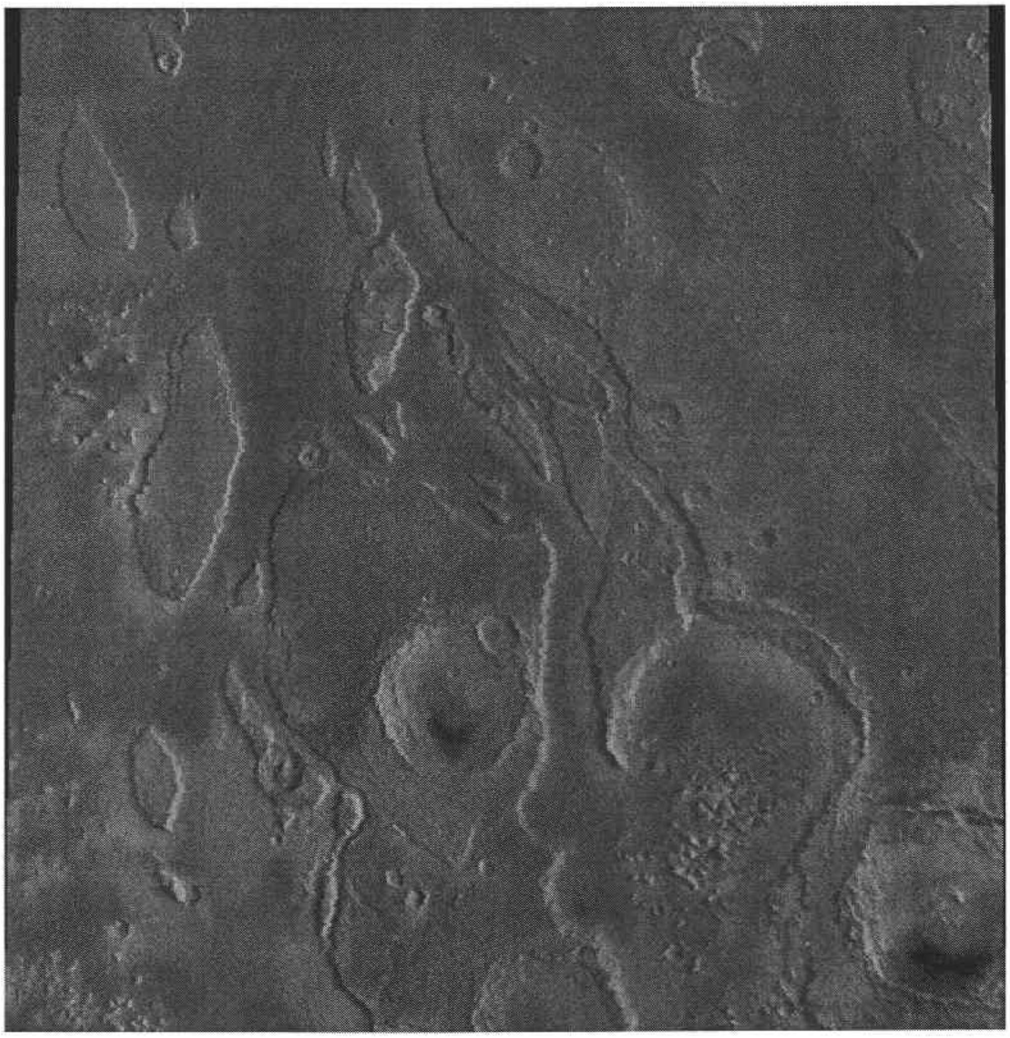

Figure 8-9. Streamlined residuals at terminus of Ares Vallis on Mars.

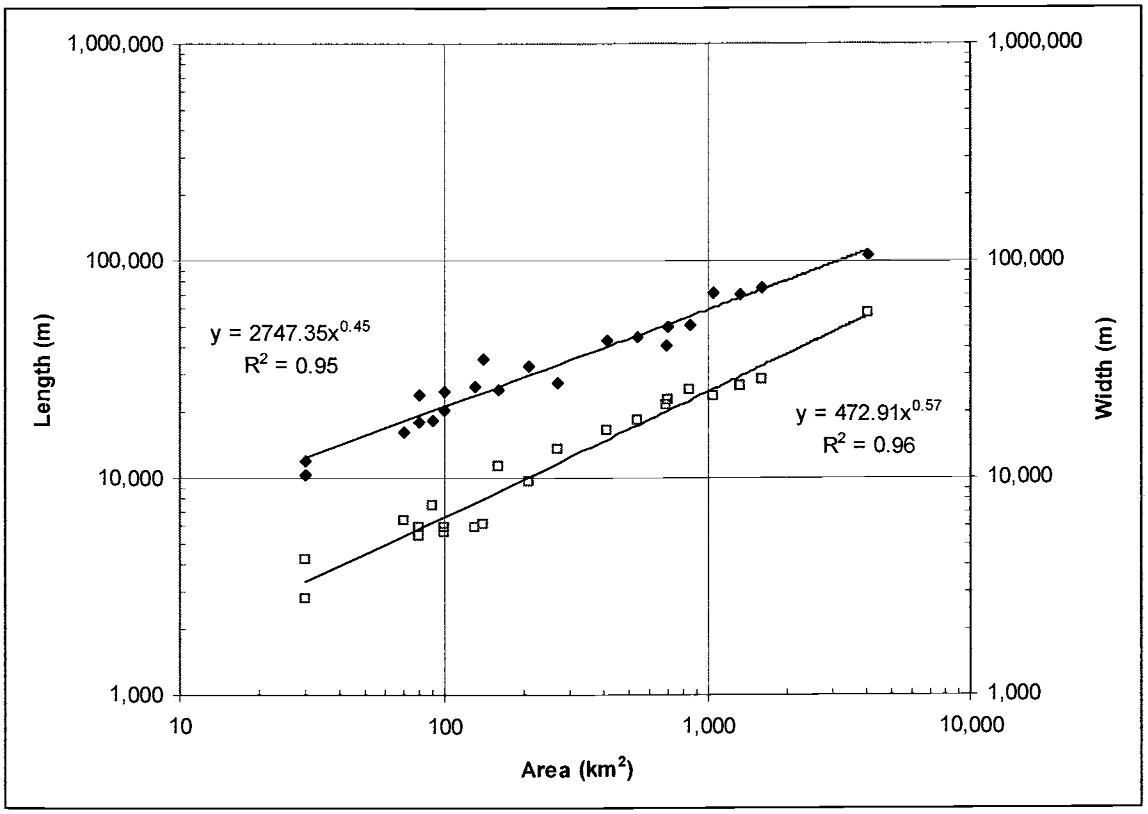

Figure 8-10. Relationship between Martian residual islands' length and width to area.

In Table 8-6, I further differentiate the analyzed islands into 'Crater' and 'Non-crater' islands. A crater island is one that is formed around and in the lee of an impact crater (e.g., Figure 8-11). A non-crater island is one that formed from eroding away the rest of the terrain (e.g., Figure 8-12), similar to residual islands in the Channeled Scablands. The reason for the separation is that the two types of islands may have been formed by different processes (though it would be difficult to actually determine this). The crater islands seem to be similar to the Lee-deposition islands discussed in Chapter 3, whereas the non-crater islands may be erosionally formed. Whether or not these islands were formed by different processes, there does seem to be a difference in their aspect ratios (Table 8-6) and a more detailed analysis of these would be necessary.

Table 8-6. Comparison of aspect ratios of islands formed in Martian megafloods

Source	Island Type	Location	Number of Islands	Average Aspect Ratio	Length v. Area*	Width v. Area*
Baker [1979]	All islands	Maja & Kasei Valles	95	4.05	$2.96A^{0.44}$ R^2=0.91	$0.50A^{0.56}$ R^2=0.95
Wyrick [2003]	Crater islands	Ares Vallis	8	2.32	$2.75A^{0.44}$ R^2=0.88	$0.70A^{0.52}$ R^2=0.96
Wyrick [2003]	Non-crater islands	Ares Vallis	14	3.41	$2.76A^{0.45}$ R^2=0.88	$0.55A^{0.54}$ R^2=0.89
This thesis		American rivers	420	4.14	$2.48A^{0.51}$ R^2=0.98	$0.60A^{0.49}$ R^2=0.97

* Units for lengths and widths are in kilometers, areas in square kilometers

The residual islands analyzed on Mars are one to three magnitudes greater in scale than those in terrestrial rivers (Figure 8-13). The length-to-width relationships, however, of the Martian islands are similar to those of the Scabland islands and terrestrial islands. The relationships between the aspect ratios and elongation factors also are similar to the relationships of the Scabland islands and terrestrial islands (Figure 8-14). These statistical similarities help show that all the islands were formed by similar fluvial processes, and therefore are able to be statistically compared with each other.

Figure 8-11. Streamlined residuals in the lee of craters in Athabasca Vallis. Flow is presumed to be towards the lower left of the photograph. Photo is centered at 9°N, 204°W and shows an area of 12 km x 13 km

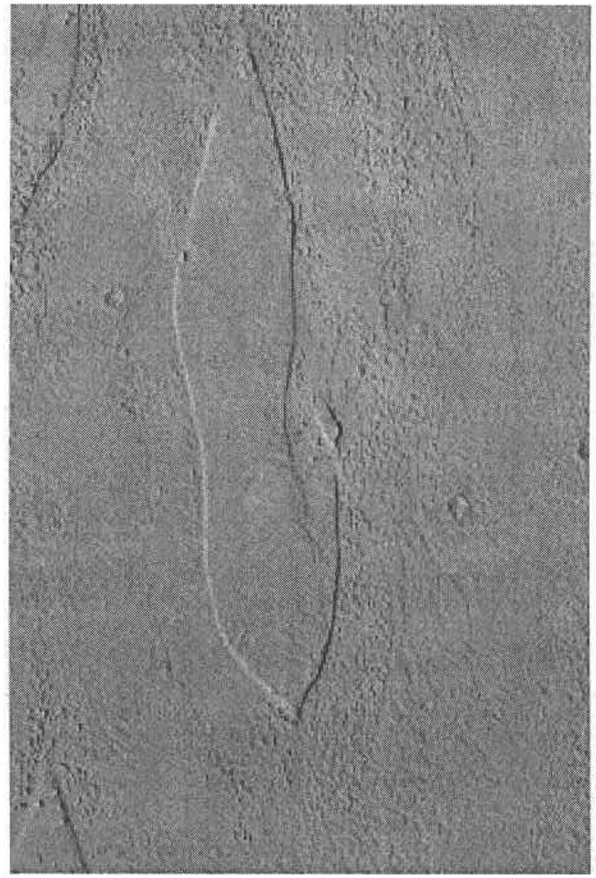

Figure 8-12. Streamlined residual in Marte Vallis. Flow is presumed to be towards the top. Photo is centered at 22°N, 175°W and shows an area of 3 km x 4.5 km

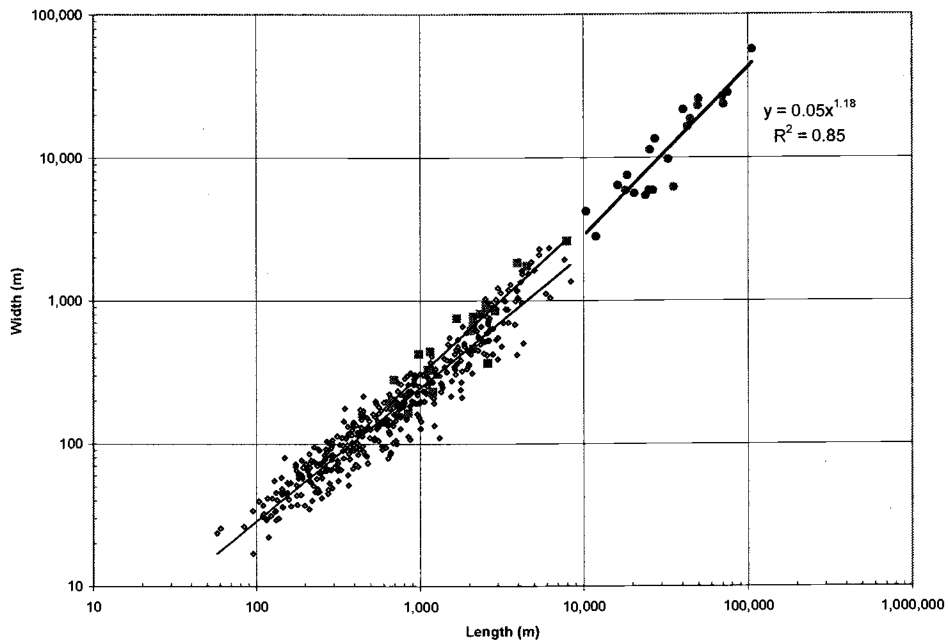

Figure 8-13. Length-Width relationships for residual islands in Martian Channels (solid circles), the Channeled Scablands (solid squares) and fluvial islands in American rivers (open diamonds). Equation for trendline of Martian islands only.

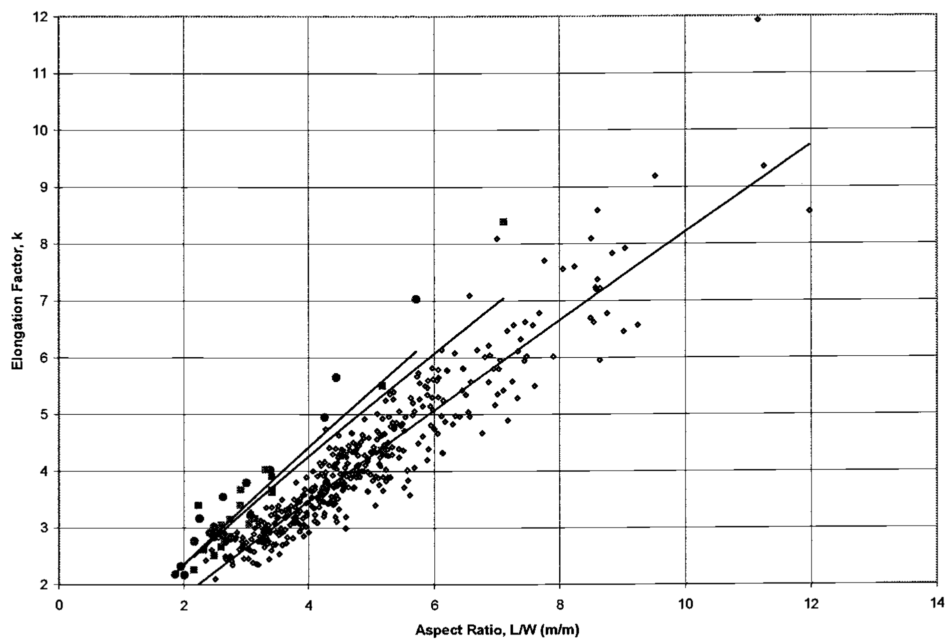

Figure 8-14. Comparison of R_A-k relationships for islands in the Martian Channels (solid circles), Channeled Scablands (solid squares), and American Rivers (open diamonds).

Differences in Sustained Flow and Pulse Flow on Island Formation

Wolman and Miller [1960] stated that the most geomorphically significant fluvial processes may not necessarily occur during the most rare or infrequent flood events. In the cases of megaflood residuals within the Scablands or on Mars, however, the rare events are significant simply because they are the only fluvial events to affect the landforms. The Snake River valley has fluvial islands that have remained unchanged since the Bonneville Flood swept through and formed them [O'Connor, 1993; Osterkamp, 1998]. Islands in the Columbia River, however, have long since lost their memory of the Missoula Floods and are continually being reshaped by the normal river flows.

The formation processes for islands created in megafloods (pulse flows) are limited to either rapid channel degradation around the residual or deposition of material in the lee of a resistant object, whereas river islands (sustained flows) can form by any of the nine processes described in Chapter 3.

The aspect ratios between megaflood regions and sustained river flow regions also show a difference. Aspect ratios range between 2.7 and 3.4 for islands in the Scablands, Souris spillway, and Martian outwash plains [Baker, 1979; Kehew and Lord, 1986; Wyrick, 2003]. The average aspect ratio for the combined suite of islands in American rivers is 4.1. Megafloods produce significantly higher shear stresses and stream powers (Table 8-2) that would be more capable of eroding islands. Rivers experience more depositional flows than erosional flows. The low, non-erosive flows may be responsible for depositing sediment along and behind the islands, thereby increasing their lengths (and hence their aspect ratios).

The megaflood islands generally have a greater elongation factor, k, for a given aspect ratio, R_A, than for river islands (Figure 8-13). Since k is a function of the frictional drag force (see Chapter 7), this discrepancy could also be a result of the difference in the duration of the flows.

Chapter 9 – Summary and Conclusions

Comparison of Islands at various Scales

This research analyzed islands with a wide range of sizes in a wide range of discharges. In order to be able to compare all the islands, I described each island with its equivalent lemniscate shape. The lemniscate provided a means of calculating dimensionless parameters, such as the length-to-width aspect ratio and the degree of elongation. This section summarizes the islands and their lemniscate equivalents through a telescoping range of island sizes.

The smallest type of island analyzed in this study was the artificial island used the flume experiments (Figure 9-1). The average discharge used in these experiments was about 0.5 cfs. The island's length was about 0.8 meters and its planform area was about 1.8 x 10^{-1} square meters.

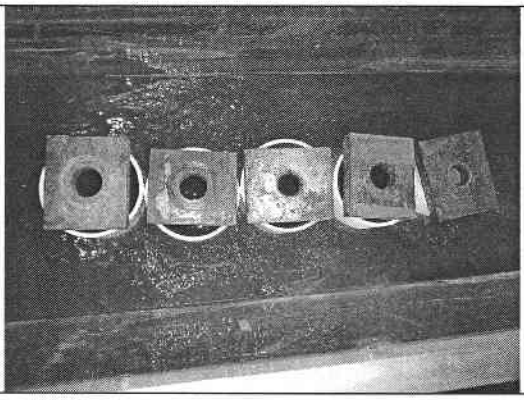	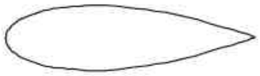
Artificial PVC Island in Flume $A \sim 10^{-1}\ m^2$ $R_A = 4.75$	Equivalent Lemniscate Shape $k = 4.95$

Figure 9-1. Equivalent lemniscate for island in flume experiment.

The next size up was the artificial island made of buckets used in the Oak Creek experiments (Figure 9-2). Its length was about 1.8 meters and its planform area was about 8.6x10^{-1} square meters. At the time of measurement, the discharge in Oak Creek was about 2 cfs.

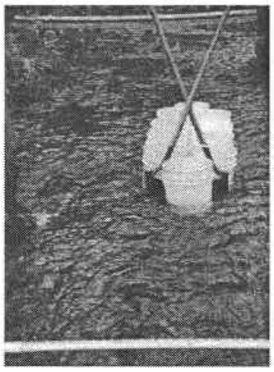	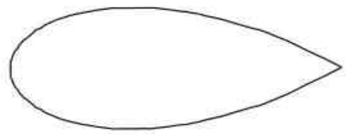
Artificial Bucket Island in Oak Creek $A \sim 10^0\ m^2 \quad R_A = 3.0$	Equivalent Lemniscate Shape $k = 2.95$

Figure 9-2. Equivalent lemniscate for artificial island in Oak Creek.

The cobble island analyzed on the Calapooia River (Figure 9-3) had a length of about 22 meters and a planform area of about 5.5×10^1 square meters. At the time of measurement, the discharge in the Calapooia River was about 220 cfs.

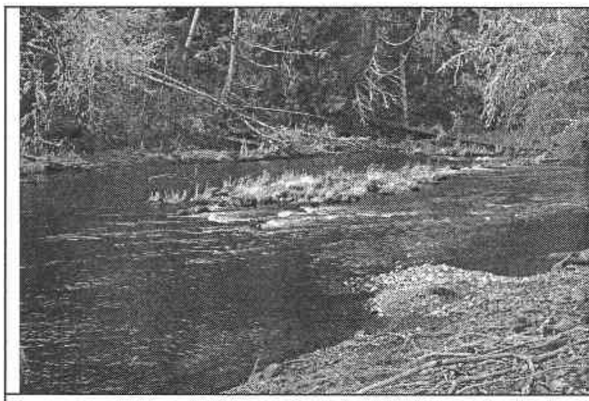	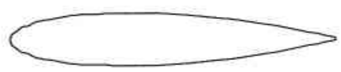
Cobble Island in Calapooia River $A \sim 10^1\ m^2 \quad R_A = 4.36$	Equivalent Lemniscate Shape $k = 6.85$

Figure 9-3. Equivalent lemniscate for Calapooia River island.

The lower section of the Colorado River carries a mean annual discharge of about 10,000 cfs. One island in this section, shown in Figure 9-4, has a length of about 120 meters and a planform area of about 2×10^3 square meters.

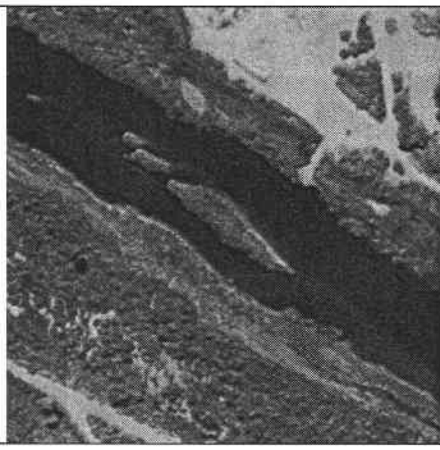	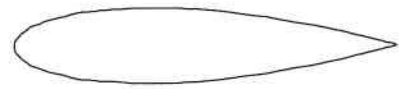
Colorado River Island $A \sim 10^3$ m^2 R_A =5.36	Equivalent Lemniscate Shape $k = 5.30$

Figure 9-4. Equivalent lemniscate for Colorado River island.

The middle section of the Snake River carries about twice as much discharge as the lower Colorado. Current Island (Figure 9-5) has a length of about 400 meters and a planform area of about 2.7×10^4 square meters.

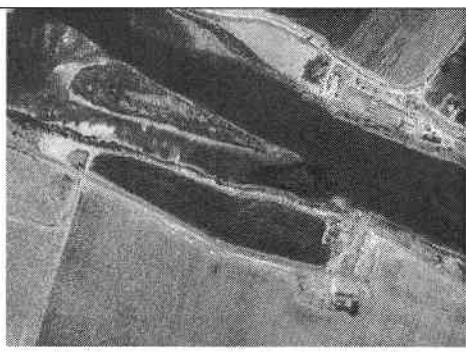	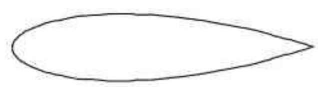
Current Island in Snake River $A \sim 10^4$ m^2 $R_A = 4.28$	Equivalent Lemniscate Shape $k = 4.89$

Figure 9-5. Equivalent lemniscate for Snake River island.

Skamania Island on the Columbia River (Figure 9-6) had a length of about 700 meters and a planform area of about 9.5×10^4 square meters. The mean annual discharge for the Columbia River below the Bonneville Dam is about 230,000 cfs.

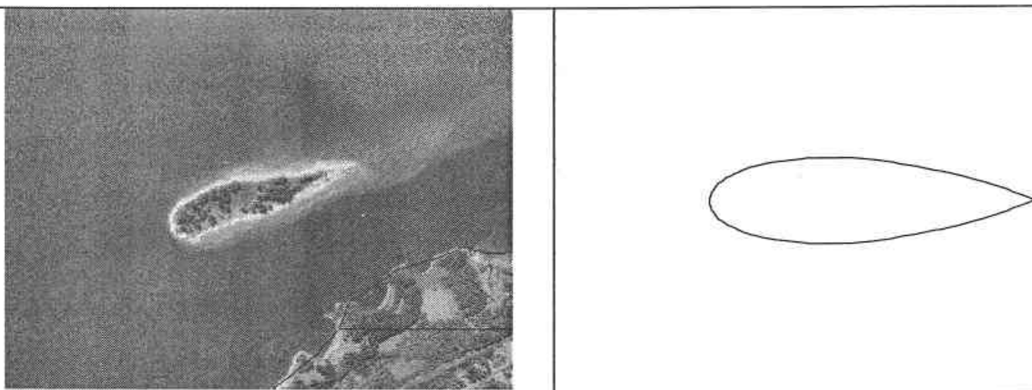

Skamania Island in Columbia River	Equivalent Lemniscate Shape
$A \sim 10^5\ m^2 \quad R_A = 3.68$	$k = 4.10$

Figure 9-6. Equivalent lemniscate for Columbia River Island.

Residual islands in the Channeled Scablands were generally a magnitude greater than river islands. For example, the residual island shown in the Figure 9-7 has a length of about 2900 meters and a planform area of about $1.8x10^6$ square meters. The peak flow for the Missoula Floods through the Channeled Scablands has been estimated to have been on the order of 10^7 cfs.

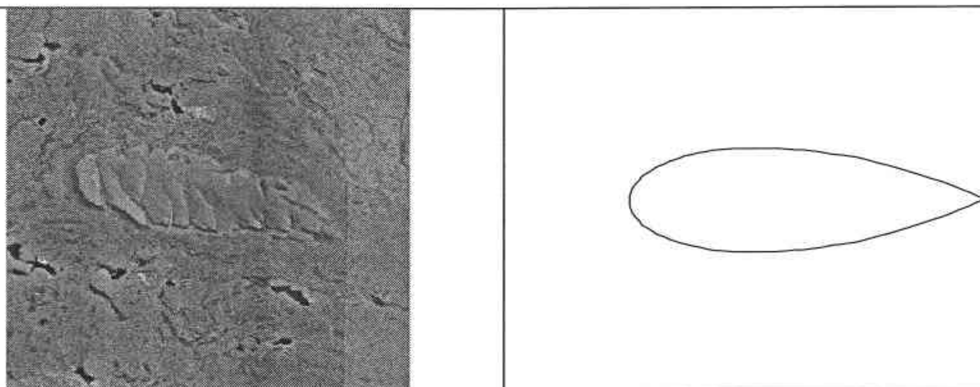

Residual Island in Channeled Scablands	Equivalent Lemniscate Shape
$A \sim 10^6\ m^2 \quad R_A = 3.41$	$k = 3.67$

Figure 9-7. Equivalent lemniscate for Scablands residual island.

Residual islands in Valles Ares on Mars are the largest scale islands analyzed in this study. The streamlined residual shown in Figure 9-8 has a length of about 35,000 meters and a planform area of about $1.4x10^8$ square meters. The residual that formed around an impact crater shown in Figure 9-8 has a length of about 106,000 meters and a planform area of about $4x10^9$ square meters. The peak flow for the floods in Ares Valles has been estimated to have been on the order of 10^8 cfs.

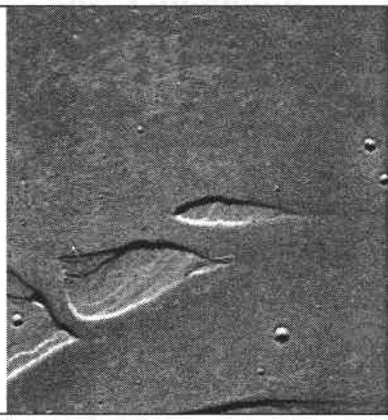	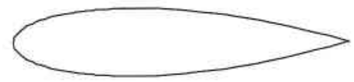
Streamlined Residual Island in Ares Vallis $A \sim 10^8$ m^2 $R_A = 5.71$	Equivalent Lemniscate Shape $k = 7.03$
	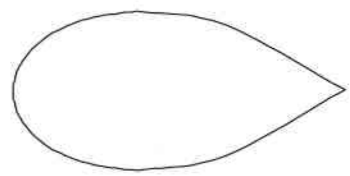
Residual Island behind Martian Crater $A \sim 10^9$ m^2 $R_A = 1.86$	Equivalent Lemniscate Shape $k = 2.18$

Figure 9-8. Equivalent lemniscates for residual islands in Ares Vallis on Mars.

Thus, from the above comparisons, it is seen that the scale for the planform areas of the analyzed fluvial islands ranges over 10 orders of magnitude. The scale for the equivalent flow ranges over 8 orders of magnitude. The aspect ratios and elongation factors, however, do not appear to be affected by the wide ranges in scale. One might then deduce that the shape parameters of fluvial islands are scale-independent.

CONCLUSIONS

This research has sought to unite the ideas of island formation and river processes. Fluvial islands are a natural part of rivers and have been shown to form by at least nine separate processes. These include flood-related processes, such as avulsions through the floodplain, rapid erosion of flood deposits, depositions in the wake of an obstacle, and mass movements from the floodplain or valley slopes. Other processes include those that not flood related, such as preferential erosion of flanking channels, lateral shifts of a meandering river, stabilization of a bar or riffle, gradual erosion through structural cracks, and isolation of riparian topography upstream of a dam. A classification scheme has been proposed here to help identify the type of island formation and to describe the relationship between island formation and river processes.

Physical experiments in laboratory flumes and natural streams were performed to better clarify the relationship of islands and rivers. Experiments in sandy, coastal streams helped show what type of conditions are necessary for island formation. Experiments in Oak Creek showed that flow patterns behind an obstacle are conducive to creating a streamlined, depositional shape. Flume experiments showed the relationship between an island's size and the flow's energy loss and drag force. Both were minimized for a length-to-width ratio of about three. Experiments on artificial islands in Oak Creek showed that islands could be an effective method of energy loss within a river system. Analyses of flows around natural islands in the Calapooia and Willamette Rivers showed the effects islands have on the velocity patterns of a river.

To determine the main relationships between fluvial islands and river processes, dimensionless properties of islands were determined as based on the lemniscate shape. This allowed for simple comparisons of islands of varying sizes to be compared within and between river basins. The shape of a fluvial island was shown to be independent of a river's discharge and sediment concentration. The shapes were found to be somewhat dependent on the ratio of the island's width to the channel width. The lengths and widths of all islands in a particular river can be fitted to a $L=aW^b$ curve, with most relationships having an exponent, b, near a value of one. The relationship between lengths and widths of all analyzed islands was shown to be $L=4.31W^{0.98}$, while the arithmetic mean value for length/width ratio of all islands was 4.14.

Comparing the shapes of terrestrial fluvial islands to the shapes of residual islands in megaflood areas, it was shown that megaflood islands in the Scablands and on Mars generally exhibit a lower length/width ratio. The differences in the flow processes that may explain the difference in length/width ratios include the duration of the flow and the lack of channel boundaries. Since it has been hypothesized that the megafloods were hyperconcentrated, the differences in island shapes could also be attributed to the dampening of the flow turbulence due to the high sediment concentrations.

Experiments described herein and cited from previous research have shown that the drag force of an object in a flow can be minimized for a length/width ratio of between three and four. If a river, therefore, does not need to maximize its energy loss, then it should reshape its islands' length/width ratios to minimize the energy loss. As an example, islands on the Columbia River downstream of the Bonneville Dam were documented to exhibit a trend of optimizing their length/width values to be between three and four.

This research can be useful for river restoration practices. Since islands are integral parts of natural rivers, the more we understand about the inter-relationship of islands and rivers, the better we can attempt to restore natural conditions to a system. This should not, however, be taken as a guide on how to 'engineer' natural islands. Like most natural river characteristics, river restoration strategies should not necessarily involve the construction of islands, but should create conditions that allow the river to construct its own islands [Ward et al., 2002a].

Recommendations for Future Research

The island classification method set forth in Chapter 3 was created without the author having visited any of the fluvial islands in person. The classification scheme would benefit greatly from first-hand knowledge of each of the islands. The river classification scheme set forth by Rosgen [1994] was created after he spent many years working the field and analyzing different river systems. That kind of 'field-truthing' should be applied to the proposed island classification scheme.

A more detailed analysis of the effect sediment concentration of the river has on island shape and formation is recommended. Limitations of equipment available for this research prevented a thorough examination of the relationship, though an effect should be expected.

The logical progression for this research would be to numerically model the flow processes around a fluvial island. Few computer models, however, have the capability to incorporate a flow separation. I have found one computer model, NETSTARS, by Sinotech, Inc., [Lee and Hsieh, 2001] that can specifically model a network of flow channels. The purpose in their design was to model flow around bridge piers, but islands could be represented similarly in the model.

References

Alden, W.C. (1927), Discussion: Channeled scabland and the Spokane flood, *Washington Academy of Science Journal, 17(8)*, 203.

Allison, I.S. (1933), New version of the Spokane Flood, *GSA Bulletin, 44*, 675-722.

Allison, I.S. (1978), Late Pleistocene sediments and floods in the Willamette Valley, *The Ore Bin, 40 (11-12),* 177-191, 193-202.

Arscott, D.B., K. Tockner, and J.V. Ward (2000) Aquatic habitat diversity along the corridor of an Alpine floodplain river (Fiume Tagliamento, Italy), *Archiv für Hydrobiologie, 149,* 679-704.

Bagnold, R.A. (1966), *An Approach to the Sediment Transport Problem from General Physics*, USGS Professional Paper, no. 422-I, 37 pp.

Baker, V.R. (1973), *Paleohydrology and Sedimentology of Lake Missoula Flooding in Eastern Washington*, GSA Special Paper 144, 79 pp.

Baker, V.R. (1978a), Large-scale erosional and depositional features of the Channeled Scabland, in *The Channeled Scabland*, edited by V.R. Baker and D. Nummedal, pp. 81-115, Comparative Planetary Geology Field Trip Conference, NASA, Washington, D.C.

Baker, V.R. (1978b), The Spokane Flood controversy and the Martian outflow channels, *Science*, *202*, 1249-1256.

Baker, V.R. (1979), Erosional processes in channelized water flows on Mars, *Journal of Geophysical Research, 81 (B14),* 7985-7993.

Baker, V.R. (1982), *The Channels of Mars*, University of Texas Press, Austin.

Baker, V.R. (2001), Water and the Martian landscape, *Nature, 412*, 228-236.

Baker, V.R. (2002a), The study of superfloods, *Science*, *295*, 2379-2380.

Baker, V.R. (2002b), High-energy megafloods: planetary settings and sedimentary dynamics, in *Flood and Megaflood Processes and Deposits: Recent and Ancient Examples*, edited by I.P. Martini, V.R. Baker, G. Garzon, pp. 3-15, Special Publ. no. 32 of Int'l Assoc. of Sedimentologists.

Baker, V.R., and D.J. Milton (1974), Erosion by catastrophic floods on Mars and Earth, *Icarus*, *23*, 27-41.

Baker, V.R., G. Benito, and A.N. Rudoy (1993), Paleohydrology of late Pleistocene superflooding, Altay Mountains, Siberia, *Science*, *259*, 348-350.

Baker, V.R., M.H. Carr, V.C. Gulick, C.R. Williams, and M.S. Marley (1992a), Channels and valley networks, In *Mars*, edited by H.H. Kieffer, B.M. Jakosky, C.W. Snyder, and M.S. Matthews, pp 493-522, University of Arizona Press, Tucson.

Baker, V.R., G. Komatsu, T.J. Parker, V.C. Gulick, J.S. Kargel, and J.S. Lewis (1992b), Channels and valleys on Venus: a preliminary analysis of Magellan data, *Journal of Geophysical Research, 97(E8)*, 13,421-13,444.

Baker, V.R., R.G. Strom, V.C. Gulick, J.S. Kargel, G. Komatsu, and V.S. Kale (1991), Ancient oceans, ice sheets, and the hydrological cycle on Mars, *Nature, 352*, 589-594.

Bartlett, R.A. (Ed.) (1984), *Rolling Rivers: An Encyclopedia of American Rivers*, McGraw-Hill Book Co.

Beckinsale, R.P. (1971), Rivers as political boundaries, in *Introduction to Geographical Hydrology,* edited by R.J. Chorley, pp. 96-107, Methuen & Co. Ltd, London, England.

Benito, G. (1997), Energy expenditure and geomorphic work of the cataclysmic Missoula flooding in the Columbia River Gorge, USA, *Earth Surface Processes and Landforms*, *22*, 457-472.

Benito, G., and J.E. O'Connor (2003), Number and size of last-glacial Missoula Floods in the Columbia River valley between the Pasco Basin, Washington and Portland, Oregon, *GSA Bulletin, 115 (5),* 624-638.

Beverage, J.P., and J.K. Culbertson (1964), Hyperconcentrations of suspended sediment, *Journal of the Hydraulics Division, HY 6*, 117-128.

Bjornstad, B.N., K.R. Fecht, and C.J. Pluhar (2001), Long history of pre-Wisconsin, ice age cataclysmic floods: evidence from southeastern Washington State, *Journal of Geology*, *109*, 695-713.

Blasius, K.R., and J.A. Cutts (1979), Erosion and transport in Martian outflow channels, paper presented at Lunar Planetary Science Conference X.

Bretz, J.H. (1923), The channeled scabland of the columbia plateau, *Journal of Geology*, *31*, 617-649.

Bretz, J.H. (1925), The spokane flood beyond the channeled scablands, *Journal of Geology*, *33*, 97-115 & 236-259.

Bretz, J.H. (1927), Channeled scabland and the spokane flood, *Washington Academy of Science Journal*, *17(8),* 200-211.

Bretz, J.H. (1928), Bars of the Channeled Scabland, *GSA Bulletin, 39*, 643-702.

Bretz, J.H. (1932), The Grand Coulee, *American Geographical Society Special Publ. #15,* 89p.

Bretz, J.H., H.T.U. Smith, and G.E. Neff (1956), Channeled Scabland of Washington: new data and interpretations, *GSA Bulletin*, *67*, 957-1049.

Bridge, J.S. (1993), The interaction between channel geometry, water flow, sediment transport, and deposition in braided rivers, in *Braided Rivers*, edited by J.L. Best and C.S. Bristow, pp. 13-72, Geological Society Special Publication No. 75.

Bridge, J.S. (2003), *Rivers and Floodplains: Forms, Processes and Sediment Record,* Blackwell Publishing, Malden, MA.

Bridge, J.S., and S.L. Gabel (1992), Flow and sediment dynamics in a low-sinuosity river: Calamus River, Nebraska Sandhills, *Sedimentology, 39*, 125-142.

Buffington, J.M., and D.R. Montgomery (1997), A systematic analysis of eight decades of incipient motion studies, with special reference to gravel-bedded rivers, *Water Resources Research, 33 (8),* 1993-2029.

Burkham, D.E. (1972), *Channel Changes of the Gila River in Safford Valley, Arizona, 1846-1970*, U.S. Geological Survey Professional Paper 422-D.

Burr, D.M. (2003), Hydraulic modeling of Athabasca Vallis, Mars, *Hydrological Sciences*, *48 (4),* 635-664.

Burr, D.M., and A.S. McEwen (2002), Recent extreme floods on Mars, in *The Extremes of the Extremes: Extraordinary Floods*, edited by A. Snorrason, H.P. Finnsdottir, and M.E. Moss, pp. 101-106, IAHS Publication no. 271.

Burr, D.M., J.A. Grier, A.S. McEwen, and L.P. Keszthelyi (2002), Repeated aqueous flooding from the Cerberus Fossae: Evidence for very recently extant, deep groundwater on Mars, *Icarus*, *159*, 53-73.

Carling, P.A. (1996), In-stream hydraulics and sediment transport, in *River Flows and Channel Forms*, edited by G. Petts and P. Calow, pp. 160-184, Blackwell Science Ltd, Oxford, UK.

Carling, P.A., A.D. Kirkbride, S. Parnachov, P.S. Borodavko, and G.W. Berger (2002), Late Quaternary catastrophic flooding in the Altai Mountains of south-central Siberia: a synoptic overview and an introduction to flood deposit sedimentology, in *Flood and Megaflood Processes and Deposits: Recent and Ancient Examples*, edited by I.P. Martini, V.R. Baker, G. Garzon, pp. 17-36, Special Publ. no. 32 of Int'l Assoc. of Sedimentologists.

Carr, M.H. (1974), The role of lava erosion in the formation of lunar rilles and Martian channels, *Icarus*, *22*, 1-23.

Carr, M.H. (1979), Formation of Martian flood features by release of water from confined aquifers. *Journal of Geophysical Research*, *84 (B6)*, 2995-3007.

Carr, M.H. (1996), *Water on Mars*, Oxford University Press, New York, NY.

Carr, M.H., and M.C. Malin (2000), Meter-scale characteristics of Martian channels and valleys, *Icarus*, *146 (2)*, 366-386.

Carr, M.H., and G.G. Schaber (1977), Martian permafrost features, *Journal of Geophysical Research, 82*, 4039-4054.

Chanson, H. (1999), *The Hydraulics of Open Channel Flow: An Introduction*, Arnold Publishing, London, England.

Chorley, R.J. (Ed.) (1971), *Introduction to Fluvial Processes*, Methuen & Co. Ltd, London, England.

Clifford, S.M. (1993), A model for the hydrologic and climatic behavior of water on Mars, *Journal of Geophysical Research*, *98*, 10,973-11,016.

Clifford, S.M., and F.P. Fanale (1985), The thermal conductivity of the Martian crust, paper presented at Lunar Planetary Science Conference XVI.

Clifford, S.M., and T.J. Parker (2001), The evolution of the Martian hydrosphere: implications for the fate of a primordial ocean and the current state of the northern plains. *Icarus*, *54*, 466-489.

Coleman, N.L. (1980), Velocity profiles with suspended sediment, *Journal of Hydraulic Research*, *19 (3)*, 211-228.

Costa, J.E. (1988), Rheologic, geomorphic, and sedimentologic differentiation of water floods, hyperconcentrated flows, and debris flows, in *Flood Geomorphology*, edited by V.R. Baker, R.C. Kochel, and P.C. Patton, pp. 113-122, John Wiley & Sons, Inc, New York.

Davis, W.M. (1899), The geographical cycle, *Geographical Journal*, *14*, 481-504.

Dietrich, W.E. (1987), Mechanics of flow and sediment transport in river bends, in *River Channels* edited by K. Richards, pp. 179-227, Basil Blackwell Inc., NY, NY.

Eisner (1929), Drag characteristics of cylinders in towing tank, *Mitt. Pr. VAWS*, #4.

Eschner, T.R., R.F. Hadley, and K.D. Crowley (1983), Hydrologic and morphologic changes in the channels of the Platte River Basin in Colorado, Wyoming, and Nebraska: a historical perspective, in *Hydrologic and Geomorphic Studies of the Platte River Basin*, pp. A1-A39, U.S. Geological Survey Professional Paper 1277.

Flammarion, C. (1892), *La Planéte Mars et ses Conditions d'Habitabilités, Volume 1*, Gouthier-Villars et Fils, Paris, France.

Flint, R.F. (1938), Origin of the Cheney-Palouse Scabland tract, *GSA Bulletin*, *49*, 461-524.

Fortier, S., and F.C. Scobey (1926), Permissible canal velocities, *Transactions of the ASCE, 89*.

Friedman, J.M., W.R. Osterkamp, and W.M. Lewis, Jr. (1996), The role of vegetation and bed-level fluctuations in the process of channel narrowing, *Geomorphology, 14*, 341-351.

Gilluly, J. (1927), Discussion: Channeled scabland and the Spokane flood, *Washington Academy of Science Journal, 17(8)*, 203-205.

Goldspiel, J.M., S.W. Squyres, and D.G. Janikowski (1993), Topography of small martian valleys, *Icarus*, *89*, 392-410.

Gottesfeld, A.S., and L.M.J. Gottesfeld (1990), Floodplain dynamics of a wandering river, dendrochronology of the Morice River, British Columbia, Canada, *Geomorphology*, *3*, 159-179.

Graf, W.L. (1978), Fluvial adjustments to the spread of tamarisk in the Colorado Plateau region, *GSA Bulletin*, *89*, 1491-1501.

Grant, G.E., S.T. Lancaster, and S Hayes (2001), Interactions among riparian vegetation, wood, and fluvial processes: a Pacific Northwest drainage basin perspective, paper presented at Fall Meeting 2001, American Geophysical Union, San Francisco, CA, abstract #H41I-02.

Gross, M.G. (1987), *Oceanography: a View of the Earth*, Prentice Hall, New Jersey.

Gurnell, A.M., G.E. Petts, D.M. Hannah, B.P.G. Smith, P.J. Edwards, J. Kollmann, J.V. Ward, and K. Tockner (2001), Riparian vegetation and island formation along the gravel-bed Fiume Tagliamento, Italy, *Earth Surf. Proc. & Landforms*, *26*, 31-62.

Gurnell, A.M., and G.E. Petts (2002), Island-dominated landscapes of large floodplain rivers, a European perspective, *Freshwater Biology, 47*, 581-600.

Head, J.W., L. Wilson, and K.L. Mitchell (2003), Generation of recent massive water floods at Cerberus Fossae, Mars by dike emplacement, cryospheric cracking, and confined aquifer groundwater release, *Geophysical Research Letters*, *30 (11)*, 31-1 – 31-4.

Hickin, E.J. (Ed.) (1995), *River Geomorphology,* Wiley, Chichester, England.

Hilbig, W. (1995), *The Vegetation of Mongolia*, SPB Academic Publishing, Amsterdam, The Netherlands.

Hjulstrom, F. (1935), The morphological activity of rivers as illustrated by River Fryis, *Bulletin of the Geological Institute, Uppsala, 25 (3)*.

Hoerner, S.F. (1965), *Fluid-Dynamic Drag*, Hoerner Fluid Dynamics, Brick Town, NJ.

Hoffman, N. (2000), White Mars: A new model for Mars' surface and atmosphere based on CO_2. *Icarus*, *146*, 326-342.

Hooke, J.M. (1986), The significance of mid-channel bars in an active meandering river, *Sedimentology, 33,* 839-850.

Hou, H., and X. Yang (1983), Effect of fine sediment on drag reduction in muddy flow, *Proceedings of 2nd International Symposium on River Sedimentation*, 47-80.

Inbar, M. (1987), Effects of high magnitude flood in a Mediterranean climate: A case study in the Jordan River basin, in *Catastrophic Flooding*, edited by L. Mayer and D. Nash, pp. 333-354, Allen and Unwin, Boston, MA.

Ingebritsen, S.E., and W.E. Sanford (1998) *Groundwater in Geologic Processes*, Cambridge University Press, Cambridge, UK.

Ippen, A.T. (1971), A new look at sedimentation in turbulent streams, *Journal of Boston Society of Civil Engineers, 58 (3)*, 131-161.

Jarrett, R.D., and H.E. Malde (1987), Paleodischarge of the late Pleistocene Bonneville Flood, Snake River, Idaho, computed from new evidence, *GSA Bulletin, 99*, 127-134.

Johnson, W.C. (1997), Equilibrium response of riparian vegetation to flow regulation in Platte River, Nebraska, *Regulated Rivers: Research & Management, 13,* 403-415.

Julien, P.Y. (1995), *Erosion and Sedimentation*, Cambridge University Press, New York.

Kehew, A.E. (1982), Catastrophic flood hypothesis for the origin of the Souris spillway, Saskatchewan and North Dakota, *GSA Bulletin, 93,* 1051-1058.

Kehew, A.E., and M.L. Lord (1986), Origin and large-scale erosional features of glacial-lake spillways in Northern Great Plains, *GSA Bulletin, 97*, 162-177.

Kellerhals, R., M. Church, and D.I. Bray (1976), Classification and analysis of river processes, *Journal of the Hydraulics Division, HY7*, 813-829.

Klingeman, P.C. (1979), *Sediment Transport Facilities, Oak Creek, Oregon,* Report F1, Water Resources Research Institute, Oregon State University, Corvallis, OR.

Knighton, D. (1998), *Fluvial Forms and Processes: A New Perspective,* Arnold, London, England.

Kochel, R.C., D.F. Ritter, and J. Miller (1987), Role of tree dams in the construction of pseudo-terraces and variable geomorphic response to floods in Little River valley, Virginia, *Geology, 15*, 718-721.

Komar, P.D. (1979), Comparisons of the hydraulics of water flows in the Martian outflow channels with flows of similar scale on Earth, *Icarus, 37*, 156-181.

Komar, P.D. (1980), Modes of sediment transport in channelized water flows with ramifications to the erosion of the Martian outflow channels, *Icarus, 42*, 317-329.

Komar, P.D. (1983), Shapes of streamlined islands on Mars and Earth: experiments and analyses of the minimum-drag form, *Geology, 11,* 651-654.

Komar, P.D. (1984), The lemniscate loop – comparisons with the shapes of streamlined landforms, *Journal of Geology, 92*, 133-145.

Komar, P.D. (1996), Cataclysmic floods on Earth and Mars – morphology and hydraulic interpretations, in *Gravel-Bed Rivers in the Environment*, edited by P.C. Klingeman, R.L. Beschta, P.D. Komar, and J.B. Bradley, pp. 677-704, Water Resource Publications, Highlands Ranch, Colorado.

Komatsu, G., and V.R. Baker (1997), Paleohydrology and flood geomorphology of Ares Vallis, *Journal of Geophysical Research, 102 (E2)*, 4151-4160.

Laity, J.E., and M.C. Malin (1985), Sapping processes and the development of theater-headed valley networks on the Colorado Plateau, *Geological Society of America Bulletin, 96*, 203-217.

Lane, E. (1940), Notes on the limit of sediment concentration, *Journal of Sedimentary Petrology, 10,* 279-300.

Lane, E. (1955), Design of stable channels, *Transactions of American Society of Engineers*, *120,* 1234-1260.

Lee, H.Y., and H.M. Hsieh (2001), Numerical solutions in a alluvial channel network, XXIX IAHR Congress Proceedings, Sept. 16-21, 2001, Beijing, China.

Leighton, R.B., B.C. Murray, R.P. Sharp, J.D. Allen, and R.K. Sloan (1965), Mariner IV photographs of Mars: initial results, *Science, 149*, 627-630.

Leighton, R.B., N.H. Horowitz, B.C. Murray, R.P. Sharp, A.G. Herriman, A.T. Young, B.A. Smith, M.E. Davies, and C.G. Leovy (1969), Mariner 6 & 7 television pictures: preliminary analysis, *Science, 166*, 49-67.

Leopold, L.B., and M.G. Wolman (1957), River channel patterns – braided, meandering, and straight, *USGS Professional Paper 282B.*

Lowell, P. (1895), *Mars*, Houghton Mifflin, Boston, MA.

Lucchitta, B.K. (1982), Ice sculpture in the Martian outflow channels, *Journal of Geophysical Research*, *87*, 9951-9973.

Maizels, J. (1989), Sedimentology, paleoflow dynamics and flood history of jökulhlaup deposits: paleohydrology of Holocene sediment sequences in southern Iceland Sandur deposits, *Journal of Sedimentary Petrology*, *59 (2),* 204-223.

Manga, M. (2004), Martian floods at Cerberus Fossae can be produced by groundwater discharge, *Geophysical Research Letters*, *31*, L02702, 4 pp.

Maser, C. and J.R. Sedell (1994), *From the Forest to the Sea,* St. Lucie Press, Delray Beach, FL.

Mavis, F.T., and L.M. Laushey (1948), A reappraisal of the beginning of bed-movement – competent velocity, *International Association for Hydraulic Structure, Second Meeting,* Stockholm, Sweden.

McKnight, E.T. (1927), The Spokane flood: a discussion, *Journal of Geology, 35*, 453-460.

Meizner, O.E. (1927), Discussion: Channeled scabland and the Spokane flood, *Washington Academy of Science Journal, 17(8)*, 207-208.

Melville, B.W., and S.E. Coleman (2000), *Bridge Scour*, Water Resources Publications, LLC, Highland Ranch, CO.

Merritt, D.M., and D.J. Cooper (2000) Riparian vegetation and channel change in response to river regulations: a comparative study of regulated and unregulated streams in the Green River basin, USA, *Regulated Rivers: Research & Management, 16,* 543-564.

Meyer-Peter, E., and R. Muller (1948), Formula for bed-load transport, *International Association for Hydraulic Structure, Second Meeting,* Stockholm, Sweden.

Milhous, R.T. (1973), Sediment transport in a gravel-bottomed stream, PhD thesis, 232 pp., Oregon State University, Corvallis, OR.

Milton, D.J. (1973), Water and processes of degradation in the Martian landscape, *Journal of Geophysical Research*, *78*, 4037-4047.

Mingfu, W., Z. Yizheng, L. Jianjun, D. Wenzhong, and W. Weimin (1983), An experimental study on turbulence characteristics of flow with hyperconcentration, in

Proceedings of the Second International Symposium on River Sedimentation, pp. 45-53, Water Resources and Electrical Power Press, Beijing.

Munson, B.R., D.F. Young, and T.H. Okiishi (1990), *Fundamentals of Fluid Mechanics*, John Wiley & Sons, New York, NY.

Nummedal, D. (1978), The role of liquefaction in channel development on Mars, *NASA Technical Memo 79729*, pp 257-259.

O'Connor, J.E. (1993), *Hydrology, Hydraulics, and Geomorphology of the Bonneville Flood,* Geological Society of America Special Paper 274.

O'Connor, J.E., and V.R. Baker (1992), Magnitudes and implications of peak discharges from glacial Lake Missoula, *GSA Bulletin, 104*, 267-279.

Osterkamp, W.R. (1998), Processes of fluvial island formation, with examples from Plum Creek, Colorado and Snake River, Idaho, *Wetlands*, *18 (4)*, 530-545.

Osterkamp, W.R., and J.E. Costa (1987), Changes accompanying an extraordinary flood on a sand-bed stream, in *Catastrophic Flooding*, edited by L. Mayer and D. Nash, pp. 201-224, Allen and Unwin, Boston, MA.

Pardee, J.T. (1910), The glacial Lake Missoula, Montana, *Journal of Geology, 18*, 376-386.

Pardee, J.T. (1942), Unusual currents in glacial Lake Missoula, Montana, *GSA Bulletin, 53*, 1569-1600.

Penn, J.R. (2001), *Rivers of the World: A Social, Geographical, and Environmental Sourcebook*, ABC-CLIO, Inc.

Petts, G., and I. Foster (1985), *Rivers and Landscapes*, Edward Arnold Publishing Ltd., London, UK.

Pierson, T.C., and K.M. Scott (1985), Downstream dilution of a lahar: transition from debris flow to hyperconcentrated streamflow, *Water Resources Research, 21 (10)*, 1511-1524.

Rakonczai, J., H. Hargitai, and Sz. Bèrczi (2001), Comparisons of the ancient meandering riverbeds in the Chryse Region, Mars, and the Tisza flooded basin in the Carpathian Basin, Earth, paper presented at Lunar and Planetery Science Conference XXXII.

Richards, K. (1982), *Rivers*, Methuen & Co., Ltd, London, UK.

Richards, K.S. (1987), *River Channels: Environment and Process,* Methuen & Co. Ltd, London, England.

Robinson, M.S., and K.L. Tanaka (1990), Magnitude of a catastrophic flood event at Kasei Valles, Mars, *Geology*, *18*, 902-905.

Rodier, J.A., and M. Roche (1984), World catalogue of maximum observed floods, *International Association of Hydrologic Sciences, Publ. No. 143*, 354 p.

Rodriguez-Iturbe, I., and A. Rinaldo (1997), *Fractal River Basins: Chance and Self-organization,* Cambridge University Press, Cambridge, UK.

Rosgen, D.L. (1994), A classification of natural rivers, *Catena, 22*, 169-199.

Rosgen, D.L. (1996), *Applied River Morphology*, Wildland Hydrology, Pagosa Springs, CO.

Rossbacher, L.A., and D.D. Rhodes (1987), Planetary analogs for geomorphic features produced by catastrophic flooding, in *Catastrophic Flooding*, edited by L. Mayer and D. Nash, pp. 289-304, Allen & Unwin, Boston, MA.

Rudoy, A.N., and V.R. Baker (1993), Sedimentary effects of cataclysmic late Pleistocene glacial outburst flooding, Altay Mountains, Siberia, *Sedimentary Geology, 85*, 53-62.

Ryan, W.B.F., and nine other authors (1997), An abrupt drowning of the Black Sea shelf, *Marine Geology, 138*, 119-126.

Schubert, G., S.C. Solomon, D.L. Turcotte, M.J. Drake, and N.H. Sleep (1992), Origin and thermal evolution of Mars, in *Mars*, edited by H.H. Kieffer, B.M. Jakosky, C.W. Snyder, and M.S. Matthews, pp 147-183, University of Arizona Press, Tucson, AZ.

Schumm, S.A. (1963), *A Tentative Classification of Alluvial River Channels*, USGS Circular #477.

Schumm, S.A. (Ed.) (1972), *River Morphology,* Dowden, Hutchinson, & Ross, Inc., Stroudsburg, PA.

Schumm, S.A. (1985), Patterns of alluvial rivers, *Annual Review of Earth & Planetary Science*, *13*, 5-27.

Shaw, J., M. Munro-Stasiuk, B. Sawyer, C. Beaney, J-E. Leseman, A. Musacchio, B.Rains, and R.R. Young (1999), The Channeled Scabland: back to Bretz?, *Geology, 27(7),* 605-608.

Shields, A. (1936), *Application of Similarity Principles, and Turbulence Research to bed-Load Movement*, (in German).

Shull, C.A. (1922), The formation of a new island in the Mississippi River, *Ecology, 3 (3)*, 202-206.

Smith, A.J. (1985), A catastrophic origin for the paleovalley system of the eastern English Channel, *Marine Geology*, *64*, 65-75.

Snorroson, A., P. Jonsson, O. Sigurdsson, S. Palsson, S. Arnason, S. Vikingsson, and I. Kaldal (2002), November 1996 jökulhlaup on Skeiðarársandur outwash plain, Iceland, in *Flood and Megaflood Processes and Deposits: Recent and Ancient Examples*, edited by I.P. Martini, V.R. Baker, G. Garzon, pp. 55-66, Special Publ. no. 32 of Int'l Assoc. of Sedimentologists.

Soderblom, L.A., and D.B. Wenner (1978), Possible fossil liquid-ice interfaces in the Martian crust, *Icarus*, *34*, 622-637.

Squyres, S.W., and J.F. Kasting (1994), Early Mars: how warm and how wet? *Science*, *265*, 744-749.

Stanford, J.A., J.V. Ward, W.J. Liss, C.A. Frissell, R.N. Williams, J.A. Lichatowich, and C.C. Coutant (1996), A general protocol for restoration of regulated rivers, *Regulated Rivers: Research & Management, 12,* 391-413.

Tanaka, K.L. and M.G. Chapman (1990), The relation of catastrophic flooding in Mangala Valles, Mars, to faulting of Memnonia Fossae and Tharsis volcanism, *Journal of Geophysical Research*, *95 (B9)*, 14,315-14,323.

Tessmer, I.H. (ed) (1991), *Colossal Cataract – the Geologic History of Niagara Falls*, State University of New York Press, Albany, NY, USA.

Thorne, C.R., A.P.G. Russell, and M.K. Alam (1993), Planform pattern and channel evolution on the Brahmaputra River, Bangladesh, in *Braided Rivers,* edited by J.L. Best and C.S. Bristow, pp. 257-276, Geological Society Special Publication 75.

Toms, B.A. (1948), Some observations on the flow of linear polymer solutions through straight tubes at large Reynold's Number, *Proceedings of 1st International Congress on Rheology, vol. II*, 135-141.

Tooth, S., and G.C. Nanson (2000), The role of vegetation in formation of anabranching channels in an ephemeral river, Northern plains, arid central Australia, *Hydrological Processes, 14*, 3099-3117.

Trevena, A.S., and M.D. Picard (1978), Morphometric comparison of braided Martian channels and some braided terrestrial features, *Icarus*, *35*, 385-394.

U.S. Army Corps of Engineers (1989), Engineering and design – sedimentation investigations of rivers and reservoirs, *Engineering Manual No. 1110-2-4000.*

U.S. Bureau of Reclamation (1977), *Hydraulic Design of Flood Control Channels*, Engineering Manual EM1110-2-1601.

van der Nat, D., K. Tockner, P.J. Edwards, J.V. Ward, and A.M. Gurnell (2003), Habitat change in braided flood plains (Tagliamento, NE-Italy), *Freshwater Biology, 48,* 1799-1812.

van Rijn, L.C. (1983), Sediment transportation in heavy sediment-laden flows, *Proceedings of the 2nd International Symposium on River Sedimentation*, Nanjing, China, 482-491.

Vanoni, V.A. (ed.) (1975), *Sedimentation Engineering*, ASCE Task Committee for the Preparation of the Manual on Sedimentation of the Sedimentation Committee of the Hydraulics Division.

Waitt, R.B. (1994), Scores of gigantic, successively smaller Lake Missoula Floods through Channeled Scabland and Columbia Valley, in *Geologic Field Trips in Pacific Northwest*, GSA Meeting 1994, edited by D.A. Swanson, R.A. Haugerud, University of Washington, Seattle.

Waitt, R.B. (2002), Great Holocene floods along Jökulsá á Fjöllum, north Iceland, in *Flood and Megaflood Processes and Deposits: Recent and Ancient Examples*, edited by I.P. Martini, V.R. Baker, G. Garzon, pp. 37-516, Special Publ. no. 32 of Int'l Assoc. of Sedimentologists.

Waitt, R.B., J.E. O'Connor, and C.J. Harpel (2000), Varying routings of repeated colossal jökulhlaups through the Channeled Scabland of Washington, USA, in *Extremes of the Extremes*, Symposium Abstracts, edited by H.P. Finnsdottir and E. Gudnadottir, Reykjavik, Iceland.

Wan, Z., and Z. Wang (1994), *Hyperconcentrated Flow*, International Association for Hydraulic Research Monography Series, AA Balkema Publishers, Brookfield, VT.

Wang, S. (1981), Variations of Karman constant in sediment laden flow, *Journal of the Hydraulics Division, ASCE, HY4.*

Ward, J.V., K. Tockner, P.J.Edwards, J. Kollmann, G. Bretschko, A.M. Gurnell, G.E. Petts, and B. Rosarro (1999) A reference river system for the Alps: the Fiume Tagliamento, *Regulated Rivers, 15*, 63-75.

Ward, J.V., F. Malard, and K. Tockner (2002a), Landscape ecology: a framework for integrating pattern and process in river corridors, *Landscape Ecology, 17 (Suppl. 1),* 35-45.

Ward, J.V., K. Tockner, D.B. Arscott, and C. Claret (2002b), Riverine landscape diversity, *Freshwater Biology, 47,* 517-539.

Weihaupt, J.G. (1974), Possible origin and probable discharges of meandering channels on the planet Mars, *Journal of Geophysical Research, 79(14),* 2073-2076.

White, C.M. (1940), The equilibrium of grains on the bed of an alluvial channel, *Proceedings of the Royal Society of London, Series A, 174*, 332-338.

Wolman, M.G., and J.P. Miller (1960), Magnitude and frequency of forces in geomorphic processes, *Journal of Geology, 68*, 54-74.

Wyrick, J.R. (2003), Fluvial indicators of hyperconcentrated flows – with application to the floods on Mars, *Hydrological Science and Technology*, *19 (1-4)*, 287-296.

Yalin, M.S. (1992), *River Mechanics*, BPCC Wheatens Ltd, Exeter, UK.

Yang, C.T. (1996), *Sediment Transport: Theory and Practice*, McGraw-Hill Companies, Inc., New York.

Yang, W., and W. Zhao (1983), An experimental study of the resistance to flow with hyperconcentration in rough flumes, *Proceedings of 2nd International Symposium on River Sedimentation*, Water Resource and Electric Press, pp. 45-55.

Yung, Y.L., and J.P. Pinto (1978), Primitive atmosphere and implications for the formation of channels on Mars, *Nature*, *273*, 730-732.

Appendices

APPENDIX I – EXAMPLES OF FLUVIAL ISLANDS AND THEIR CLASSIFICATION

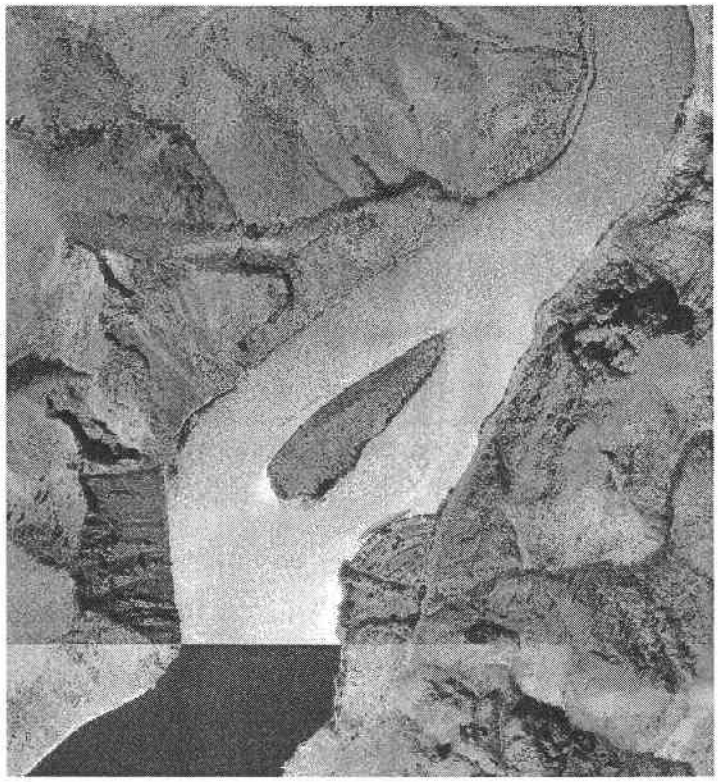

Figure A1-1. Big Bar, Snake River, river mile 256

Determinable Characteristics:
- In or near main flow
- Streamlined shape
- No other significant islands nearby
- Relatively equal width
- Vegetation – sparse shrubs (similar to surrounding floodplain)

From the classification matrix (Table 3-5), the island types that fit these known characteristics are either 'Gradual Degradation of Channel' or 'Rapid Incision of Flood Deposits'. A deciding factor in the determination of the island type could be the age of the island. If it is known that it formed recently, then it would more likely be a Rapid Incision type island, especially if it is known that a large flood has occurred recently. Another deciding factor would be the sediment that makes up the island. If the sediment is generally finer than the surrounding floodplain, then it is more likely to be a Rapid Incision type island. Also, if a sediment coring shows an upward fining of the sediment, this would point towards the Rapid Incision type island.

Island Type: *Gradual Degradation of Channel Branches* or *Rapid Incision of Flood Deposits*. More detailed analysis of the island is necessary.

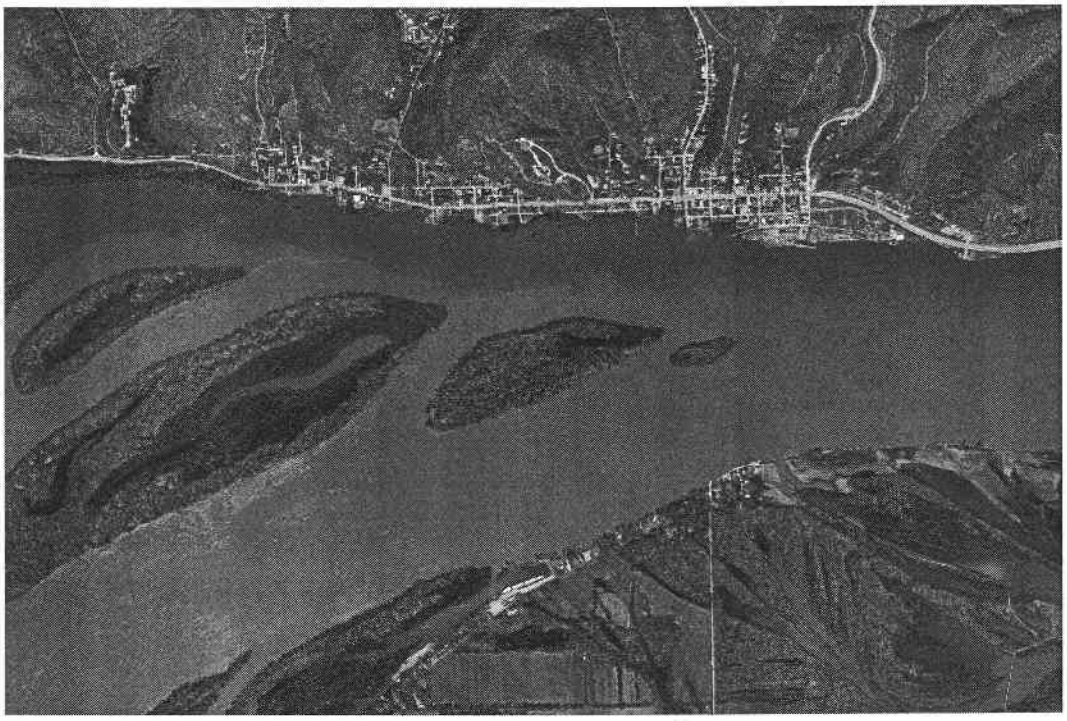

Figure A1-2. Island 526, Mississippi River, river mile 220

Determinable Characteristics:

- Away from main flow
- Irregular shape
- Several islands nearby (classified as *split*)
- Relatively narrow width
- Mature/mixed vegetation present

From the classification matrix (Table 3-5), the only island type that fits these known characteristics is the 'Lateral Shifts' type. The other main clue for this determination is the presence of the Illinois River that joins the Mississippi River at this location. The interactions of these two rivers created the islands seen in the above figure. From this classification, we can expect that these islands are highly changeable in shape due to future channel flow realignments and may only persist in the short-term.

Island Type: *Lateral Shifts*

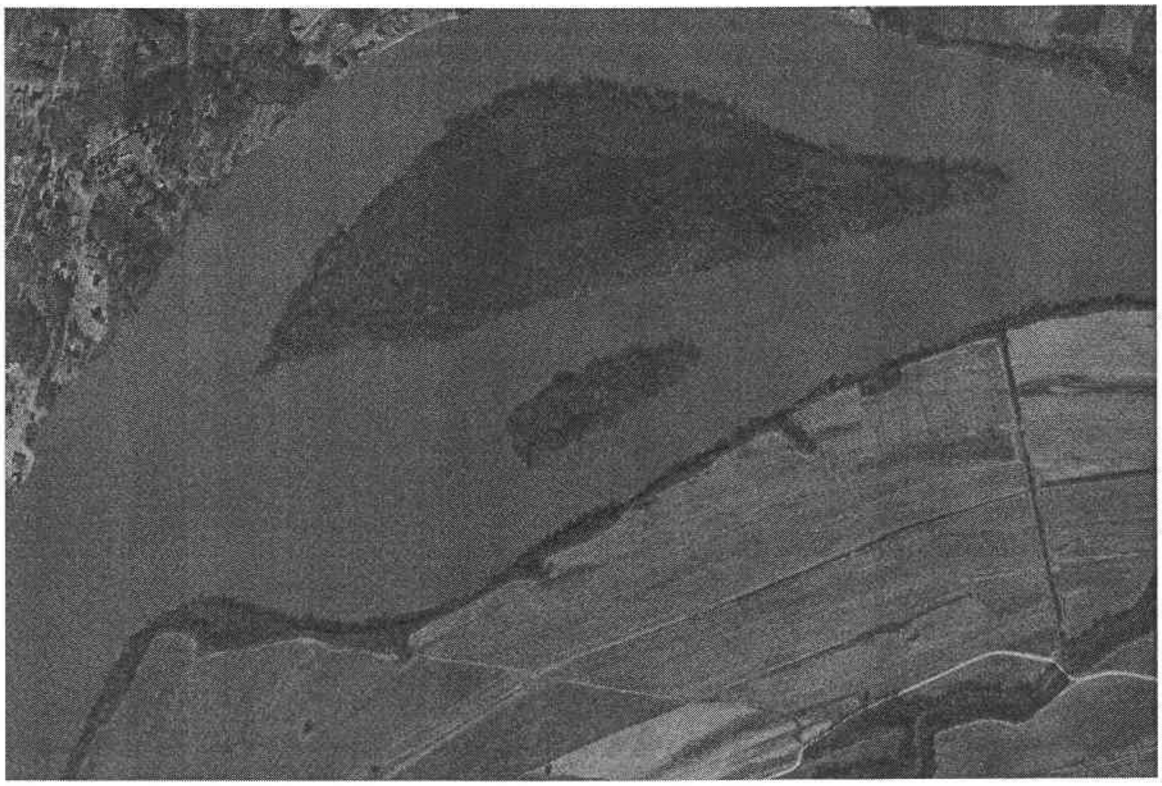

Figure A1-3. Wolf Island, Tennessee River, river mile 193

Determinable Characteristics:

Away from main flow

Triangular shape

The two islands seen in the figure are the only ones for several river miles either direction. Therefore, they could be classified as either Occasional or Frequent.

Relatively wide width

Mature/mixed vegetation

From the classification matrix (Table 3-5), the island types that fit these known characteristics are 'Avulsion' or 'Lateral Shifts'.

Island Type: *Avulsion* or *Lateral Shifts*. More detailed analysis of the island is necessary.

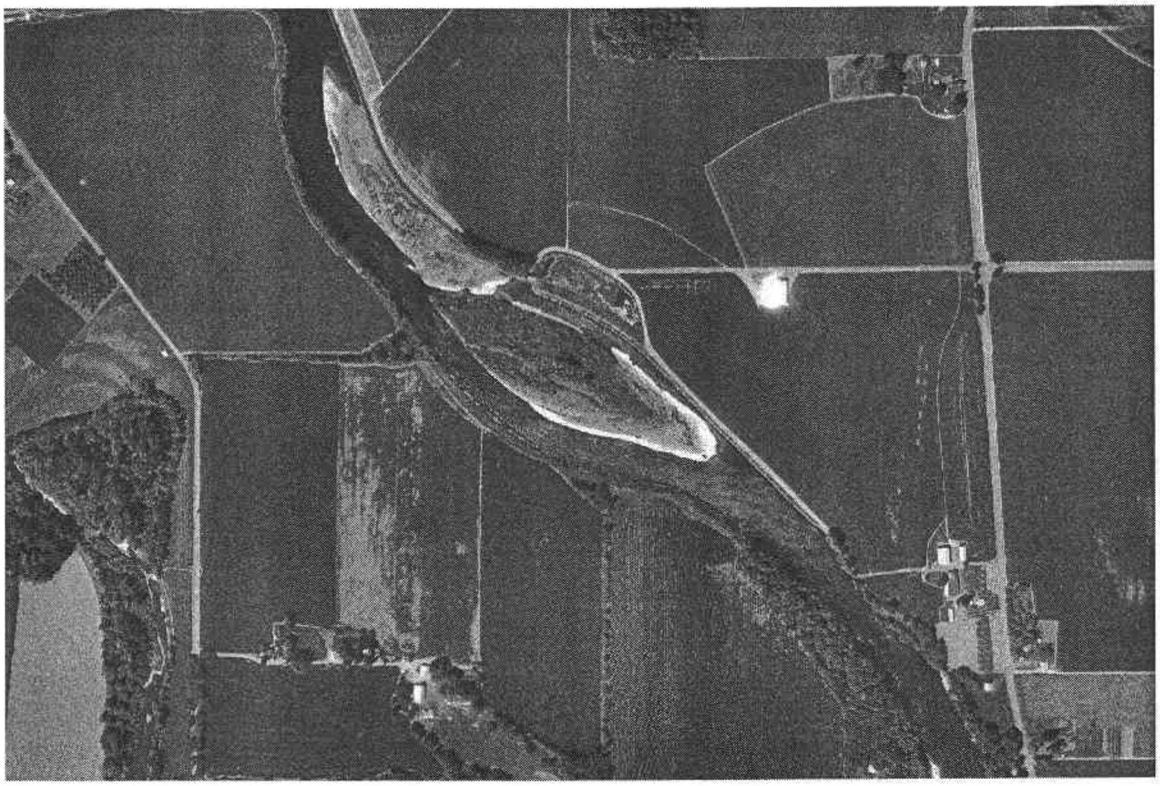

Figure A1-4. Island on the Willamette River, river mile 137

Determinable Characteristics:

- In or near main flow
- Streamlined shape
- No other islands in vicinity
- Relatively wide width
- Pioneer vegetation species

From the classification matrix (Table 3-5), the island types that fit these known characteristics are 'Bar Stabilization' and 'Rapid Incision of Flood Deposits'. Some history of this island is known from aerial photograph sequences. It is known that the island is about 20-25 years old and has increased in size since original formation. The known accretion, therefore, eliminates the 'Rapid Incision' type.

Island Type: *Bar Stabilization*

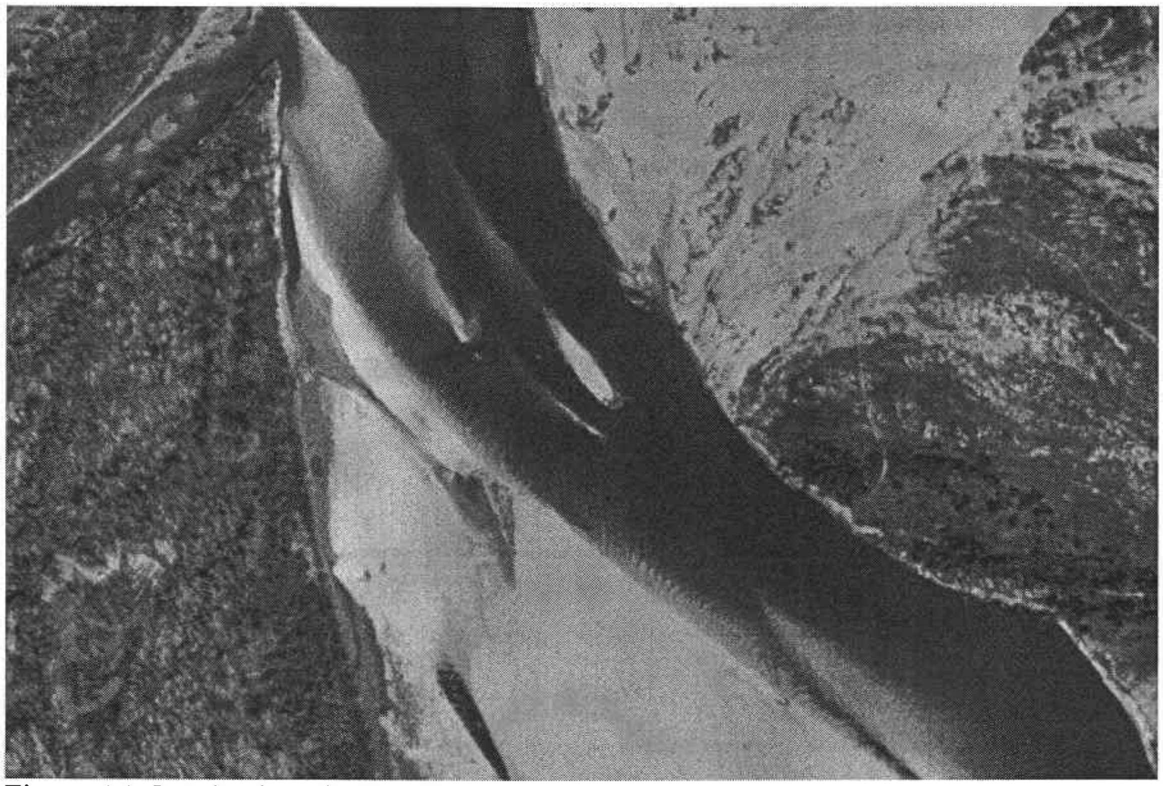

Figure A1-5. Island on the Red River

Determinable Characteristics:

- In or near main flow
- Streamlined shape
- Sparse islands/bars nearby
- Relative narrow width
- No vegetation
- Sand/silt sediment composition

From the classification matrix (Table 3-5), the island types that fit these known characteristics are 'Gradual Degradation of Channel Branches', 'Rapid Incision of Flood Deposits', and 'Lee Deposits'. By examining the island in question, we can see that the upstream end consists of a tangle of woody debris.

Island Type: *Lee Deposition*

APPENDIX II – CHARACTERISTICS OF FLUVIAL ISLANDS IN AMERICAN RIVERS

Island characteristics were determined using aerial photographs available from www.mapcard.com. Aerial photos, however, were not available for the Yukon River in Alaska. Characteristics of Yukon River islands were determined from topographic maps available from Mapcard. Characteristics can be separated into four main categories: Island location, Actual geometry, Lemniscate geometry, and River dimensions.

Island Location Characteristics:

- Island Name (if available)
- Latitude
- Longitude
- River mile (if available)
- Distance from left edge to left bank
- Distance from right edge to right bank
- Distance from island centerline to left bank, in percent of channel width

Actual Geometry Characteristics:

- Length, L, (m)
- Width, W, (m)
- Distance from upstream end to cross-section of maximum width, x, (m)
- Aspect Ratio, R_A
- Area, A, (km^2)
- Ratio of x/L
- Ratio of A/(L*W)
- Angle, theta, from island centerline to edge at maximum width
- Shape of island

Lemniscate Geometry Characteristics:

- Degree of elongation, $k = (\pi L)/(4A)$
- Angle, θ, to point of maximum width: $k \tan(\theta) \tan(k\,\theta) = 1$
- Ratio of distance from downstream end to cross-section of maximum width to total island length, $x/L = k \sin(\theta) \sin(k\,\theta)$
- Length/Width, $L/W = k \tan(k\,\theta) / 2(x/L)$

River Dimensions:

- Channel width
- Active channel width, ACW = channel width – island width
- Downstream channel width
- Upstream channel width
- Ratio of island width to total channel width
- Ratio of island width to active channel width

Other Notable Characteristics:

- Vegetation type
- Presence of nearby islands
- Presence of nearby river engineering projects, e.g. spur dikes or dams

Averages and standard deviations were calculated for the following characteristics: Distance from island centerline to left bank, Aspect ratio, Actual ratio of x/L, Ratio of A/LW, Actual theta, Lemniscate L/W, Degree of elongation, Lemniscate theta, Lemniscate x/L, and all the channel width ratios.

Colorado River

			Island Location			
Name	Lat (N)	Long (W)	RM	LB (m)	RB (m)	D from LB
	32.72	-114.719	23.5	44	17	66%
	32.741	*-114.693*	*26*	*43*	*14*	*67%*
	32.723	*-114.588*		*72*	*24*	*67%*
	32.726	*-114.585*		*37*	*39*	*49%*
	32.721	*-114.568*		*18*	*38*	*39%*
Laguna Dam			44			
Imperial Dam			49			
	32.939	-114.48	53.5	126	56	62%
	32.964	-114.467	55.5	144	54	66%
	33.027	-114.6	67.5	49	159	29%
	33.043	-114.638	70	140	82	59%
	33.046	-114.675		149	69	65%
	33.065	-114.682		104	114	48%
	33.18	-114.676		79	234	32%
	33.182	-114.676		119	136	48%
	33.212	-114.677		108	132	47%
	33.599	-114.535		33	113	32%
	33.601	-114.533		45	100	38%
	33.607	-114.528		31	116	31%
	33.966	-114.496	156	104	84	54%
	33.966	-114.495	156	57	124	36%
	33.972	-114.488	156	44	135	41%
	33.986	-114.472		89	53	59%
	33.987	-114.472		157	33	75%
	34.004	-114.467	160	64	129	41%
	34.011	-114.454	161	39	35	52%
	34.094	-114.427	167	102	30	69%
Headgate Rock Dam			178			
Parker Dam						
Davis Dam			276			
Hoover Dam			342			
Glen Canyon Dam						
	38.354	-109.756		56	188	28%
	38.431	-109.737		37	127	30%
	38.518	-109.649		29	124	34%
	35.558	-109.586		95	73	54%
	38.576	-109.579		56	153	32%
	38.602	-109.586		58	113	40%
	38.704	-109.399		64	83	47%
	count =	32				50.80%

					Actual Geometry				
Lat (N)	Long (W)	L (m)	W (m)	x	R_A	A(km^2)	x/L act.	A=x*LW	theta
32.72	-114.719	119	22.2	43.8	5.36	0.0021	63.19%	0.79	8.40
32.741	*-114.693*	*137*	*30*	43.4	4.57	0.0029	68.32%	0.71	9.10
32.723	*-114.588*	*142*	*45.6*	38	3.11	0.0049	73.24%	0.76	12.37
32.726	*-114.585*	*192*	*57.2*	77	3.36	0.0085	59.90%	0.77	13.97
32.721	*-114.568*	*111*	*32.3*	43.7	3.44	0.0022	60.63%	0.61	13.49
32.939	-114.48	427	115	135	3.71	0.0325	68.38%	0.66	11.14
32.964	-114.467	261	75.8	116	3.44	0.014	55.56%	0.71	14.65
33.027	-114.6	176	51.2	65.6	3.44	0.0056	62.73%	0.62	13.06
33.043	-114.638	340	89.3	164	3.81	0.0213	51.76%	0.70	14.24
33.046	-114.675	281	53	164	5.30	0.0104	41.64%	0.70	12.76
33.065	-114.682	394	89.5	137	4.40	0.0275	65.23%	0.78	9.88
33.18	-114.676	526	106	140	4.96	0.0412	73.38%	0.74	7.82
33.182	-114.676	475	128	279	3.71	0.0375	41.26%	0.62	18.08
33.212	-114.677	498	126	253	3.95	0.0415	49.20%	0.66	14.42
33.599	-114.535	473	81.7	142	5.79	0.029	69.98%	0.75	7.04
33.601	-114.533	149	79.7	84	1.87	0.0081	43.62%	0.68	31.51
33.607	-114.528	175	71.7	57	2.44	0.009	67.43%	0.72	16.90
33.966	-114.496	288	65.6	85	4.39	0.0124	70.49%	0.66	9.18
33.966	-114.495	142	58	37	2.45	0.0047	73.94%	0.57	15.44
33.972	-114.488	1242	334	374	3.72	0.2613	69.89%	0.63	10.89
33.986	-114.472	129	55	77	2.35	0.0047	40.31%	0.66	27.87
33.987	-114.472	212	60.4	111	3.51	0.0085	47.64%	0.66	16.65
34.004	-114.467	433	173	196	2.50	0.0537	54.73%	0.72	20.05
34.011	-114.454	235	56.9	56	4.13	0.0098	76.17%	0.73	9.03
34.094	-114.427	248	62.3	98	3.98	0.0113	60.48%	0.73	11.73
38.354	-109.756	318	54.8	155	5.80	0.0123	51.26%	0.71	9.54
38.431	-109.737	363	60.4	172	6.01	0.0152	52.62%	0.69	8.98
38.518	-109.649	553	144	207	3.84	0.056	62.57%	0.70	11.76
35.558	-109.586	294	83.6	116	3.52	0.0152	60.54%	0.62	13.22
38.576	-109.579	316	65	157	4.86	0.0147	50.32%	0.72	11.55
38.602	-109.586	846	112	256	7.55	0.0698	69.74%	0.74	5.42
38.704	-109.399	451	215	297	2.10	0.0639	34.15%	0.66	34.92
				Average	3.98		59.07%	0.69	13.91
				Std Dev	1.27		11.44%	0.05	6.66

Lemniscate Geometry

Lat (N)	Long (W)	L/W	k	theta	x/L	Shape
32.72	-114.719	4.74	5.30	9.28	0.65	lemn d/s
32.741	*-114.693*	4.55	5.08	9.66	0.65	horseshoe
32.723	*-114.588*	2.91	3.23	15.12	0.64	lemn d/s
32.726	*-114.585*	3.07	3.41	14.36	0.64	irregular
32.721	*-114.568*	3.94	4.40	11.15	0.64	lemn d/s
32.939	-114.48	3.95	4.41	11.14	0.64	lemn d/s

32.964	-114.467	3.43	3.82	12.82	0.64	elliptical
33.027	-114.6	3.90	4.34	11.29	0.64	lemn d/s
33.043	-114.638	3.82	4.26	11.51	0.64	lemn d/s
33.046	-114.675	5.33	5.96	8.25	0.65	lenticular
33.065	-114.682	3.98	4.43	11.07	0.64	lemn d/s
33.18	-114.676	4.72	5.27	9.32	0.65	irregular
33.182	-114.676	4.23	4.73	10.39	0.64	irregular
33.212	-114.677	4.21	4.69	10.46	0.64	irregular
33.599	-114.535	5.42	6.06	8.12	0.65	elliptical
33.601	-114.533	1.97	2.15	22.46	0.61	irregular
33.607	-114.528	2.42	2.67	18.21	0.63	irregular
33.966	-114.496	4.70	5.25	9.35	0.65	lemn d/s
33.966	-114.495	3.04	3.37	14.51	0.64	lemn d/s
33.972	-114.488	4.16	4.64	10.59	0.64	lemn d/s
33.986	-114.472	2.52	2.78	17.52	0.63	lenticular
33.987	-114.472	3.73	4.15	11.81	0.64	irregular
34.004	-114.467	2.48	2.74	17.76	0.63	irregular
34.011	-114.454	3.97	4.43	11.09	0.64	lemn d/s
34.094	-114.427	3.84	4.27	11.47	0.64	elliptical
38.354	-109.756	5.77	6.46	7.62	0.65	triangular
38.431	-109.737	6.08	6.81	7.23	0.65	lenticular
38.518	-109.649	3.85	4.29	11.44	0.64	dissected
35.558	-109.586	4.00	4.47	10.99	0.64	lemn d/s
38.576	-109.579	4.77	5.34	9.21	0.65	elliptical
38.602	-109.586	7.19	8.05	6.11	0.65	trapezoidal
38.704	-109.399	2.27	2.50	19.43	0.62	irregular
		4.03	4.49	11.90	0.64	
		1.16	1.31	3.78	0.01	

			River Dimensions				
Lat (N)	Long (W)	ACW	width	d/s width	u/s width	IW/TW	IW/ACW
32.72	-114.719	57.8	80	70	75	27.8%	38.4%
32.741	*-114.693*	60	90	60	75	33.3%	50.0%
32.723	*-114.588*	84.4	130	90	95	35.1%	54.0%
32.726	*-114.585*	77.8	135	95	70	42.4%	73.5%
32.721	*-114.568*	57.7	90	45	90	35.9%	56.0%
32.939	-114.48	175	290	145	190	39.7%	65.7%
32.964	-114.467	199.2	275	155	195	27.6%	38.1%
33.027	-114.6	203.8	255	205	230	20.1%	25.1%
33.043	-114.638	225.7	315	150	180	28.3%	39.6%
33.046	-114.675	237	290	165	270	18.3%	22.4%
33.065	-114.682	220.5	310	170	260	28.9%	40.6%
33.18	-114.676	304	410	195	245	25.9%	34.9%
33.182	-114.676	262	390	315	175	32.8%	48.9%
33.212	-114.677	254	380	205	205	33.2%	49.6%

33.599	-114.535	171.3	253	150	215	32.3%	47.7%
33.601	-114.533	150.3	230	250	130	34.7%	53.0%
33.607	-114.528	151.3	223	165	85	32.2%	47.4%
33.966	-114.496	189.4	255	145	275	25.7%	34.6%
33.966	-114.495	182	240	275	300	24.2%	31.9%
33.972	-114.488	161	495	185	110	67.5%	207.5%
33.986	-114.472	150	205	70	160	26.8%	36.7%
33.987	-114.472	199.6	260	80	130	23.2%	30.3%
34.004	-114.467	197	370	160	150	46.8%	87.8%
34.011	-114.454	83.1	140	250	155	40.6%	68.5%
34.094	-114.427	122.7	185	130	215	33.7%	50.8%
38.354	-109.756	270.2	325	195	275	16.9%	20.3%
38.431	-109.737	169.6	230	265	220	26.3%	35.6%
38.518	-109.649	171	315	235	230	45.7%	84.2%
35.558	-109.586	161.4	245	195	215	34.1%	51.8%
38.576	-109.579	220	285	200	205	22.8%	29.5%
38.602	-109.586	158	270	255	140	41.5%	70.9%
38.704	-109.399	135	350	155	100	61.4%	159.3%
						32.7%	53.3%

Columbia River

Island Location

Name	Lat (N)	Long (W)	RM	LB (m)	RB (m)	D from LB
Sandy I.	46.006	-122.863	76	415	755	42%
St. Helens Bar	45.867	-122.792	85.5	286	667	34%
Willamette River			101			
Tri-Club	45.594	-122.556	112	1245	524	69%
Lemon	45.589	-122.562	112	448	1116	32%
Government	45.576	-122.503	115	725	663	51%
McGuire I.	45.563	-122.46	118	305	234	53%
Ackerman I.	45.575	-122.46	118	380	347	52%
Gary I.	45.555	-122.347	124	275	1203	24%
Flag	45.547	-122.337	125	276	1027	24%
Chatham	45.541	-122.333	125	66	1438	8%
Reed I.	45.553	-122.294	127	722	203	64%
Sand I.	45.554	-122.2	130	224	1032	28%
Skamania I.	45.589	-122.124	136	900	472	64%
Bonneville Dam			146			
Wells I.	45.718	-121.533	168	264	1128	23%
The Dalles Dam			191			
Browns I.	45.655	-121.039	197	595	666	48%
John Day Dam			215			
McNary Dam			292			
Badger I.	46.11	-118.938	318	970	2226	31%

Snake River			325			
Richland Bar	46.237	-119.199	334	422	251	61%
Nelson I.	46.306	-119.261	340	707	157	77%
	46.313	-119.254	340	300	441	42%
	count =	19				43.45%

Lat (N)	Long (W)	L (m)	W (m)	*Actual Geometry* x (m)	R_A	A(km^2)	x/L act.	A=x*LW	theta
46.006	-122.863	2748	865	1720	3.18	1.64	37.41%	0.69	22.82
45.867	-122.792	1349	257	572	5.25	0.23	57.60%	0.67	9.39
45.594	-122.556	1014	143	214	7.09	0.12	78.90%	0.85	5.11
45.589	-122.562	1372	247	404	5.55	0.26	70.55%	0.76	7.27
45.576	-122.503	8311	1356	4883	6.13	8.11	41.25%	0.72	11.19
45.563	-122.46	2786	635	833	4.39	1.03	70.10%	0.58	9.23
45.575	-122.46	2075	310	1132	6.69	0.40	45.45%	0.62	9.33
45.555	-122.347	1098	294	379	3.73	0.21	65.48%	0.64	11.55
45.547	-122.337	710	145	159	4.90	0.06	77.61%	0.54	7.50
45.541	-122.333	755	127	120	5.94	0.06	84.11%	0.63	5.71
45.553	-122.294	3835	985.7	793	3.89	2.18	79.32%	0.58	9.20
45.554	-122.2	2271.1	550.4	675	4.13	0.79	70.28%	0.63	9.78
45.589	-122.124	704.1	191.5	263	3.68	0.10	62.65%	0.70	12.25
45.718	-121.533	765	220	254	3.48	0.12	66.80%	0.71	12.15
45.655	-121.039	829	297	378	2.79	0.20	54.40%	0.80	18.23
46.11	-118.938	1214	192	442	*6.32*	0.16	63.59%	0.67	7.09
46.237	-119.199	716.7	99.6	322	*7.20*	0.05	55.07%	0.66	7.19
46.306	-119.261	852.7	159.5	159	*5.35*	0.10	81.35%	0.71	6.56
46.313	-119.254	867.2	184	475	*4.71*	0.12	45.23%	0.73	13.20
				Average	4.97		63.53%	0.68	10.25
				Std Dev	1.35		14.16%	0.08	4.35

Lat (N)	Long (W)	*Lemniscate Geometry* L/W	k	theta	x/L	shape
46.006	-122.863	3.25	3.62	13.55	0.64	semicircle
45.867	-122.792	5.49	6.14	8.01	0.65	elliptical
45.594	-122.556	5.86	6.55	7.50	0.65	elliptical
45.589	-122.562	5.16	5.77	8.53	0.65	elliptical
45.576	-122.503	5.98	6.69	7.35	0.65	elliptical
45.563	-122.46	5.28	5.90	8.33	0.65	lemn d/s

45.575	-122.46	7.58	8.49	5.80	0.65	irregular
45.555	-122.347	4.09	4.56	10.76	0.64	elliptical
45.547	-122.337	6.41	7.17	6.86	0.65	rhombic
45.541	-122.333	6.64	7.44	6.62	0.65	lemn d/s
45.553	-122.294	4.74	5.30	9.27	0.65	lemn d/s
45.554	-122.2	4.59	5.12	9.59	0.65	elliptical
45.589	-122.124	3.68	4.10	11.96	0.64	lemn d/s
45.718	-121.533	3.44	3.82	12.81	0.64	irregular
45.655	-121.039	2.50	2.76	17.68	0.63	irregular
46.11	-118.938	6.59	7.38	6.67	0.65	elliptical
46.237	-119.199	7.66	8.58	5.74	0.65	elliptical
46.306	-119.261	5.26	5.89	8.35	0.65	lemn d/s
46.313	-119.254	4.56	5.09	9.65	0.65	elliptical
		5.20	5.81	9.21	0.65	
		1.44	1.62	3.04	0.01	

River Dimensions

Lat (N)	Long (W)	ACW	width	d/s width	u/s width	IW/TW	IW/ACW
46.006	-122.863	1200	2065	1095	940	41.89%	72.08%
45.867	-122.792	923	1180	975	830	21.78%	27.84%
45.594	-122.556	1802	1945	1225	2545	7.35%	7.94%
45.589	-122.562	1603	1850	1225	2545	13.35%	15.41%
45.576	-122.503	1459	2815	1070	760	48.17%	92.94%
45.563	-122.46	1000	1635	705	915	38.84%	63.50%
45.575	-122.46	835	1145	685	905	27.07%	37.13%
45.555	-122.347	1421	1715	1390	1540	17.14%	20.69%
45.547	-122.337	1375	1520	1570	2275	9.54%	10.55%
45.541	-122.333	1528	1655	1660	2115	7.67%	8.31%
45.553	-122.294	964.3	1950	1675	1680	50.55%	102.22%
45.554	-122.2	1304.6	1855	1280	1960	29.67%	42.19%
45.589	-122.124	1358.5	1550	1395	1895	12.35%	14.10%
45.718	-121.533	1400	1620	1265	1300	13.58%	15.71%
45.655	-121.039	1268	1565	1060	1250	18.98%	23.42%
46.11	-118.938	3153	3345	3410	4675	5.74%	6.09%
46.237	-119.199	685.4	785	690	915	12.69%	14.53%
46.306	-119.261	790.5	950	730	870	16.79%	20.18%
46.313	-119.254	691	875	890	825	21.03%	26.63%
						21.80%	32.71%

Upper Mississippi River

		Island Location				
Name	RM	Lat (N)	Lon (W)	LB (m)	RB (m)	D from LB
Lock & Dam No.26	203					
Piasa I.	208.5	38.931	90.277	242	1117	26%
Eagle's Nest I.	210	38.927	90.302	655	570	53%
Portage I.	213.5	38.939	90.355	498	309	58%
Elsah Bar	214	38.947	90.366	530	489	52%
	214	38.94	90.36	171	297	38%
	214	38.939	90.358	72	359	20%
Island 526	219.5	38.964	90.441	517	652	45%
	219.5	38.964	90.435	504	458	52%
Illinois River	220					
	226	38.885	90.516	95	324	28%
Island 508	233	38.89	90.634	821	112	80%
Lock & Dam No.25	241.5					
Turner I.	245	39.05	90.708	412	569	45%
Willow I.	245	39.058	90.703	375	238	61%
Hausgen I.	247	39.079	90.702	858	158	79%
	258	39.22	90.726	793	76	87%
Mozier I.	260	39.252	90.737	508	432	52%
Howard I.	261	39.256	90.747	185	246	45%
	261	39.259	90.745	128	161	46%
	261	39.257	90.75	177	65	68%
	262	39.27	90.751	169	482	32%
Lock & Dam No. 24	273.5					
Hope I.	297	39.597	91.202	155	101	58%
Polly I.		40.183	91.496	120	385	31%
	count =	21				50.3%

						Actual Geometry			
Lat (N)	Lon (W)	L (m)	W (m)	x	R_A	A(km^2)	x/L act.	A=x*LW	theta
38.931	90.277	2342.7	494	875	4.7	0.72	62.65%	0.62	9.55
38.927	90.302	1310	298.5	751	4.4	0.30	42.67%	0.76	14.95
38.939	90.355	1763.4	440	1070	4.0	0.50	39.32%	0.65	17.60
38.947	90.366	177	43.4	123	4.1	0.01	30.51%	0.73	21.89
38.94	90.36	274.9	44.8	141	6.1	0.01	48.71%	0.79	9.50
38.939	90.358	242.3	46	115	5.3	0.01	52.54%	0.72	10.24
38.964	90.441	1097.6	312	352	3.5	0.24	67.93%	0.71	11.82
38.964	90.435	288.4	93.4	96.5	3.1	0.02	66.54%	0.76	13.68
38.885	90.516	556	105	237	5.3	0.04	57.37%	0.74	9.35
38.89	90.634	1078.6	231.1	293	4.7	0.15	72.84%	0.61	8.37
39.05	90.708	1510.2	548.6	478	2.8	0.56	68.35%	0.67	14.88
39.058	90.703	163	36.6	43.6	4.5	0.00	73.25%	0.75	8.71
39.079	90.702	882	187	141	4.7	0.11	84.01%	0.67	7.19

39.22	90.726	268	91.6	95.3	2.9	0.02	64.44%	0.64	14.85
39.252	90.737	2848	897	458	3.2	1.75	83.92%	0.69	10.63
39.256	90.747	1088	224	422	4.9	0.17	61.21%	0.71	9.55
39.259	90.745	362	132	166	2.7	0.03	54.14%	0.72	18.61
39.257	90.75	213	68.3	64.3	3.1	0.01	69.81%	0.60	12.93
39.27	90.751	889	199	280	4.5	0.12	68.50%	0.67	9.28
39.597	91.202	315.4	76.2	99.5	4.1	0.02	68.45%	0.70	10.01
40.183	91.496	984.7	191.3	285	5.1	0.13	71.06%	0.70	7.78
				Average	4.18		62.3%	0.70	11.97
				Std Dev	0.95		13.72%	0.05	3.93

Lemniscate Geometry

Lat (N)	Lon (W)	L/W	k	theta	x/L	shape
38.931	90.277	5.36	6.00	8.20	0.65	lemniscate
38.927	90.302	4.06	4.53	10.83	0.64	elliptical
38.939	90.355	4.35	4.85	10.12	0.64	elliptical
38.947	90.366	3.94	4.39	11.17	0.64	elliptical
38.94	90.36	5.47	6.12	8.04	0.65	elliptical
38.939	90.358	5.16	5.76	8.53	0.65	elliptical
38.964	90.441	3.47	3.87	12.68	0.64	trapezoidal
38.964	90.435	2.87	3.19	15.33	0.63	elliptical
38.885	90.516	5.03	5.62	8.75	0.65	lenticular
38.89	90.634	5.41	6.05	8.13	0.65	lemniscate
39.05	90.708	2.89	3.21	15.24	0.63	lemniscate
39.058	90.703	4.16	4.64	10.59	0.64	elliptical
39.079	90.702	4.94	5.52	8.90	0.65	lemniscate
39.22	90.726	3.23	3.59	13.62	0.64	lemniscate
39.252	90.737	3.27	3.63	13.48	0.64	lemniscate
39.256	90.747	4.83	5.40	9.11	0.65	lenticular
39.259	90.745	2.71	3.00	16.26	0.63	elliptical
39.257	90.75	3.68	4.10	11.97	0.64	lemniscate
39.27	90.751	4.66	5.20	9.44	0.65	lenticular
39.597	91.202	4.14	4.62	10.62	0.64	lemniscate
40.183	91.496	5.20	5.81	8.46	0.65	elliptical
		4.23	4.72	10.93	0.64	
		0.91	1.03	2.60	0.00	

River Dimensions

Lat (N)	Lon (W)	ACW	width	d/s width	u/s width	IW/TW	IW/ACW
38.931	90.277	1431	1925	1320	1400	25.66%	34.52%
38.927	90.302	1216.5	1515	1850	1445	19.70%	24.54%
38.939	90.355	820	1260	1030	900	34.92%	53.66%
38.947	90.366	1051.6	1095	1305	910	3.96%	4.13%
38.94	90.36	1230.2	1275	1160	945	3.51%	3.64%
38.939	90.358	1249	1295	1100	1020	3.55%	3.68%

38.964	90.441	1168	1480	835	730	21.08%	26.71%
38.964	90.435	996.6	1090	835	1015	8.57%	9.37%
38.885	90.516	410	515	250	315	20.39%	25.61%
38.89	90.634	948.9	1180	1185	1755	19.58%	24.35%
39.05	90.708	1056.4	1605	1025	1125	34.18%	51.93%
39.058	90.703	1433.4	1470	1280	1045	2.49%	2.55%
39.079	90.702	1013	1200	1485	1045	15.58%	18.46%
39.22	90.726	958.4	1050	1900	530	8.72%	9.56%
39.252	90.737	963	1860	670	935	48.23%	93.15%
39.256	90.747	1286	1510	1290	910	14.83%	17.42%
39.259	90.745	1288	1420	1730	880	9.30%	10.25%
39.257	90.75	1351.7	1420	1730	880	4.81%	5.05%
39.27	90.751	671	870	1480	1100	22.87%	29.66%
39.597	91.202	463.8	540	375	310	14.11%	16.43%
40.183	91.496	1528.7	1720	1040	1340	11.12%	12.51%
						16.53%	22.72%

Middle Mississippi River

Island Location

Name	RM	Lat (N)	Long (W)	LB (m)	RB (m)	D from LB
Browns Bar	23	36.998	89.278	405	599	45%
	30	37.04	89.373	269	433	39%
Burnham I.	37	37.14	89.416	260	533	43%
Marquette I.	50	37.263	89.513	378	575	45%
	79	37.608	89.512	525	411	55%
	99	37.806	89.685	648	104	80%
	99	37.809	89.691	630	82	85%
	122	37.975	89.999	296	791	39%
Mosenthein I.	188	38.725	90.2	585	592	50%
	195	38.804	90.125	644	214	68%
Missouri River	195.5					
						55.0%

count = 10

Actual Geometry

Lat (N)	Lon (W)	L (m)	W (m)	x	R_A	A(km^2)	x/L act.	A=x*LW	theta
36.998	89.278	2129	784	648	2.7	1.0643	69.56%	0.64	14.83
37.04	89.373	263	77.7	124	3.4	0.0146	52.85%	0.71	15.62
37.14	89.416	5880	1116	3098	5.3	5.0797	47.31%	0.77	11.34
37.263	89.513	3486	1184	1276	2.9	2.833	63.40%	0.69	15.00
37.608	89.512	930	302	389	3.1	0.1797	58.17%	0.64	15.60
37.806	89.685	394	141	150	2.8	0.0432	61.93%	0.78	16.12

37.809	89.691	320	67.5	75	4.7	0.0188	76.56%	0.87	7.84
37.975	89.999	2991	1219	930	2.5	2.3702	68.91%	0.65	16.47
38.725	90.2	4112	1350	1559	3.0	3.9583	62.09%	0.71	14.81
38.804	90.125	1408	344	315	4.1	0.3263	77.63%	0.67	8.94
				Average	3.45		63.8%	0.71	13.66
				Std Dev	0.94		9.68%	0.07	3.12

Lemniscate Geometry

Lat (N)	Lon (W)	L/W	k	theta	x/L	shape
36.998	89.278	3.01	3.34	14.62	0.64	lemniscate
37.04	89.373	3.35	3.72	13.16	0.64	lenticular
37.14	89.416	4.78	5.35	9.19	0.65	elliptical
37.263	89.513	3.03	3.37	14.52	0.64	semicircle
37.608	89.512	3.40	3.78	12.96	0.64	lenticular
37.806	89.685	2.55	2.82	17.27	0.63	elliptical
37.809	89.691	3.84	4.28	11.47	0.64	elliptical
37.975	89.999	2.68	2.96	16.46	0.63	lenticular
38.725	90.2	3.02	3.35	14.58	0.64	elliptical
38.804	90.125	4.28	4.77	10.29	0.64	lenticular
		3.39	3.78	13.45	0.64	
		0.71	0.80	2.58	0.01	

River Dimensions

Lat (N)	Lon (W)	ACW	width	d/s width	u/s width	IW/TW	IW/ACW
36.998	89.278	1111	1895	680	870	41.37%	70.57%
37.04	89.373	752.3	830	560	1325	9.36%	10.33%
37.14	89.416	894	2010	740	845	55.52%	124.83%
37.263	89.513	996	2180	530	705	54.31%	118.88%
37.608	89.512	933	1235	645	925	24.45%	32.37%
37.806	89.685	734	875	850	760	16.11%	19.21%
37.809	89.691	732.5	800	855	890	8.44%	9.22%
37.975	89.999	1096	2315	535	715	52.66%	111.22%
38.725	90.2	1225	2575	625	995	52.43%	110.20%
38.804	90.125	881	1225	635	785	28.08%	39.05%
						34.27%	64.59%

Lower Mississippi River

Name	Island Location					
	Lat (N)	Long (W)	RM	LB (m)	RB (m)	
Bayou Goula Towhead	30.199	91.159	195	269	658	36%
	30.311	91.214	210	345	753	34%
Fancy Point Towhead	30.665	91.33	258	302	523	43%
St. Maurice Towhead	30.739	91.488	272	744	207	66%
Miles Bar	30.921	91.641	299	541	1715	27%
Shreves Bar	30.983	91.656	304	364	739	39%
	31.2	91.601	325	896	367	65%
St. Catherine Bend Bar	31.405	91.476		584	740	45%
	31.5	91.504	356	200	678	39%
	31.505	91.494	356	109	143	46%
	31.753	91.377	377	816	498	57%
	31.834	91.343	383	393	729	37%
	31.888	91.227	392	761	462	58%
Middle Ground Island	32.054	91.072		834	735	52%
Racetrack Island	32.279	90.967		1644	271	78%
	32.337	90.937		1211	264	76%
	32.4	91.003		1387	121	83%
	32.527	91.107	459	780	450	62%
Stack Island	32.831	91.134	490	778	823	49%
	33.015	91.165	507	1117	417	66%
	33.043	91.162	510	1233	343	74%
	33.035	91.158	510	1420	302	79%
	33.079	91.156	513	349	161	65%
	33.091	91.158	514	328	892	36%
	33.173	91.09	523	874	460	60%
Choctaw Bar Island	33.607	91.144	562	772	467	54%
	33.67	91.214	570	302	712	40%
	33.739	91.137	577	250	857	31%
Arkansas River			580			
Cessions Towhead	34.058	90.899	615	768	305	66%
	34.115	90.947	619	500	491	50%
	34.297	90.746	639	687	327	59%
Montezuma Towhead	34.408	90.602		965	252	70%
	34.416	90.578		354	1211	27%
St. Francis Towhead	34.629	90.58	673	142	854	24%
	34.849	90.379	699	1491	301	78%
Harkleroad/Catisland Thd.	34.933	90.256	710	712	325	57%
	35.026	90.268	718	1258	174	80%
Loosahatchie Bar	35.183	90.076	739	762	305	59%
	35.44	90.002	759	798	348	63%
Lookout Bar	35.531	89.911	772	1872	509	76%
	35.533	89.913	772	213	213	50%
Plum Point Bar	35.656	89.901	782	418	900	34%

	35.787	89.747	799	238	1048	24%
	35.86	89.756	807	887	596	59%
	35.897	89.741	811	268	1539	22%
Island No. 21	35.975	89.703	826	291	1336	37%
	36.029	89.699	830	1211	604	65%
	36.089	89.668	835	517	827	40%
Madrid Bar	36.575	89.546	888	1525	350	75%
	36.53	89.46	895	1154	251	76%
	36.57	89.24	920	718	349	65%
Middle Bar	36.723	89.149	934	849	550	55%
Ohio River			953			
						54.0%
	count =	52				

Actual Geometry

Lat (N)	Lon (W)	L (m)	W (m)	x	R_A	A(km^2)	x/L act.	A=x*LW	theta
30.199	91.159	2460	429	1382	5.73	0.8273	43.82%	0.78	11.25
30.311	91.214	1172	216	227	5.43	0.1675	80.63%	0.66	6.52
30.665	91.33	2615	708	1157	3.69	1.1386	55.76%	0.61	13.65
30.739	91.488	3798	681	1072	5.58	1.5641	71.77%	0.60	7.12
30.921	91.641	1560	276	256	5.65	0.3151	83.59%	0.73	6.04
30.983	91.656	1823	663	795	2.75	0.8033	56.39%	0.66	17.87
31.2	91.601	3158	481	375	6.57	0.8472	88.13%	0.56	4.94
31.405	91.476	*820*	*223*	*486*	*3.68*	*0.1229*	40.73%	*0.67*	18.46
31.5	91.504	3599	1296	1927	2.78	3.0468	46.46%	0.65	21.18
31.505	91.494	519	161	181	3.22	0.0623	65.13%	0.75	13.40
31.753	91.377	3335	870	985	3.83	1.7402	70.46%	0.60	10.49
31.834	91.343	*984*	*152*	*371*	*6.47*	*0.1062*	62.30%	*0.71*	7.07
31.888	91.227	2669	752	1222	3.55	1.2806	54.22%	0.64	14.57
32.054	91.072	4293	1650	1663	2.60	4.25	61.26%	0.60	17.42
32.279	90.967	2264	564	785	4.01	0.7236	65.33%	0.57	10.79
32.337	90.937	1619	346	337	4.68	0.4396	79.18%	0.78	7.69
32.4	91.003	1179	408	256	2.89	0.3497	78.29%	0.73	12.46
32.527	91.107	590	139	255	4.24	0.0532	56.78%	0.65	11.72
32.831	91.134	2556	873	779	2.93	1.4766	69.52%	0.66	13.80
33.015	91.165	3234	698	1150	4.63	1.8309	64.44%	0.81	9.51
33.043	91.162	1248	309	245	4.04	0.275	80.37%	0.71	8.76
33.035	91.158	*730*	*234*	*389*	*3.12*	*0.1294*	46.71%	*0.76*	18.94
33.079	91.156	636	134	256	4.75	0.0593	59.75%	0.70	10.00
33.091	91.158	3440	864	1284	3.98	1.9416	62.67%	0.65	11.33
33.173	91.09	2612	683	970	3.82	1.0249	62.86%	0.57	11.75
33.607	91.144	6163	2317	2554	2.66	9.071	58.56%	0.64	17.80
33.67	91.214	3115	1130	1174	2.76	2.3209	62.31%	0.66	16.23
33.739	91.137	2658	527	959	5.04	0.8484	63.92%	0.61	8.82
34.058	90.899	1654	355	917	4.66	0.4126	44.56%	0.70	13.54
34.115	90.947	*933*	*261*	*459*	*3.57*	*0.122*	50.80%	*0.50*	15.39

34.297	90.746	3239	1009	1202	3.21	2.2575	62.89%	0.69	13.91
34.408	90.602	2358	539	568	4.37	0.9365	75.91%	0.74	8.56
34.416	90.578	1203	323	410	3.72	0.2679	65.92%	0.69	11.51
34.629	90.58	*2981*	*387*	*408*	*7.70*	*0.9002*	86.31%	*0.78*	4.30
34.849	90.379	920	298	247	3.09	0.202	73.15%	0.74	12.48
34.933	90.256	4997	1620	2290	3.08	4.737	54.17%	0.59	16.66
35.026	90.268	1526	376	246	4.06	0.3217	83.88%	0.56	8.36
35.183	90.076	4223	1527	2107	2.77	4.171	50.11%	0.65	19.84
35.44	90.002	*1703*	*534*	*655*	*3.19*	*0.4955*	61.54%	*0.54*	14.29
35.531	89.911	1211	208	590	5.82	0.193	51.28%	0.77	9.51
35.533	89.913	189	76.5	42.4	2.47	0.0103	77.57%	0.71	14.62
35.656	89.901	725	155	298	4.68	0.0881	58.90%	0.78	10.29
35.787	89.747	807	285	218	2.83	0.1802	72.99%	0.78	13.60
35.86	89.756	*698*	*205*	*302*	*3.40*	*0.087*	56.73%	*0.61*	14.51
35.897	89.741	1627	424	520	3.84	0.4585	68.04%	0.66	10.84
35.975	89.703	5366	2283	2314	2.35	7.0746	56.88%	0.58	20.51
36.029	89.699	722	165	183	4.38	0.0901	74.65%	0.76	8.70
36.089	89.668	961	230	257	4.18	0.1469	73.26%	0.66	9.28
36.575	89.546	4283	500	1114	8.57	1.2032	73.99%	0.56	4.51
36.53	89.46	1976	359	784	5.50	0.4033	60.32%	0.57	8.56
36.57	89.24	*1059*	*198*	*545*	*5.35*	*0.1356*	48.54%	*0.65*	10.90
36.723	89.149	4203	1610	1837	2.61	4.5467	56.29%	0.67	18.79
			Average		4.13		64.0%	0.67	12.17
			Std Dev		1.4		11.82%	0.1	4.3

Lemniscate Geometry

Lat (N)	Lon (W)	L/W	k	theta	x/L	shape
30.199	91.159	5.14	5.75	8.56	0.65	elliptical
30.311	91.214	5.76	6.44	7.64	0.65	lemniscate
30.665	91.33	4.23	4.72	10.41	0.64	lenticular
30.739	91.488	6.47	7.24	6.79	0.65	lenticular
30.921	91.641	5.42	6.07	8.11	0.65	semicircle
30.983	91.656	2.93	3.25	15.04	0.64	lenticular
31.2	91.601	8.25	9.25	5.33	0.65	irregular
31.405	91.476	3.85	4.30	11.42	0.64	irregular
31.5	91.504	3.01	3.34	14.64	0.64	lenticular
31.505	91.494	3.06	3.40	14.40	0.64	lemniscate
31.753	91.377	4.50	5.02	9.78	0.64	lemniscate
31.834	91.343	6.40	7.16	6.87	0.65	elliptical
31.888	91.227	3.92	4.37	11.23	0.64	lenticular
32.054	91.072	3.07	3.41	14.36	0.64	lenticular
32.279	90.967	4.98	5.56	8.83	0.65	irregular
32.337	90.937	4.20	4.68	10.48	0.64	lemniscate
32.4	91.003	2.82	3.12	15.64	0.63	lemniscate
32.527	91.107	4.60	5.14	9.56	0.65	lenticular
32.831	91.134	3.13	3.47	14.08	0.64	lemniscate

33.015	91.165	4.02	4.49	10.94	0.64	elliptical
33.043	91.162	3.99	4.45	11.03	0.64	lemniscate
33.035	91.158	2.92	3.23	15.11	0.64	elliptical
33.079	91.156	4.79	5.36	9.17	0.65	lenticular
33.091	91.158	4.29	4.79	10.26	0.64	irregular
33.173	91.09	4.68	5.23	9.40	0.65	irregular
33.607	91.144	2.96	3.29	14.86	0.64	semicircle
33.67	91.214	2.96	3.28	14.89	0.64	semicircle
33.739	91.137	5.84	6.54	7.52	0.65	lemniscate
34.058	90.899	4.66	5.21	9.43	0.65	elliptical
34.115	90.947	5.01	5.60	8.77	0.65	irregular
34.297	90.746	3.28	3.65	13.41	0.64	lenticular
34.408	90.602	4.18	4.66	10.53	0.64	lemniscate
34.416	90.578	3.81	4.24	11.56	0.64	lemniscate
34.629	90.58	6.92	7.75	6.35	0.65	elliptical
34.849	90.379	2.97	3.29	14.85	0.64	lemniscate
34.933	90.256	3.72	4.14	11.84	0.64	semicircle
35.026	90.268	5.09	5.69	8.65	0.65	lemniscate
35.183	90.076	3.03	3.36	14.56	0.64	irregular
35.44	90.002	4.12	4.60	10.68	0.64	lemniscate
35.531	89.911	5.34	5.97	8.24	0.65	lenticular
35.533	89.913	2.47	2.72	17.88	0.63	lemniscate
35.656	89.901	4.20	4.69	10.48	0.64	lenticular
35.787	89.747	2.57	2.84	17.17	0.63	elliptical
35.86	89.756	3.94	4.40	11.16	0.64	lemniscate
35.897	89.741	4.06	4.53	10.82	0.64	lemniscate
35.975	89.703	2.88	3.20	15.28	0.63	lenticular
36.029	89.699	4.07	4.54	10.80	0.64	lemniscate
36.089	89.668	4.42	4.94	9.95	0.64	lemniscate
36.575	89.546	10.68	11.97	4.11	0.65	elliptical
36.53	89.46	6.79	7.60	6.47	0.65	lenticular
36.57	89.24	5.81	6.50	7.57	0.65	lenticular
36.723	89.149	2.76	3.05	16.00	0.63	semicircle
		4.40	4.91	11.02	0.64	
		1.55	1.75	3.25	0.01	

River Dimensions

Lat (N)	Lon (W)	ACW	width	d/s width	u/s width	IW/TW	IW/ACW
30.199	91.159	1041	1470	780	1120	29.18%	41.21%
30.311	91.214	1104	1320	555	1295	16.36%	19.57%
30.665	91.33	882	1590	975	1160	44.53%	80.27%
30.739	91.488	1034	1715	675	815	39.71%	65.86%
30.921	91.641	2329	2605	830	1315	10.60%	11.85%
30.983	91.656	1117	1780	1045	1380	37.25%	59.36%
31.2	91.601	1294	1775	900	1100	27.10%	37.17%
31.405	91.476	1312	1535	1220	1545	14.53%	17.00%

31.5	91.504	874	2170	1140	1315	59.72%	148.28%
31.505	91.494	244	405	185	560	39.75%	65.98%
31.753	91.377	1825	2695	1430	1495	32.28%	47.67%
31.834	91.343	1083	1235	815	1880	12.31%	14.04%
31.888	91.227	1298	2050	1215	1620	36.68%	57.94%
32.054	91.072	1555	3205	1200	790	51.48%	106.11%
32.279	90.967	1986	2550	1865	1210	22.12%	28.40%
32.337	90.937	1454	1800	1170	1105	19.22%	23.80%
32.4	91.003	1557	1965	865	1500	20.76%	26.20%
32.527	91.107	1236	1375	865	1625	10.11%	11.25%
32.831	91.134	1487	2360	1710	1950	36.99%	58.71%
33.015	91.165	1632	2330	1400	1600	29.96%	42.77%
33.043	91.162	1611	1920	2330	680	16.09%	19.18%
33.035	91.158	1981	2215	2330	690	10.56%	11.81%
33.079	91.156	531	665	540	435	20.15%	25.24%
33.091	91.158	1286	2150	1280	915	40.19%	67.19%
33.173	91.09	1227	1910	1110	1455	35.76%	55.66%
33.607	91.144	1343	3660	825	820	63.31%	172.52%
33.67	91.214	1015	2145	935	1030	52.68%	111.33%
33.739	91.137	1153	1680	995	1360	31.37%	45.71%
34.058	90.899	1140	1495	1995	1460	23.75%	31.14%
34.115	90.947	1029	1290	820	1970	20.23%	25.36%
34.297	90.746	1006	2015	855	755	50.07%	100.30%
34.408	90.602	1281	1820	1210	1895	29.62%	42.08%
34.416	90.578	1537	1860	1820	1160	17.37%	21.01%
34.629	90.58	1018	1405	825	850	27.54%	38.02%
34.849	90.379	1782	2080	1980	1635	14.33%	16.72%
34.933	90.256	1175	2795	1590	915	57.96%	137.87%
35.026	90.268	1454	1830	1640	2170	20.55%	25.86%
35.183	90.076	1138	2665	1085	2525	57.30%	134.18%
35.44	90.002	1186	1720	1180	1660	31.05%	45.03%
35.531	89.911	2457	2665	835	1225	7.80%	8.47%
35.533	89.913	2588.5	2665	835	1225	2.87%	2.96%
35.656	89.901	1300	1455	1225	1670	10.65%	11.92%
35.787	89.747	1275	1560	1275	1000	18.27%	22.35%
35.86	89.756	1550	1755	1100	1720	11.68%	13.23%
35.897	89.741	1736	2160	1625	1185	19.63%	24.42%
35.975	89.703	1622	3905	1350	1970	58.46%	140.75%
36.029	89.699	1835	2000	1920	1720	8.25%	8.99%
36.089	89.668	1350	1580	985	1825	14.56%	17.04%
36.575	89.546	1860	2360	1480	1120	21.19%	26.88%
36.53	89.46	1401	1760	1270	1245	20.40%	25.62%
36.57	89.24	1052	1250	1185	1585	15.84%	18.82%
36.723	89.149	1420	3030	1880	890	53.14%	113.38%
						28.33%	48.55%

Ohio River

	Island Location					
Name	Lat (N)	Long (W)	RM	LB (m)	RB (m)	D from LB
Lock & Dam No.			939			
Owens I.	37.077	88.581	932	259	934	31%
Cuba Towhead	37.067	88.571	932	134	268	40%
Tennessee River			932			
Towhead I.	37.113	88.43	923	228	1030	24%
Cumberland I.	37.136	88.418	921	368	816	37%
Stewart Isl. Towhead	37.2	88.437	916	161	843	18%
Stewart I.	37.223	88.463	914	510	316	55%
Smithland L&D			911			
Rondeau I.	37.389	88.465	901	286	610	39%
Hurricane I.	37.446	88.271	886	553	532	50%
Cave In Rock I.	37.462	88.146	880	102	545	31%
Sturgeon I.	37.539	88.088	870	957	155	80%
	37.658	88.155	860	384	538	43%
	37.724	88.074	854	462	530	47%
Little Wabash I.	37.785	87.999	846	133	245	43%
Uniontown L&D			846			
Towhead I.	37.839	87.904	837	257	621	31%
Slim I.	37.876	87.931	833	376	500	47%
Slim Isl. Towhead	37.888	87.934	833	92	540	20%
Mt. Vernon Towhead	37.916	87.874	828	479	388	54%
Diamond I.	37.883	87.752	816	415	273	53%
Deadmans I.	37.822	87.655	808	495	376	55%
Henderson I.	37.82	87.631	806	257	517	39%
	37.926	87.625	797	673	243	70%
Newburgh L&D			776			
	37.926	87.367	776	521	424	55%
	37.917	87.35	775	566	378	59%
French Isl. No. 2	37.857	87.242	767	736	144	73%
French Isl. No. 1	37.848	87.233	767	455	165	64%
Little French I.	37.841	87.223	766	300	336	47%
Cannelton L&D			721			
McAlpine L&D			606			
Sixmile I.	38.31	85.666	597	566	87	78%
Twelvemile I.	38.374	85.632	593	454	366	54%
Markland L&D			531			
Capt Anth Meldehl L&D			436			
Manchester Isl. No. 2	38.688	83.584	396	420	191	63%
Manchester Isl. No. 1	38.686	83.575	396	293	238	54%
Brush Creek I.	38.671	83.459	388	184	382	36%
Greenup L&D			341			
Gallipolis L&D			281			
Racine L&D			238			

Buffington I.	38.992	81.771	217	388	73	67%
Mustapha I.	39.21	81.728	197	283	191	57%
Newberry I.	39.221	81.694	195	146	387	29%
Neal I.	39.308	81.559	182	149	354	38%
Eureka I.	39.374	81.292	160	255	228	52%
Broadback I.	39.383	81.272	159	338	179	60%
Willow Island L&D			152			
Grape I.	39.431	81.181	152	187	226	47%
Lock & Dam No. 16			147			
Wells I.	39.551	81.019	139	119	384	32%
Hannibal L&D			126			
Fish Creek I.	39.817	80.818	113	157	331	38%
Pike Island L&D			84			
Babbs I.	40.626	80.555	42	284	117	66%
Phillis I.	40.622	80.445	35	112	335	31%
Montgomery L&D			32			
Dashields Dam			13			
	count =	42				47.8%

						Actual Geometry			
Lat (N)	Lon (W)	L (m)	W (m)	x	R_A	A(km^2)	x/L act.	A=x*LW	theta
37.077	88.581	2232.7	612.8	641	3.6	0.79	71.29%	0.58	10.90
37.067	88.571	732	268	292	2.7	0.12	60.11%	0.59	16.94
37.113	88.43	1093	295.1	376	3.7	0.23	65.60%	0.72	11.63
37.136	88.418	2933	533	448	5.5	1.15	84.73%	0.74	6.12
37.2	88.437	368	51	87.3	7.2	0.01	76.28%	0.66	5.19
37.223	88.463	2519.7	1025.8	933	2.5	1.64	62.97%	0.63	17.91
37.389	88.465	2989.7	550.7	918	5.4	0.99	69.29%	0.60	7.57
37.446	88.271	6276	1042	1733	6.0	4.14	72.39%	0.63	6.54
37.462	88.146	1860.8	499.4	856	3.7	0.63	54.00%	0.68	13.96
37.539	88.088	1341	231	821	5.8	0.20	38.78%	0.66	12.52
37.658	88.155	908.8	262.6	308	3.5	0.15	66.11%	0.63	12.33
37.724	88.074	617	94	307	6.6	0.04	50.24%	0.68	8.62
37.785	87.999	1156.9	369.8	397	3.1	0.28	65.68%	0.65	13.68
37.839	87.904	656.7	83.8	246	7.8	0.04	62.54%	0.70	5.83
37.876	87.931	3990	1038	1690	3.8	2.24	57.64%	0.54	12.72
37.888	87.934	1006	127	262	7.9	0.09	73.96%	0.69	4.88
37.916	87.874	1542.9	213.4	532	7.2	0.22	65.52%	0.66	6.03
37.883	87.752	4820	1854	1930	2.6	5.95	59.96%	0.67	17.78
37.822	87.655	1802.7	322	767	5.6	0.42	57.45%	0.73	8.84
37.82	87.631	2267	448	703	5.1	0.71	68.99%	0.70	8.15
37.926	87.625	824	148	374	5.6	0.08	54.61%	0.64	9.34
37.926	87.367	237	45.5	95.2	5.2	0.01	59.83%	0.72	9.11
37.917	87.35	1312	110	166	11.9	0.12	87.35%	0.84	2.75
37.857	87.242	3910	418	2078	9.4	1.07	46.85%	0.65	6.51
37.848	87.233	2796	422	1501	6.6	0.82	46.32%	0.70	9.25

37.841	87.223	639	79	412	8.1	0.05	35.52%	0.91	9.87
38.31	85.666	1803	210	1329	8.6	0.30	26.29%	0.78	12.49
38.374	85.632	1971	349	667	5.6	0.50	66.16%	0.73	7.62
38.688	83.584	1646	305	561	5.4	0.40	65.92%	0.79	8.00
38.686	83.575	579	171	188	3.4	0.07	67.53%	0.76	12.33
38.671	83.459	439	130	132	3.4	0.04	69.93%	0.65	11.95
38.992	81.771	1698	474	706	3.6	0.58	58.42%	0.72	13.44
39.21	81.728	823	155	175	5.3	0.09	78.74%	0.69	6.82
39.221	81.694	131	33.6	54.8	3.9	0.00	58.17%	0.59	12.43
39.308	81.559	1936	335	698	5.8	0.47	63.95%	0.73	7.71
39.374	81.292	866	107	259	8.1	0.07	70.09%	0.75	5.04
39.383	81.272	917	257	215	3.6	0.16	76.55%	0.66	10.37
39.431	81.181	846	259	286	3.3	0.14	66.19%	0.65	13.02
39.551	81.019	1045	234	450	4.5	0.18	56.94%	0.74	11.12
39.817	80.818	987	252	332	3.9	0.18	66.36%	0.74	10.89
40.626	80.555	1221	133	547	9.2	0.12	55.20%	0.76	5.63
40.622	80.445	761	153	339	5.0	0.07	55.45%	0.64	10.27
			Average		5.44		62.3%	0.69	9.86
			Std Dev		2.14		12.12%	0.07	3.58

Lemniscate Geometry

Lat (N)	Lon (W)	L/W	k	theta	x/L	shape
37.077	88.581	4.43	4.95	9.92	0.64	lemniscate
37.067	88.571	3.28	3.64	13.44	0.64	lenticular
37.113	88.43	3.64	4.06	12.08	0.64	lemniscate
37.136	88.418	5.23	5.85	8.40	0.65	elliptical
37.2	88.437	7.72	8.65	5.69	0.65	lenticular
37.223	88.463	2.74	3.04	16.07	0.63	lemniscate
37.389	88.465	6.35	7.11	6.92	0.65	lenticular
37.446	88.271	6.67	7.47	6.59	0.65	lenticular
37.462	88.146	3.86	4.30	11.40	0.64	lenticular
37.539	88.088	6.21	6.95	7.08	0.65	lenticular
37.658	88.155	3.89	4.34	11.30	0.64	lenticular
37.724	88.074	6.76	7.57	6.50	0.65	lenticular
37.785	87.999	3.40	3.78	12.95	0.64	irregular
37.839	87.904	7.89	8.84	5.57	0.65	lenticular
37.876	87.931	4.99	5.58	8.81	0.65	semicircle
37.888	87.934	8.07	9.04	5.45	0.65	elliptical
37.916	87.874	7.65	8.57	5.74	0.65	lenticular
37.883	87.752	2.77	3.07	15.93	0.63	lenticular
37.822	87.655	5.40	6.04	8.14	0.65	lenticular
37.82	87.631	5.09	5.69	8.65	0.65	lenticular
37.926	87.625	6.13	6.86	7.17	0.65	elliptical
37.926	87.367	5.06	5.66	8.69	0.65	elliptical
37.917	87.35	9.95	11.15	4.42	0.65	elliptical
37.857	87.242	10.03	11.24	4.38	0.65	lenticular

37.848	87.233	6.66	7.45	6.60	0.65	lenticular
37.841	87.223	6.26	7.00	7.03	0.65	elliptical
38.31	85.666	7.68	8.60	5.73	0.65	elliptical
38.374	85.632	5.42	6.06	8.12	0.65	elliptical
38.688	83.584	4.79	5.35	9.18	0.65	elliptical
38.686	83.575	3.16	3.52	13.92	0.64	elliptical
38.671	83.459	3.64	4.06	12.08	0.64	lemniscate
38.992	81.771	3.53	3.93	12.48	0.64	lemniscate
39.21	81.728	5.42	6.06	8.12	0.65	lemniscate
39.221	81.694	4.64	5.18	9.48	0.65	lenticular
39.308	81.559	5.54	6.20	7.93	0.65	elliptical
39.374	81.292	7.59	8.50	5.79	0.65	lenticular
39.383	81.272	3.79	4.23	11.60	0.64	lemniscate
39.431	81.181	3.57	3.97	12.35	0.64	lemniscate
39.551	81.019	4.26	4.75	10.33	0.64	elliptical
39.817	80.818	3.72	4.14	11.84	0.64	lemniscate
40.626	80.555	8.50	9.53	5.17	0.65	elliptical
40.622	80.445	5.47	6.11	8.04	0.65	semicircle
		5.50	6.15	8.98	0.65	
		1.89	2.13	3.09	0.00	

River Dimensions

Lat (N)	Lon (W)	ACW	width	d/s width	u/s width	IW/TW	IW/ACW
37.077	88.581	1222.2	1835	1180	1480	33.40%	50.14%
37.067	88.571	1457	1725	1425	1540	15.54%	18.39%
37.113	88.43	1274.9	1570	1315	1655	18.80%	23.15%
37.136	88.418	1157	1690	1190	1160	31.54%	46.07%
37.2	88.437	1019	1070	1115	965	4.77%	5.00%
37.223	88.463	824.2	1850	1075	620	55.45%	124.46%
37.389	88.465	834.3	1385	905	775	39.76%	66.01%
37.446	88.271	1118	2160	610	655	48.24%	93.20%
37.462	88.146	705.6	1205	745	735	41.44%	70.78%
37.539	88.088	1104	1335	670	1090	17.30%	20.92%
37.658	88.155	947.4	1210	660	975	21.70%	27.72%
37.724	88.074	991	1085	880	950	8.66%	9.49%
37.785	87.999	410.2	780	370	720	47.41%	90.15%
37.839	87.904	891.2	975	970	970	8.59%	9.40%
37.876	87.931	887	1925	975	475	53.92%	117.02%
37.888	87.934	1458	1585	1715	535	8.01%	8.71%
37.916	87.874	856.6	1070	605	950	19.94%	24.91%
37.883	87.752	816	2670	755	540	69.44%	227.21%
37.822	87.655	933	1255	765	1240	25.66%	34.51%
37.82	87.631	782	1230	1255	850	36.42%	57.29%
37.926	87.625	927	1075	765	610	13.77%	15.97%
37.926	87.367	894.5	940	785	1060	4.84%	5.09%
37.917	87.35	990	1100	820	970	10.00%	11.11%

37.857	87.242	942	1360	925	1015	30.74%	44.37%
37.848	87.233	1028	1450	1065	845	29.10%	41.05%
37.841	87.223	1241	1320	1480	845	5.98%	6.37%
38.31	85.666	850	1060	560	795	19.81%	24.71%
38.374	85.632	876	1225	755	870	28.49%	39.84%
38.688	83.584	615	920	530	700	33.15%	49.59%
38.686	83.575	899	1070	785	625	15.98%	19.02%
38.671	83.459	595	725	500	635	17.93%	21.85%
38.992	81.771	476	950	320	360	49.89%	99.58%
39.21	81.728	470	625	445	475	24.80%	32.98%
39.221	81.694	526.4	560	400	485	6.00%	6.38%
39.308	81.559	505	840	440	390	39.88%	66.34%
39.374	81.292	498	605	425	485	17.69%	21.49%
39.383	81.272	528	785	485	365	32.74%	48.67%
39.431	81.181	411	670	330	420	38.66%	63.02%
39.551	81.019	506	740	330	390	31.62%	46.25%
39.817	80.818	533	785	400	350	32.10%	47.28%
40.626	80.555	402	535	365	375	24.86%	33.08%
40.622	80.445	467	620	375	405	24.68%	32.76%
						27.11%	45.27%

Platte River

Island Location

Name	Lat (N)	Long (W)	RM	LB (m)	RB (m)	D fro LB
	41.061	-96.064		83	352	31%
	41.05	-96.101		335	133	67%
	41.021	-96.272		54	288	27%
	41.041	-96.309		139	78	59%
	41.316	-96.406		230	122	60%
	41.317	-96.403		71	116	41%
	41.354	-96.418		332	108	69%
	41.362	-96.431		81	118	44%
	41.387	-96.469		328	144	60%
	41.393	-96.476		205	270	45%
	41.437	-96.573		134	329	32%
	41.437	-96.576		85	366	22%
	41.442	-96.64		74	56	55%
	41.444	-96.957		196	135	57%
	41.399	-97.313		117	168	45%
	count =	15				47.58%

Actual Geometry

Lat (N)	Lon (W)	L (m)	W (m)	x	R_A	A(km^2)	x/L act.	A=x*LW	theta
41.061	-96.064	1155	269	370	4.29	0.1968	67.97%	0.63	9.72
41.05	-96.101	361	113	83.4	3.19	0.0281	76.90%	0.69	11.50
41.021	-96.272	766	157	217	4.88	0.0747	71.67%	0.62	8.14
41.041	-96.309	444	113	221	3.93	0.0353	50.23%	0.70	14.22
41.316	-96.406	928	194	492	4.78	0.1262	46.98%	0.70	12.54
41.317	-96.403	157.5	52.3	52.4	3.01	0.005	66.73%	0.61	13.97
41.354	-96.418	451	155	143	2.91	0.0473	68.29%	0.68	14.12
41.362	-96.431	419	120	140	3.49	0.0314	66.59%	0.62	12.14
41.387	-96.469	1656	455	618	3.64	0.5314	62.68%	0.71	12.36
41.393	-96.476	1006	198	493	5.08	0.1329	50.99%	0.67	10.92
41.437	-96.573	405	71.4	87.8	5.67	0.0225	78.32%	0.78	6.42
41.437	-96.576	188	43.9	40.8	4.28	0.0058	78.30%	0.70	8.48
41.442	-96.64	132	33.9	29	3.89	0.0026	78.03%	0.58	9.35
41.444	-96.957	447	96	289	4.66	0.0306	35.35%	0.71	16.90
41.399	-97.313	846	232	381	3.65	0.1138	54.96%	0.58	14.01
				Average	4.09		63.60%	0.67	11.65
				Std Dev	0.81		13.18%	0.06	2.83

Lemniscate Geometry

Lat (N)	Lon (W)	L/W	k	theta	x/L
41.061	-96.064	4.76	5.32	9.23	0.65
41.05	-96.101	3.28	3.64	13.44	0.64
41.021	-96.272	5.52	6.17	7.97	0.65
41.041	-96.309	3.93	4.39	11.19	0.64
41.316	-96.406	4.80	5.36	9.17	0.65
41.317	-96.403	3.50	3.90	12.58	0.64
41.354	-96.418	3.04	3.38	14.48	0.64
41.362	-96.431	3.94	4.39	11.17	0.64
41.387	-96.469	3.64	4.05	12.10	0.64
41.393	-96.476	5.35	5.98	8.22	0.65
41.437	-96.573	5.12	5.73	8.59	0.65
41.437	-96.576	4.29	4.79	10.26	0.64
41.442	-96.64	4.71	5.26	9.33	0.65
41.444	-96.957	4.59	5.13	9.58	0.65
41.399	-97.313	4.42	4.94	9.94	0.64
		4.33	4.83	10.48	0.64
		0.75	0.85	1.95	0.00

River Dimensions

Lat (N)	Lon (W)	ACW	width	d/s width	u/s width	IW/TW	IW/ACW
41.061	-96.064	401	670	525	345	40.15%	67.08%
41.05	-96.101	467	580	410	500	19.48%	24.20%
41.021	-96.272	343	500	525	430	31.40%	45.77%
41.041	-96.309	757	870	625	715	12.99%	14.93%

41.316	-96.406	361	555	600	455	34.95%	53.74%
41.317	-96.403	502.7	555	600	455	9.42%	10.40%
41.354	-96.418	445	600	535	830	25.83%	34.83%
41.362	-96.431	900	1020	600	475	11.76%	13.33%
41.387	-96.469	610	1065	495	500	42.72%	74.59%
41.393	-96.476	452	650	905	435	30.46%	43.81%
41.437	-96.573	468.6	540	530	430	13.22%	15.24%
41.437	-96.576	436.1	480	500	450	9.15%	10.07%
41.442	-96.64	866.1	900	1200	455	3.77%	3.91%
41.444	-96.957	329	425	410	475	22.59%	29.18%
41.399	-97.313	293	525	340	760	44.19%	79.18%
						23.47%	34.68%

Red River

Island Location

Name	RM	Lat	Lon	LB (m)	RB (m)	D from LB
Hollingsworth Cutoff I.		31.991	-93.354	193	237	46%
Homan Ditch Bar		33.551	-93.95	43.2	87.9	41%
		33.556	-94.026	166	121	57%
		33.587	-94.18	132	172	44%
		33.558	-94.249	326	226	59%
		33.547	-94.371	341	84	77%
		33.621	-94.564	150	95	60%
		33.621	-94.564	41.5	207	24%
		33.66	-94.577	72	92	45%
		33.66	-94.577	64	92	44%
		33.676	-94.623	72	82	47%
		33.742	-94.832	92	155	40%
		33.742	-94.832	101	77	54%
		33.771	-94.9	95	94	50%
Mud Lake Bar		33.916	-95.249	68	73	49%
		33.851	-95.759	57	136	37%
Indian Treaty Bayou Bar		33.848	-96.095	88	65	57%
Choctaw Slough I.		33.698	-96.359	205	117	60%
		33.781	-96.467	63	120	40%
	count = 19					48.98%

Actual Geometry

Lat (N)	Lon (W)	L (m)	W (m)	x	R_A	A(km^2)	x/L act.	A=x*LW	theta
31.991	-93.354	550.9	134.7	160	4.1	0.0463	70.96%	0.62	9.78
33.551	-93.95	492.8	109.75	170	4.5	0.0332	65.50%	0.61	9.65
33.556	-94.026	210.7	35	41.7	6.0	0.0044	80.21%	0.60	5.91
33.587	-94.18	155.3	53.25	44.8	2.9	0.0047	71.15%	0.57	13.55

33.558	-94.249	84.14	26.4	20.7	3.2	0.0013	75.40%	0.56	11.75
33.547	-94.371	275.8	47.54	57.9	5.8	0.0085	79.01%	0.65	6.23
33.621	-94.564	115.75	29.7	33.8	3.9	0.0022	70.80%	0.64	10.27
33.621	-94.564	247.1	72	134	3.4	0.0121	45.77%	0.68	17.66
33.66	-94.577	134.3	40.3	44	3.3	0.0032	67.24%	0.58	12.58
33.66	-94.577	206.5	64.5	98.4	3.2	0.0079	52.35%	0.59	16.61
33.676	-94.623	123.4	31.3	26.3	3.9	0.0024	78.69%	0.62	9.16
33.742	-94.832	162.5	53.2	57.3	3.1	0.0056	64.74%	0.65	14.19
33.742	-94.832	450.75	123.2	157	3.7	0.0308	65.17%	0.55	11.84
33.771	-94.9	198.25	37	43	5.4	0.0044	78.31%	0.60	6.80
33.916	-95.249	453.5	87.75	132	5.2	0.0232	70.89%	0.58	7.77
33.851	-95.759	528.7	109.3	181	4.8	0.0400	65.77%	0.69	8.93
33.848	-96.095	95.6	17	22.7	5.6	0.0012	76.26%	0.74	6.65
33.698	-96.359	388.3	102.5	134	3.8	0.0259	65.49%	0.65	11.39
33.781	-96.467	391.2	90	231	4.3	0.0241	40.95%	0.68	15.69
				Average	4.22		67.61%	0.63	10.86
				St Dev	0.99		10.94%	0.05	3.54

Lemniscate Geometry

Lat (N)	Lon (W)	L/W	k	theta	x/L
31.991	-93.354	4.60	5.14	9.55	0.65
33.551	-93.95	5.14	5.75	8.56	0.65
33.556	-94.026	7.06	7.90	6.23	0.65
33.587	-94.18	3.59	4.00	12.26	0.64
33.558	-94.249	3.97	4.43	11.07	0.64
33.547	-94.371	6.28	7.03	7.00	0.65
33.621	-94.564	4.31	4.81	10.20	0.64
33.621	-94.564	3.56	3.96	12.37	0.64
33.66	-94.577	4.02	4.49	10.94	0.64
33.66	-94.577	3.81	4.24	11.56	0.64
33.676	-94.623	4.46	4.98	9.86	0.64
33.742	-94.832	3.33	3.70	13.22	0.64
33.742	-94.832	4.64	5.18	9.48	0.65
33.771	-94.9	6.27	7.02	7.01	0.65
33.916	-95.249	6.22	6.96	7.07	0.65
33.851	-95.759	4.91	5.49	8.95	0.65
33.848	-96.095	5.35	5.98	8.22	0.65
33.698	-96.359	4.10	4.57	10.73	0.64
33.781	-96.467	4.47	4.99	9.85	0.64
		4.74	5.30	9.69	0.64
		1.06	1.20	2.00	0.00

River Dimensions

Lat (N)	Lon (W)	ACW	width	d/s width	u/s width	IW/TW	IW/ACW
31.991	-93.354	430.3	565	400	380	23.84%	31.30%

33.551	-93.95	140.25	250	100	120	43.90%	78.25%
33.556	-94.026	275	310	270	300	11.29%	12.73%
33.587	-94.18	301.75	355	285	650	15.00%	17.65%
33.558	-94.249	563.6	590	355	760	4.47%	4.68%
33.547	-94.371	437.46	485	350	325	9.80%	10.87%
33.621	-94.564	240.3	270	330	225	11.00%	12.36%
33.621	-94.564	258	330	380	230	21.82%	27.91%
33.66	-94.577	169.7	210	190	245	19.19%	23.75%
33.66	-94.577	165.5	230	190	265	28.04%	38.97%
33.676	-94.623	168.7	200	245	200	15.65%	18.55%
33.742	-94.832	251.8	305	310	260	17.44%	21.13%
33.742	-94.832	181.8	305	300	275	40.39%	67.77%
33.771	-94.9	193	230	250	230	16.09%	19.17%
33.916	-95.249	152.25	240	280	155	36.56%	57.64%
33.851	-95.759	190.7	300	260	180	36.43%	57.32%
33.848	-96.095	158	175	200	130	9.71%	10.76%
33.698	-96.359	317.5	420	315	215	24.40%	32.28%
33.781	-96.467	200	290	135	215	31.03%	45.00%
						21.90%	30.95%

Sacramento River

Island Location

Name	Lat (N)	Long (W)	RM	LB (m)	RB (m)	D from LB
	39.335	-122.03		192	59	72%
	39.562	-121.99		100	98	50%
	39.663	-121.978		57	143	37%
	39.671	-121.994		180	81	63%
	39.675	-121.961		119	98	54%
	39.676	-121.961		141	113	55%
	39.688	-121.954		123	51	63%
	39.735	-121.964		32	118	28%
	39.747	-121.991		181	64	69%
	39.876	-122.053		161	47	73%
	39.914	-122.092		118	41	63%
	39.997	-122.11		86	53	58%
	count =	12				57.07%

Actual Geometry

Lat (N)	Lon (W)	L (m)	W (m)	x	R_A	A(km^2)	x/L act.	A=x*LW	theta
39.335	-122.03	238	48.3	22.8	4.93	0.0086	90.42%	0.75	6.40
39.562	-121.99	361	98.1	118	3.68	0.026	67.31%	0.73	11.41
39.663	-121.978	446	122	237	3.66	0.0388	46.86%	0.71	16.27
39.671	-121.994	313	113	132	2.77	0.0238	57.83%	0.67	17.34

39.675	-121.961	132	29.3	23.1	4.51	0.0026	82.50%	0.67	7.66
39.676	-121.961	156	45.1	81	3.46	0.0045	48.08%	0.64	16.73
39.688	-121.954	336	110	166	3.05	0.0226	50.60%	0.61	17.93
39.735	-121.964	242	46.1	97.8	5.25	0.0088	59.59%	0.79	9.08
39.747	-121.991	188	61.3	56.8	3.07	0.008	69.79%	0.69	13.15
39.876	-122.053	253	41.9	108	6.04	0.0073	57.31%	0.69	8.22
39.914	-122.092	615	145	228	4.24	0.0664	62.93%	0.74	10.61
39.997	-122.11	269	64.9	120	4.14	0.0136	55.39%	0.78	12.29
				Average	4.07		62.38%	0.71	12.26
				Std Dev	0.98		13.34%	0.05	4.05

Lemniscate Geometry

Lat (N)	Lon (W)	L/W	k	theta	x/L
39.335	-122.03	4.63	5.17	9.50	0.65
39.562	-121.99	3.54	3.94	12.45	0.64
39.663	-121.978	3.62	4.03	12.17	0.64
39.671	-121.994	2.91	3.23	15.12	0.64
39.675	-121.961	4.71	5.26	9.33	0.65
39.676	-121.961	3.81	4.25	11.55	0.64
39.688	-121.954	3.52	3.92	12.49	0.64
39.735	-121.964	4.68	5.23	9.40	0.65
39.747	-121.991	3.12	3.47	14.10	0.64
39.876	-122.053	6.15	6.89	7.14	0.65
39.914	-122.092	4.01	4.47	10.97	0.64
39.997	-122.11	3.75	4.18	11.74	0.64
		4.04	4.50	11.33	0.64
		0.88	1.00	2.22	0.00

River Dimensions

Lat (N)	Lon (W)	ACW	width	d/s width	u/s width	IW/TW	IW/ACW
39.335	-122.03	256.7	305	340	320	15.84%	18.82%
39.562	-121.99	196.9	295	100	140	33.25%	49.82%
39.663	-121.978	198	320	145	230	38.13%	61.62%
39.671	-121.994	257	370	95	90	30.54%	43.97%
39.675	-121.961	225.7	255	75	100	11.49%	12.98%
39.676	-121.961	209.9	255	75	100	17.69%	21.49%
39.688	-121.954	195	305	120	160	36.07%	56.41%
39.735	-121.964	148.9	195	150	140	23.64%	30.96%
39.747	-121.991	243.7	305	185	195	20.10%	25.15%
39.876	-122.053	208.1	250	120	170	16.76%	20.13%
39.914	-122.092	155	300	110	155	48.33%	93.55%
39.997	-122.11	140.1	205	235	200	31.66%	46.32%
						26.96%	40.10%

Snake River

		Island Location				
Name	Lat (N)	Long (W)	RM	LB (m)	RB (m)	D from LB
Ice Harbor Dam			9.7			
Lower Monumental Dam			41.6			
Little Goose Dam			70.3			
New York I.	46.606	-117.874	79	673	459	58%
Lower Granite Dam			107.5			
Tenmile Rapids I.	46.305	-117.005	149	104	118	48%
Steamboat I.	46.183	-116.94	159.5	40.6	101	39%
Zigzag Rapids I.	45.826	-116.724	194	44.9	29.4	58%
Dry Creek I.	45.783	-116.627	200.5	29.8	44.8	45%
Pleasant Valley I.	45.641	-116.483	214	50.7	61	47%
Hells Canyon Dam			247			
Big Bar	45.134	-116.74	256	221	183	53%
Oxbow Dam			273			
Brownlee Dam			285			
Farewell Bend I.	44.304	-117.218	333.5	136	192	45%
Darrows I.	44.257	-117.149	339	134	195	43%
	44.269	-117.13	340	256	111	64%
	44.265	-117.13	340	241	211	53%
Porters I.	44.277	-117.106	342	111	197	44%
	44.242	-117.043	348	64	72	48%
	44.242	-117.04	348	104	39	67%
	44.242	-117.042	348	133	82	59%
McRae I.	44.247	-117.017	349	143	44	60%
Smith I.	44.196	-116.968	355	174	101	58%
	44.193	-116.941	356	80	111	44%
	44.176	-116.901	358.5	50	179	30%
	44.179	-116.905	358.5	77	113	44%
	44.15	-116.899	360.5	78	98	47%
	44.113	-116.928	363.5	75	82	48%
Ontario I.	44.045	-116.963	370	76	88	49%
	44.005	-116.945	374	87	105	46%
Crow I.	43.935	-116.965	381	120	75	57%
	43.89	-116.977	384	134	72	57%
	43.864	-116.998	390	58	41	55%
Prati I.	43.866	-117.003	390	90	117	47%
Boise River			395.5			
Goose Egg I.	43.764	-117.026	399	110	171	43%
	River miles offset by three miles here -- RM 397 = RM 400 (no correction)					
	43.737	-117.066	398.5	47	176	30%
	43.746	-117.045	397	141	141	50%
	43.741	-117.057	398	152	59	65%
	43.742	-117.05	397.5	253	65	76%
Suzy I.	43.724	-117.078	400	105	73	55%

	43.713	-117.086	401	59	168	37%
	43.679	-117.062	405	139	200	42%
	43.682	-117.059	405	115	88	54%
	43.684	-117.054	405	117	77	57%
	43.686	-117.05	405.5	133	39.5	72%
	43.674	-117.004	408	130	101	56%
	43.671	-116.983	409	58	146	32%
Goat I.	43.649	-116.962	411	127	72	58%
	43.641	-116.959	411.5	137	41	71%
Heltons I.	43.625	-116.935	415	76	169	39%
	43.61	-116.914	416.5	67	33	57%
	43.609	-116.915	417	84	33	64%
Rabbit I.	43.604	-116.909	417	119	154	46%
	43.595	-116.884	419	76	142	39%
Clarks I.	43.596	-116.873	419	191	95	59%
	43.593	-116.872	419.5	48.8	19	62%
Smiths I.	43.593	-116.869	419.5	67	312	27%
	43.593	-116.845	420.5	94	154	43%
	43.575	-116.815	422	220	138	60%
	43.54	-116.795	424.5	43	127	37%
	43.503	-116.785	427.5	83	76	51%
Dredge I.	43.438	-116.727	432.5	78	46	55%
Raccoon I.	43.411	-116.693	435	81.5	43	59%
Hermit I.	43.401	-116.78	436	104	66	58%
Rippee I.	43.394	-116.675	436	82	159	42%
	43.4	-116.679	436	46	56	47%
	43.394	-116.672	436	67	57	53%
Current I.	43.384	-116.658	437.5	131	54	64%
Ware I.	43.379	-116.646	438	63	104	46%
Papike I.	43.363	-116.619	440	64	165	36%
Becky/Argy I.	43.368	-116.623	440	78	142	41%
Bayha I.	43.37	-116.626	440	76	169	38%
Brooks I.	43.355	-116.61	441	144	53.5	65%
Blind I.	43.349	-116.604	441.5	152	46	65%
Big Rocky I.	43.331	-116.547	443	94	89	51%
	43.302	-116.56	445.5	99	66	57%
Guffey I.	43.3	-116.536	447	125	46	61%
Rail I.	43.297	-116.518	448	71	58	53%
	43.267	-16.403	456	81	73	52%
	43.206	-116.384	460.5	96	241	33%
	43.12	-116.303	468.5	54	116	35%
	43.119	-116.3	468.5	58	124	36%
	43.097	-116.244	472	47	103	38%
	43.046	-116.191	478.5	107	66	60%
	42.962	-116.03	491	122	78	59%
	42.95	-116	493	121	46	63%

CJ Strike Dam 494

50.7%

count = 80

Lat (N)	Lon (W)	L (m)	W (m)	x	R_A	A(km^2)	x/L act.	A=x*LW	theta
					Actual Geometry				
46.606	-117.874	1124.6	284.3	255	3.96	0.2205	77.33%	0.69	9.28
46.305	-117.005	366.6	117.5	158	3.12	0.0278	56.90%	0.65	15.73
46.183	-116.94	389.7	137.7	79.7	2.83	0.0405	79.55%	0.75	12.52
45.826	-116.724	60.2	25.5	19.2	2.36	0.0009	68.11%	0.59	17.27
45.783	-116.627	240.3	91.7	84.4	2.62	0.0157	64.88%	0.71	16.39
45.641	-116.483	211.6	84.8	76.4	2.50	0.0132	63.89%	0.74	17.41
45.134	-116.74	684.6	197	223	3.48	0.096	67.43%	0.71	12.05
44.304	-117.218	664.2	210	383	3.16	0.0887	42.34%	0.64	20.48
44.257	-117.149	540	134	233	4.03	0.0481	56.85%	0.66	12.31
44.269	-117.13	634	148	250	4.28	0.0604	60.57%	0.64	10.91
44.265	-117.13	685	133	349	5.15	0.0621	49.05%	0.68	11.20
44.277	-117.106	1400	395	652	3.54	0.3717	53.43%	0.67	14.79
44.242	-117.043	132	45.2	73	2.92	0.0048	44.70%	0.80	20.96
44.242	-117.04	148	45.6	33.5	3.25	0.0045	77.36%	0.67	11.26
44.242	-117.042	262	83.5	88.1	3.14	0.0175	66.37%	0.80	13.50
44.247	-117.017	876	312	477	2.81	0.1861	45.55%	0.68	21.35
44.196	-116.968	725	191	259	3.80	0.1086	64.28%	0.78	11.58
44.193	-116.941	212	72.5	130	2.92	0.01	38.68%	0.65	23.85
44.176	-116.901	425	91.5	142.5	4.64	0.0292	66.47%	0.75	9.20
44.179	-116.905	374	95.4	152	3.92	0.0259	59.36%	0.73	12.13
44.15	-116.899	909	197	200	4.61	0.1117	78.00%	0.62	7.91
44.113	-116.928	390	67.1	190	5.81	0.0185	51.28%	0.71	9.52
44.045	-116.963	1256	299	551	4.20	0.2107	56.13%	0.56	11.97
44.005	-116.945	57.4	23.7	25	2.42	0.0011	56.45%	0.81	20.09
43.935	-116.965	431	120	251	3.59	0.0346	41.76%	0.67	18.43
43.89	-116.977	860	229	431	3.76	0.1134	49.88%	0.58	14.94
43.864	-116.998	176	65	85.2	2.71	0.007	51.59%	0.61	19.69
43.866	-117.003	792	200	269	3.96	0.117	66.04%	0.74	10.82
43.764	-117.026	959	161	318	5.96	0.0836	66.84%	0.54	7.16
43.737	-117.066	685	101	281	6.78	0.048	58.98%	0.69	7.13
43.746	-117.045	661	87	187	7.60	0.0417	71.71%	0.73	5.24
43.741	-117.057	712	105	203	6.78	0.0455	71.49%	0.61	5.89
43.742	-117.05	125	41.4	31.7	3.02	0.0031	74.64%	0.60	12.51
43.724	-117.078	531	154	186	3.45	0.0555	64.97%	0.68	12.58
43.713	-117.086	542	190	192	2.85	0.0588	64.58%	0.57	15.19
43.679	-117.062	179	37.3	110	4.80	0.0046	38.55%	0.69	15.13
43.682	-117.059	657	143	271	4.59	0.0684	58.75%	0.73	10.49
43.684	-117.054	271	104	83.4	2.61	0.0236	69.23%	0.84	15.49
43.686	-117.05	145	36.5	53	3.97	0.0036	63.45%	0.68	11.22
43.674	-117.004	109	30.9	47.2	3.53	0.0023	56.70%	0.68	14.04

43.671	-116.983	219	40	98.8	5.48	0.0064	54.89%	0.73	9.45
43.649	-116.962	634	136	159	4.66	0.0467	74.92%	0.54	8.15
43.641	-116.959	224	50.6	90.6	4.43	0.0074	59.55%	0.65	10.74
43.625	-116.935	749	176	254	4.26	0.0957	66.09%	0.73	10.08
43.61	-116.914	440	147	109	2.99	0.0331	75.23%	0.51	12.52
43.609	-116.915	269	67.5	56.7	3.99	0.0115	78.92%	0.63	9.03
43.604	-116.909	947	191	221	4.96	0.1273	76.66%	0.70	7.49
43.595	-116.884	343	79.4	160	4.32	0.0205	53.35%	0.75	12.24
43.596	-116.873	650	223	288	2.91	0.0931	55.69%	0.64	17.12
43.593	-116.872	191	59.2	61.6	3.23	0.0078	67.75%	0.69	12.88
43.593	-116.869	559	163	260	3.43	0.0555	53.49%	0.61	15.25
43.593	-116.845	437	162	164	2.70	0.0419	62.47%	0.59	16.53
43.575	-116.815	420	69.1	125	6.08	0.0219	70.24%	0.75	6.68
43.54	-116.795	692	160	208	4.33	0.0614	69.94%	0.55	9.39
43.503	-116.785	730	195	171	3.74	0.0937	76.58%	0.66	9.89
43.438	-116.727	821	211	202	3.89	0.1112	75.40%	0.64	9.67
43.411	-116.693	587	96	350	6.11	0.0369	40.37%	0.65	11.45
43.401	-116.78	481	73.2	105	6.57	0.025	78.17%	0.71	5.56
43.394	-116.675	966	220	388	4.39	0.1349	59.83%	0.63	10.78
43.4	-116.679	226	94.8	64	2.38	0.0129	71.68%	0.60	16.31
43.394	-116.672	243	62.4	94.2	3.89	0.0117	61.23%	0.77	11.84
43.384	-116.658	407	95.1	85.2	4.28	0.0266	79.07%	0.69	8.41
43.379	-116.646	1158	349	298	3.32	0.2999	74.27%	0.74	11.47
43.363	-116.619	573	140	136	4.09	0.0613	76.27%	0.76	9.10
43.368	-116.623	473	152	264	3.11	0.0395	44.19%	0.55	19.98
43.37	-116.626	345	143	118	2.41	0.0338	65.80%	0.69	17.48
43.355	-116.61	340	97.4	116	3.49	0.0254	65.88%	0.77	12.27
43.349	-116.604	492	144	82.8	3.42	0.0441	83.17%	0.62	9.98
43.331	-116.547	994	308	382	3.23	0.1891	61.57%	0.62	14.12
43.302	-116.56	175	69	36.1	2.54	0.0068	79.37%	0.56	13.95
43.3	-116.536	761	177	307	4.30	0.1036	59.66%	0.77	11.03
43.297	-116.518	354	109	146	3.25	0.0285	58.76%	0.74	14.68
43.267	-16.403	144	44	70.6	3.27	0.0053	50.97%	0.84	16.68
43.206	-116.384	419	84	163	4.99	0.0244	61.10%	0.69	9.32
43.12	-116.303	158	40.8	30.8	3.87	0.0042	80.51%	0.65	9.11
43.119	-116.3	229	46	71.8	4.98	0.0065	68.65%	0.62	8.32
43.097	-116.244	225	75.3	52.4	2.99	0.0121	76.71%	0.71	12.31
43.046	-116.191	130	33.5	41.2	3.88	0.0026	68.31%	0.60	10.68
42.962	-116.03	254	57.6	80.2	4.41	0.0117	68.43%	0.80	9.41
42.95	-116	653	117	233	5.58	0.0509	64.32%	0.67	7.93
			Average		3.94		63.5%	0.68	12.49
			Std Dev		1.15		11.09%	0.07	4.03

Lemniscate Geometry

Lat (N)	Lon (W)	L/W	k	theta	x/L	shape
46.606	-117.874	4.04	4.50	10.89	0.64	lemniscate

46.305	-117.005	3.41	3.80	12.90	0.64	lemniscate
46.183	-116.94	2.66	2.95	16.56	0.63	lemniscate
45.826	-116.724	2.85	3.16	15.45	0.63	lemniscate
45.783	-116.627	2.61	2.89	16.88	0.63	elliptical
45.641	-116.483	2.42	2.66	18.27	0.63	rhombic
45.134	-116.74	3.45	3.83	12.78	0.64	lemniscate
44.304	-117.218	3.51	3.91	12.54	0.64	rhombic
44.257	-117.149	4.27	4.76	10.31	0.64	lenticular
44.269	-117.13	4.68	5.23	9.40	0.65	elliptical
44.265	-117.13	5.31	5.93	8.29	0.65	lenticular
44.277	-117.106	3.72	4.14	11.84	0.64	lenticular
44.242	-117.043	2.58	2.85	17.10	0.63	elliptical
44.242	-117.04	3.44	3.82	12.81	0.64	elliptical
44.242	-117.042	2.78	3.08	15.85	0.63	elliptical
44.247	-117.017	2.92	3.24	15.09	0.64	semicirc
44.196	-116.968	3.42	3.80	12.89	0.64	lenticular
44.193	-116.941	3.18	3.53	13.86	0.64	irregular
44.176	-116.901	4.35	4.86	10.11	0.64	elliptical
44.179	-116.905	3.81	4.24	11.56	0.64	lenticular
44.15	-116.899	5.20	5.81	8.46	0.65	lemniscate
44.113	-116.928	5.77	6.46	7.62	0.65	elliptical
44.045	-116.963	5.26	5.88	8.36	0.65	irregular
44.005	-116.945	2.14	2.35	20.61	0.62	rhombic
43.935	-116.965	3.78	4.22	11.63	0.64	lemniscate
43.89	-116.977	4.59	5.12	9.59	0.65	triangular
43.864	-116.998	3.13	3.48	14.08	0.64	lenticular
43.866	-117.003	3.78	4.21	11.65	0.64	semicirc
43.764	-117.026	7.71	8.64	5.70	0.65	lemniscate
43.737	-117.066	6.86	7.68	6.41	0.65	elliptical
43.746	-117.045	7.35	8.23	5.98	0.65	elliptical
43.741	-117.057	7.81	8.75	5.63	0.65	elliptical
43.742	-117.05	3.56	3.96	12.38	0.64	elliptical
43.724	-117.078	3.58	3.99	12.28	0.64	rhombic
43.713	-117.086	3.52	3.92	12.49	0.64	semicirc
43.679	-117.062	4.90	5.47	8.98	0.65	irregular
43.682	-117.059	4.44	4.96	9.91	0.64	irregular
43.684	-117.054	2.22	2.44	19.87	0.62	irregular
43.686	-117.05	4.11	4.59	10.70	0.64	elliptical
43.674	-117.004	3.64	4.06	12.08	0.64	elliptical
43.671	-116.983	5.26	5.89	8.35	0.65	lemniscate
43.649	-116.962	6.04	6.76	7.28	0.65	semicirc
43.641	-116.959	4.77	5.33	9.23	0.65	irregular
43.625	-116.935	4.13	4.60	10.66	0.64	elliptical
43.61	-116.914	4.12	4.59	10.68	0.64	lemniscate
43.609	-116.915	4.43	4.94	9.94	0.64	elliptical
43.604	-116.909	4.95	5.53	8.88	0.65	elliptical

43.595	-116.884	4.04	4.51	10.89	0.64	rhombic
43.596	-116.873	3.21	3.56	13.73	0.64	semicirc
43.593	-116.872	3.30	3.67	13.33	0.64	elliptical
43.593	-116.869	3.97	4.42	11.10	0.64	triangular
43.593	-116.845	3.22	3.58	13.67	0.64	triangular
43.575	-116.815	5.65	6.33	7.77	0.65	elliptical
43.54	-116.795	5.48	6.13	8.03	0.65	rhombic
43.503	-116.785	4.01	4.47	10.99	0.64	elliptical
43.438	-116.727	4.27	4.76	10.31	0.64	lemniscate
43.411	-116.693	6.55	7.33	6.71	0.65	elliptical
43.401	-116.78	6.49	7.27	6.77	0.65	elliptical
43.394	-116.675	4.86	5.43	9.05	0.65	elliptical
43.4	-116.679	2.81	3.11	15.70	0.63	triangular
43.394	-116.672	3.56	3.96	12.36	0.64	elliptical
43.384	-116.658	4.38	4.89	10.04	0.64	lemniscate
43.379	-116.646	3.16	3.51	13.93	0.64	irregular
43.363	-116.619	3.77	4.21	11.66	0.64	elliptical
43.368	-116.623	3.99	4.45	11.03	0.64	irregular
43.37	-116.626	2.50	2.77	17.61	0.63	irregular
43.355	-116.61	3.22	3.57	13.69	0.64	elliptical
43.349	-116.604	3.87	4.31	11.38	0.64	lemniscate
43.331	-116.547	3.68	4.10	11.95	0.64	irregular
43.302	-116.56	3.18	3.54	13.84	0.64	elliptical
43.3	-116.536	3.94	4.39	11.18	0.64	lemniscate
43.297	-116.518	3.11	3.45	14.17	0.64	lenticular
43.267	-16.403	2.77	3.07	15.89	0.63	elliptical
43.206	-116.384	5.06	5.65	8.70	0.65	elliptical
43.12	-116.303	4.18	4.67	10.52	0.64	lemniscate
43.119	-116.3	5.66	6.34	7.76	0.65	lemniscate
43.097	-116.244	2.96	3.29	14.88	0.64	irregular
43.046	-116.191	4.57	5.11	9.62	0.65	lenticular
42.962	-116.03	3.88	4.33	11.33	0.64	elliptical
42.95	-116	5.88	6.58	7.48	0.65	lenticular
		4.15	4.62	11.52	0.64	
		1.25	1.41	3.25	0.01	

River Dimensions

Lat (N)	Lon (W)	ACW	width	d/s width	u/s width	IW/TW	IW/ACW
46.606	-117.874	1130.7	1415	810	1015	20.09%	25.14%
46.305	-117.005	212.5	330	215	260	35.61%	55.29%
46.183	-116.94	137.3	275	165	205	50.07%	100.29%
45.826	-116.724	94.5	120	110	90	21.25%	26.98%
45.783	-116.627	73.3	165	65	90	55.58%	125.10%
45.641	-116.483	120.2	205	50	70	41.37%	70.55%
45.134	-116.74	493	690	265	450	28.55%	39.96%
44.304	-117.218	355	565	430	210	37.17%	59.15%

44.257	-117.149	646	780	355	420	17.18%	20.74%
44.269	-117.13	387	535	390	330	27.66%	38.24%
44.265	-117.13	477	610	430	340	21.80%	27.88%
44.277	-117.106	335	730	290	265	54.11%	117.91%
44.242	-117.043	399.8	445	175	240	10.16%	11.31%
44.242	-117.04	399.4	445	175	240	10.25%	11.42%
44.242	-117.042	361.5	445	175	240	18.76%	23.10%
44.247	-117.017	238	550	260	240	56.73%	131.09%
44.196	-116.968	294	485	205	220	39.38%	64.97%
44.193	-116.941	212.5	285	230	410	25.44%	34.12%
44.176	-116.901	248.5	340	275	190	26.91%	36.82%
44.179	-116.905	199.6	295	205	340	32.34%	47.80%
44.15	-116.899	203	400	190	195	49.25%	97.04%
44.113	-116.928	162.9	230	160	205	29.17%	41.19%
44.045	-116.963	181	480	170	150	62.29%	165.19%
44.005	-116.945	216.3	240	235	195	9.88%	10.96%
43.935	-116.965	285	405	140	170	29.63%	42.11%
43.89	-116.977	236	465	165	180	49.25%	97.03%
43.864	-116.998	355	420	140	125	15.48%	18.31%
43.866	-117.003	220	420	140	125	47.62%	90.91%
43.764	-117.026	299	460	345	285	35.00%	53.85%
43.737	-117.066	189	290	295	215	34.83%	53.44%
43.746	-117.045	288	375	260	335	23.20%	30.21%
43.741	-117.057	220	325	340	320	32.31%	47.73%
43.742	-117.05	313.6	355	325	315	11.66%	13.20%
43.724	-117.078	216	370	200	205	41.62%	71.30%
43.713	-117.086	240	430	205	200	44.19%	79.17%
43.679	-117.062	347.7	385	350	200	9.69%	10.73%
43.682	-117.059	242	385	350	200	37.14%	59.09%
43.684	-117.054	281	385	350	200	27.01%	37.01%
43.686	-117.05	168.5	205	305	245	17.80%	21.66%
43.674	-117.004	254.1	285	195	240	10.84%	12.16%
43.671	-116.983	220	260	195	130	15.38%	18.18%
43.649	-116.962	209	345	195	185	39.42%	65.07%
43.641	-116.959	184.4	235	195	210	21.53%	27.44%
43.625	-116.935	269	445	95	150	39.55%	65.43%
43.61	-116.914	233	380	215	375	38.68%	63.09%
43.609	-116.915	292.5	360	205	400	18.75%	23.08%
43.604	-116.909	274	465	270	170	41.08%	69.71%
43.595	-116.884	245.6	325	270	330	24.43%	32.33%
43.596	-116.873	347	570	300	245	39.12%	64.27%
43.593	-116.872	505.8	565	305	230	10.48%	11.70%
43.593	-116.869	402	565	305	230	28.85%	40.55%
43.593	-116.845	248	410	245	310	39.51%	65.32%
43.575	-116.815	365.9	435	350	390	15.89%	18.88%
43.54	-116.795	170	330	300	210	48.48%	94.12%

43.503	-116.785	195	390	150	110	50.00%	100.00%
43.438	-116.727	154	365	280	160	57.81%	137.01%
43.411	-116.693	189	285	190	195	33.68%	50.79%
43.401	-116.78	291.8	365	185	395	20.05%	25.09%
43.394	-116.675	245	465	240	185	47.31%	89.80%
43.4	-116.679	270.2	365	185	395	25.97%	35.09%
43.394	-116.672	402.6	465	240	185	13.42%	15.50%
43.384	-116.658	169.9	265	135	380	35.89%	55.97%
43.379	-116.646	166	515	230	110	67.77%	210.24%
43.363	-116.619	200	340	390	140	41.18%	70.00%
43.368	-116.623	238	390	265	340	38.97%	63.87%
43.37	-116.626	272	415	85	370	34.46%	52.57%
43.355	-116.61	222.6	320	145	250	30.44%	43.76%
43.349	-116.604	171	315	275	195	45.71%	84.21%
43.331	-116.547	207	515	170	200	59.81%	148.79%
43.302	-116.56	166	235	90	140	29.36%	41.57%
43.3	-116.536	173	350	120	130	50.57%	102.31%
43.297	-116.518	211	320	125	260	34.06%	51.66%
43.267	-16.403	151	195	170	235	22.56%	29.14%
43.206	-116.384	331	415	170	200	20.24%	25.38%
43.12	-116.303	174.2	215	165	235	18.98%	23.42%
43.119	-116.3	189	235	185	180	19.57%	24.34%
43.097	-116.244	149.7	225	125	140	33.47%	50.30%
43.046	-116.191	181.5	215	155	165	15.58%	18.46%
42.962	-116.03	207.4	265	225	210	21.74%	27.77%
42.95	-116	168	285	185	165	41.05%	69.64%
						32.24%	55.32%

Susquehanna River

						Actual Geometry			
Lat (N)	Lon (W)	L (m)	W (m)	x	R_A	A(km^2)	x/L act.	A=x*LW	theta
40.559	-76.976	146.1	35.9	48.3	4.1	0.0038	0.67	72.45%	10.40
40.557	-76.974	360.2	89.4	144	4.0	0.0195	0.60	60.56%	11.68
40.555	-76.976	243.3	72.4	85.4	3.4	0.0123	0.65	69.83%	12.91
40.551	-76.979	144.1	48.1	68.9	3.0	0.0052	0.52	75.02%	17.73
40.528	-76.97	243	90	68.2	2.7	0.0135	0.72	61.73%	14.44
40.523	-76.976	103.7	39.4	29.2	2.6	0.0028	0.72	68.53%	14.81
40.526	-76.981	116.8	41.4	47.5	2.8	0.0042	0.59	86.86%	16.63
40.522	-76.981	278.1	65.8	66	4.2	0.0123	0.76	67.22%	8.82
40.522	-76.975	389.9	131.7	95.2	3.0	0.0354	0.76	68.94%	12.60
40.527	-76.975	109.8	36.9	36.8	3.0	0.0029	0.66	71.58%	14.18
40.521	-76.976	181	61	56.2	3.0	0.0071	0.69	64.31%	13.73
40.52	-76.982	115.5	29.3	27.5	3.9	0.0023	0.76	67.96%	9.45
40.49	-76.944	292.9	106	161	2.8	0.023	0.45	74.08%	21.89

40.49	-76.942	95.2	33.8	39.4	2.8	0.0019	0.59	59.05%	16.85
40.369	-77.006	437.1	154.2	204	2.8	0.041	0.53	60.83%	18.30
40.365	-77	153.5	44.4	68	3.5	0.0048	0.56	70.43%	14.56
40.289	-76.919	878.7	233.8	224	3.8	0.1363	0.75	66.35%	10.12
40.292	-76.918	325.1	98.7	142	3.3	0.0215	0.56	67.00%	15.08
40.256	-76.89	1183.8	326	460	3.6	0.2575	0.61	66.72%	12.69
40.21	-76.82	763.4	183.3	317	4.2	0.1075	0.58	76.82%	11.60
40.205	-76.814	418.5	113.4	150	3.7	0.0302	0.64	63.64%	11.92
40.206	-76.807	710.3	157.2	264	4.5	0.082	0.63	73.44%	9.99
40.18	-76.739	559.8	181.2	183	3.1	0.0658	0.67	64.87%	13.52
40.094	-76.68	1633.5	331.7	835	4.9	0.4283	0.49	79.05%	11.73
40.064	-76.648	293.2	100	103	2.9	0.0175	0.65	59.69%	14.73
39.895	-76.377	1477.8	494.5	456	3.0	0.5171	0.69	70.76%	13.60
39.861	-76.363	616	150.1	363	4.1	0.0608	0.41	65.76%	16.52
39.608	-76.133	652.8	176	186	3.7	0.0607	0.72	52.83%	10.68
				Average	3.44		0.63	68.1%	13.61
				Std Dev	0.6		0.09	6.9%	3.00

Lemniscate Geometry

Lat (N)	Lon (W)	L/W	k	theta	x/L
40.559	-76.976	3.96	4.41	11.12	0.64
40.557	-76.974	4.68	5.23	9.40	0.65
40.555	-76.976	3.40	3.78	12.96	0.64
40.551	-76.979	2.83	3.14	15.57	0.63
40.528	-76.97	3.09	3.44	14.24	0.64
40.523	-76.976	2.72	3.02	16.18	0.63
40.526	-76.981	2.32	2.55	19.06	0.62
40.522	-76.981	4.42	4.94	9.94	0.64
40.522	-76.975	3.04	3.37	14.50	0.64
40.527	-76.975	2.94	3.27	14.97	0.64
40.521	-76.976	3.26	3.62	13.51	0.64
40.52	-76.982	4.08	4.56	10.77	0.64
40.49	-76.944	2.65	2.93	16.65	0.63
40.49	-76.942	3.37	3.75	13.07	0.64
40.369	-77.006	3.29	3.66	13.38	0.64
40.365	-77	3.46	3.86	12.71	0.64
40.289	-76.919	3.99	4.45	11.03	0.64
40.292	-76.918	3.47	3.86	12.69	0.64
40.256	-76.89	3.83	4.27	11.48	0.64
40.21	-76.82	3.82	4.26	11.52	0.64
40.205	-76.814	4.08	4.55	10.78	0.64
40.206	-76.807	4.33	4.83	10.16	0.64
40.18	-76.739	3.36	3.74	13.09	0.64
40.094	-76.68	4.38	4.89	10.04	0.64
40.064	-76.648	3.47	3.86	12.70	0.64
39.895	-76.377	2.99	3.32	14.74	0.64

39.861	-76.363	4.39	4.90	10.02	0.64
39.608	-76.133	4.93	5.51	8.91	0.65
		3.59	4.00	12.69	0.64
		0.66	0.75	2.45	0.00

River Dimensions

Lat (N)	Lon (W)	ACW	width	d/s width	u/s width	IW/TW	IW/ACW
40.559	-76.976	1314.1	1350	1280	975	2.66%	2.73%
40.557	-76.974	1260.6	1350	1280	975	6.62%	7.09%
40.555	-76.976	1277.6	1350	1280	975	5.36%	5.67%
40.551	-76.979	1301.9	1350	1280	975	3.56%	3.69%
40.528	-76.97	1040	1130	945	1100	7.96%	8.65%
40.523	-76.976	1090.6	1130	945	1100	3.49%	3.61%
40.526	-76.981	1088.6	1130	945	1100	3.66%	3.80%
40.522	-76.981	1064.2	1130	945	1100	5.82%	6.18%
40.522	-76.975	998.3	1130	945	1100	11.65%	13.19%
40.527	-76.975	1093.1	1130	945	1100	3.27%	3.38%
40.521	-76.976	1069	1130	945	1100	5.40%	5.71%
40.52	-76.982	1100.7	1130	945	1100	2.59%	2.66%
40.49	-76.944	1084	1190	1230	1130	8.91%	9.78%
40.49	-76.942	1156.2	1190	1230	1130	2.84%	2.92%
40.369	-77.006	1495.8	1650	1095	775	9.35%	10.31%
40.365	-77	1605.6	1650	1095	775	2.69%	2.77%
40.289	-76.919	1296.2	1530	1285	1510	15.28%	18.04%
40.292	-76.918	1431.3	1530	1285	1510	6.45%	6.90%
40.256	-76.89	774	1100	835	1300	29.64%	42.12%
40.21	-76.82	1356.7	1540	1065	675	11.90%	13.51%
40.205	-76.814	1426.6	1540	1065	675	7.36%	7.95%
40.206	-76.807	1382.8	1540	1065	675	10.21%	11.37%
40.18	-76.739	848.8	1030	865	1240	17.59%	21.35%
40.094	-76.68	858.3	1190	1265	915	27.87%	38.65%
40.064	-76.648	1175	1275	535	1330	7.84%	8.51%
39.895	-76.377	1015.5	1510	680	1285	32.75%	48.70%
39.861	-76.363	764.9	915	835	850	16.40%	19.62%
39.608	-76.133	1094	1270	1315	1250	13.86%	16.09%
						10.11%	12.32%

Tennessee River

Island Location

Name	RM	Lat	Lon	LB (m)	RB (m)	
Kentucky Dam	22					
Kellys I.	143	35.524	87.978			
Double I.	149	35.465	88.033	351	184	60%
Beech Creek I.	155	35.42	87.99	233	201	52%
Glenkirk I.	156	35.409	87.97	459	120	76%
Eagle Nest I.	164	35.414	88.079	255	217	52%
Little Swallow Bluff I.	170	35.387	88.169	157	163	49%
Swallow Bluff I.	170	35.39	88.165	234	214	51%
Wolf I.	193	35.219	88.3	157	397	37%
Little Wolf I.	193	35.215	88.299	132	148	48%
Diamond I.	196	35.175	88.313	332	103	63%
Pickwick Dam	207					
Wilson Dam	260					
Wheeler Dam	275					
Guntersville Dam	349					
Crow Creek I.	401	34.813	85.822	271	199	55%
Nickajack Dam	425					
Chickamauga Dam	471					
Watts Bar Dam	530					
Ft. Loudon Dam	602					
Looney I.	643	35.929	83.955	174	123	55%
	count = 12					54.4%

Actual Geometry

Lat (N)	Lon (W)	L (m)	W (m)	x	R_A	A(km^2)	x/L act.	A=x*LW	theta
35.524	87.978	212.6	54.4	51.6	3.91	0.007	0.76	0.61	9.59
35.465	88.033	918.8	282.1	489	3.26	0.1559	0.47	0.60	18.17
35.42	87.99	1771.75	383	625	4.63	0.4784	0.65	0.71	9.48
35.409	87.97	232	73.3	83.2	3.17	0.0121	0.64	0.71	13.84
35.414	88.079	1975	438	1185	4.51	0.6501	0.40	0.75	15.49
35.387	88.169	259	76.4	118	3.39	0.0104	0.54	0.53	15.16
35.39	88.165	1105.5	294.6	401	3.75	0.2186	0.64	0.67	11.81
35.219	88.3	1452	384	668	3.78	0.3654	0.54	0.66	13.76
35.215	88.299	384.3	114.6	132	3.35	0.0349	0.66	0.79	12.80
35.175	88.313	1866	478.3	850	3.90	0.5679	0.54	0.64	13.25
34.813	85.822	1756	238	767	7.38	0.2816	0.56	0.67	6.86
35.929	83.955	602	195	186	3.09	0.0759	0.69	0.65	13.19
				Average	4.01		0.59	0.66	12.78
				Std Dev	1.17		0.10	0.07	3.04

Lemniscate Geometry

Lat (N)	Lon (W)	L/W	k	theta	x/L
35.524	87.978	4.54	5.07	9.69	0.65
35.465	88.033	3.82	4.25	11.53	0.64
35.42	87.99	4.61	5.15	9.53	0.65
35.409	87.97	3.14	3.49	14.01	0.64
35.414	88.079	4.22	4.71	10.42	0.64
35.387	88.169	4.54	5.07	9.70	0.65
35.39	88.165	3.94	4.39	11.17	0.64
35.219	88.3	4.06	4.53	10.83	0.64
35.215	88.299	2.99	3.32	14.71	0.64
35.175	88.313	4.31	4.82	10.20	0.64
34.813	85.822	7.68	8.60	5.72	0.65
35.929	83.955	3.37	3.75	13.06	0.64
		4.27	4.76	10.88	0.64
		1.20	1.36	2.37	0.00

River Dimensions

Lat (N)	Lon (W)	ACW	width	d/s width	u/s width	IW/TW	IW/ACW
35.524	87.978	470.6	525	390	435	10.36%	11.56%
35.465	88.033	562.9	845	285	275	33.38%	50.12%
35.42	87.99	442	825	535	235	46.42%	86.65%
35.409	87.97	591.7	665	255	435	11.02%	12.39%
35.414	88.079	502	940	285	330	46.60%	87.25%
35.387	88.169	698.6	775	255	325	9.86%	10.94%
35.39	88.165	480.4	775	255	325	38.01%	61.32%
35.219	88.3	581	965	375	320	39.79%	66.09%
35.215	88.299	850.4	965	375	320	11.88%	13.48%
35.175	88.313	431.7	910	320	360	52.56%	110.79%
34.813	85.822	482	720	450	465	33.06%	49.38%
35.929	83.955	410	605	230	165	32.23%	47.56%
						30.43%	50.63%

Willamette River

Island Location

Name	Lat (N)	Long (W)	RM	LB (m)	RB (m)	D from LB
East I.	45.479	-122.659	15.5	86	137	43%
Hog I.	45.401	-122.643	22	64	105	44%
	45.394	-122.631	23	60	181	31%
	45.372	-122.612	25	108	154	45%
Willamette Falls			27			
Ash I.	45.273	-122.984	51.5	79	125	46%
	44.962	-123.038	83	90	61	55%

	44.912	-123.119	89.5	96	45	61%
	44.823	-123.116	100	86	68	53%
Wells I.	44.775	-123.143	106	95	127	47%
	44.778	-123.141	106	20	41	42%
	44.608	-123.187	125	48	50	50%
	44.552	-123.25	132.5	41	41	50%
	44.512	-123.222	136.5	56	32	55%
	44.211	-123.158	166	43	46	49%
	44.131	-123.116	174	37	49	46%
	44.052	-123.073	183	54	38	55%
	count =	16				48.29%

Actual Geometry

Lat (N)	Lon (W)	L (m)	W (m)	x	R_A	A(km^2)	x/L act.	A=x*LW	theta
45.479	-122.659	480	131	175	3.7	0.040	63.54%	0.63	12.12
45.401	-122.643	348	177	155	2.0	0.043	55.46%	0.70	24.63
45.394	-122.631	266	81	73	3.3	0.015	72.56%	0.70	11.85
45.372	-122.612	702	188	435	3.7	0.094	38.03%	0.71	19.40
45.273	-122.984	1992	450	1298	4.4	0.619	34.84%	0.69	17.96
44.962	-123.038	645	122	255	5.3	0.045	60.47%	0.57	8.89
44.912	-123.119	465	83	116	5.6	0.029	75.05%	0.75	6.78
44.823	-123.116	728	186	150	3.9	0.090	79.40%	0.67	9.14
44.775	-123.143	1781	269	649	6.6	0.292	63.56%	0.61	6.78
44.778	-123.141	236	69.9	92	3.4	0.011	61.02%	0.65	13.64
44.608	-123.187	555	130	263	4.3	0.046	52.61%	0.64	12.55
44.552	-123.25	278	101	125	2.8	0.019	55.04%	0.68	18.27
44.512	-123.222	621	176	321	3.5	0.075	48.31%	0.69	16.35
44.211	-123.158	588	91	169	6.5	0.030	71.26%	0.56	6.20
44.131	-123.116	374	78	90	4.8	0.021	75.94%	0.71	7.82
44.052	-123.073	216	54	68	4.0	0.009	68.52%	0.77	10.34
				Average	4.23		60.97%	0.67	12.67
				Std Dev	1.27		13.11%	0.06	5.36

Lemniscate Geometry

Lat (N)	Lon (W)	L/W	k	theta	x/L
45.479	-122.659	4.08	4.55	10.79	0.64
45.401	-122.643	2.01	2.20	21.97	0.62
45.394	-122.631	3.31	3.68	13.31	0.64
45.372	-122.612	3.68	4.10	11.95	0.64
45.273	-122.984	4.51	5.03	9.76	0.65
44.962	-123.038	6.54	7.33	6.72	0.65
44.912	-123.119	5.27	5.90	8.34	0.65
44.823	-123.116	4.13	4.60	10.66	0.64
44.775	-123.143	7.63	8.55	5.76	0.65

44.778	-123.141	3.64	4.05	12.10	0.64
44.608	-123.187	4.72	5.27	9.32	0.65
44.552	-123.25	2.88	3.19	15.29	0.63
44.512	-123.222	3.63	4.04	12.14	0.64
44.211	-123.158	8.05	9.02	5.46	0.65
44.131	-123.116	4.75	5.31	9.26	0.65
44.052	-123.073	3.66	4.07	12.04	0.64
		4.53	5.06	10.93	0.64
		1.65	1.86	4.00	0.01

River Dimensions

Lat (N)	Lon (W)	ACW	width	d/s width	u/s width	IW/TW	IW/ACW
45.479	-122.659	204	335	130	535	39.10%	64.22%
45.401	-122.643	183	360	225	125	49.17%	96.72%
45.394	-122.631	234	315	140	320	25.71%	34.62%
45.372	-122.612	252	440	245	200	42.73%	74.60%
45.273	-122.984	240	690	215	170	65.22%	187.50%
44.962	-123.038	168	290	185	180	42.07%	72.62%
44.912	-123.119	147	230	150	150	36.09%	56.46%
44.823	-123.116	154	340	195	160	54.71%	120.78%
44.775	-123.143	216	485	150	185	55.46%	124.54%
44.778	-123.141	415.1	485	150	185	14.41%	16.84%
44.608	-123.187	95	225	110	95	57.78%	136.84%
44.552	-123.25	74	175	145	105	57.71%	136.49%
44.512	-123.222	109	285	160	85	61.75%	161.47%
44.211	-123.158	94	185	70	120	49.19%	96.81%
44.131	-123.116	112	190	65	110	41.05%	69.64%
44.052	-123.073	101	155	140	145	34.84%	53.47%
						45.44%	93.98%

Wisconsin River

Island Location

Name	Lat (N)	Long (W)	RM	LB (m)	RB (m)	L from LB
	43.023	-91.001		99	159	41%
	43.023	-90.999		64	221	28%
	43.0272	-90.9846		128	95	56%
	43.0306	-90.9741		176	122	57%
	43.0306	-90.9741		56	52	51%
	43.043	-90.9532		162	116	57%
	43.091	-90.8171		91	193	36%
	43.1815	-90.6274		79	119	43%
	43.1848	-90.6237		262	121	65%
	43.1865	-90.6053		72	207	30%
Steamboat I.	43.2094	-90.5432		171	155	52%

	43.208	-90.522	241	175	57%
	43.198	-90.428	110	346	30%
Muscoda I.	43.2	-90.422	266	173	57%
	43.202	-90.396	137	150	48%
	43.208	-90.349	161	195	47%
	43.21	-90.357	263	68	73%
	43.205	-90.319	165	360	33%
	43.204	-90.317	44	456	13%
	43.207	-90.316	305	161	63%
	43.204	-90.207	240	117	65%
	43.166	-90.162	140	324	35%
	43.165	-90.152	85	315	28%
	43.151	-90.07	264	136	63%
	43.147	-90.07	38	448	13%
	43.148	-90.067	201	198	50%
	43.16	-90.05	269	99	69%
	43.194	-89.961	395	56	74%
	43.189	-89.929	170	231	44%
	43.187	-89.924	98	305	33%
	43.196	-89.887	156	186	48%
	43.199	-89.884	469	68	80%
	43.226	-89.818	224	169	56%
Sauk City Dam	43.3103	-89.7252			
	count =	33			48.31%

Actual Geometry

Lat (N)	Lon (W)	L (m)	W (m)	x	R_A	A(km^2)	x/L act.	A=x*LW	theta
43.023	-91.001	213	59.4	57	3.59	0.0091	73.24%	0.72	10.78
43.023	-90.999	290.6	77.1	110	3.77	0.0148	62.15%	0.66	12.05
43.0272	-90.9846	316.5	73.1	89	4.33	0.0155	71.88%	0.67	9.13
43.0306	-90.9741	227	94.1	57	2.41	0.0146	74.89%	0.68	15.47
43.0306	-90.9741	301	68.5	72	4.39	0.0138	76.08%	0.67	8.51
43.043	-90.9532	202	72.1	42	2.80	0.0104	79.21%	0.71	12.70
43.091	-90.8171	293.6	82.1	85	3.58	0.016	71.05%	0.66	11.13
43.1815	-90.6274	368.6	85	94	4.34	0.0227	74.50%	0.72	8.80
43.1848	-90.6237	288	82.4	65	3.50	0.0173	77.43%	0.73	10.47
43.1865	-90.6053	203.3	66.5	46	3.06	0.0084	77.37%	0.62	11.94
43.2094	-90.5432	792.2	182.9	203	4.33	0.0979	74.38%	0.68	8.82
43.208	-90.522	331	66	168	5.02	0.0169	49.24%	0.77	11.45
43.198	-90.428	549	127	134	4.32	0.0456	75.59%	0.65	8.70
43.2	-90.422	802	193	324	4.16	0.1133	59.60%	0.73	11.41
43.202	-90.396	296	82.9	56.7	3.57	0.0155	80.84%	0.63	9.83
43.208	-90.349	451	169	135	2.67	0.0544	70.07%	0.71	14.97
43.21	-90.357	414	101	194	4.10	0.0311	53.14%	0.74	12.93
43.205	-90.319	292	49	58	5.96	0.0095	80.14%	0.66	5.98
43.204	-90.317	184	58	63.2	3.17	0.007	65.65%	0.66	13.50

43.207	-90.316	217	76.2	102	2.85	0.0115	53.00%	0.70	18.33
43.204	-90.207	182	57.2	46	3.18	0.0074	74.73%	0.71	11.88
43.166	-90.162	594	137	339	4.34	0.0586	42.93%	0.72	15.04
43.165	-90.152	416	120	95	3.47	0.0322	77.16%	0.65	10.59
43.151	-90.07	271	88.1	65.9	3.08	0.0167	75.68%	0.70	12.12
43.147	-90.07	265	64.4	88	4.11	0.0115	66.79%	0.67	10.31
43.148	-90.067	458	156	213	2.94	0.05	53.49%	0.70	17.66
43.16	-90.05	194	68.4	63.1	2.84	0.0089	67.47%	0.67	14.64
43.194	-89.961	763	261	403	2.92	0.1399	47.18%	0.70	19.93
43.189	-89.929	409	135	162	3.03	0.0411	60.39%	0.74	15.28
43.187	-89.924	535	198	171	2.70	0.0764	68.04%	0.72	15.22
43.196	-89.887	1044	302	435	3.46	0.205	58.33%	0.65	13.93
43.199	-89.884	385	125	96	3.08	0.0303	75.06%	0.63	12.20
43.226	-89.818	187	58.8	71	3.18	0.0073	62.03%	0.66	14.22
				Average	3.58		73.83%	0.69	12.42
				Std Dev	0.775		4.58%	0.037	3.074

Lemniscate Geometry

Lat (N)	Lon (W)	L/W	k	theta	x/L
43.023	-91.001	3.52	3.92	12.51	0.64
43.023	-90.999	4.02	4.48	10.95	0.64
43.0272	-90.9846	4.54	5.08	9.68	0.65
43.0306	-90.9741	2.51	2.77	17.57	0.63
43.0306	-90.9741	4.62	5.16	9.53	0.65
43.043	-90.9532	2.78	3.08	15.85	0.63
43.091	-90.8171	3.80	4.23	11.59	0.64
43.1815	-90.6274	4.21	4.70	10.44	0.64
43.1848	-90.6237	3.38	3.77	13.01	0.64
43.1865	-90.6053	3.47	3.86	12.68	0.64
43.2094	-90.5432	4.51	5.03	9.76	0.65
43.208	-90.522	4.56	5.09	9.65	0.65
43.198	-90.428	4.65	5.19	9.46	0.65
43.2	-90.422	4.00	4.46	11.01	0.64
43.202	-90.396	3.98	4.44	11.05	0.64
43.208	-90.349	2.65	2.94	16.61	0.63
43.21	-90.357	3.88	4.33	11.33	0.64
43.205	-90.319	6.30	7.05	6.98	0.65
43.204	-90.317	3.41	3.80	12.90	0.64
43.207	-90.316	2.90	3.22	15.19	0.63
43.204	-90.207	3.16	3.52	13.92	0.64
43.166	-90.162	4.24	4.73	10.38	0.64
43.165	-90.152	3.79	4.22	11.62	0.64
43.151	-90.07	3.11	3.45	14.16	0.64
43.147	-90.07	4.30	4.80	10.24	0.64
43.148	-90.067	2.97	3.29	14.84	0.64
43.16	-90.05	2.99	3.32	14.72	0.64

43.194	-89.961	2.95	3.27	14.96	0.64
43.189	-89.929	2.88	3.20	15.28	0.63
43.187	-89.924	2.66	2.94	16.58	0.63
43.196	-89.887	3.75	4.18	11.74	0.64
43.199	-89.884	3.45	3.84	12.75	0.64
43.226	-89.818	3.38	3.76	13.02	0.64
		3.68	4.09	12.48	0.64

Yukon River

	Island Location					
Name	Lat (N)	Long (W)	RM	LB (m)	RB (m)	D from LB
	62.079	-163.653		805	630	54%
	61.819	-163.093		691	279	62%
	61.874	-161.254		1077	933	52%
	61.954	-160.471		1134	273	74%
Carlo I.	62.409	-160.011		663	841	47%
Elkhorn I.	62.546	-160.189		1482	529	63%
Alice I.	63.302	-159.659		1025	404	59%
	63.761	-159.276		775	563	55%
	63.883	-159.157		1238	187	76%
	63.884	-159.135		992	1008	50%
	64.355	-158.676		619	838	46%
Nulato I.	64.71	-158.09		777	720	51%
Gemodedon I.	64.81	-157.954		1498	277	79%
Yuki I.	64.722	-156.062		735	607	53%
Fox I.	64.902	-154.848		1123	807	55%
Emerald I.	64.919	-154.578		797	1017	45%
Henry I.	65.026	-154.019		619	833	46%
Lady I.	65.064	-153.868		605	335	59%
Burns I.	65.056	-153.85		637	490	54%
	65.043	-153.907		322	958	31%
Lange I.	65.13	-153.194		297	536	42%
Station I.	65.139	-152.55		755	380	63%
Twelvemile I.	65.494	-150.554		560	389	57%
Sixmile I.	65.488	-150.352		498	122	68%
Minook I.	65.531	-150.142		425	204	59%
Crescent I.	65.752	-149.83		423	294	55%
Kalka I.	65.769	-150.007		275	515	43%
	66.049	-148.975		231	876	26%
Gull I.	66.152	-148.525		433	762	38%
	count =	29				53.85%

Actual Geometry

Lat (N)	Lon (W)	L (m)	W (m)	x	R_A	A(km^2)	x/L act.	A=x*LW	theta
62.079	-163.653	2596	523	464	4.96	0.807	82.13%	0.59	6.99
61.819	-163.093	2573	769	1004	3.35	1.27	60.98%	0.64	13.77
61.874	-161.254	3904	1188	1046	3.29	3.35	73.21%	0.72	11.74
61.954	-160.471	2577	415	1333	6.21	0.76	48.27%	0.71	9.47
62.409	-160.011	7666	1915	2192	4.00	9.4563	71.41%	0.64	9.92
62.546	-160.189	4589	1533	2522	2.99	4.65	45.04%	0.66	20.35
63.302	-159.659	5357	2077	2302	2.58	7.2152	57.03%	0.65	18.77
63.761	-159.276	3307	986	910	3.35	2.11	72.48%	0.65	11.62
63.883	-159.157	1919	596	850	3.22	0.729	55.71%	0.64	15.58
63.884	-159.135	615	150	248	4.10	0.062	59.67%	0.67	11.55
64.355	-158.676	3923	1166	2084	3.36	2.9	46.88%	0.63	17.59
64.71	-158.09	3971	1047	1450	3.79	2.88	63.49%	0.69	11.73
64.81	-157.954	1453	317	389	4.58	0.34	73.23%	0.74	8.47
64.722	-156.062	3473	700	1069	4.96	1.48	69.22%	0.61	8.28
64.902	-154.848	2913	1015	1004	2.87	1.89	65.53%	0.64	14.89
64.919	-154.578	1341	265	756	5.06	0.2597	43.62%	0.73	12.76
65.026	-154.019	4200	962	1878	4.37	2.5162	55.29%	0.62	11.70
65.064	-153.868	2486	517	1114	4.81	0.817	55.19%	0.64	10.67
65.056	-153.85	2615	596	1085	4.39	1.128	58.51%	0.72	11.02
65.043	-153.907	1548	381	663	4.06	0.411	57.17%	0.70	12.15
65.13	-153.194	2558	593	1081	4.31	0.991	57.74%	0.65	11.35
65.139	-152.55	1683	363	611	4.64	0.43	63.70%	0.70	9.61
65.494	-150.554	1198	269	676	4.45	0.235	43.57%	0.73	14.45
65.488	-150.352	2044	423	677	4.83	0.5215	66.88%	0.60	8.79
65.531	-150.142	2378	656	1106	3.63	1.0623	53.49%	0.68	14.46
65.752	-149.83	2676	631	1311	4.24	1.0352	51.01%	0.61	13.01
65.769	-150.007	2758	942	1191	2.93	1.7162	56.82%	0.66	16.73
66.049	-148.975	1108	253	609	4.38	0.2028	45.04%	0.72	14.23
66.152	-148.525	798	216	302	3.69	0.1187	62.16%	0.69	12.28
				Average	4.05		59.12%	0.67	12.55
				Std Dev	0.82		10.02%	0.04	3.19

Lemniscate Geometry

Lat (N)	Lon (W)	L/W	k	theta	x/L
62.079	-163.653	5.86	6.56	7.50	0.65
61.819	-163.093	3.68	4.09	11.98	0.64
61.874	-161.254	3.21	3.57	13.70	0.64
61.954	-160.471	6.13	6.86	7.17	0.65
62.409	-160.011	4.37	4.88	10.06	0.64
62.546	-160.189	3.20	3.56	13.76	0.64
63.302	-159.659	2.82	3.12	15.63	0.63
63.761	-159.276	3.65	4.07	12.04	0.64

63.883	-159.157	3.56	3.97	12.35	0.64
63.884	-159.135	4.29	4.79	10.25	0.64
64.355	-158.676	3.74	4.17	11.77	0.64
64.71	-158.09	3.86	4.30	11.41	0.64
64.81	-157.954	4.37	4.88	10.07	0.64
64.722	-156.062	5.72	6.40	7.68	0.65
64.902	-154.848	3.17	3.53	13.88	0.64
64.919	-154.578	4.87	5.44	9.04	0.65
65.026	-154.019	4.93	5.51	8.93	0.65
65.064	-153.868	5.31	5.94	8.28	0.65
65.056	-153.85	4.27	4.76	10.31	0.64
65.043	-153.907	4.10	4.58	10.72	0.64
65.13	-153.194	4.64	5.19	9.47	0.65
65.139	-152.55	4.63	5.17	9.50	0.65
65.494	-150.554	4.30	4.80	10.24	0.64
65.488	-150.352	5.62	6.29	7.82	0.65
65.531	-150.142	3.75	4.18	11.73	0.64
65.752	-149.83	4.86	5.43	9.05	0.65
65.769	-150.007	3.13	3.48	14.06	0.64
66.049	-148.975	4.26	4.75	10.33	0.64
66.152	-148.525	3.78	4.21	11.64	0.64
		4.28	4.78	10.70	0.64
		0.88	0.99	2.18	0.00

Residual Islands in the Channeled Scablands

Location			*Geometry*							
N	W	Quad	L (m)	W (m)	R_A	A (km^2)	A=x*LW	k	theta	x/L
46,56	118,6.5	Benge	2038	615	3.3	0.81	0.65	4.03	12.17	64.1%
46,56	118,6.5	Benge	7905	2595	3.0	16.0	0.78	3.07	15.92	63.3%
46,57	118,8.5	Benge	1192	231	5.2	0.26	0.93	4.38	11.21	64.3%
46,57	118,8.5	Benge	2594	365	7.1	0.63	0.67	8.39	5.87	65.0%
46,57	118,8.5	Benge	846	163.5	5.2	0.10	0.74	5.51	8.92	64.6%
47, 1.5	118,3	Macall	1115	327	3.4	0.27	0.74	3.62	13.54	63.8%
47, 1.5	118,3	Macall	692	279	2.5	0.15	0.78	2.51	19.38	62.4%
47, 1.5	118,3	Macall	2346	808	2.9	1.27	0.67	3.39	14.41	63.7%
47,4.5	118,5	Macall	2885	846	3.41	1.78	0.73	3.67	13.35	63.9%
47,2	118,8	Marengo	1673	750	2.2	0.65	0.52	3.39	14.42	63.7%
47,2	118,8	Marengo	981	423	2.3	0.29	0.70	2.61	18.66	62.6%
47,2	118,8	Marengo	2527	923	2.7	1.59	0.68	3.15	15.52	63.4%
47,2	118,8	Marengo	1146	442	2.6	0.39	0.76	2.67	18.26	62.7%
47,4.5	118,8	Marengo	2115	462	4.6	0.82	0.84	4.28	11.46	64.2%
47,4	118,12	Marengo	2577	885	2.9	1.42	0.62	3.67	13.33	63.9%
46,57	117,56.5	Honn Lakes	4500	1731	2.6	5.22	0.67	3.05	16.02	63.3%
47,3.5	117,53.5	Revere	654	192	3.4	0.09	0.68	3.91	12.55	64.0%
47,3.5	117,53.5	Revere	3942	1827	2.2	5.41	0.75	2.26	21.47	61.8%
47,5	117,58.5	Revere	2115	769	2.8	1.24	0.76	2.84	17.16	63.0%
47,20.5	117,44.5	Amber	2106	671	3.1	1.10	0.78	3.15	15.49	63.4%

	R_A	A=x*LW	k	theta	x/L
Average	3.37	0.72	3.7	14.5	63.6%
Std Dev	1.2	0.09	1.3	3.7	0.0

Residual Islands in Outwash Plains of Mars

Streamlined Islands

Location		*Geometry*									
N	W	L (m)	W (m)	R_A	A (km^2)	A=x*LW	k	theta	x/L	L (km)	W (km)
13.75	34.1	18100	5900	3.1	80.0	0.7	3.22	15.19	63.5%	18.10	5.90
13.77	34.1	20500	5600	3.7	100.0	0.9	3.30	14.81	63.6%	20.50	5.60
15.8	36.8	27300	13600	2.0	270.0	0.7	2.17	22.30	61.5%	27.30	13.60
18.9	31.25	16200	6400	2.5	70.0	0.7	2.94	16.57	63.2%	16.20	6.40
15.75	30.55	26600	5900	4.5	130.0	0.8	4.27	11.47	64.2%	26.60	5.90
15.25	33.85	25100	5900	4.3	100.0	0.7	4.95	9.93	64.5%	25.10	5.90
15.83	37.25	75200	28300	2.7	1610.0	0.8	2.76	17.66	62.9%	75.20	28.30
14.83	33.9	24000	5400	4.4	80.0	0.6	5.65	8.69	64.7%	24.00	5.40
14.18	35.03	32800	9700	3.4	210.0	0.7	4.02	12.18	64.1%	32.80	9.70
16.13	29.98	11900	2800	4.3	30.0	0.9	3.71	13.21	63.9%	11.90	2.80
16.38	35.55	35400	6200	5.71	140.0	0.6	7.03	7.00	64.9%	35.40	6.20
17.93	32.88	25400	11300	2.2	160.0	0.6	3.17	15.43	63.4%	25.40	11.30
20.3	37.18	18600	7500	2.5	90.0	0.6	3.02	16.17	63.3%	18.60	7.50
26.33	36.32	10400	4200	2.5	30.0	0.7	2.83	17.21	63.0%	10.40	4.20
			Average	3.41		0.71	3.8	14.13	63.6%		
			Std Dev	1.1		0.10	1.3	4.0	0.0		

Residual Islands in Outwash Plains on Mars

Crater Islands

Location		*Geometry*									
N	W	L (m)	W (m)	R_A	A (km^2)	A=x*LW	k	theta	x/L	L (km)	W (km)
18	36.23	44700	18500	2.4	540.0	0.7	2.91	16.78	63.1%	44.70	18.50
17.18	38.67	49600	22900	2.2	700.0	0.6	2.76	17.65	62.9%	49.60	22.90
16.97	32.08	105900	56900	1.86	4040.0	0.7	2.18	22.18	61.5%	105.90	56.90
19.93	31.47	43000	16400	2.6	410.0	0.6	3.54	13.82	63.8%	43.00	16.40
20.5	31.78	70900	23600	3.0	1040.0	0.6	3.80	12.90	64.0%	70.90	23.60
26.23	33.85	50100	25700	1.9	850.0	0.7	2.32	20.90	61.9%	50.10	25.70
26.7	37.85	40500	21500	1.9	690.0	0.8	1.87	25.72	60.2%	40.50	21.50
22.5	31.62	69900	26600	2.6	1330.0	0.7	2.89	16.90	63.1%	69.90	26.60
			Average	2.32		0.66	2.8	18.36	62.6%		
			Std Dev	0.42		0.07	0.66	4.32	0.01		

APPENDIX III – RAW DATA FROM FIELD WORK

Flume Experiments

Manometer Equation for flume: $Q = 0.522 * \Delta h_m^{0.353}$ $r^2 = 0.989$

Slope Calculation:
- upstream elevation = 6.426 ft
- downstream elevation = 6.500 ft
- distance between measurements = 23 ft
- Slope (S) = (6.500-6.426)/23 = 0.003217 ft/ft

Flume width (B) = 449 mm = 1.474 ft
Large PVC pipe diameter = 169 mm = 0.554 ft
Small PVC pipe diameter = 127 mm = 0.417 ft

Assumed properties:
- gravity (g) = 32.2 ft/s^2
- specific weight of water (γ) = 62.4 lb/ft^3
- density of water (ρ) = 1.94 slug/ft^3
- kinematic viscosity of water (υ) = 1.21×10^{-5} ft^2/sec

Distance between upstream and downstream measurements = 8 ft
Difference in elevation between measurement locations (Δz) = 8*0.003217 = 0.02574 ft

Location of island in flume:
- Left edge: 150 mm from left wall
- Right edge: (449-319) = 130 mm from right wall

Actual Measurements:
- Island length in millimeters (L)
- Flow depth upstream of island in millimeters (u/s d)
  - (measured 3 ft upstream from upstream nose of island)
- Flow depth downstream of island in millimeters (d/s d)
  - (measured 5 ft downstream from upstream nose of island)
- Difference in manometer heads (Δh) in feet (Δh 1 & 2)
  - (read twice: before and after flow depths were measured)

Calculated Measurements:
- Aspect ratio (R_a) = length/width (ft/ft)
- Discharge (Q), calculated from manometer equation, values averaged (ft^3/sec)
- upstream and downstream flow area (A) = B * d (ft^2)
- upstream and downstream wetted perimeter (P) = B + 2*d (ft)
- upstream and downstream hydraulic radius (R) = A/P (ft)
- upstream and downstream shear stress = γ*R*S (lb/ft^2)
- upstream and downstream velocity (V) = Q/A (ft/sec)

upstream and downstream energy head (E) = d + $V^2/2g$ (ft)
head loss = (u/s E + Δz) – d/s E (ft)
head loss percentage = (head loss)/(u/s E)
upstream and downstream Reynold's Number (Re) = $(V*d)/\upsilon$ (unitless)
total frictional drag force (lb):

$$F = \left(\frac{1}{2}\rho g B\right)(d_1^2 - d_2^2) - \rho Q(V_2 - V_1)$$

drag force only on island = total F – F calculated without any island (no pipes)
drag coefficient (C_D) = $F/(0.5*\rho*V^2*A)$ (unitless)
Manning's roughness coefficient (n) = $(1.49/V)*R^{2/3}*S^{1/2}$ (unitless)

Flume Data:

	No pipes	1 pipe	2 pipes	3 pipes	4 pipes	5 pipes
width (mm)		169	169	169	169	169
width (ft)		0.554	0.554	0.554	0.554	0.554
length (mm)		169	296	465	634	803
length (ft)		0.554	0.971	1.526	2.080	2.635
R_a		1.0	1.751	2.751	3.751	4.751
u/s d (mm)	34	70	70	70	72	74
u/s d (ft)	0.112	0.230	0.230	0.230	0.236	0.243
d/s d (mm)	39	35	33	29	29.33	30
d/s d (ft)	0.128	0.115	0.108	0.095	0.096	0.098
Δh 1	0.59	0.51	0.49	0.49	0.52	0.50
Δh 2	0.56	0.51	0.52	0.52	0.51	0.50
Q 1	0.433	0.412	0.406	0.406	0.414	0.409
Q 2	0.425	0.412	0.410	0.410	0.413	0.409
avg Q	0.429	0.412	0.410	0.410	0.413	0.409
u/s A	0.164	0.339	0.339	0.339	0.348	0.358
u/s P	1.697	1.933	1.933	1.933	1.946	1.960
u/s R	0.097	0.175	0.175	0.175	0.179	0.183
u/s shear	0.019	0.035	0.035	0.035	0.036	0.037
u/s V	2.611	1.216	1.211	1.211	1.186	1.142
u/s E	0.217	0.253	0.252	0.252	0.258	0.263
d/s A	0.189	0.169	0.160	0.140	0.142	0.145
d/s P	1.730	1.704	1.690	1.664	1.666	1.671
d/s R	0.109	0.099	0.094	0.084	0.085	0.087
d/s shear	0.022	0.020	0.019	0.017	0.017	0.017
d/s V	2.276	2.432	2.57	2.924	2.911	2.817
d/s E	0.208	0.207	0.211	0.228	0.228	0.222
head loss (ft)	0.0347	0.0717	0.0674	0.0503	0.0560	0.0671
head loss (%)	15.98	28.39	26.69	19.91	21.68	25.51
u/s Re	2.1E04	1.8E04	1.8E04	1.8E04	1.8E04	1.7E04
d/s Re	2.1E04	2.0E04	2.0E04	2.0E04	2.1E04	2.0E04
F (total)	0.098	0.850	0.819	0.663	0.756	0.939
F (island)		0.752	0.721	0.565	0.658	0.842
C_D		4.121	3.978	3.117	3.679	4.941
n	0.0077	0.015	0.014	0.014	0.014	0.015

Oak Creek Experiments

Flow patterns behind object

Date: 3/23/2004
Time: 12:00 pm
Water temperature: 52 F
Discharge measured by automatic recorder 37.5 feet downstream = 4.3 cfs

	0 feet downstream		0.5 feet downstream		1.0 feet downstream	
Station	Depth	Velocity	Depth	Velocity	Depth	Velocity
13	0.28	1.65	0.3	1.68	0.19	1.56
12.75	0.25	1.59	0.27	1.58	0.23	1.32
12.5	0.25	1.76	0.35	0.91	0.3	1.25
12.25	0.35	1.72	0.25	1.69	0.3	1.67
12	0.3	1.71	0.31	1.61	0.3	1.62
11.75	0.32	1.43	0.33	1.75	0.3	1.43
11.5	0.35	-0.04	0.38	0.03	0.36	0.3
11.25	0.35	-0.09	0.38	-0.07	0.35	-0.09
11	0.38	-0.07	0.38	-0.15	0.3	-0.16
10.75	0.4	0.55	0.29	0.4	0.35	0.53
10.5	0.36	1.51	0.3	0.86	0.38	1.15
10.25	0.35	1.83	0.3	1.73	0.3	1.48
10	0.35	1.52	0.33	1.49	0.32	1.51
9.75	0.3	1.53	0.31	1.36	0.31	1.19
9.5	0.4	1.64	0.31	1.61	0.3	1.39
9.25	0.33	1.53	0.4	1.4	0.3	1.8
9	0.37	1.35	0.35	1.35	0.35	1.43

	1.5 feet downstream		2.0 feet downstream		2.5 feet downstream	
Station	Depth	Velocity	Depth	Velocity	Depth	Velocity
13	0.28	1.32	0.38	1.13	0.2	1.23
12.75	0.33	1.14	0.3	1.4	0.3	1.44
12.5	0.3	1.02	0.33	1.15	0.28	1.28
12.25	0.3	1.04	0.3	1.09	0.3	1.26
12	0.25	1.42	0.25	1.64	0.3	1.12
11.75	0.3	0.81	0.25	1.25	0.29	1.53
11.5	0.3	0.44	0.25	1.02	0.29	0.76
11.25	0.3	-0.23	0.3	0.19	0.2	0.58
11	0.3	-0.07	0.3	-0.1	0.25	-0.08
10.75	0.32	0.49	0.3	0.3	0.25	0.14
10.5	0.3	1.1	0.3	0.83	0.3	0.56
10.25	0.3	1.32	0.35	1.33	0.22	1.05
10	0.32	1.46	0.31	1.3	0.3	1.36
9.75	0.35	1.04	0.25	1.08	0.3	1.19
9.5	0.35	1.25	0.39	1.42	0.32	1.02
9.25	0.3	1.73	0.35	1.6	0.3	1.47
9	0.33	1.46	0.29	1.59	0.3	1.23

	3.0 feet downstream		3.5 feet downstream		4.0 feet downstream	
Station	Depth	Velocity	Depth	Velocity	Depth	Velocity
13	0.3	1.21	0.22	1.29	0.2	1.01
12.75	0.2	1.35	0.25	1.48	0.25	1.29
12.5	0.3	1.18	0.25	1.36	0.3	1.53
12.25	0.3	1.08	0.23	1.39	0.25	1.36
12	0.35	1.04	0.3	1.13	0.22	1.41
11.75	0.35	1.34	0.25	1.5	0.3	1.5
11.5	0.37	0.8	0.25	1.37	0.22	1.27
11.25	0.32	0.58	0.3	0.84	0.3	0.73
11	0.32	0.23	0.35	0.4	0.31	0.41
10.75	0.32	0.19	0.38	0.27	0.31	0.72
10.5	0.35	0.66	0.38	0.6	0.25	1.04
10.25	0.35	0.9	0.33	1.18	0.31	1.05
10	0.39	0.92	0.3	1.18	0.29	1.22
9.75	0.26	1.04	0.3	1.27	0.33	1.2
9.5	0.3	1.1	0.3	1.23	0.3	1.28
9.25	0.3	1.46	0.28	1.36	0.25	1.7
9	0.3	1.44	0.25	1.53	0.35	1.33

Date: 5/23/2004
Time: 12:00 pm
Water temperature not recorded
Discharge measured by automatic recorder 37.5 feet downstream = 3.0 cfs

	0.5 feet upstream		1.0 feet upstream	
Station	Depth	Velocity	Depth	Velocity
13				
12.75				
12.5	0.21	0.97		
12.25	0.3	1	0.21	1.02
12	0.21	1.04	0.2	0.96
11.75				
11.5				
11.25	Object		Object	
11				
10.75				
10.5	0.2	0.85	0.25	0.49
10.25	0.3	0.92	0.25	0.71
10	0.32	0.97	0.3	0.97
9.75				
9.5				

	0 feet downstream		0.5 feet downstream		1.0 feet downstream	
Station	Depth	Velocity	Depth	Velocity	Depth	Velocity
13	0.2	0.98	0.2	0.87	0.18	0.65
12.75	0.22	1.31	0.2	1.2	0.2	1.03
12.5	0.27	1.07	0.25	1.16	0.21	1.28

12.25	0.2	1.31	0.22	0.91	0.2	0.95
12	0.3	1.46	0.21	1.3	0.22	1.18
11.75	0.3	0.1	0.3	0.7	0.2	0.72
11.5	0.3	-0.13	0.28	-0.07	0.25	0.15
11.25	0.3	-0.1	0.28	-0.14	0.21	-0.13
11	0.25	-0.1	0.3	-0.08	0.3	-0.12
10.75	0.31	0.32	0.23	0.1	0.3	0.24
10.5	0.37	0.42	0.3	0.41	0.26	0.52
10.25	0.3	0.77	0.32	0.64	0.29	0.87
10	0.28	0.99	0.27	1.05	0.28	0.99
9.75	0.31	0.77	0.25	0.87	0.22	0.75
9.5	0.31	0.73	0.25	0.74	0.22	0.86

	1.5 feet downstream		2.0 feet downstream		2.5 feet downstream		3.0 feet downstream	
Station	Depth	Velocity	Depth	Velocity	Depth	Velocity	Depth	Velocity
13	Too Shallow							
12.75								
12.5	0.2	1.28	0.28	1.07	0.3	0.87	0.2	1.03
12.25	0.2	1.05	0.21	1	0.25	0.81	0.2	0.97
12	0.24	1.14	0.22	0.86	0.2	0.87	0.2	0.65
11.75	0.25	0.83	0.22	0.96	0.2	0.99	0.21	0.87
11.5	0.21	0.31	0.2	0.42	0.22	1	0.2	0.88
11.25	0.21	0.01	0.2	0.03	0.22	0.48	0.23	0.39
11	0.23	-0.08	0.2	0.09	0.22	0.28	0.25	0.31
10.75	0.28	0.15	0.2	0.33	0.23	0.35	0.26	0.53
10.5	0.28	0.64	0.22	0.6	0.3	0.67	0.3	0.59
10.25	0.27	0.84	0.3	0.86	0.28	0.85	0.3	0.81
10	0.27	0.94	0.25	0.79	0.2	0.75	0.2	0.85
9.75	0.25	0.76	0.25	0.62	0.18	0.64	0.2	0.5
9.5	0.2	0.93	0.27	0.69	0.2	0.83	0.2	0.64

Artificial Islands in Oak Creek

No Island setup:
Determination of water surface slope

Surface Profile			**No island**
BS	100		
HI	7.125	staff gage	0.165

Pipe #	Sight	Elev	read depth	Surf Elev	Loc	Slope
BS	7.125	100	0.22	100.22	0	0.0044
8	5.72	101.405	1.11	100.295	17.0612	0.0217
7	6.285	100.84	0.36	100.48	25.5918	0.0090
6L	5.78	101.345	0.8	100.545	32.81	0.0116
6R	5.6	101.525	1.03	100.495	32.81	
5	5.645	101.48	0.88	100.6	37.56745	0.0086
4L	5.645	101.48	0.88	100.6	43.9654	
4R	5.34	101.785	1.13	100.655	43.9654	0.0111
3	5.29	101.835	1.1	100.735	51.1836	0.0127
2	5.3	101.825	0.94	100.885	62.9952	0.0051
1	5.265	101.86	0.91	100.95	75.7911	
					average	0.0114

Velocity Profiles at each cross-section

XS 1

Station	Depth	Velocity	Area	Q
5.3	0	0	0.1	0
6.3	0.2	0.28	0.2	0.056
7.3	0.3	0.73	0.3	0.219
8.3	0.25	1.82	0.25	0.455
9.3	0.4	1.73	0.4	0.692
10.3	0.32	1.06	0.32	0.3392
11.3	0.24	1.1	0.168	0.1848
11.7	0.14	0.92	0.07	0.0644
12.3	0.14	-0.19	0.077	-0.01463
12.8	0.15	0.64	0.075	0.048
13.3	0.2	0.73	0.15	0.1095
14.3	0.25	0.15	0.25	0.0375
15.3	0.25	0.06	0.25	0.015
16.3	0.25	-0.09	0.1625	-0.01463
16.6	0	0	0.0375	0
Total	0.24	0.69	2.81	2.19

XS 2

Station	Depth	Velocity	Area	Q
5.2	0	0	0.15	0
7.2	0.15	0.37	0.225	0.08325

8.2	0.15	0.62	0.15	0.093
9.2	0.22	1.39	0.22	0.3058
10.2	0.4	1.2	0.4	0.48
11.2	0.42	1.33	0.42	0.5586
12.2	0.42	1.63	0.42	0.6846
13.2	0.34	0.85	0.34	0.289
14.2	0.27	0.88	0.27	0.2376
15.2	0.16	0.1	0.128	0.0128
15.8	0	0	0.048	0
Total	0.28	0.93	2.77	2.74

XS 3

Station	Depth	Velocity	Area	Q
5.7	0	0	0.0375	0
6.2	0.15	-0.17	0.1125	-0.01913
7.2	0.26	0.55	0.26	0.143
8.2	0.25	0.73	0.25	0.1825
9.2	0.32	1.18	0.32	0.3776
10.2	0.27	0.89	0.27	0.2403
11.2	0.35	1.31	0.35	0.4585
12.2	0.4	1.54	0.4	0.616
13.2	0.33	1.14	0.33	0.3762
14.2	0.3	0.9	0.3	0.27
15.2	0.18	0.9	0.162	0.1458
16	0.12	-0.15	0.084	-0.0126
16.6	0	0	0.036	0
Total	0.27	0.80	2.91	2.78

XS 4

Station	Depth	Velocity	Area	Q
4.6	0	0	0.09	0
5.6	0.18	0.22	0.18	0.0396
6.6	0.25	0.14	0.25	0.035
7.6	0.25	0.33	0.25	0.0825
8.6	0.27	0.94	0.27	0.2538
9.6	0.5	0.46	0.5	0.23
10.6	0.4	0.87	0.4	0.348
11.6	0.43	1.37	0.43	0.5891
12.6	0.27	1.36	0.27	0.3672
13.6	0.25	0.88	0.25	0.22
14.6	0.15	0.77	0.135	0.10395
15.4	0	0	0.06	0
Total	0.30	0.73	3.09	2.27

XS 5

Station	Depth	Velocity	Area	Q
4.7	0	0	0.11	0
5.7	0.22	0.39	0.22	0.0858
6.7	0.22	0.88	0.22	0.1936

7.7	0.27	0.87	0.27	0.2349
8.7	0.3	0.79	0.3	0.237
9.7	0.3	1.31	0.3	0.393
10.7	0.38	1.46	0.38	0.5548
11.7	0.28	1.45	0.28	0.406
12.7	0.32	1.36	0.32	0.4352
13.7	0.2	1.14	0.2	0.228
14.7	0.12	0.13	0.156	0.02028
16.3	0	0	0.096	0
Total	0.26	0.98	2.85	2.79

XS 6

Station	Depth	Velocity	Area	Q
5	0	0	0.1	0
6	0.2	0.29	0.2	0.058
7	0.22	1	0.22	0.22
8	0.24	0.6	0.24	0.144
9	0.2	0.77	0.2	0.154
10	0.26	1.31	0.26	0.3406
11	0.26	1.6	0.26	0.416
12	0.27	1.25	0.27	0.3375
13	0.22	1.3	0.22	0.286
14	0.26	1.53	0.26	0.3978
15	0.2	1.37	0.26	0.3562
16.6	0	0	0.16	0
Total	0.23	1.10	2.65	2.71

XS 7

Station	Depth	Velocity	Area	Q
4.8	0	0	0.065	0
6.1	0.1	0.35	0.115	0.04025
7.1	0.12	0.45	0.12	0.054
8.1	0.24	0.4	0.24	0.096
9.1	0.26	0.64	0.26	0.1664
10.1	0.26	0.99	0.26	0.2574
11.1	0.2	0.98	0.2	0.196
12.1	0.24	0.93	0.24	0.2232
13.1	0.28	1.28	0.28	0.3584
14.1	0.33	1.28	0.33	0.4224
15.1	0.32	1.05	0.32	0.336
16.1	0.21	0.18	0.1575	0.02835
16.6	0	0	0.0525	0
Total	0.23	0.78	2.64	2.18

Small Island:

Determination of water surface slope:

Surface Profile

BS	100		
HI	7.195	staff gage	0.149

Pipe #	Sight	Elev	read depth	Surf Elev	Loc	Slope
BS	7.195	100	0.205	100.205	0	0.0032
8	5.8	101.395	1.135	100.26	17.0612	0.0229
7	6.45	100.745	0.29	100.455	25.5918	0.0083
6L	5.85	101.345	0.83	100.515	32.81	0.0042
6R	5.695	101.5	1.06	100.44	32.81	
5	5.73	101.465	0.93	100.535	37.56745	0.0102
4L	5.722	101.473	0.9	100.573	43.9654	
4R	5.425	101.77	1.17	100.6	43.9654	0.0104
3	5.37	101.825	1.15	100.675	51.1836	0.0127
2	5.37	101.825	1	100.825	62.9952	0.0082
1	5.285	101.91	0.98	100.93	75.7911	
					average	0.0110

Velocity profiles at each cross-section:

XS 2

Station	Depth	Velocity	Area	Discharge
5.5	0	0	0.15	0
8	0.12	0.58	0.18	0.1044
8.5	0.12	1.43	0.06	0.0858
9	0.1	0.6	0.075	0.045
10	0.35	1.52	0.35	0.532
11	0.4	1.56	0.4	0.624
12	0.33	1.28	0.33	0.4224
13	0.37	0.78	0.37	0.2886
14	0.33	0.44	0.33	0.1452
15	0.24	0.62	0.276	0.17112
16.3	0	0	0.156	0
Total	0.26	0.98	2.68	2.42

XS 3 Just u/s of buckets

Station	Depth	Velocity	angle	Velocity	Area	Discharge
5.7	0	0	0	0	0.09	0
6.7	0.18	0.18	10	0.182777	0.18	0.0329
7.7	0.2	0.53	20	0.564014	0.2	0.112803
8.7	0.25	0.56	25	0.617892	0.25	0.154473
9.7	0.33	0.52	30	0.600444	0.33	0.198147
10.7	0.4	0.36	10	0.365554	0.4	0.146221
11.7	0.4	1.12	15	1.159509	0.4	0.463804
12.7	0.36	1.08	10	1.096661	0.36	0.394798
13.7	0.37	0.71	5	0.712712	0.37	0.263703
14.7	0.2	0.54	0	0.54	0.2	0.108
15.7	0.23	0.09	0	0.09	0.2185	0.019665
16.6	0	0	0	0	0.1035	0
Total	0.29			0.59	3.10	1.89

XS 3.5 Middle of bucket island

Station	Depth	Velocity	angle	Velocity	Area	Discharge
5	0	0	0	0	0.07	0
5.7	0.2	-0.08	0	-0.08	0.17	-0.0136
6.7	0.2	0.48	10	0.487405	0.2	0.097481
7.7	0.2	0.6	10	0.609256	0.2	0.121851
8.7	0.25	1.31	10	1.330209	0.2125	0.282669
9.4	0.3	1.36	0	1.36	0.15	0.204
9.7		0	Island of Buckets			
11.7		0				
12	0.15	1.51	0	1.51	0.075	0.11325
12.7	0.3	1.63	10	1.655145	0.255	0.422062
13.7	0.35	1.03	5	1.033934	0.35	0.361877
14.7	0.2	0.82	0	0.82	0.2	0.164
15.7	0.15	-0.09	0	-0.09	0.1125	-0.01013
16.2	0	0	0	0	0.0375	0
Total	0.23			0.86	2.03	1.74

XS 4

Station	Depth	Velocity	angle	Velocity	Area	Discharge
4.7	0	0	0	0	0.13	0
6	0.2	0.38	0	0.38	0.23	0.0874
7	0.25	0.38	0	0.38	0.25	0.095
8	0.21	0.92	0	0.92	0.21	0.1932
9	0.32	1.27	10	1.289592	0.32	0.412669
10	0.4	0.01	10	0.010154	0.4	0.004062
11	0.3	-0.04	0	-0.04	0.3	-0.012
12	0.4	1.38	10	1.401289	0.4	0.560515
13	0.25	1.64	0	1.64	0.25	0.41
14	0.25	0.85	0	0.85	0.25	0.2125
15	0.1	0.38	0	0.38	0.075	0.0285
15.5	0	0	0	0	0.025	0
Total	0.27			0.72	2.84	1.99

XS 5

Station	Depth	Velocity	Area	Discharge
4.5	0	0	0.0625	0
5	0.25	0	0.1875	0
6	0.2	0.95	0.2	0.19
7	0.15	0.56	0.15	0.084
8	0.2	0.2	0.2	0.04
9	0.25	0.74	0.25	0.185
10	0.3	0.63	0.3	0.189
11	0.33	1.02	0.33	0.3366
12	0.3	1.5	0.3	0.45
13	0.25	1.71	0.25	0.4275
14	0.15	0.63	0.15	0.0945
15	0.1	0.33	0.105	0.03465
16.1	0	0	0.055	0
Total	0.23	0.75	2.54	2.03

XS 6

Station	Depth	Velocity	angle	Velocity	Area	Discharge
5	0	0	0	0	0.07	0
5.7	0.2	-0.01	0	-0.01	0.17	-0.0017
6.7	0.15	0.76	0	0.76	0.15	0.114
7.7	0.18	0.81	0	0.81	0.18	0.1458
8.7	0.2	0.47	0	0.47	0.2	0.094
9.7	0.21	0.79	10	0.802187	0.21	0.168459
10.7	0.25	1.04	15	1.076687	0.25	0.269172
11.7	0.22	1	20	1.064178	0.22	0.234119
12.7	0.1	1.51	10	1.533294	0.1	0.153329
13.7	0.2	1.53	20	1.628192	0.2	0.325638
14.7	0.25	1.49	20	1.585625	0.25	0.396406
15.7	0.1	0.3	15	0.310583	0.1	0.031058
16.7	0	0	0	0	0.05	0
Total	0.19			0.77	2.15	1.93

Large Island Setup:
Determination of water surface slope:

Surface Profile

BS	100			
HI	7.195		staff gage	0.145

Pipe #	Sight	Elev	read depth	Surf Elev	Loc	Slope
BS	7.195	100	0.205	100.205	0	0.0035
8	5.8	101.395	1.13	100.265	17.0612	0.0258
7	6.45	100.745	0.26	100.485	25.5918	0.0028
6L	5.85	101.345	0.84	100.505	32.81	0.0063
6R	5.695	101.5	1.05	100.45	32.81	
5	5.73	101.465	0.93	100.535	37.56745	0.0133
4L	5.722	101.473	0.9	100.573	43.9654	
4R	5.425	101.77	1.15	100.62	43.9654	0.0062
3	5.37	101.825	1.16	100.665	51.1836	0.0127
2	5.37	101.825	1.01	100.815	62.9952	0.0082
1	5.285	101.91	0.99	100.92	75.7911	
					average	0.0108

Velocity profiles at each cross-section

XS 2

Station	Depth	Velocity	Area	Discharge
5.5	0	0	0.225	0
8	0.18	0.59	0.27	0.1593
8.5	0.13	1.12	0.065	0.0728
9	0.1	0.43	0.075	0.03225
10	0.35	1.53	0.35	0.5355
11	0.45	1.44	0.45	0.648

12	0.23	1.62	0.23	0.3726
13	0.35	0.96	0.35	0.336
14	0.3	0.43	0.3	0.129
15	0.22	0.71	0.253	0.17963
16.3	0	0	0.143	0
Total	0.26	0.98	2.71	2.47

XS 3	Just u/s of buckets					
Station	Depth	Velocity	angle	Velocity	Area	Discharge
5.5	0	0	0	0	0.1	0
6.5	0.2	0.36	20	0.383104	0.22	0.084283
7.7	0.22	0.37	30	0.427239	0.242	0.103392
8.7	0.23	0.45	20	0.47888	0.23	0.110142
9.7	0.23	0.78	40	1.018218	0.23	0.23419
10.7	0.4	0.72	20	0.766208	0.4	0.306483
11.7	0.4	0.77	10	0.781878	0.4	0.312751
12.7	0.35	0.95	10	0.964655	0.35	0.337629
13.7	0.37	0.65	15	0.67293	0.37	0.248984
14.7	0.15	0.69	10	0.700644	0.15	0.105097
15.7	0.15	0.12	0	0.12	0.135	0.0162
16.5	0	0	0	0	0.06	0
Total	0.27			0.63	2.89	1.86

XS 3.5	Middle of bucket island					
Station	Depth	Velocity	angle	Velocity	Area	Discharge
4.8	0	0	0	0	0.0675	0
5.7	0.15	0.36	10	0.365554	0.1425	0.052091
6.7	0.25	0.77	10	0.781878	0.25	0.19547
7.7	0.2	0.77	10	0.781878	0.2	0.156376
8.7	0.32	0.97	10	0.984964	0.272	0.26791
9.4	0.25	1.12	0	1.12	0.125	0.14
9.7		Island of Buckets			0.0375	
11.7					0.0465	
12	0.31	1.18	0	1.18	0.155	0.1829
12.7	0.35	1.44	5	1.445501	0.2975	0.430036
13.7	0.38	1.13	10	1.147432	0.38	0.436024
14.7	0.2	0.87	10	0.883421	0.2	0.176684
15.7	0	0	0	0	0	0
16.2	0	0	0	0	0	0
Total	0.24			0.87	2.17	2.04

XS 4						
Station	Depth	Velocity	angle	Velocity	Area	Discharge
4.7	0	0	0	0	0.13	0
6	0.2	0.5	0	0.5	0.23	0.115
7	0.2	0.46	0	0.46	0.2	0.092
8	0.23	1.01	10	1.025581	0.23	0.235884
9	0.2	1.14	10	1.157586	0.16	0.185214
9.6	0.4	0.35	25	0.386182	0.18	0.069513
9.9		Island		0	0.06	0

11.9				0	0.048	0
12.2	0.32	1.34	20	1.425998	0.176	0.250976
13	0.25	1.91	20	2.03258	0.225	0.45733
14	0.25	0.91	0	0.91	0.25	0.2275
15	0.18	0.69	0	0.69	0.144	0.09936
15.6	0	0	0	0	0.054	0
Total	0.20			0.95	2.09	1.73

XS 5

Station	Depth	Velocity	angle	Velocity	Area	Discharge
4.5	0	0	0	0	0.0525	0
5	0.21	-0.09	0	-0.09	0.1575	-0.01418
6	0.15	1.02	0	1.02	0.15	0.153
7	0.13	0.35	0	0.35	0.13	0.0455
8	0.1	0.49	0	0.49	0.1	0.049
9	0.27	0.54	15	0.559049	0.27	0.150943
10	0.3	0.57	10	0.578793	0.3	0.173638
11	0.33	0.89	0	0.89	0.33	0.2937
12	0.24	1.53	0	1.53	0.24	0.3672
13	0.25	1.72	0	1.72	0.25	0.43
14	0.1	0.85	0	0.85	0.1	0.085
15	0.1	0.47	0	0.47	0.11	0.0517
16.2	0	0	0	0	0.06	0
Total	0.17			0.77	2.25	1.79

XS 6

Station	Depth	Velocity	angle	Velocity	Area	Discharge
5	0	0	0	0	0.07	0
5.7	0.2	0	0	0	0.17	0
6.7	0.15	0.77	0	0.77	0.15	0.1155
7.7	0.15	0.26	0	0.26	0.15	0.039
8.7	0.2	0.44	0	0.44	0.2	0.088
9.7	0.2	0.31	0	0.31	0.2	0.062
10.7	0.25	1.09	10	1.106815	0.25	0.276704
11.7	0.25	0.28	20	0.29797	0.25	0.074492
12.7	0.1	1.21	30	1.397188	0.1	0.139719
13.7	0.23	1.43	25	1.57783	0.23	0.362901
14.7	0.23	1.94	0	1.94	0.23	0.4462
15.7	0.15	1.18	0	1.18	0.1575	0.18585
16.8	0	0	0	0	0.0825	0
Total	0.16			0.71	2.24	1.79

Determination of Energy head:

XS #	Date	# buckets	matting	width	avg depth	avg vel	area	discharge
1	12/16/04	0	no	11.3	0.24	0.69	2.81	2.19
2	12/16/04	0	no	10.6	0.28	0.93	2.77	2.74
	12/16/04	4	yes	10.6	0.31	0.75	3.03	2.25
	12/17/04	4	no	10.8	0.26	0.98	2.68	2.42

	12/17/04	10	no	10.8	0.26	0.98	2.71	2.47
3	12/16/04	0	no	10.9	0.27	0.8	2.91	2.78
	12/16/04	4	yes	11	0.29	0.92	3.18	3.19
	12/17/04	4	no	10.9	0.29	0.59	3.1	1.89
	12/17/04	10	no	11	0.27	0.63	2.89	1.86
4	12/16/04	0	no	10.8	0.3	0.73	3.09	2.27
	12/16/04	4	yes	10.9	0.3	0.94	3.16	2.56
	12/17/04	4	no	10.8	0.27	0.72	2.84	1.99
	12/17/04	10	no	10.9	0.2	0.95	2.09	1.73
5	12/16/04	0	no	11.6	0.26	0.98	2.85	2.79
	12/16/04	4	yes	11.4	0.24	1.16	2.65	2.91
	12/17/04	4	no	11.6	0.23	0.75	2.54	2.03
	12/17/04	10	no	11.7	0.17	0.77	2.25	1.79
6	12/16/04	0	no	11.6	0.23	1.1	2.65	2.71
	12/16/04	4	yes	11.6	0.25	1.2	2.86	3.14
	12/17/04	4	no	11.7	0.19	0.77	2.15	1.93
	12/17/04	10	no	11.8	0.16	0.71	2.24	1.79
7	12/16/04	0	no	11.8	0.23	0.78	2.64	2.18
	12/16/04	4	yes	11.8	0.26	0.76	2.98	2.14
							average	2.336957

XS #	location	$y+v^2/2g$ energy	% of no isl energy	QV force
1	53.81	0.247		1.51
2	49.22	0.293	100.0%	2.55
		0.319	108.6%	1.69
		0.275	93.7%	2.37
		0.275	93.7%	2.42
3	44.95	0.280	100.0%	2.22
		0.303	108.3%	2.93
		0.295	105.5%	1.12
		0.276	98.7%	1.17
4	40.03	0.308	100.0%	1.66
		0.314	101.8%	2.41
		0.278	90.2%	1.43
		0.214	69.4%	1.64
5	36.42	0.275	100.0%	2.73
		0.261	94.9%	3.38
		0.239	86.8%	1.52
		0.179	65.2%	1.38

6	32.81	0.249	100.0%	2.98
		0.272	109.5%	3.77
		0.199	80.1%	1.49
		0.168	67.5%	1.27
7	28.05	0.239		1.70
		0.269		1.63

Calapooia River Island

Date: 2/16/05
Water Temperature: 43 F (kinematic viscosity = $1.59\text{x}10^{-5}$ ft^2/sec)

Cross-section data:
Transect 1 - 137.5 ft upstream of island

Station (ft)	Depth (ft)	2/10 V (ft/s)	6/10 V (ft/s)	8/10 V (ft/s)	angle	Avg V	A (ft^2)	Q (cfs)
1.8	0	Left Edge of Water				0	0.825	0
4	1.5		-0.1		0	-0.1	3.15	-0.315
6	2.2		-0.9		0	-0.9	4.4	-3.96
8	2.9		-0.12		0	-0.12	8.7	-1.044
12	3.5		-0.04		0	-0.04	14	-0.56
16	3.5		0.08		0	0.08	10.5	0.84
18	3.6		0.1		0	0.1	7.2	0.72
20	3.7		0.05		0	0.05	11.1	0.555
24	3.2		0.18		0	0.18	9.6	1.728
26	2.9		0.37		0	0.37	5.8	2.146
28	2.6		0.37		0	0.37	5.2	1.924
30	2.4	0.53	0.67	0.67	0	0.635	4.8	3.048
32	2.6	0.7	0.68	1.05	0	0.7775	5.2	4.043
34	2.9	0.96	1.28	1.69	0	1.3025	5.8	7.5545
36	3.2	1.05	1.46	2.04	0	1.5025	6.4	9.616
38	3.2	1.09	1.74	2.46	0	1.7575	6.4	11.248
40	3	1.47	1.73	2.48	0	1.8525	6	11.115
42	2.9	1.62	1.66	2.39	0	1.8325	5.8	10.6285
44	2.8	1.43	1.67	2.26	0	1.7575	5.6	9.842
46	2.8	0.43	1.77	2.28	0	1.5625	5.6	8.75
48	2.6	1.25	1.65	2.31	0	1.715	5.2	8.918
50	2.4	1.59	1.87	2.06	0	1.8475	4.8	8.868
52	2.2	1.61	1.81	2.56	0	1.9475	4.4	8.569
54	1.9	2.13	2.34	2.79	0	2.4	3.8	9.12
56	2.3	1.87	2.16	2.55	0	2.185	4.6	10.051
58	2.1	2.36	2.34	3.11	0	2.5375	4.2	10.6575
60	2.3	1.9	2.17	2.98	0	2.305	4.6	10.603
62	2.3	1.81	2.66	3.42	0	2.6375	4.6	12.1325
64	2.3	1.57	1.74	2.73	0	1.945	4.6	8.947
66	2.1	1	1.28	2.11	0	1.4175	4.2	5.9535
68	1.9	0.67		1.81	0	1.24	3.8	4.712
70	2	1.22		2.43	0	1.825	4	7.3
72	2.1	1.27		2.4	0	1.835	4.2	7.707
74	2.1	1.3		1.93	0	1.615	4.2	6.783
76	2.3	0.67		1.22	0	0.945	4.6	4.347
78	2.1	0.54		1.07	0	0.805	4.2	3.381
80	1.6	0.2		0.78	0	0.49	3.2	1.568
82	1.9	0.23		0.31	0	0.27	3.8	1.026
84	2		0.33		0	0.33	4	1.32
86	1.6		0.32		0	0.32	3.2	1.024

88	1.5		0.51		0	0.51	3	1.53
90	1.4		0.28		0	0.28	2.8	0.784
92	1.5		0.24		0	0.24	2.7	0.648
93.6	0	Right Edge of Water				0	0.6	0
91.8	2.315909		3.42			1.01392	225.375	213.8285
						0.948768	2.455065	
			Re=	1.57E+05				
						E =	2.331872	

Transect 2 - 20 ft upstream of island

Station (ft)	Depth (ft)	2/10 V (ft/s)	6/10 V (ft/s)	8/10 V (ft/s)	angle	Avg V	A (ft^2)	Q (cfs)
13.5	0	LEW				0	1.575	0
18	1.4		0.05		0	0.05	5.25	0.2625
21	1.7		-0.21		0	-0.21	5.1	-1.071
24	2.2		-0.11		0	-0.11	5.5	-0.605
26	2.1		-0.04		0	-0.04	4.2	-0.168
28	2.15		0.1		0	0.1	4.3	0.43
30	2.15		0.33		20	0.351179	4.3	1.510068
32	2.2		0.59		20	0.627865	4.4	2.762605
34	2.3	0.77	0.99	0.94	10	0.936731	4.6	4.308963
36	2.4	1.29	1.37	1.41	10	1.38098	4.8	6.628705
38	2.6	0.96	1	1.42	15	1.133627	5.2	5.894863
40	2.6	1.15	1.57	2.15	20	1.713326	5.2	8.909296
42	2.5	1.72	2.06	2.29	20	2.162941	5	10.81471
44	2.6	1.39	2.01	2.23	20	2.03258	5.2	10.56941
46	2.7	1.24	1.92	2.44	20	2.000654	5.4	10.80353
48	2.8	1.3	1.78	2.29	20	1.902218	5.6	10.65242
50	2.8	1.83	2.05	2.37	20	2.208169	5.6	12.36575
52	2.75	1.41	1.89	2.32	20	1.997994	5.5	10.98897
54	2	1.54	2.19	2.55	30	2.445078	5	12.22539
57	2	1.68	2.03	2.11	10	1.992775	5	9.963874
59	1.6	0.55	1.04	2.21	10	1.228666	3.2	3.931732
61	1.3	0.48		2.21	0	1.345	2.6	3.497
63	1.3	1.8		2.1	-10	1.980082	2.6	5.148213
65	1.5	1.84		2.46	-10	2.183167	3	6.549502
67	1.3	0.81		2.52	-10	1.690685	2.6	4.395782
69	1.3	1.4		2.56	-10	2.010545	2.6	5.227416
71	1.4	0.25		2.79	-10	1.543448	4.2	6.482483
75	1.8	2.12		1.16	-20	1.745252	6.3	10.99508
78	1.5	1.42		2.8	-20	2.245415	3.75	8.420307
80	1.5	0.91		2.65	-20	1.894236	3	5.682709
82	1.5	1.84		2.45	-20	2.282661	3	6.847984
84	1.4	2.16		2.48	-20	2.468892	2.8	6.912899
86	1.6	2.18		2.23	-20	2.346512	3.2	7.508838
88	1.1	2.24		2.75	-20	2.655124	2.2	5.841272
90	0.9	-0.38	1.12	3.2	-10	1.284515	1.8	2.312126
92	0.95	2.12		1.88	-5	2.00764	1.9	3.814515
94	1.1	1.95		2.68	0	2.315	2.2	5.093

96	1.25	1.98		2.47	0	2.225	2.5	5.5625
98	1.25	1.27		2.36	10	1.842999	2.5	4.607498
100	0.85		2.01		20	2.138997	1.7	3.636295
102	0.6		2.43		10	2.467487	1.2	2.960984
104	0.3		1.64		0	1.64	0.675	1.107
106.5	0	REW				0	0.1875	0
93	1.656977		3.2			1.53994	156.4375	233.7822
						1.494413	1.682124	
			Re =	1.63E+05				
						E =	1.6938	

Transect 4 - middle of island

Station (ft)	Depth (ft)	2/10 V (ft/s)	6/10 V (ft/s)	8/10 V (ft/s)	angle	Avg V	A (ft^2)	Q (cfs)
8	0	LEW				0	0.75	0
12	0.75		0.85		0	0.85	2.25	1.9125
14	1.35		0.58		0	0.58	2.7	1.566
16	1.35		0.58		0	0.58	2.7	1.566
18	0.9		0.98		0	0.98	1.8	1.764
20	1.5		0.84		5	0.843209	3	2.529626
22	1.45		0.35		5	0.351337	2.9	1.018877
24	1.4		1.8		5	1.806876	2.8	5.059252
26	1.2		1.83		5	1.83699	2.4	4.408777
28	1.2		1.84		5	1.847029	2.4	4.432868
30	1.2		1.95		5	1.957449	2.4	4.697877
32	1.4	1.72	1.88	2.17	5	1.919805	2.8	5.375455
34	1.6	1.85	2.17	2.24	5	2.11555	3.2	6.769761
36	1.8	2.21	2.12	2.31	0	2.19	3.6	7.884
38	2.75	1.54	1.72	2.18	0	1.79	5.5	9.845
40	2.4	1.51	1.47	1.9	0	1.5875	4.8	7.62
42	2.4	2.03	2.37	2.57	0	2.335	4.8	11.208
44	2.4	2.11	2.26	2.41	0	2.26	4.8	10.848
46	2.5	1.86	1.96	1.93	0	1.9275	5	9.6375
48	2.3	1.3	1.43	1.84	0	1.5	4.6	6.9
50	2.05	0.87	0.98	1.31	0	1.035	4.1	4.2435
52	1.95	0.35	0.7	1.69	0	0.86	3.9	3.354
54	1.5	0.44	0.82	1.42	0	0.875	3	2.625
56	0.9	0.65		0.42	0	0.535	1.8	0.963
58	0.6		-0.02		0	-0.02	1.5	-0.03
61	0	Left edge of Island					0.45	
77.5	0	Right edge of Island					0.13125	
78	1.05		0.38		0	0.38	1.3125	0.49875
80	1.9	0.72	0.9	0.88	0	0.85	3.8	3.23
82	1.8	1.01	1.37	2.01	0	1.44	3.6	5.184
84	1.7	1.57	1.85	2.6	5	1.975016	3.4	6.715053
86	1.9	1.63	2.11	2.99	5	2.218442	3.8	8.430079
88	2.1	1.54	1.89	2.63	5	1.995092	4.2	8.379386
90	2.1	1.18	1.79	2.36	0	1.78	4.2	7.476

92	1.9	1.4	1.38	1.18	0	1.335	3.8	5.073
94	2	1.6	1.68	1.48	0	1.61	4	6.44
96	1.85	1.43	2.27	2.1	0	2.0175	3.7	7.46475
98	1.9	1.57	1.94	2.77	0	2.055	3.8	7.809
100	1.7	2.51	3.17	3.46	0	3.0775	3.4	10.4635
102	1.5	3.57	3.93	4.37	0	3.95	3	11.85
104	1.5	4.24	4.64	4.65	0	4.5425	3	13.6275
106	1.4	2.4	2.87	3.57	0	2.9275	2.8	8.197
108	1.05	1.72	1.81	2.5	0	1.96	2.2575	4.4247
110.3	0	REW				0	0.60375	0
102.3			4.65			1.587067	134.755	231.4617
						1.717648		
53	1.554		Re L =	1.29E+05	Left	1.355969	79.95	
32.8	1.608824		Re R =	2.24E+05	Right	2.132097	54.805	
16.5								
					Left	E =	1.58255	
					Right	E =	1.679411	

Transect 5 - 43 ft downstream of island

Station (ft)	Depth (ft)	2/10 V (ft/s)	6/10 V (ft/s)	8/10 V (ft/s)	angle	Avg V	A (ft^2)	Q (cfs)
6	0	LEW				0	2.085	0
12	1.39		0.06		0	0.06	5.56	0.3336
14	1.6		0.31		0	0.31	3.2	0.992
16	1.8		0.28		0	0.28	3.6	1.008
18	1.75		-0.01		0	-0.01	3.5	-0.035
20	1.5		-0.09		0	-0.09	3	-0.27
22	1.5		-0.01		0	-0.01	3	-0.03
24	1.35	0.62	1.32	1.91	10	1.312439	2.7	3.543585
26	1.3	1.2	1.32	1.38	10	1.325132	2.6	3.445342
28	1.45	1.16	1.4	1.41	25	1.481285	2.9	4.295726
30	1.5	0.76	1.28	1.87	50	2.018552	3	6.055655
32	1.2	-0.98	0.17	1.97	50	0.517278	2.4	1.241468
34	1.3	-1.05	-0.29		60	-0.815	2.6	-2.119
36	1.4	0.12	0.55	1.32	25	0.700645	2.8	1.961806
38	1.2	1.85	2.26	2.4	20	2.33321	2.4	5.599703
40	1.65	2.04	2.4	2.71	20	2.540724	3.3	8.384391
42	1.5	1.7	2.24	2.21	20	2.232113	3	6.696339
44	1.45	2.2	2.09	2.31	20	2.311926	2.9	6.704586
46	1.3	0.62	0.47	2.3	20	1.026932	2.6	2.670022
48	1.2	2.33	3.03	3.76	10	3.084358	2.4	7.40246
50	1.3	-0.06	1.24	3.67	20	1.620211	2.6	4.212548
52	1.3	2.51	2.92	3.14	15	2.973831	2.6	7.73196
54	1.5	1.38	2.28	2.75	15	2.249138	3	6.747413
56	1.5	2.02		2.55	20	2.431646	3	7.294939
58	1.5	1.89		2.24	20	2.197527	3	6.592581
60	1.25	2.14		2.9	10	2.558875	2.5	6.397188
62	1.8	0.97		2.23	10	1.624683	3.6	5.848857
64	1.7	1.7		1.9	10	1.827768	3.4	6.214411

66	0.95	1.5		2.01	10	1.782074	1.9	3.38594
68	1.8	2.39		1.94	5	2.17327	3.6	7.823772
70	1.5	0.54		0.96	5	0.752865	3	2.258595
72	1.9	0.93		1.45	0	1.19	3.8	4.522
74	1.5	1.8		1.95	15	1.941143	3	5.823429
76	1.6	0.42		1.76	20	1.159954	3.2	3.711852
78	1.2	1.14		2.39	20	1.878274	2.4	4.507857
80	1.5	0.82		2.8	10	1.837922	3	5.513767
82	1.6	1.46		2.82	20	2.27734	3.2	7.287489
84	1.6	1.11		3.06	15	2.158551	3.2	6.907363
86	1.5	0.01	1.89	3.35	5	1.791818	3	5.375455
88	1.9	2.21		2.77	5	2.499511	3.8	9.498143
90	2.3	1.65	2.12	2.38	0	2.0675	4.6	9.5105
92	2.1	1.32	1.75	2.16	0	1.745	4.2	7.329
94	1.8	1.33		1.99	0	1.66	3.6	5.976
96	1.8	1.61		2.11	0	1.86	3.6	6.696
98	1.5	1.24		1.84	0	1.54	3	4.62
100	0.7		1.46		0	1.46	1.4	2.044
102	0.2		0.75		0	0.75	0.5	0.375
105	0	REW				0	0.15	0
99	1.419583		3.76			1.471219	141.395	212.0867
						1.499959	1.428232	
			Re =	1.32E+05				
						E =	1.453193	

APPENDIX IV – SATELLITE IMAGES OF MARTIAN MEGAFLOOD REGIONS

Figure A4-1. Viking satellite image of outwash plain from Vallis Ares. Center of image is located at 15 °N, 35 °W.

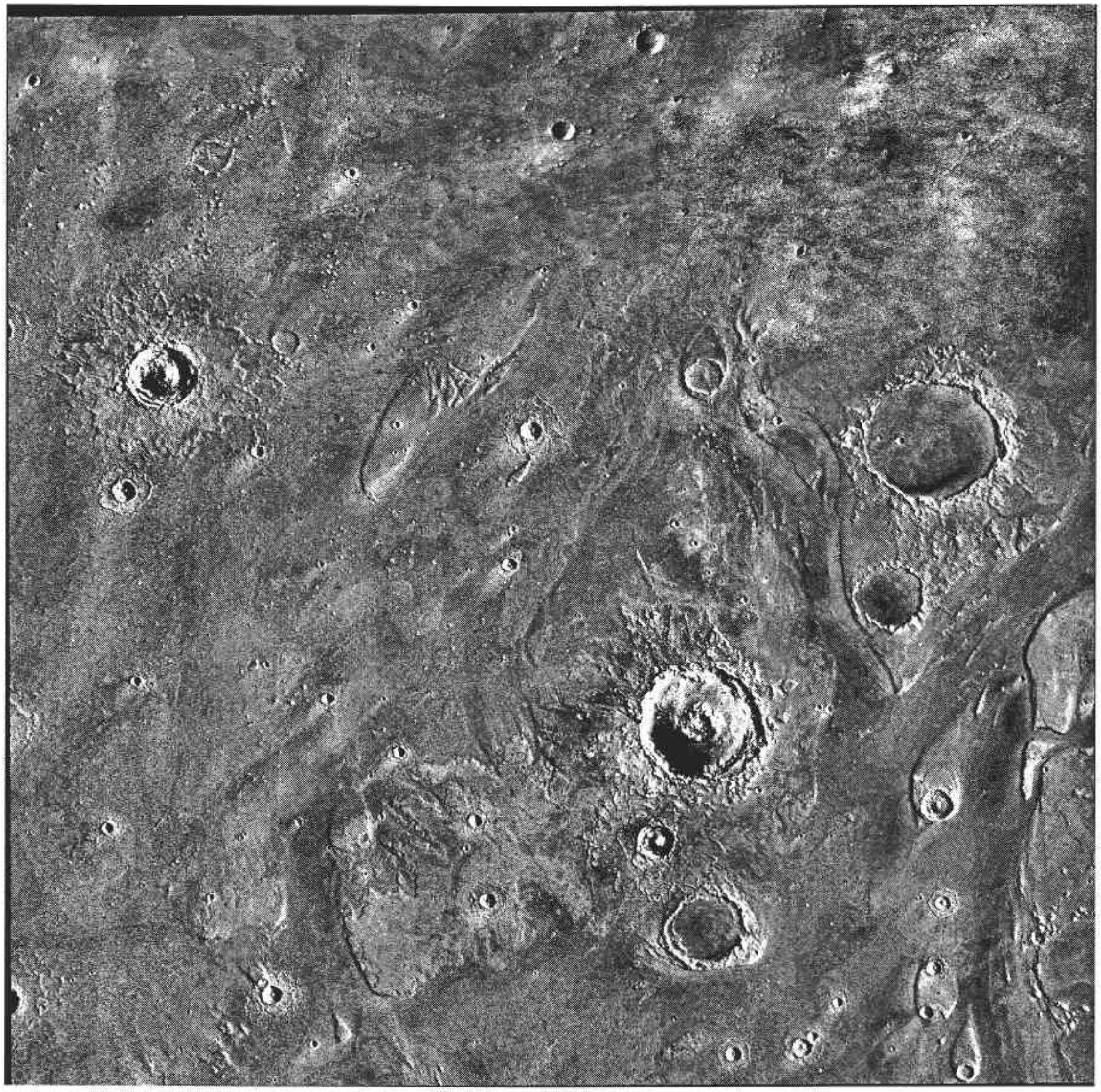

Figure A4-2. Viking satellite image of outwash plain from Vallis Ares. Center of image is located at 25 °N, 35 °W.

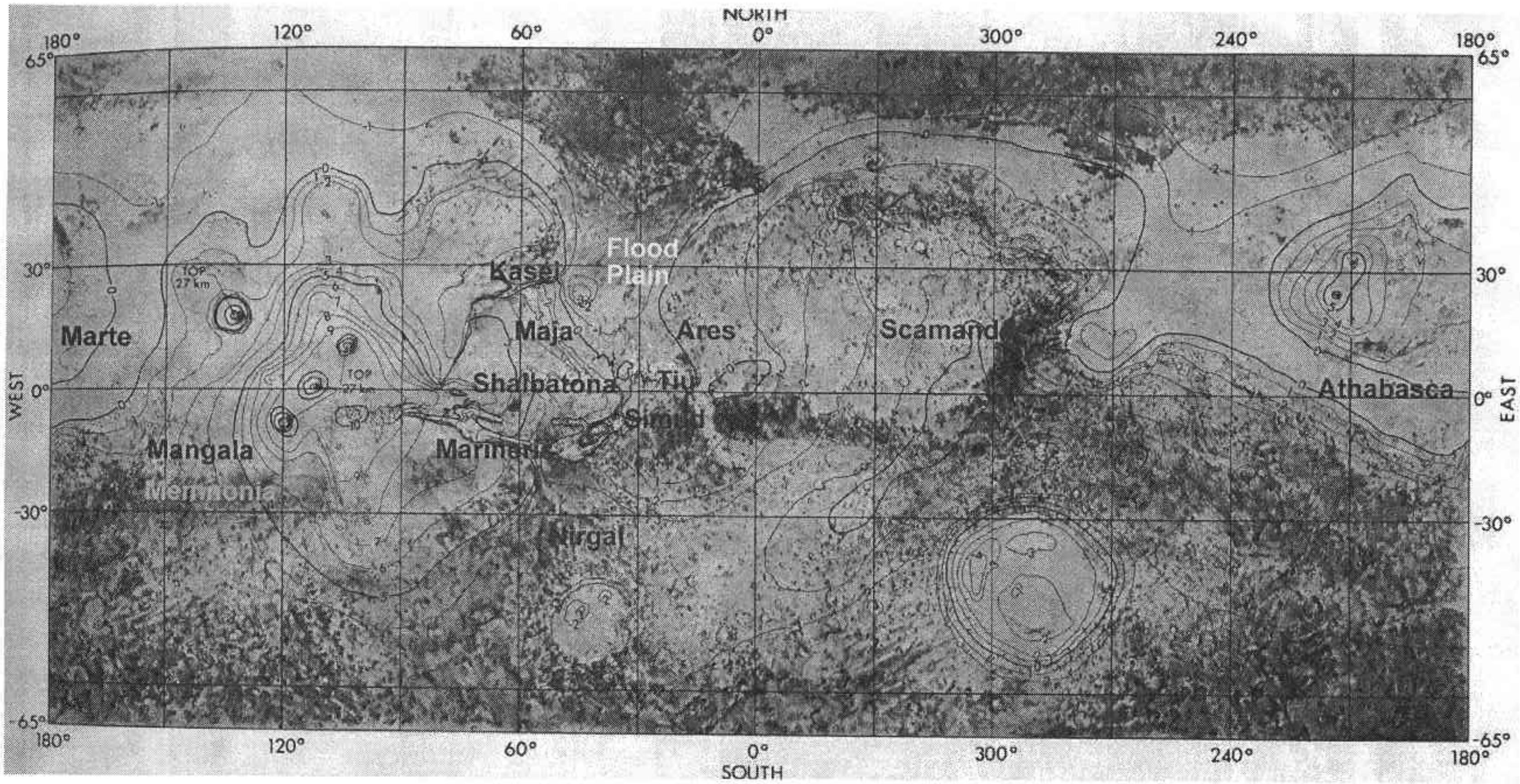

Figure A4-3. Map of martian surface with areas of suggested flooding labeled.